



**HAL**  
open science

# Role of ATG16L1-IFT20 crosstalk in autophagy and primary cilium interplay

Asma Boukhalfa

► **To cite this version:**

Asma Boukhalfa. Role of ATG16L1-IFT20 crosstalk in autophagy and primary cilium interplay. Cellular Biology. Université Paris Cité, 2019. English. NNT : 2019UNIP5041 . tel-03971342

**HAL Id: tel-03971342**

**<https://theses.hal.science/tel-03971342>**

Submitted on 3 Feb 2023

**HAL** is a multi-disciplinary open access archive for the deposit and dissemination of scientific research documents, whether they are published or not. The documents may come from teaching and research institutions in France or abroad, or from public or private research centers.

L'archive ouverte pluridisciplinaire **HAL**, est destinée au dépôt et à la diffusion de documents scientifiques de niveau recherche, publiés ou non, émanant des établissements d'enseignement et de recherche français ou étrangers, des laboratoires publics ou privés.



UNIVERSITÉ  
PARIS  
DESCARTES



Université de Paris

# Université de Paris

École doctorale **BIO SORBONNE PARIS CITÉ (BIOSPC)**

Laboratoire: **AUTOPHAGY PATHWAY and INTRACELLULAR  
COMPARTMENTS DYNAMICS** – Institut Necker Enfants malades  
Inserm U1151/ CNRS UMR 8253

## **Role of ATG16L1-IFT20 crosstalk in autophagy and primary cilium interplay**

Par **Asma BOUKHALFA**

Thèse de doctorat de **Biologie Cellulaire**

Dirigée par **Etienne MOREL**

Présentée et soutenue publiquement le **26 Novembre 2019**

Devant un jury composé de :

Pr. Alexandre BENMERAH (Université Paris Descartes)	President
Pr. Bénédicte DURAND (Université Claude Bernard, Lyon)	Reporter
Dr. Pascale BOMONT (Université de Montpellier)	Reporter
Dr. Philippe BASTIN (Sorbonne Université, Paris)	Examinator
Dr. Cédric DELEVOYE (Université Paris Descartes)	Examinator
Pr. David STEPHENS (University of Bristol, UK)	Examinator
Dr. Etienne MOREL (Université Paris Descartes)	Thesis Director



UNIVERSITÉ  
PARIS  
DESCARTES



Université de Paris

# Université de Paris

École doctorale **BIO SORBONNE PARIS CITÉ (BIOSPC)**

Laboratoire: **AUTOPHAGY PATHWAY and INTRACELLULAR  
COMPARTMENTS DYNAMICS** – Institut Necker Enfants malades  
Inserm U1151/ CNRS UMR 8253

## **Role of ATG16L1-IFT20 crosstalk in autophagy and primary cilium interplay**

Par **Asma BOUKHALFA**

Thèse de doctorat de **Biologie Cellulaire**

Dirigée par **Etienne MOREL**

Présentée et soutenue publiquement le **26 Novembre 2019**

Devant un jury composé de :

Pr. Alexandre BENMERAH (Université Paris Descartes)	President
Pr. Bénédicte DURAND (Université Claude Bernard, Lyon)	Reporter
Dr. Pascale BOMONT (Université de Montpellier)	Reporter
Dr. Philippe BASTIN (Sorbonne Université, Paris)	Examinator
Dr. Cédric DELEVOYE (Université Paris Descartes)	Examinator
Pr. David STEPHENS (University of Bristol, UK)	Examinator
Dr. Etienne MOREL (Université Paris Descartes)	Thesis Director



## Acknowledgements

First and foremost, I would like to express my deep and sincere gratitude to our former head of the lab: Patrice Codogno for giving me the opportunity to start and to do my PhD in his lab, I will be grateful to Dr Patrice Codogno all my life.

Foremost, I would like to thank the members of the jury: Bénédicte Durand and Pascale Bomont for accepting to evaluate this manuscript, Alexandre Benmarah for accepting to be the president of the jury and Cedric Delevoye and Philippe Bastin for accepting to be examiners of this work.

I am greatly thankful to Pr David Stephens from Bristol University (UK) for accepting our invitation to be part of the jury.

I warmly thank my thesis director, Etienne Morel, without whom this work could not have been done. Thank you for having accompanied me during these four years through the phases, far from being all the time easy.

Thank you for giving me the opportunity to work on several projects and for providing me invaluable guidance throughout this research.

I will be all the time extremely thankful to my PhD Supervisor, he has taught me the methodology to carry out the research and to present the research works as clearly as possible.

I would like to express my thanks to Nicolas Dupont for his continuous help, scientific discussions, advices and ideas.

Very special thanks for Pr Sophie Lotersztajn and Pr Bruno Crestani for the time they gave me during several meetings and for sharing interesting ideas with us about my project.

I am greatly thankful to Diana Molino, a senior post doc in the lab, for all advices, ideas and inspiration. I would like to thank her for giving me the idea to take a look to phosphoinositides in my story of IFT20 and ATG16L1 trafficking.

I am extremely grateful to Anna Chiara Nascimbeni and Naima Zemirli, both amazing collaborators and scientists. I feel lucky to have worked with them and learnt from, and hope to work with again.

I feel lucky to meet these brilliant scientists and researchers during my thesis.

I would like to thank Jani Riddhi and Cedric Delevoye from Graça Raposo lab at Curie Institute, for sharing with us several ideas and tools concerning recycling endosomes.

I'd like to thank sincerely to all the other members from Codogno Team with whom I started this journey: Ahmed Hamaï who was ready to answer all my questions at any time with a smile. Amadine David for her friendship and help. Maryam Mehrpour and Joelle Botti for their kindness.

I want to thank Christine and Valérie for their management skills.

I would like to thank sincerely all my friends (PhD students and post docs) from Codogno lab and Pende lab, I felt very lucky to daily work with them, such as Caterina Miceli, Mouradi El Hout, Martina Bonucci, Manuella Barilari, Chantal Al Khoury, Irene Pila-Castellanos, François Brazier and Talha Rashid.

I would also like to thank postdocs and students from Morel lab: Nina Fenouille, Clemence Bor, Morgane Djebar, Federica Roccio, Karla Alvarez, Lucille Penalva and Lukas Bögge.

Last but not least, I have to thank my family, my dear sister and my dear brother. I am also thinking of my precious and dear mother who passed away 2 years ago, I wished she could have seen the end of it all.

I would like to thank the person who has always encouraged, supported me and also inspired me even when he was so far in Canada or Edinburgh, my future husband Fayez. I hope one day we will create our lab and we will collaborate on "a project in the interface of cell biology and Biophysics should be interesting".

I would like also to thank my friends Insaf Farah, Marie Elisa Pinson, Cecile Mons, friends with whom I kept contact also after the end of the Master 2 at the university Paris Diderot.



# TABLE of CONTENT

Abbreviations	4
Illustrations and figures	6
Summary	8
Résumé (français)	10
Preface	12
I. INTRODUCTION	16
<b>1. The primary cilium: structure, dynamics and associated signaling</b>	<b>16</b>
1.1) The primary cilium structure	16
1.2) Ciliogenesis	20
1.3) Molecular regulation for ciliary trafficking	25
1.3.1) Intraflagellar transport system	25
1.3.2) Molecular regulation of trafficking toward the cilium	30
1.3.3) The phosphoinositides turnover: linking PC and endomembranes trafficking	32
1.4) The primary cilium functions: a biological stress sensor	34
1.4.1) Ciliary signaling in response to nutritional stress	34
1.4.2) Ciliary signaling in response to biomechanical stress	39
1.5) The ciliopathies	41

<b>2. The autophagic pathway and machinery</b>	<b>43</b>
2.1) The different forms of autophagy	44
2.2) The regulation of autophagy	46
2.3) ATG16L1: roles and functions	52
2.4) The autophagy and primary cilium interconnection	57
II. AIMS OF THE STUDY	60
III. RESULTS	63
IV. DISCUSSION	66
V. APPENDIX	76
VI. BIBLIOGRAPHY	78

## **ABBREVIATIONS**

ADPKD: autosomal dominant polycystic kidney disease

AMPK: AMP-activated protein kinase complex

ATG: autophagy related

ATP: adenosine triphosphate

BB : Basal body

BBS: Bardet–Biedl syndrome

Bcl-2: B cell lymphomas

CMA: chaperone-mediated autophagy

CTS: Ciliary targeting sequence

DN: diabetic nephropathy

EndoMT: endothelial-to-mesenchymal transition

Gli: glioma-associated oncogene family

GPCRs: G-protein-coupled receptors HDAC6: histone deacetylase-6

Hh: Hedgehog

IFT: Intraflagellar transport

KEC: Kidney epithelial cell

LKB1: Liver kinase B1

MAPK: mitogen-activated protein kinase

MC: motile cilium

MCF7: Michigan Cancer Foundation - 7

mTORC1: mammalian target of rapamycin complex 1

GFP: green fluorescent protein

OFD1: oral-facial-digital syndrome type 1

PAS: pre-autophagosomal structure

PC: Primary cilia  
PC1: polycystin 1  
PC2: polycystin 2  
PCP: planar cell polarity  
PDGF: platelet-derived growth factor  
PI3KC3: class III phosphatidylinositol 3-kinase  
PI3P: phosphatidylinositol 3-phosphate  
PI4P: phosphatidylinositol 4-phosphate  
PI4,5P2: phosphatidylinositol 4,5-biphosphate  
INPP5E: inositol polyphosphate 5-phosphatase  
PKD: polycystic kidney disease  
Ptc1: patched 1  
RFP: red fluorescent protein  
Shh: sonic hedgehog  
Smo: smoothened  
Sufu: suppressor of fused protein  
TFEB: transcription factor EB  
TGN: trans-Golgi networks  
UUO: Unilateral ureteral obstruction  
Vangl2: Van Gogh-like 2 protein

## **ILLUSTRATIONS AND FIGURES**

Figure 01: Primary cilia structure

Figure 02: Structure of the basal body

Figure 03: Synchronization of the assembly of the PC with the cell cycle.

Figure 04: The centrosome cycle

Figure 05: Intraflagellar transport machinery

Figure 06: phosphoinositides and endomembranes

Figure 07: Shh signaling pathway (SMO localisations)

Figure 08: Dysfunctions in motile and/or non-motile cilia cause ciliopathies

Figure 09: Human diseases associated with autophagy defects

Figure 10: The different types of autophagy

Figure 11: the formation of the autophagosome

Figure 12: Early steps of autophagy machinery

Figure 13: ATG16L1 and partners in autophagosome biogenesis

Figure 14: ATG16 interacting proteins, binding regions, and functions of interactions

Figure 15: Interaction between ATG16L1 and PI3P

Figure 16: Phosphoinositide Regulation at Distinct Cellular Membranes

Figure 17: ATG16L1 and phosphoinositides membranes dialog

Figure 18. A specific post-Golgian trafficking to PC for phosphoinositides turnover?

Figure 19: The ATG16L1 partners and functions at a glance



## **SUMMARY:**

Primary cilia are microtubule-based structures located at the cell surface of many cell types and directly participating in integration of mechanical and chemical stresses related signaling. In parallel, the macro-autophagy pathway is a lysosomal degradative system that allows cells to adapt to various stress situations. In this work, we investigated the molecular and the functional relationship between autophagy and primary cilium. Indeed, recent literature show that many stress situations that trigger primary cilium signaling or induce ciliogenesis also stimulates autophagy. Moreover, previous work of our laboratory suggested a direct crosstalk between primary cilium and autophagy pathways in response to serum deprivation by a dual mobilization of ATG16L1 (a key player in autophagy regulation) and IFT20 (an essential regulator of primary cilium associated trafficking). In this context, the precise goal of my PhD project was to characterize the role of ATG16L1/IFT20 mobilization in the complex interplay between autophagy and primary cilium in response to nutritional stress, by analyzing the physiological conditions, and protein domains, that regulate ATG16L1/IFT20 complex.

We first showed that IFT20 and ATG16L1 are part of the same protein complex independently of the ciliogenesis status but that they colocalized only at primary cilium and/or Golgi structures. Moreover, ATG16L1 engagement with IFT20 occurs independently of key regulators of autophagy such as ATG3 and ATG5 (the ATG16L1 direct partner in autophagosome biogenesis sequence) suggesting that the ATG16L1 mobilization we observed is not related to its canonical implication in autophagy. Interestingly, we identified the Sec8 protein (from the exocyst post-Golgi trafficking machinery) as a new partner in the IFT20/ATG16L1 complex, but only when cells are engaged in primary cilium biogenesis. We finally showed that this ATG16L1/ITF20 interaction was mediated by the ATG16L1 WD40 domain and by a newly identified motif in the IFT20 protein.

In addition, we showed that invalidation of ATG16L1 expression induced an increase of primary cilium length and that ATG16L1 participates, directly or indirectly, in ciliary signaling (like hedgehog signaling pathway) to control primary cilium functions and stress response. To go further in the role of ATG16L1/IFT20 complex in primary cilium signaling in response to stress, we investigated a putative link between ATG16L1 and phosphatidylinositol-4-phosphate (PI4P) turnover, a key lipid in membrane trafficking also known to participate in primary cilium

membrane dynamics. Interestingly, we show that absence of ATG16L1 alters the phosphoinositides equilibrium at primary cilium since PI4P is no longer present on the ciliary membrane, while phosphatidylinositol-4,5-bisphosphate (PI4,5P2,) which is normally excluded from cilia structures, was found to be present on abnormal cilia observed in ATG16L1 KO cells. We finally show that INPP5E, the Golgi to PC phosphatase responsible for PI4P production from PI4,5P2 membranes, was a partner of ATG16L1/IFT20 complex during ciliogenesis and that destabilization of the this complex alters the proper INPP5E targeting to primary cilium (and thus affecting its local function), highlighting the key role of ATG16L1 in PI4P production and trafficking at primary cilium.

In conclusion, the findings presented in my thesis manuscript suggest a non-canonical role of ATG16L1 in targeting and trafficking to PC structure and strongly support the idea that IFT20-ATG16L1 crosstalk has a functional role in the control of cilium homeostasis.

## **RESUME (français):**

Le cil primaire est une structure présente à la surface de nombreux types cellulaires et participant directement à l'intégration de la signalisation associée aux contraintes mécaniques et chimiques. Par ailleurs, la voie macro-autophagique est un système de dégradation lysosomal qui permet aux cellules de s'adapter à diverses situations de stress. Au cours de ce travail de thèse, nous avons étudié la relation moléculaire et fonctionnelle entre l'autophagie et le cil primaire. En effet, la littérature récente montre que de nombreux types de stress cellulaire associés la signalisation du cil primaire et à la ciliogenèse stimulent également la machinerie autophagique. En outre, des travaux issus de notre équipe ont suggéré une connexion directe entre les voies ciliaire et autophagique, en réponse à la privation de sérum, par une mobilisation de vésicules transportant ATG16L1 (un acteur clé de la voie de l'autophagie) et d'IFT20 (un régulateur essentiel du trafic vésiculaire lié au cil primaire). Dans ce contexte, l'objectif précis de mon projet de doctorat était de caractériser le rôle de la mobilisation du complexe ATG16L1/IFT20 dans le dialogue encore mal caractérisé entre autophagie et le cil primaire en réponse au stress nutritionnel. Dans ce contexte, nous avons analysé les conditions physiologiques et les domaines protéiques qui régulent le complexe ATG16L1/IFT20, ainsi que l'aspect fonctionnel de l'interaction entre ces deux protéines au niveau de la ciliogenèse.

Nous avons tout d'abord pu montrer qu'IFT20 et ATG16L1, qui colocalisent au niveau du centrosome, du cil primaire et du Golgi, interagissent indépendamment de l'état de la ciliogenèse. De façon originale, l'interaction entre ATG16L1 et IFT20 se produit également en absence des principaux régulateurs de l'autophagie (tels que ATG3 ou ATG5) suggérant que la mobilisation ATG16L1 que nous observons n'est pas liée à son implication classique dans l'autophagie. Nous avons de plus identifié la protéine Sec8 (associée au complexe Exocyst, impliqué dans le trafic post-Golgien) comme un nouveau partenaire dans le complexe IFT20/ATG16L1, mais seulement lorsque les cellules sont engagées dans la biogénèse du cil primaire.

Notre étude nous a permis de démontrer que l'interaction entre ATG16L1 et IFT20 est dépendante du domaine WD40 d'ATG16L1 et qu'elle nécessite un motif nouvellement identifié dans la protéine IFT20. Enfin, nous avons montré que l'inactivation de l'expression d'ATG16L1 induit une augmentation de la longueur du cil primaire et affecte la signalisation ciliaire en réponse au stress. De façon intéressante, l'absence d'ATG16L1 altère la présence du PI4P au cil primaire (un

lipide clé dans le trafic membranaire, également connu pour participer à la dynamique du cil primaire) n'est plus présent sur la membrane ciliaire, tandis que PI4,5P2, qui est normalement exclu des structures ciliaires, est artificiellement adressé aux cils anormaux observés dans les cellules ATG16L1 KO.

Nous montrons enfin que la phosphatase INPP5E, localisée au niveau du Golgi et du cil primaire et responsable de la production PI4P à partir du PI4,5P2, est un partenaire du complexe ATG16L1/IFT20 au cours de la ciliogenèse et que la déstabilisation du complexe altère le ciblage de cette enzyme vers le cil primaire et affecte donc sa fonction locale. Ces résultats soulignent le rôle, jusqu'alors inconnu, d'ATG16L1 dans la production et le trafic du PI4P au niveau du cil primaire.

Ainsi, les résultats présentés dans mon manuscrit de thèse suggèrent un rôle non canonique d'ATG16L1 dans le ciblage et le trafic vésiculaire vers le cil primaire et soutiennent l'idée que le dialogue entre IFT20 et ATG16L1 joue un rôle fonctionnel dans le contrôle de l'homéostasie cellulaire via le cil primaire.

## PREFACE

The study of molecular aspects and physiological implications of the autophagic pathway is experiencing significant growth in the field of cell biology these last years. The interest of the scientific community in its understanding was notably illustrated by the recent awarding of the 2016 Nobel Prize in Medicine to Professor Yoshinori Oshumi, for the discovery of yeast autophagy genes. Thus, many studies highlight and try to address the link(s) between autophagy regulation and many cellular processes with pathophysiological implications.

In this context, our team "Autophagy pathway and intracellular dynamic compartments" in the cell biology department of Institut Necker Enfants Malades, currently headed by Etienne Morel and created by Patrice Codogno, is interested to understand how mammalian cells organelles and endomembranes cooperate with autophagic machinery to adapt to stress situations and external stimuli.

My doctoral study was devoted at a better understanding of the complex interplay between autophagic machinery and primary cilia in response to stress and during cellular adaptation. Beside my main doctoral project, I directly participated to two distinct projects dedicated to the role of the folliculin (FLCN) protein and PI3KC2alpha lipid kinase in the autophagy and primary cilium dialog in epithelial cells. I contributed to these studies along with my main project, especially by shear stress (i.e. mechanical forces) experiments, cell biology, imaging and biochemistry experiments. This led first to a publication of the FLCN story, in Cell Stress journal (N.Zemirli\*, A.Boukhalfa\* *et al*, 2019). I present this article in my thesis manuscript, in the Annexes section.

The second side-project was specifically aimed at understanding the precise contribution of lipid kinases associated with the primary cilium and phosphoinositides, in shear stress conditions, namely the PI3KCIII (also known as Vps34) and PI3C2 $\alpha$ . I contributed significantly to this study along with my main project, especially by shear stress experiments analyses, cell biology, imaging, lipid biochemistry and molecular biology experiments. This work gave rise to interesting results about a yet unreported role of PI3KC2 $\alpha$ -dependent PI3P that regulates primary cilium-mediated autophagy in response to shear stress. This paper is under reviewing in Nature

Communications Journal (A.Boukhalifa\*, A. Nascimbeni\* *et al*, in revision). I present as well this article in my thesis manuscript, in Annexes section.

My main project in the lab was to study the dialogue between autophagic machinery and ciliogenesis upon nutritional stress in epithelial cells. This project originated from a previous collaboration between our lab and Ana Maria Cuervo's lab (Albert Einstein college of Medicine, Bronx, NY) that gave rise to an original story showing for the first time an interplay between primary cilia and autophagy in nutritional stress conditions (Pampliega *et al.*, 2013). As a direct follow-up of this study, my current study aimed at deciphering precisely the crosstalk suggested between the ciliary protein IFT20 and the autophagic regulator ATG16L1. Thus, the introduction of my thesis manuscript mainly concerns this last project and addresses both the basics of ciliary proteins and functions as well as autophagy processes.

I therefore organized the introduction section by treating first different aspects of primary cilia, from structure, dynamics to associated signaling, followed by the vesicular transport associated with ciliary structures and more precisely about polarized vesicular trafficking to the primary cilium, notably the IFT proteins, the small Rab GTPases, the ARL proteins, the exocyst and the microtubules. Finally, I detailed some functions of the primary cilium as a biological sensor in response to nutritional stress or biomechanical stress.

Thereafter, I described autophagy process from biological roles to defects and diseases and I particularly detailed the role and functions of ATG16L1, which is an important partner of the ciliary protein IFT20. Finally, I summarized ideas from previous studies about the interconnection between the autophagy and primary cilium.

After the presentation of the aims of the study, the results obtained as part of my main project are presented in a format of a paper manuscript (comprising methods section), which we wish to submit very soon ("*The autophagy protein ATG16L1 cooperates with IFT20 and INPP5E to regulate the turnover of phosphoinositides at the primary cilium*". Boukhalifa *et al*, in preparation) for publication.

In the discussion part, the part of this manuscript where i felt free to propose ideas off the beaten track. I present some ideas on the results that I have obtained as part of my project and I present the perspectives for the team to answer the unresolved questions.

# I. INTRODUCTION

## **1. The primary cilium: structure, dynamics and associated signaling**

### **1.1) The primary cilium structure**

A cilium is a cytoplasmic cell extension described for the first time among protozoa in 1675 by Anton van Leeuwenhoek (Haimo and Rosenbaum, 1981) but the term cilium was attributed in 1786 by Otto Muller (Satir, 2017) and described in mammals in 1898 by a Swiss anatomist KW Zimmerman (KW Zimmerman, *Arch Mikrosk Anat*, 1898 (in German)). Cilia are found on the surface of most differentiated mammalian cells. Depending on their motor capacity and its ultrastructure, cilia have been classified into two categories: motile cilium and non-motile cilium, still called primary cilium (PC), which is one of the key aspects of this thesis work. The PC is thus defined as an immobile structure localized at the surface of quiescent cells, and notably characterized by sensory functions, notably illustrated on epithelial cells of the retina, of kidney, endothelial cells, chondrocytes and neurons (Satir, 2017). Unlike PC that is only present in one copy per cell, the motile cilia are over a hundred copies on the surface of some specialized epithelial cells. Through their coordinated beating movement, motile cilia are indeed able to generate fluid movement to allow proper evacuation of the mucus (Ishikawa and Marshall, 2014), the circulation of the cerebrospinal fluid (Hagenlocher *et al.*, 2013), or movement of oocytes (Talbot, Geiske and Knoll, 1999). From the dedicated literature, it appears that most of the knowledge we have about the PC comes indirectly from what has been discovered on the motile cilium such as the flagella of the spermatozoa, or motile cilia of the respiratory epithelium in different organisms such as sea urchin, and some vertebrate cells, (Takeda and Narita, 2012). In the rest of the chapter, I will mostly focus on PC: for detailed information on motile cilia, readers can refer to (Al Jord, Spassky and Meunier, 2019).

In terms of functions, and membrane identity, the PC constitutes a well-individualized cellular compartment, separated from the rest of the cell and its structure is extremely well preserved. The PC consists of three distinct parts, connecting the cytoplasm and the plasma membrane: the basal body (derived from the mother centriole) directly anchored to the plasma membrane, the axoneme forming an external projection to the cell surrounded by its own membrane and the transition zone,

lying between the basal body and the axoneme (Figure 01). The PC often partially externalized and a ciliary pocket created by membrane invagination is observed near the basal body. Different studies on the PC show that its architecture can vary from one cellular type to another. As an example, in cells of the renal epithelium, the symmetry of the nine lining microtubules assembled in a ring is progressively lost to the distal region of the cilium (Gluenz *et al.*, 2010). This loss of symmetry results in a progressive incursion of the microtubule doublets towards the center of the axoneme.

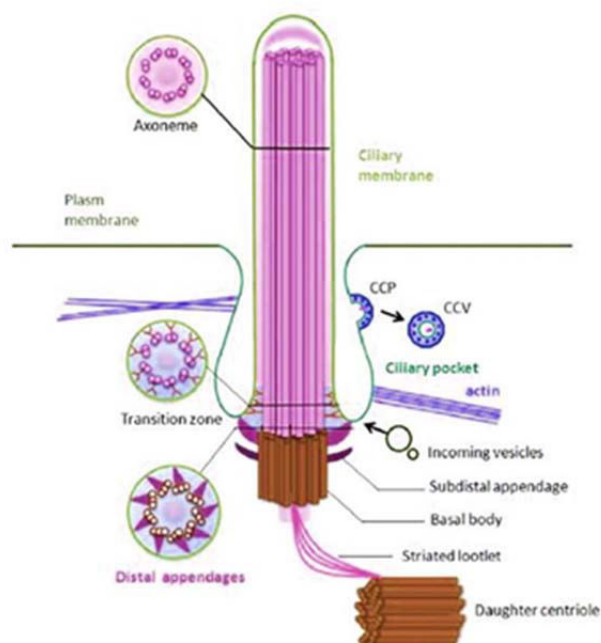


**Figure 01: Primary cilia structure**

We distinguish the skeleton of the PC from its membrane. The skeleton is composed of a 9 + 0 axoneme and basal body. The transition zone is in the region immediately following the loss of the microtubule triplet organization where Y-shaped bridges are found. The mother and daughter centriole are connected by striated rootlets.

Adapted from (Joukov and De Nicolo, 2019)

### 1.1.1) The axoneme

The axoneme corresponds to the cilium projection from the plasma membrane. The axoneme of the PC is composed of 9 peripheral microtubule doublets (microtubules A and B) giving an axonemal structure called "9 + 0". In comparison, the one of the mobile cilium is provided with central pair additional singlet microtubules (axonemal structure called "9 + 2").

PC may also show a 7+2 or 8+1 structure within different tissues and organisms (Webber and Lee, 1975). In osteocytes, the primary cilium is very small and has irregular microtubule doublets, which means that the bone extracellular matrix can have an effect in maintaining the structure of the cilium (Uzbekov *et al.*, 2012).

The hybrid nature of the PC can be observed in different tissues and organisms. For example, the nodal cilia found at the embryonic node have a 9+0 axoneme, but is motile. These cilia have dynein arms that allow causing a rotation of the structure, but in a completely different way than that of the canonical motile cilia. The beating of these cilia will enable the right left symmetry of the embryo to be established in vertebrates by ensuring the diffusion of morphogens (Okada *et al.*, 2005). Other primary cilia have motility. This is the case, for example, with the cilium of the neonatal cells of the choroidal plexus that beat vigorously, and whose motility gradually decreases during the two weeks required for cell differentiation (Narita *et al.*, 2012).

Each doublet of microtubules consists of a complete microtubule (microtubule A), and an incomplete adjacent microtubule (microtubule B). Microtubule A consists of thirteen tubulin protofilaments and B consists of ten (Downing and Sui, 2007). The protofilaments are assembled by longitudinal polymerization of  $\alpha$  and  $\beta$ -tubulin heterodimers in the presence of GTPs. Tubulin protofilaments are very dynamic structures, and their polymerization is oriented: the “minus” end is subject to depolymerization, while the protofilament polymerization is at the “plus” end (Haimo and Rosenbaum, 1981); (Sui and Downing, 2006). Thus, the assembly of a functional, stable microtubule requires a number of reversible post-translational changes to the tubulin (Janke and Kneussel, 2010). These changes are particularly important at the ciliary level, where there are various combinations of post-translational modifications, such as acetylation, palmitoylation, tyrosination/detyrosination, glutamylation, and glycylation. Acetylation is the most common post-translation modification associated with microtubule stabilization. However, it is not yet known whether tubulin acetylation is a cause or consequence of microtubule stabilization (Sharma *et al.*, 2011). After polymerization,  $\alpha$ -tubulin acetylation occurs on lysine 40 (Jenkins *et al.*, 2017).

### **1.1.2) The basal body**

The basal body, which corresponds to the mother centriole, is located at the base of the cilium (Vertii *et al.*, 2016). The centrioles consist of nine triplets of microtubules with microtubules A and B extending to form the axoneme (Figure 02). The basal body comes from the maturation of the mother centriole, the oldest centriole of the centrosome (Division, 2017). The immature centriole (or daughter centriole) remains physically associated with the mother centriole

and the latter two are connected and surrounded by a pericentriolar matrix. The differentiation of the mother centriole into PC associated basal body takes place during the early stages of the ciliogenesis as soon as the cell enters G0phase (Love *et al.*, 2010).

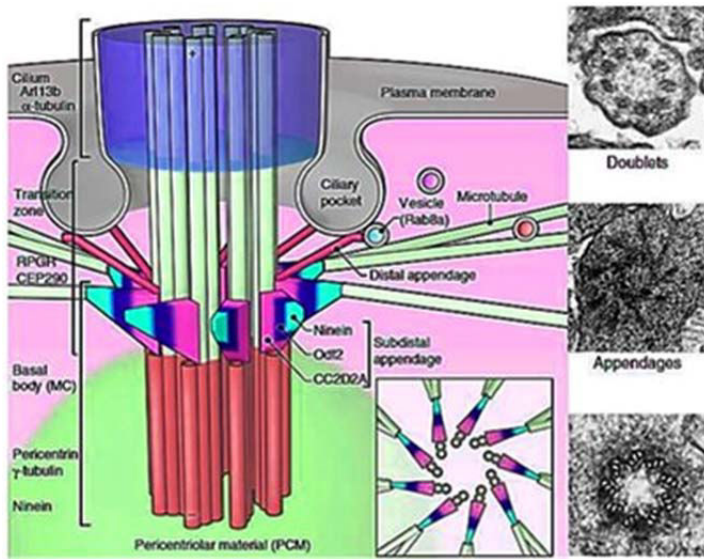


**Figure 02: Structure of the basal body.**

The basal body is organized in a triplet of microtubules (pink cylinders) which extend into doublets of microtubules at the level of the axoneme (green cylinders). The localized proteins at the level of the primary cilium and the basal body are indicated. The nine lateral extensions of each microtubule doublet at the edge of the mother centriole and the transition zone represent the subdistal appendages (pink, blue, green, pyramid) and the distal appendages (pink sticks). The subdistal appendages are attached to the microtubule network and help transport the vesicles to the base of the cilium. The distal appendages attach the maternal centriole to the membrane and separate the ciliary compartment from the cytoplasm. The electron micrographs on the right show the cross-sections of the indicated levels. Adapted from (Veleri *et al.*, 2014)

### 1.1.3) The transition zone

The transition zone, constitutes a real barrier between the PC and the cytoplasm preventing the free passage of vesicles between the two compartments. In addition, the transition zone constitutes a sorting platform area for the 17 IFT protein complexes that will be assembled and translocated in the axoneme. Although the ciliary membrane is in continuity with the plasma membrane, the composition of these two membranes is different (Garcia, Raleigh and Reiter, 2018). The ciliary membrane is enriched with sterols, glycolipids and sphingolipids and some studies show possible enrichment of phosphatidylinositol-4-phosphate and phosphatidylinositol 3,4-bisphosphate ((Schurmans, Inoue and Reiter, 2016); (Jacoby *et al.*, 2009). This composition is ensured by a diffusion barrier that prevents lipid diffusion by separating the ciliary membrane from the plasma membrane (Nachury, Seeley and Jin, 2010). Various studies found that the septins protein family, present at the base of the cilium, forms a barrier that restricts the diffusion of

membrane proteins inside and outside the PC. (Malicki and Avidor-Reiss, 2014; Garcia, Raleigh and Reiter, 2018).

## **1.2) Ciliogenesis**

Ciliogenesis corresponds to the cilium biogenesis and maintenance and may differ from one organism to another. However, it must include several key steps, common to all cellular models and conserved during evolution: centriole / basal body duplication, basal body maturation, membrane migration and anchorage, and membrane growth from the basal body. In addition to a correct synthesis of the proteins involved, the construction of this complex organelle depends on the good progress of the molecular interactions in a space and time.

### **1.2.1) Replication of centrioles**

Replication of centrioles occurs during cell division and can be divided into 4 major steps and each pre-existing centriole is able to form a new centriole (Figure 03). During the cell cycle, ciliogenesis occurs in the G0 / G1 phase. The cilium is then disassembled to allow the centriole to be replicated. The mother and daughter centrioles will separate while remaining connected by a fibrous link so that each initiates the formation of procentrioles that will be perpendicular to their base during the S phase (Figure 03). The duplication of centrioles thus takes place at the same time as the replication of the nuclear DNA. In particular the newly formed centrioles display “symmetry 9” and the SAS-6 protein organizes a wheel-shaped structure called the "cartwheel" (Kitagawa *et al.*, 2011). SAS-4 / CPAP and CEP120 proteins regulate centriole elongation during the G2 phase by binding directly to SAS-6 to polymerize microtubules (Comartin *et al.*, 2013), (Lin *et al.*, 2013). In fact, the loss of one of these proteins inhibits the elongation of the centriole, and their overexpression leads to the assembly of very long centrioles (Comartin *et al.*, 2013). The procentrioles will grow to the same size as the original centriole in phase G2 and the son centriole will thus become in turn a new mother centriole, so it will acquire the appropriate appendages. During the G2 / M phase the two pairs of centrioles will lose the link that united them to segregate in each future cell during the mitosis. Many proteins have been implicated in the separation,

duplication, elongation, and maturation stages of centrioles (Figure 03) (Fu, Hagan and Glover, 2015).

### 1.2.2) Differentiation of the mother centriole in basal body

Before initiation of ciliogenesis, the mother centriole acquires distal appendages and subdistals that play essential roles in initiating proper ciliogenesis. The identified proteins in the formation of appendages of the mother centrioles are OFD1 (oro facial digital syndrome 1) (Singla *et al.*, 2010), C2CD3 (C2 calcium-dependent domain containing 3) (Thauvin-robinet *et al.*, 2015), ODF2 / Cenexine1 (Outer Dense Fiber 2), DZIP1 (DAZ interacting zinc finger protein) (C. Wang *et al.*, 2018). The loss of these proteins leads to a lack of formation of distal and / or subdistal appendages and defects of ciliogenesis. DZIP1, C2CD3 and ODF2 / Cenexine1 are required for both appendix assembly distal and subdistal (Ishikawa *et al.*, 2005), (Thauvin-Robinet *et al.*, 2014). The absence of one of these three proteins leads to defects in protein recruitment from distal appendages, as it is the case for the absence of CEP164 in the mutant DZIP1 condition (Wang *et al.*, 2018). In the same way, the absence of C2CD3 prevents the recruitment of the core proteins involved in the formation of distal appendages like CEP83, CEP89, SCLT1 and FBF1.

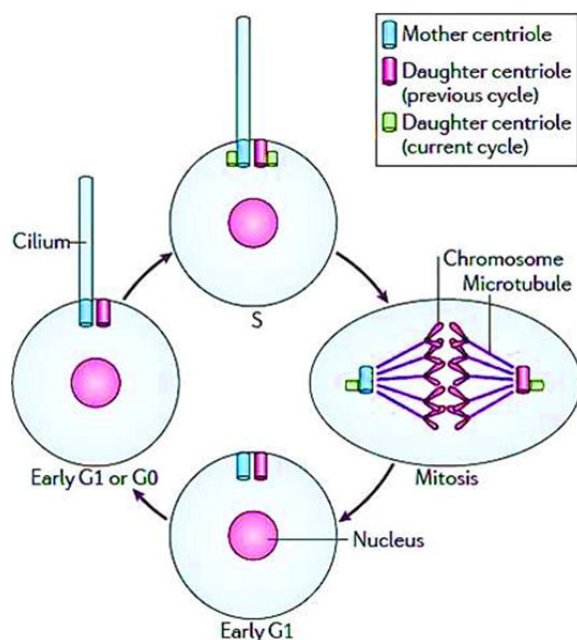


**Figure 03: Synchronization of the assembly of the PC with the cell cycle.**

The cells at the end of mitosis do not have a cilium. During the G0 / G1 phase, the parent centriole attaches to the membrane and forms a PC. During phase S, the mother and daughter centrioles duplicate each other. Before mitosis, in most cells the PC is resorbed, allowing the centriole pair to detach from the membrane and move to the cell poles to produce the mitotic spindle. The PC is again generated in the two child cells in G0 / G1.

Adapted from (Ishikawa and Marshall, 2011)

Among the important proteins in the maturation of the mother centriole, OFD1 is required only for the formation of distal appendages but is not involved in the formation of the subdistal appendages. Indeed, after the loss of OFD1 in cells of mammals, only the subdistal appendages are present. In addition, the CEP164 protein is not recruited to distal appendages in the absence of OFD1 (Singla *et al.*, 2010). The DZIP1, C2CD3, ODF2 and OFD1 proteins thus play a functional role in the maturation of the centriole in the basal body by recruiting the proteins necessary for the function of the distal appendages and are necessary to allow initiation of ciliogenesis.

### **1.2.3) Control of ciliogenesis**

As mentioned above, ciliogenesis is a mechanism which is strongly coordinated with cell cycle. A set of regulatory proteins is required to avoid non-programmed conversion from mother centriole to basal body in dividing cells. This control is ensured by the recruitment of negative and positive factors of ciliogenesis at the level of the mother centriole during the formation of the basal body. CP110 (centrosomal protein 110) and its interaction partners such as Cep97 and kinesin Kif24 have been identified as negative regulators of cilia formation (Spektor *et al.*, 2007). Their levels decrease during the assembly of the cilia and the overexpression of these proteins suppresses the formation of the cilia, whereas their suppression generates an aberrant ciliogenesis (Walentek *et al.*, 2016), (Spektor *et al.*, 2007). Moreover, CP110 is located at the distal end of the centriole, to regulate its size, and its stability is ensured by its interaction with Cep97 (Spektor *et al.*, 2007). At the mother centriole, the loss of CP110 and Cep97 occurs at the end of G1 and is sufficient to induce ciliogenesis (Schmidt *et al.*, 2009). Kif24 is a member of the family of depolymerizing kinesins from microtubules and colocalizes with CP110 (Kobayashi *et al.*, 2011). The depolymerization action of centric microtubules is important for the assembly of the axoneme of the cilia (Kobayashi *et al.*, 2011). Other proteins, close to CP110, have been identified for their negative impact on ciliogenesis. This is the case of trichoplein, which is no longer found in the basal body during ciliogenesis, and whose depletion favors ciliogenesis, whereas its overexpression prevents the growth of the cilia (Inoko *et al.*, 2012) (Figure 04). On the other hand, specific proteins are known to promote ciliogenesis, such as Ser / Thr kinase TTBK2 (Goetz, Liem and Anderson, 2012): in cells depleted in serum, TTBK2 is localized at the distal end of the basal body where it displaces CP110 and recruits the intraflagellar transport complex. Ablation of this

kinase in mice leads to loss of the cilia and induces cerebrosplinal ataxia in humans. In addition, cells disabled for TTBK2 are distinguished by a persistent presence of CP110 at the basal body level (Goetz, Liem and Anderson, 2012). Other studies point to the importance of phosphorylation of certain substrates and try to determine if these substrates are directly involved in the early phases of ciliogenesis.

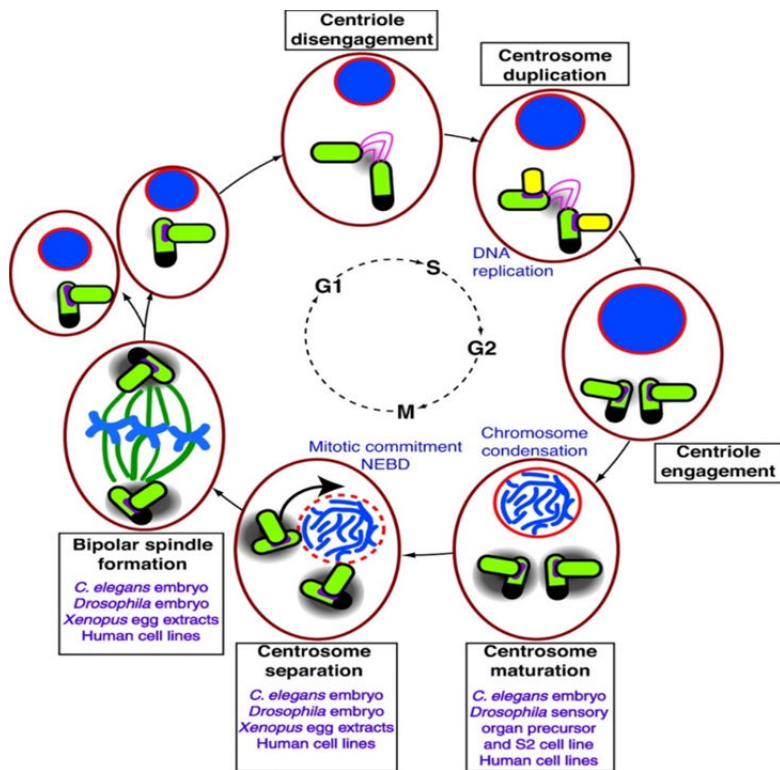


**Figure 04: The centrosome cycle**

At the beginning of G1 phase, cells contain a single centrosome with two perpendicularly aligned, closely associated centrioles. The two centrioles are not identical at this stage. The daughter centriole originates from the previous cell cycle, whereas the mother centriole (centriole with black cap) assembled at least two cell cycles ago. During G1 phase, the tight link (purple bar) between the centrioles is dissolved (centriole disengagement), but centrioles remain connected by a loose fibrous structure. Centriole disengagement is a prerequisite for centrosome duplication. In S phase, the centrosome duplicates simultaneously with EndoMT A replication. Duplication involves the assembly of two new centrioles perpendicular to the existing centrioles. Note that at this point there are three different types of centriole in the cell: two newly formed centrioles, the daughter and the mother centriole. Next, the daughter centriole finally acquires the same molecular characteristics as the mother centriole and the fibrous tether between the mother and daughter centriole is severed. Due to the tight link (purple bars) between the old centrioles and the newly formed ones, the two centrosomes are now engaged and prevented from further replication. In late G2 phase, the two centrosomes undergo maturation by recruiting additional PCM (grey circle) components to prepare for their role as spindle poles. The centrosomes then separate and move to the opposite side of the nucleus. The bipolar nature of mitosis ensures that each daughter cell inherits one centrosome.

Adapted from (Werner, Pimenta-marques and Bettencourt-dias, 2017)

Finally, the Ser / Thr kinase MARK4 promotes the assembly of the cilia (Kuhns *et al.*, 2013). The loss of MARK4 is reminiscent of the loss of TTBK2 since it disrupts the CP110-Cep97 complex in the basal body and leads to the lack of the axoneme assembly, whereas the attachment of the basal body to the ciliary vesicle is not impacted (Figure 04).

This observation suggests that MARK4 activity, such as CP110 displacement, is part of a regulatory process that occurs when the ciliary vesicle fuses with the plasma membrane before axoneme growth.

In addition to required proteins for the assembly of the axoneme, the control of ciliogenesis is also done on earlier stages such as anchoring of the basal body, or fusion of vesicles at the base of the cilia structure. For example, GTPase Rab8a GTP targeting at the distal appendage by its guanine nucleotide exchange factor (GEF) Rabin8 seems to promote anchoring and fusion of vesicles at the base of the ciliary membrane and thus promoting ciliogenesis (Nachury *et al.*, 2007). The Cdc42-Tuba GTPase-GEF pair plays also a critical role during ciliogenesis by contributing to address the exocytosis complex at the PC level (Zuo, Fogelgren and Lipschutz, 2011).

Finally, centriole anchoring to the membrane requires other centrosomal proteins such as Talpid3 (Yin *et al.*, 2009), Chibby (Love *et al.*, 2010), OFD1 (Love *et al.*, 2010), ODF2 (Tateishi *et al.*, 2013), and other proteins that are generally associated with different ciliopathies and found in the transition zone in the distal part of the basal body (Tateishi *et al.*, 2013).

At last, numerous studies point to the role of the actin cytoskeleton on the control of ciliogenesis and the size of the cilia. Indeed, in many cases, it appears that cortical actin allows ciliogenesis, whereas actin stress fibers inhibit cilia formation. The destruction of the actin filament network by cytochalasin D treatment, which preferentially destroys the stress fibers in cultured mammalian cells, elongates the cilia (Bershteyn *et al.*, 2010; Sharma *et al.*, 2011; Nechipurenko, Doroquez and Sengupta, 2013). Nevertheless, the preferential targeting of stress fibers by cytochalasin D is not yet clearly demonstrated and seems to be more specific cell (Kim *et al.*, 2012). Indeed, in primary dermal cells, the destruction of the actin network by a Cytochalasin D treatment results in elongation of the cilia and resistance to induced cilia dislocation (Bershteyn *et al.*, 2010). Finally, in endothelial cells, an increase in the level of cAMP results in activation of PKA and PKC and causes a redistribution of actin cytoskeleton as well as an increase in the size of the cilia (Abdul-Majeed, Moloney and Nauli, 2012). In all cases, a destruction of the stress fibers, or a redistribution of the actin cytoskeleton seems to stabilize the cilia and inhibit its disassembly.

### **1.3 Molecular regulation of ciliary trafficking**

Primary cilia have tightly controlled lengths, and the axoneme, which forms the core structure, has exceptionally high stability. This is despite being composed of microtubules that are often characterized as highly dynamic. In addition, a crosstalk between *Cis* and *trans* Golgi vesicles and primary cilia mediate the assembly of the ciliary structure.

#### **1.3.1 Intraflagellar transport system**

In the following chapter, I will describe the IFT proteins system, a key player protein such as IFT20, The molecular motors involved in ciliogenesis, the crosstalk between PC and cytoskeleton, the BBSome and then the ciliary pocket crosstalk with protein trafficking.

The transport of proteins at the level of the primary cilium is ensured by a specialized system called IFT (intraflagellar transport). IFT transports proteins in the form of a large complex, called cargo, whose size varies from the base of the primary cilium, along the axoneme to the summit by kinesin motors (anterograde transport), and from the top of the primary cilium at its base by dynein molecular motors (retrograde transport) (Figure 05).

Different proteins that make up each functional unit of intraflagellar transport have been identified and characterized. Most of them are conserved in ciliate organisms, but are not present in non-ciliate organisms such as plants or fungi (Avidor-reiss *et al.*, 2004). Each unit of IFT is composed of at least three sub-complexes whose composition will depend on the function: the motor proteins of the primary cilium, the proteins of complex A and complex B (Cole and Snell, 2009). The proteins forming the BBSome, which is an octameric protein complex involved in the trafficking of membrane proteins at the level of the primary cilium are also found. It moves along the axoneme with the same velocity as the units of the IFT this which leads to consider them as a subgroup of units associated with intraflagellar transport (Blacque *et al.*, 2004; Nachury *et al.*, 2007; Lechtreck *et al.*, 2009).

The IFT particles consist of two sub-complexes, each made up of several individual IFT proteins. The two complexes, known as “A” and “B”, are composed of approximately 17 proteins arranged

into these two A and B complexes. Proteins identified in complex A so far include: IFT43, IFT122A, IFT122B, IFT139, IFT140 and IFT144, while IFT20, IFT27, IFT46, IFT52, IFT57, IFT72, IFT74, IFT80, IFT81, IFT88 and IFT172 have been found in complex B (Tobin and Beales, 2009). Each functional unit of intraflagellar transport consists of an assembly of two complexes (IFT-A and IFT-B) that dissociate in the presence of strong ionic forces (Blacque and Leroux, 2006; Follit *et al.*, 2009).

The distinction between these two complexes is not only biochemical but also functional. In fact, mutations of complex A proteins produce a short, stocky cilium with bulges filled with IFT proteins whereas mutations of proteins of the B complex lead to an absence of cilium or a very short cilium (Iomini *et al.*, 2002). These phenotype differences suggest that complex A proteins work in retrograde transport and that B-complex proteins are involved in anterograde transport.

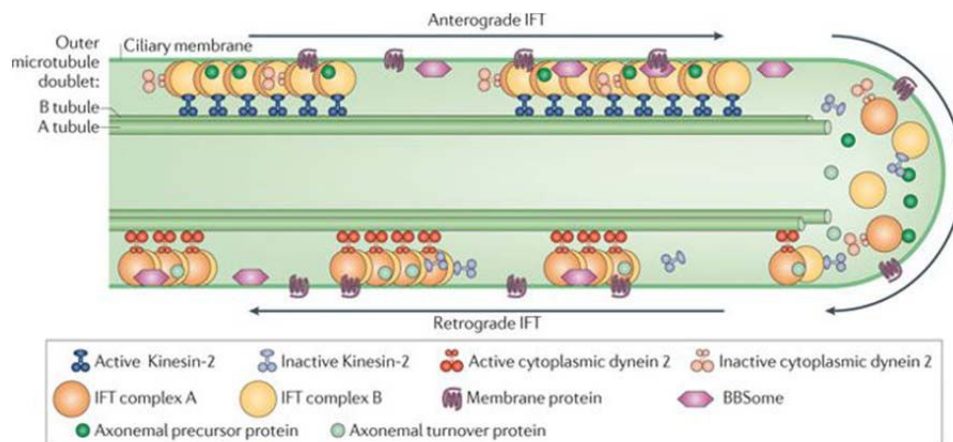


**Figure 05: Intraflagellar transport machinery.**

The canonical anterograde intraflagellar transport (IFT) motor, heterotrimeric Kinesin-2, transports IFT complexes A and B, axonemal proteins and cytoplasmic dynein 2 (previously known as cytoplasmic dynein 1b) to the tip of cilium. During this anterograde motion, Kinesin-2 is active and the retrograde motor, cytoplasmic dynein 2, is somehow kept inactive to allow smooth processive anterograde movement. At the tip of cilium, anterograde IFT trains release axonemal proteins and rearrange their conformation for retrograde IFT. Cytoplasmic dynein 2 is activated and transports retrograde IFT trains to the cell body. Subsets of IFT trains are involved in transporting membrane proteins and the BBSome (a complex comprised of at least seven Bardet–Biedl syndrome proteins). Adapted from (Ishikawa and Marshall, 2011).

The precise function of complex A and B proteins is not known, however, more and more evidence tends to show that they form an intermediate between motor proteins and cargos. IFT20 is localized at the level of the Golgi apparatus and at the level of the cilium and seems to play an important role in the addressing of proteins at the level of the primary cilium (Follit *et al.*, 2006).

The IFT172 of B complex protein is required in the transition from anterograde transport to retrograde transport at the tip of the cilium (Pedersen and Rosenbaum, 2008), (Tsao and Gorovsky, 2008).

### 1.3.1.1) IFT20: an actor of IFTB proteins

IFT20, for intraflagellar transport protein 20, is a protein encoded by the *IFT20* gene in humans, located on chromosome 17p11.1. According to the human protein Atlas (<https://www.proteinatlas.org/ENSG00000109083-IFT20/tissue>), IFT20 transcript is mostly present in human brain, lung, kidney and pancreas, and lower expression has been detected in human placenta, liver, thymus, prostate and testis. IFT20 subunit of the complex IFTB is localized at the Golgi apparatus in addition to the PC basal body and axoneme, along with other IFT proteins and complexes. In living cells, fluorescently tagged IFT20 was shown to move between the Golgi apparatus and the PC as well as along ciliary microtubules, inside axonemal lumen ((Follit *et al.*, 2006)). This perpetual IFT20 protein commuting between Golgi and PC seems to be crucial for ciliogenesis and PC dependent signalizations, (Keady *et al.*, 2013). However, several studies, using ciliary proteins depletion *via* RNA interference approaches in cell culture or *in vivo* models, suggest that some observed defects may have an extra-ciliary origin. These defects include: 1) alterations of Golgi vesicular transport, independently of the formation of the PC (Jurczyk *et al.*, 2004; Kim *et al.*, 2004), 2) deregulation of the cell cycle (Bull, 2008), 3) anomalies of cell division and spindle orientation (Patel *et al.*, 2008; Luyten *et al.*, 2010), 4) chromosomes alignment and segregation defects (Abou Alaiwi *et al.*, 2014), 5) defects in the number of centrosomes (Burtey *et al.*, 2008), 6) defects in cytokinesis (Wood *et al.*, 2012). Altogether, these studies suggest that protein such as IFT20, mostly characterized for its pivotal role in ciliary related processes can bear extra-ciliary functions, notably in membrane trafficking and cell division.

Among these PC unrelated IFT20 associated functions, we can mention its role in the specific transport of certain ciliary proteins in compartments other than the PC itself, such as transport of centrosomal proteins to the basal body (Jurczyk *et al.*, 2004). Interestingly, IFT20 has been also reported to be associated with transport of vesicles in non-ciliated compartments of ciliated cells, such as premature photoreceptor outer segment; indeed, Sedmak and collaborators (Sedmak and

Wolfrum, 2010) speculate that IFT20 may play a role in the delivery of vesicles to differentiating membrane discs in the premature photoreceptor outer segment. This suggests that the vesicular transport functions of IFT20 may not be limited to ciliated cells only. A strictly extra-ciliary role has even been proposed for IFT20 protein, since it is involved in the polarized traffic during immune synapse assembly as it is required for the delivery of the intracellular pool of LAT (linker for activation of T cells) to the immune synapse in naïve primary T lymphocytes and for effective T-cell responses *in vivo* (Vivar *et al.*, 2016). Alongside, IFT20 acts as unconventional regulator in immune system assembly by selectively controlling the recycling TCRs (T-cells receptor) polarized trafficking in T cells, which are naturally non-ciliated cells.

### **1.3.1.2) The molecular motors involved in ciliogenesis**

The molecular motor involved in the PC transport is kinesin-II, a heterotrimeric complex that belongs to the kinesin-2 family (Miki, Okada and Hirokawa, 2005). Kinesin II consists of an assembly of two motor subunits, KIF3A and KIF3B, and a non-motor subunit KAP3 (Cole *et al.*, 1992). Inactivation of kinesin-II inhibits cilia assembly and intraflagellar transport in different species such as *Chlamydomonas*, *Drosophila* and mice (Kozminski, Beech and Rosenbaum, 1995; Nonaka *et al.*, 1998; Marszalek *et al.*, 1999). The motor protein complex responsible for retrograde transport is cytoplasmic dynein-2. Dynein 2 is composed of a homodimeric heavy chain, DYNC2-H1, an intermediate light chain, DYNC2LI1, two intermediate chains WDR34 and WDR60 (Taylor *et al.*, 2015). Mutants for the different components of dynein 2 in *Chlamydomonas*, *C. elegans* and the mouse show reduced size cilium with saturated intraflagellar transport (Hou *et al.*, 2004).

### **1.3.1.3) The regulation of intraflagellar transport**

As we have seen with the PC associated diffusion barrier, the PC is an isolated compartment from the rest of the cell. Protein synthesis is carried out in the cytoplasm of the cell but does not take place in the PC. There is thus an active transport mechanism called the intraflagellar transport (IFT) that is required for the training and maintenance of the PC. Ciliary

protein transport is a bi-directional transport that is visualized in the form of IFT trains that come and go along the axoneme visualized in contrast microscopy interference. There is anterograde and retrograde transport that allows the transportation of cytoplasmic proteins in the PC (Fort and Bastin 2014). The many proteins of IFTs have been classified into two complexes, IFT-A and IFT-B (as detailed previously) (For review on components Taschner, Bhogaraju, and Lorentzen 2012). The proteins of IFTB are rather involved in anterograde transport and defects in these transport proteins anterograde lead to a reduction in the size of the PC (Absalon et al. Chia and Gorovsky Martin A 2008). Mutations affecting the proteins of IFTA are characterized by reduced activity of retrograde transport and an accumulation of IFTB proteins at the end of the primary cilium (Absalon et al., 2008). Kinesin-2 is the driving force behind anterograde transport while dyneins are necessary for the retrograde transport.

Intraflagellar transport has a role in the delivery of the various ciliary components, from the base of the PC at its end, which are grouped under the term "cargoes" as the components of the axoneme, the ciliary membrane or the proteins involved in signaling pathways. More specifically, the IFT process can be divided into several distinct phases. First, IFT particles and axonemal precursors are recruited at the base of the PC. Then the assembly of the IFT particles and the loading of the axonemal precursors takes place at the level of the transition fibers. The organization of the proteins is then modified at the distal end. Dynein and the IFT-A complex is needed for protein recycling and retrograde transport (Fort and Bastin 2014). Two structurally different types of IFT trains have been observed in *Chlamydomonas*, "long" and "short". Long IFT trains are more abundant at the beginning of the lengthening of the PC while the short IFT trains increase the longer the primary cilium lengthens (Pigino et al. 2009). Each train has a specific ultrastructure that is closely related to their function during the genesis of a PC. It has been shown that long trains predominate at the beginning of the growth of PC while the shorts are rather present for the maintenance of PC, once it has reached the right length (Vannuccini et al., 2016). IFT also plays a role in the control of PC length (Fort and Bastin 2014). It has been recently discovered that there is specific intraflagellar transport lipids which consists of driving some proteins in the PC that are not soluble as NPHP3 or INPP5E. This transport was called LIFT (lipidated protein intraflagellar targeting) and would deliver the proteins to the ciliary membrane through UNC119B or PDE6D, but would also be in functional interaction with IFT (Jensen and Leroux 2017).

### **1.3.2 Molecular regulation of trafficking toward the cilium**

The biogenesis of cilia requires both the assembly of a microtubule based core structure (the axoneme), and the establishment/maintenance of the ciliary membrane. Emerging evidence suggests that specialized and dedicated vesicular trafficking is critical for the formation and maintenance of the cilium structure and the ciliary membrane, whose composition is distinct from that of the surrounding plasma membrane.

In the following chapter, I will describe the polarized vesicular trafficking to the PC with a focus on the small Rab GTPases, the ARL proteins, the exocyst and the microtubules.

#### **1.3.2.1) Polarized vesicular trafficking to the primary cilium**

The polarized vesicular trafficking is a specialized and vectored cellular transport mechanism important for delivering of proteins and membranes to their specific compartments. Cell functions could be significantly disturbed when this process is perturbed ((Cohen, Valm and Lippincott-Schwartz, 2018)).

Polarized vesicle trafficking is mediated by some Rabs proteins along with Arf/Arl (members of the Ras superfamily of small GTPases) which assist in the recruitment of vesicle coating complexes during vesicle budding, docking and fusion of vesicles ((Stenmark, 2009)).

#### **1.3.2.2) Arl proteins in ciliary trafficking**

Arl6 is exclusively expressed in ciliated organisms (Avidor-reiss *et al.*, 2004)) and its human ortholog ARL6, encoded by BBS3, was the first identified small GTPase protein that was linked to the human ciliopathy Bardet-Biedl syndrome (BBS). The abnormalities associated with the loss of BBS3 in BBS are thought to arise due to dysfunctional primary cilia (Wiens *et al.*, 2010). Arl6 is localized at the distal end of the basal body, near or at the TFs, a region of the ciliary compartment that controls the entry of proteins into the primary cilium. Arl6 functions as a recruiter of the BBSome to the basal body and as a regulator of the function of the BBSome in

ciliary protein trafficking. ARL13B is another small GTPase protein connected to the human ciliopathy, Joubert syndrome, an inherited neurodevelopmental disorder with midbrain-hindbrain malformations, retinal dystrophy.

### **1.3.2.3) Rab small GTPases and the exocyst**

The distribution of several Rab GTPases at the primary cilium was only recently discovered. Disruption of the ciliary localization or the activities of these Rab GTPases are associated with several ciliopathies due to impairments in cilium formation and function. For example, Rab8 is a critical modulator for the formation and the function of primary cilia in addition to having an important role in vesicular trafficking between the trans-Golgi and the basolateral membrane ((Leroux, 2007).

The exocyst is a conserved octameric protein complex consisting of Sec3, Sec5, Sec6, Sec8, Sec10, Sec15, Exo70, and Exo84, and it is involved in basolateral protein sorting and membrane trafficking (Kang and Fölsch, 2009). The distribution of exocyst proteins in cells is observed in cell-cell junctions, but also at the primary cilium in polarized cells. Compromising the function of exocyst by knockdown of Sec10 results in the formation of shortened primary cilia, along with reduced levels of Sec8, Exo70, and Ift88 ((Zuo, Fogelgren and Lipschutz, 2011)). This suggests a central role for Sec10 in stabilizing the exocyst complex and possibly a role of Sec10 in trafficking Ift88 to the primary cilium.

### **1.3.2.4) Microtubules**

EB1 and EB3 are microtubule plus end tracking proteins that localize to the base of the PC in human fibroblasts and RPE cells. Both proteins are important for cilia formation, likely through a role in microtubule minus end-basal body anchoring activity, since the microtubule array anchored at the basal body is disorganized in EB1 and EB3 knockdown cells having aberrant vesicle accumulation and impaired ciliogenesis. These results demonstrate the relevance of microtubules in anchoring to the basal body thereby providing a 'roadmap' for the targeting of

vesicles carrying ciliary proteins to the vicinity of the basal body where they are exocytosed (Schröder *et al.*, 2011).

### **1.3.3) The phosphoinositides turnover: linking PC and endomembranes trafficking**

The maintenance and the turnover of the phosphoinositides lipid family is crucial for endomembranes identity and functions (Di Paolo and De Camilli, 2006; De Craene *et al.*, 2017) (Figure 06). This is particularly true for PI3,4,5P3 and Pi4,5P2 which are mostly localized at plasma membrane and engaged in many cell surface biological processes such as signaling regulation and actin-based internalization. Interestingly, PI3P has been shown to be essential for both endosomal membrane regulation (Schink, Tan and Stenmark, 2016), but also for autophagy initiation (see “autophagy regulation” chapter) in which PI3P orchestrates the membrane recruitment of early stage autophagosome biogenesis regulators such as WIPI2, and consequently ATG16L1-ATG5-ATG12, to promote LC3 lipidation (Nascimbeni, Codogno and Morel, 2017) and promotes a space and time local membrane identity for autophagosomal membranes. The turnover of phosphoinositides, and in particular of PI3P, is mostly based on the mobilization of enzymes responsible for modulating their phosphate content. This is notably well illustrated by the multiple steps and interconnected regulation of PI3P metabolism. Indeed, the PI3P synthesis is ensured by two majors lipid kinases: PI3KCIII, also known as VPS34 (see autophagy chapter) and PI3KC2alpha, the latter being directly associated with PC regulation, via the Rab11 GTPase local recruitment to PI3P positive membranes at the base of the PC (Franco *et al.*, 2014). Finally, PI3P could be metabolize by myotubularins phosphatases (which lead to PI synthesis) or by PIKfyve kinase (to promote PI3,5P2) (Figure 06) (Nascimbeni, Codogno and Morel, 2017), a phenomenon which is particularly important for endosomal PI3P content regulation in time.

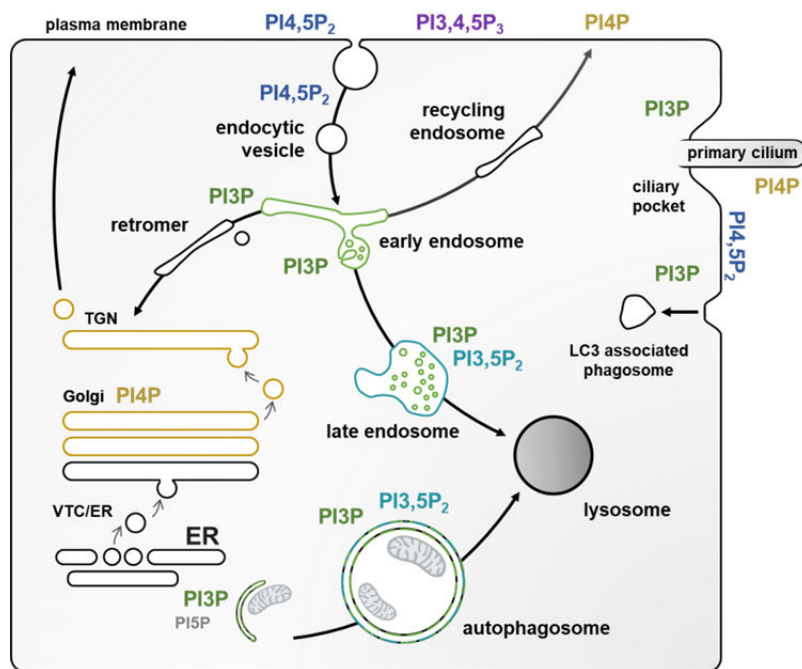


**Figure 06: phosphoinositides and endomembranes**

The main phosphoinositides subcellular distributions are shown. (VTC: vesiculo-tubular-clusters, ER: Endoplasmic Reticulum, TGN: Trans Golgi Network)

Importantly, it was recently proposed that the turnover between PI4,5P<sub>2</sub> and PI4P is crucial for PC functions (Phua, Nihongaki and Inoue, 2018). Indeed the inhibition of PI4,5P<sub>2</sub> synthesis in the PC, and the local delivery of PI4P (which is also found at Golgi level), favors the proper identity of PC, as an extension of the plasma membrane but with specialized properties and functions. It is now proposed that this ciliary segregation is notably ensured by a local metabolism of PI4,5P<sub>2</sub> which is processed by the 5-phosphatase INPP5E to produce PI4P (Chávez *et al.*, 2015; Garcia-Gonzalo *et al.*, 2015). Importantly, INPP5E appears to be essential for PI4P maintenance at PC, and is associated with the Joubert syndrome, related ciliopathy (Xu *et al.*, 2016, 2017, 2019). The PI4,5P<sub>2</sub> exclusion is then probably seen as a plasma membrane exclusion signal by the cell, and thus favors the local inhibition of biological membrane processes normally associated with plasma membrane via PI4,4P<sub>2</sub>, including internalization and actin based remodeling (Nakatsu, 2015).

## **1.4 The primary cilium functions: a biological stress sensor**

Primary cilium is a real sensory antenna with different receptors of signaling pathways that participates directly or indirectly in many cell processes. In the following chapter, I will describe some ciliary pathway in response to nutritional stress and others in response to biomechanical stress.

### **1.4.1 Ciliary signaling in response to nutritional stress**

#### **1.4.1.1 Shh signaling pathway (Sonic hedgehog)**

The Hh-dependent signaling pathway (Hedgehog) is involved in the regulation of cell proliferation, differentiation, epithelial-mesenchymal transition (EMT) and maintenance of cellular homeostasis in adulthood (Briscoe and Théron, 2013). There are 3 secreted ligands of Hh: Shh (Sonic hedgehog), Ihh (Indian Hedgehog), and Dhh62 (Desert Hedgehog). Although Shh seems to be the most widely expressed morphogen, each of its proteins has tissue-specificities (Briscoe and Théron, 2013). The Hh signaling depends on a balance between two states Gli (Glioma associated oncogene family) transcription factors that can oscillate between activating or repressor states of the transcription depending on the presence or absence of Hh and its binding on Ptch1 (Patched -1, Hh receptor with 12 transmembrane segments).

In the absence of Hh ligand, the Ptch1 receptor is in an inactive state and localized at the base of the primary cilium and represses the Smo (Smoothed) receptor activity (receptor with seven transmembrane domains) via an unknown mechanism to date. In this case, the SuFu (Suppressor of Fused) protein is active, initiates the partial degradation of Gli2 / 3 via the ubiquitin-proteasome pathway, and the short form of Gli2 / 3-R then functions as a transcription repressor target genes of the Hh pathway. On the other hand, in the presence of the ligand Hh, activated Ptch1 induces an inhibition rise on Smo, which is translocated towards the primary cilia. Smo inhibits SuFu allowing the translocation of Gli2 / 3 from the cilia to the cytoplasm. Gli2 / 3 then play their role as a transcription factor and activate target genes such as cyclin and myc leading to cell proliferation or the bcl-2 gene that regulates cell death and again the bmi-1 gene that regulates cell renewal (Rohatgi, Milenkovic and Scott, 2007; Wong and Reiter, 2009) (Figure 07).

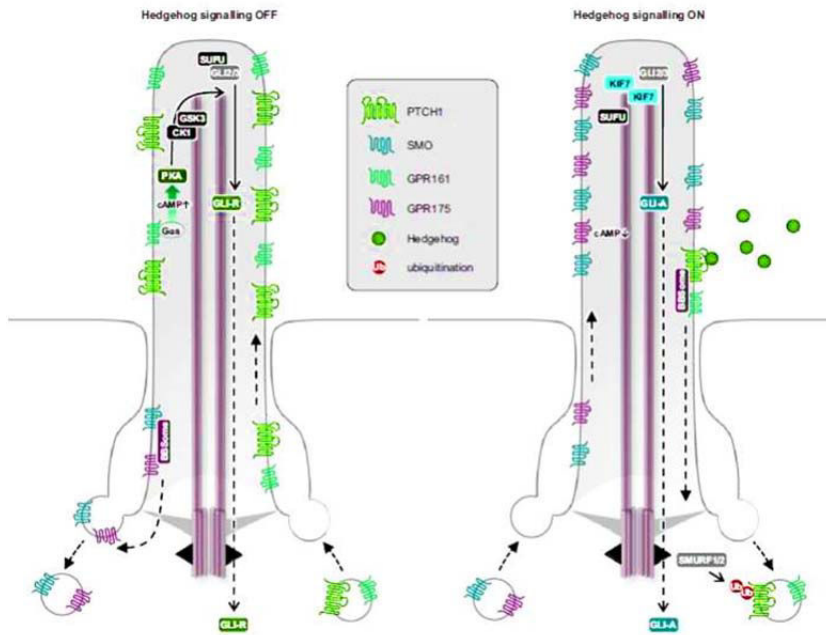


**Figure 07. Shh signaling pathway (SMO localisations)**

In the absence of Sonic Shh ligand so when the pathway is turned off, SMO is out of cilia and Patch1 is localized at axoneme. When Shh ligand is present, it binds to Patch, by the way Patch1 exit the cilium and SMO is recruited to the axoneme.

Adapted from (Pedersen, Mogensen and Christensen, 2016)

#### 1.4.1.1.1) The Hedgehog signaling pathway in cilia

The importance of the cilia during vertebrate development was observed in genetic experiments that showed the importance of the cilia in survival and in the arrangement of embryonic motifs in mice (Huangfu et al., 2003). The genetic and biochemical analyzes of these embryos made it possible to demonstrate that these phenotypes were generated by disturbances of the Hedgehog signal transduction. These observations have raised many questions, such as the reasons for its location in the cilia, or why the cilia is required for vertebrate hedgehog signaling, but not for invertebrate signaling.

#### 1.4.1.1.2) The Hedgehog signaling pathway is dependent on intraflagellar transport

Hedgehog signaling pathway strongly depends on the primary cilia. These phenotypes have significant developmental defects, including loss of ventral cells of the neural tube, as well as organogenesis problems (Huangfu et al., 2003). The genes affected in these mutants encode

several components of intraflagellar transport, including B complex proteins, IFT172, IFT88 and DYNC2H1, a subunit of the dynein responsible for the retrograde transport (Huangfu *et al.*, 2003; Huangfu and Anderson, 2005). Disturbance of kinesin-2 in Kif3a embryos leads to similar defects in neural tube development depending on the pathway Hedgehog. Genetic studies have determined that IFT proteins act at the heart of Hedgehog signaling, downstream of transmembrane patched 1 (PTCH1) and smoothed (SMO) receptors, and upstream of Gli transcription factors (Huangfu *et al.*, 2003; Huangfu and Anderson, 2005).

The role of IFT proteins in Hedgehog signaling is complex. In the absence of hedgehog ligands, the Gli transcript factors, by a proteolytic method, are converted into their repressive form (GliRs) which makes it possible to keep the target genes of the hedgehog pathway inactive. In response to hedgehog ligands, this conversion process is blocked allowing the activation of Glis transcription factors (GliA) and hedgehog target genes. Intraflagellar transport is required for the production of GliAs and GliRs (Huangfu and Anderson, 2005; Liu, Wang and Niswander, 2005), with the result that IFT mutants show a loss of hedgehog phenotypes in some cell types, and a gain in others. For example, GliAs have a central role in development, and IFT mutants show a loss of Hedgehog signaling in the neural tube. In contrast, GliRs play a central role in limb development, and IFT mutants that survive to late stages of embryogenesis exhibit preaxial polydactyly, characteristic of GliR loss (Huangfu and Anderson, 2005; Bangs and Anderson, 2017).

Recent studies have highlighted the importance of intraflagellar transport in hedgehog signaling in zebrafish. Mutations for IFT88 in this organism result in disturbances of Hedgehog signaling in the neural tube and somites (Huang and Schier, 2009). However, the problems of arrangement of embryonic patterns caused by the loss of IFT88 in zebrafish are somewhat different from those observed in mammals. The mutated IFT88 mice lose Sonic Hedgehog-dependent neural tube cells (Huangfu *et al.*, 2003) and the IFT88<sup>-/-</sup> zebrafish lose some cells such as V3 interneuronal progenitors and pioneering muscle cells, which require the highest level of activation of the Hedgehog pathway. However, neural tube cell types and somites defined by weak activation of the hedgehog pathway have expanded (Huang and Schier, 2009). These contrasts may be due to a different balance between GliAs and GliRs between zebrafish and mice (Huang and Schier, 2009).

#### **1.4.1.1.3) The importance of basal body proteins in Hedgehog signaling**

Intraflagellar transport proteins are not the only ones that are important for the Hedgehog pathway. Recent studies have highlighted the role of proteins associated with the basal body. As we have seen, some of them are involved in ciliogenesis. In all the cases analyzed so far, these proteins seem to be required for Hedgehog signaling. For example, the mutation of *talpid3* was first known to generate polydactyly and developmental problems consistent with Hedgehog pathway disruption (Rohatgi *et al.*, 2009). The *talpid3*<sup>-/-</sup> mouse embryos show an inability to form a cilia, and it has been observed that the affected gene encodes a centrosomal protein (Yin *et al.*, 2009).

Mutations affecting other basal body proteins such as OFD1, ghost (FTM, also known as RPGRIP1L), MKS1 (meckel syndrome type1 and ECV (Ellis-van Creveld syndrome protein) are responsible for ciliopathy in humans and affect the Hedgehog signaling in mammals. The mutant mice for OFD1, MKS1 or FTM, have an abnormal or absent cilia and mount disturbances of Hedgehog signaling proportional to the severity of the disturbances of the cilia (Delous *et al.*, 2007; Weatherbee, Niswander and Anderson, 2009). EVC is a protein located in the basal body that is responsible for a skeletal pathology: Ellis-van Creveld syndrome (Ruiz-Perez *et al.*, 2003). In contrast to other basal body proteins, the expression of EVC in mice is limited to the development of bone structures, and it does not seem important for the formation of the cilia of chondrocytes. Nevertheless, *EVC*<sup>-/-</sup> mice show a reduction in Indian Hedgehog signaling (IHH) specifically within skeletal structures. That's why EVC does not seem to affect ciliogenesis but is important in Hedgehog signaling of specific cell types.

#### **1.4.1.1.4) The ciliary localization of the actors of the Hedgehog signaling pathway**

Interestingly, all the key players in the Hedgehog signaling pathway are enriched in the primary cilium. Notably, the two transmembrane proteins PTCH1 (the hedgehog receptor) and SMO (which acts downstream of PTCH1) are dynamically displaced at the level of the cilium after

activation of the Hedgehog pathway (Corbit *et al.*, 2005). In the absence of stimulation PTCH1 is present at the base of the cilia and SMO is not associated with the cilium. Upon activation of the PTCH1 pathway is excluded from the ciliary space, and SMO moves to the level of the cilia (Corbit *et al.*, 2005; Rohatgi, Milenkovic and Scott, 2007). Accordingly, the constitutively active forms of SMO lead to its permanent location in the cilia (Corbit *et al.*, 2005). Despite enrichment of ciliated SMO in response to Hedgehog ligands, in the absence of SMO ligands also accumulates in cells invalidated for the retrograde transport dynein (Ocbina, Tuson and Anderson, 2009), suggesting that SMO is constitutively addressed to the cilia and that activation of the hedgehog pathway increases the accumulation of SMO in the cilia.

Gli transcription factors are also enriched in the cilia. Indeed, Gli2, whose primary function is to be a transcriptional activator of mammalian Hedgehog signaling, and GLi3, which can be converted into a transcriptional repressor, are located at the top of the cilia (Haycraft *et al.*, 2005). Recent studies show an enrichment of these two factors at the top of the fibroblast cilia following activation of the Hedgehog pathway (Endoh-Yamagami *et al.*, 2009). In addition, ciliary enrichment of Gli2 at the top of the cilia depends on the activation of SMO (Kim, Kato and Beachy, 2009). Like SMO, Gli2 accumulates strongly at the level of the cilia in cells invalidated for Dync2h1 (Kim, Kato and Beachy, 2009), which demonstrates the constant trafficking of Gli2 within the cilia.

SUFU, an important mammalian Hedgehog repressor, is also found at the apex of the PC (Haycraft *et al.*, 2005; Endoh-Yamagami *et al.*, 2009). SUFU has the ability to inhibit Hedgehog, despite the absence of cilia. However, a partial deletion of SUFU generates activation of the pathway only in cells with a functional PC (Ocbina, Tuson and Anderson, 2009), highlighting the complex role of SUFU in the cilia. Although the relationship between SUFU and the eyelid remains to be defined, the data are in agreement with the model in which SMO activates Hedgehog at the top of the cilia by inhibiting SUFU activity, which leads to the activation of Gli transcription factors.

Mice strains invalidated for intraflagellar transport B-complex proteins lose cilia and all responses to Hedgehog ligands (Huangfu *et al.*, 2003; Wong and Reiter, 2009). On the contrary, the mutations of complex A proteins allow the formation of the cilium (with abnormal morphology),

give rise to very different developmental phenotypes of mice incapable of forming an cilia, which seem to be caused by activation of the hedgehog pathway rather than by his loss. The mutated mice for the two complex A proteins, IFT139 and IFT122, show an expansion of neural-type cells dependent on Hedgehog signaling, and an increase in the expression of its target genes (Huangfu *et al.*, 2003; Huang and Schier, 2009). The opposite phenotypes of knockout mice for complex A and B complex proteins are of interest. Indeed, both DYNC2H1 and complex A proteins are important for retrograde transport, but loss of complex A proteins results in increased Hedgehog signaling (Goetz and Anderson, 2010; Larkins *et al.*, 2011), whereas DYNC2H1 mutations block response to Hedgehog ligands (Huangfu and Anderson, 2005). These results suggest that the loss of complex A proteins could disrupt the ciliary traffic of Hedgehog pathway components in different ways, thereby explaining this diversity of phenotypes. Finally, as we have seen above, Smo is able to move laterally from the plasma membrane to the ciliary membrane (Milenkovic, Scott and Rohatgi, 2009), which is why it would be particularly interesting to study the Smo displacement in invalidated models for complex A proteins.

#### **1.4.2) Signaling pathways in response to biomechanical stress**

Various biomechanical forces (including arterial or osmotic pressure, tensile force, stretching force or shear force) can be integrated by the cell through different types of mechanoreceptors such as adherent junctions, desmosomes, integrins, several types of membrane receptors, actin microtubules and PC. These biomechanical signals are converted into a chemical signal via activation of different signaling pathways that may involve cytosolic proteins, calcium, and/or transcription factors. The PC proves to be a powerful mechanosensor. Many proteins such as PC1 (Polycystine 1), PC2 (Polycystine 2), TRPV4 (Transient receptor potential vanilloid 4), AC6 (Adenylyl cyclase 6), or Piezo 1 are considered to be major players in mechano-transduction at the primary cilia level (Gradilone *et al.*, 2007; Kwon *et al.*, 2010; Lee *et al.*, 2015). In this section, I will essentially describe its role in the amplification and transduction of signals induced by shear forces, namely calcium-dependent signaling pathways and autophagic pathways.

The role of polycystins PC1 and PC2 has been studied in the PC in the integration of biomechanical signals driven by shear forces. I will mainly detail the transduction mechanisms of the signals transmitted by these two proteins in response to shear forces. PC1 / PC2 polycystins are encoded by two different Pkd1 / Pkd2 genes and are widely expressed in human tissues, including kidneys, blood vessels, heart, liver, pancreas, bone, and brain. These proteins are more particularly localized at the level of the primary cilia, but are also found at the level of the plasma membrane and the endoplasmic reticulum (Retailleau and Duprat, 2014). PC1 (460 kDa) is a protein of 11 transmembrane domains with an intracellular C-terminal portion (200 aa) and a N-terminal portion extracellular (3000 aa). It is composed of the following domains: a GPCR domain, two leucine-rich domains, sixteen Ig-like domains and a C-lectin domain. The C-terminal Region contains a Coiled Coil Domain (CC) and a G protein binding site.

PC1 located at the primary cilia interacts with PC2. PC2 (or TRPP2 Transient receptor potential 2, 110 kDa) is composed of six transmembrane segments, an intracellular N-terminal part, an intracellular C-terminal part with a calcium binding domain, a retention domain to Endoplasmic reticulum and a CC domain. PC1 and PC2 can interact via their CC domains located in their cytoplasmic C-terminus to form a ion channel complex (Qian *et al.*, 2002). An activation model of these channels has been proposed to allow the activation of calcium signaling pathways in response to shear forces. Following the flexion of the primary cilia under the influence of shear forces, PC1 via its extracellular domain is suggested to act as a mechanosensor by detecting these forces, its activation leads to the opening of the PC2 channel allowing the entry of calcium into the cilioplasm (cilioplasm being a cellular compartment for calcium signaling). This calcium influx spreads to the level of the cytoplasm and triggers the release of intracellular calcium via the ryanodine or inositol 1,4,5-trisphosphate (IP3) receptors located at the ER, which in turn is supposed to amplify the calcium signal (Nauli *et al.*, 2003; Cheng *et al.*, 2014), although the precise role of PC2 as calcium transporter in the PC is still under debate (Delling *et al.*, 2016). Thus, this calcium signaling pathway in response to shear forces could be important since its disruption can lead to a major defect in tissue function such as the appearance of polycystic kidney disease. This phenotype is notably observed in the Autosomal Dominant Polycystic Kidney Disease (ADPKD) syndrome. a ciliopathy caused by Pkd1 and Pkd2 mutations (Nauli *et al.*, 2003).

## 1.5 The ciliopathies

The PC thus plays many important roles during development in mammals. All malfunctions associated with the PC, in the assembly of the constituents and in their functions, lead to genetic diseases in humans that are grouped together under the term ciliopathies (Marko, 2015). In this chapter, a brief definition of the different types of ciliopathies is described but their implications for humans will not be detailed in this manuscript.

"Ciliopathies" are complex diseases that can sometimes be multi-systemic with involvement of all organs that have ciliated cells such as the kidney, the brain, eyes, airways (Figure 08) (Goetz and Anderson, 2010). They are rare human genetic diseases caused by a defect in the structure of the cilia (motile / primary) or centrosome or a defect of function of this organelle Figure 08.

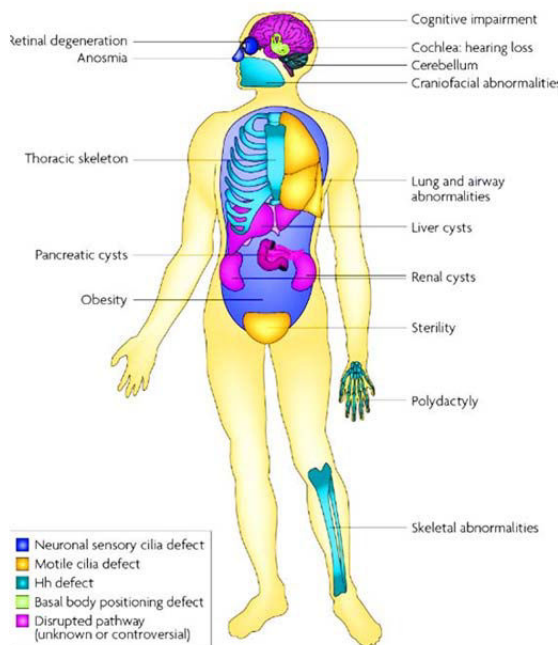


**FIGURE 08: Dysfunctions in motile and/or non-motile cilia cause ciliopathies that encompass most human organ systems**

The figure shows the different organ systems or tissues that are affected in diverse ciliopathies, and the principle phenotypic manifestations of the disease in each organ. Ciliopathies that are caused primarily by defects in motile cilia and others that result from defects in non-motile (primary) cilia.

Adapted from (Goetz and Anderson, 2010)

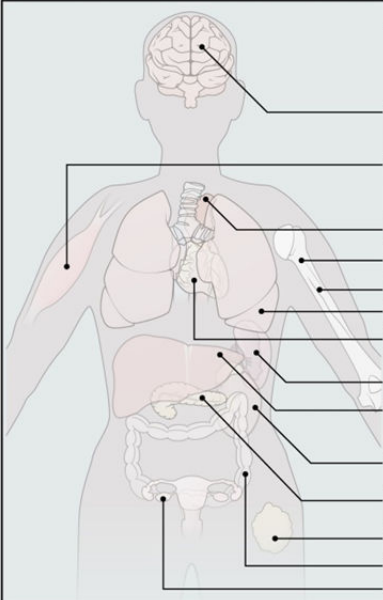
Since the majority of cells in the body carry PC, ciliopathies show a wide spectrum of abnormalities observed in multiple organs of the human body that can be redundant between the syndromes considered. Nevertheless, recurring clinical signs are mostly observed and are considered a signature ciliopathies such as cysts in the kidney, brain malformations, retinal

dystrophy. There are other "secondary" signs that can be observed such as skeletal abnormalities, *situs-inversus*, fertility abnormalities, fibrosis of the liver, obesity or diabetes (Baker and Beales, 2009; Monis, Faundez and Pazour, 2017). Currently, 35 different ciliopathies have been referenced involving directly 187 genes. This list could increase since 241 genes associated with the expression of ciliary proteins participating in the structure or function of the cilia could help identify new ciliopathies or improve understanding of a phenotype of a known ciliopathy if they were deficient or mutated in humans (Reiter and Leroux, 2017). Among the most frequent ciliopathies specifically characterized by a primary cilia defect several dominant syndromes can be described, such as: ADPKD (Autosomal Dominant Polycystic Kidney Disease) or Von Hippel-Lindeau Disease and recessive syndromes such as: ARPKD (Autosomal Recessive Polycystic Kidney Disease), Joubert Syndrome, Bardet-Biedl, Meckel-Grüber, Young, Orophacia-digital or Nephronophthisis (Konno, Setou and Ikegami, 2012).

Ciliopathies are thus very variable groups of diseases, genes can be involved in different syndromes: different mutations in the same gene lead to various clinical manifestations. This reveals the molecular complexity and the diversity of ciliary components between organs (Kim *et al.*, 2010). This is the case, for example, of CEP290 which is a transitional zone protein that is implicated in Meckel's lethal disease Gruber (MKS) or nephronophthisis (NPHP) (Kobayashi *et al.*, 2014).

## 2. The autophagic pathway and machinery

The maintenance of cellular homeostasis depends on a finely regulated balance between biosynthesis and catabolism of macromolecules and cellular components, such as defective organelles. In order to maintain this homeostatic balance, the cell has two degradation processes depending on the characteristics of cellular elements to degrade. The majority of proteins whose half-life is short, are degraded specifically by the proteasome, after being ubiquitinated. Proteins with a longer half-life are degraded by the lysosomal. The mechanism for degrading cytoplasmic or cellular components via the lysosomal pathway is called autophagy. The term autophagy comes from the Greek word "auto", meaning "self", and "phago" meaning "to eat". In summary, autophagy is a process that involves self-digestion of cellular components in response to environmental stress such as amino acid deprivation, endoplasmic reticulum stress, or certain viral and bacterial infections. Whatever the conditions under which autophagy is induced, it allows both the recycling of the elements of the cytoplasm (long half-life proteins, with conformational abnormalities or insoluble aggregates) and injured organelles. This process contributes directly to the maintenance of cellular homeostasis, thus protecting cells from various environmental stresses through energy production and components turnover regulation. Naturally, autophagy deficiency is often associated with many conditions such as neurodegenerative diseases, age-related diseases and cancer (Figure 09).



Organ	Roles of Autophagy	Diseases
General function	Starvation-induced amino acid production; constitutive turnover of cytoplasmic contents; selective degradation of p62, damaged mitochondria, microbes, etc.; life-span extension/antiaging	Tumor suppression and progression
Brain	Prevention of aggregate formation; Parkinson-dependent mitophagy; regulation of food intake and energy balance	Parkinson disease Alzheimer disease
Muscle	Maintenance of muscle mass	Myopathies : (Danon disease, XMEA, Bethlem myopathies, UCMD) Lysosomal storage diseases
Thymus	Negative selection	
Bone marrow / Hematopoiesis	Erythropoiesis; maintenance of hematopoietic stem cell	
Bone		Paget disease?
Lung	Regulation of airway responsiveness	Cystic fibrosis
Heart	Adaptation to hemodynamic stress; prevention of age-dependent dysfunction	Cardiac hypertrophy
Immune/ lymphoid system	Regulation of cytokine production; development of T cells and B cells	Infection
Liver	Prevention of hepatocellular degeneration; suppression of hepatic tumors; lipid droplet elimination; gluconeogenesis	$\alpha_1$ -antitrypsin deficiency Hepatocellular carcinoma?
Kidney	Maintenance of podocyte and tubular cell integrity	
Pancreas	$\beta$ -cell adaptation to high-fat diet; prevention of trypsin autoactivation	Diabetes Acute pancreatitis
Adipose tissue	Adipogenesis	Obesity
Intestine	Maintenance of Paneth cell function	Crohn disease
Embryos	Preimplantation development	

**Figure 09:**

**Human diseases associated with autophagy defects.**

Adapted from (Mizushima and Komatsu, 2011)

## **2.1 The different forms of Autophagy**

According to the mechanism by which the cytoplasmic material is brought to the lysosome to be there degraded, it has been characterized 3 forms of autophagy (Codogno, Mehrpour and Proikas-Cezanne, 2011; Boya, Reggiori and Codogno, 2013; Fenouille *et al.*, 2017) (Figure 10).

### **2.1.1 Macroautophagy or Autophagy**

Macroautophagy (Figure 10), more commonly known as autophagy, is a major process responsible for cellular catabolism. This conserved process is characterized by the cytoplasmic formation of a double membrane organelle called autophagosome that will later fuse with lysosome to form an autolysosome. Lysosomal hydrolases, mainly cathepsins, will degrade sequestered proteins and protein aggregates, while other lysosomal hydrolases are involved in the degradation of sugars and complex lipids. The products of this hydrolysis will be transported to the cytoplasm where they will be reused. In yeast, the phagophore membrane is derived from a membrane whose composition is close to that of the vacuole and is called PAS for Pre-Autophagosomal Structure (Suzuki and Ohsumi, 2007). In mammals, the origin of the membrane of the phagophore is not yet clearly determined (Molino, Zemirli, *et al.*, 2017). Many studies have suggested that this membrane is derived from the Endoplasmic Reticulum but it is also suggested that plasma membrane, Golgi and endosomes contribute to autophagosome biogenesis. In addition to its non-selective appearance, this autophagy can also be specific to the degradation of specific organelles. Indeed, autophagy has long been considered a non-selective process for degrading long-lived proteins or cytoplasmic components. Since then, many types of selective autophagy have been discovered. Depending on the type of stress induced, autophagosomes can specifically sequester and degrade mitochondria, ER or insoluble protein aggregates (Klionsky, 2007)). Finally, the elimination of microorganisms (bacteria or parasites) present in the cell is called xenophagy which plays a vital role in the response and maintenance of cellular immunity.

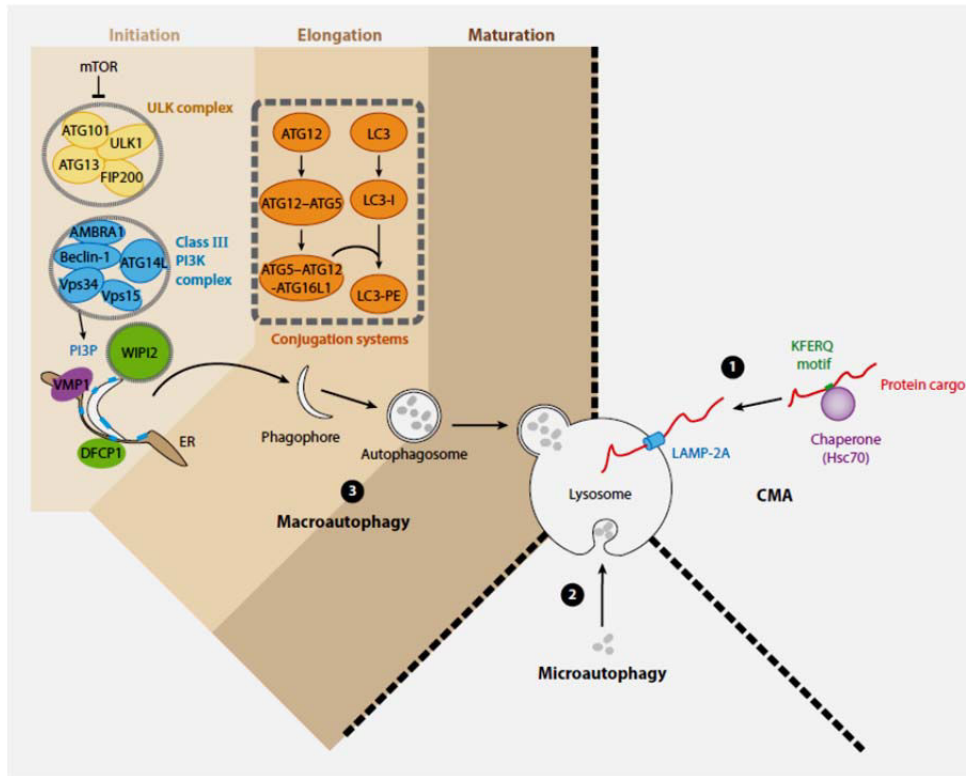


**Figure 10: The different types of autophagy**

(1) During chaperone-mediated autophagy, proteins with KFERQ motifs are recognized by the Hsc70 chaperone. Later they associate with the integral lysosome membrane protein LAMP-2A. (2) Microautophagy entails the recruitment of targeted components in proximity with the lysosomal membrane, which subsequently invaginates and pinches off. (3) Macroautophagy is characterized by the sequestration of cytosolic material in double-membrane vesicles called autophagosomes.

Adapted from (Morel et al., 2017).

### 2.1.2 Microautophagy

Microautophagy (Figure 10) is a non-selective lysosomal degradation process. In direct contact with the lysosome, the cytoplasmic content to be degraded will be sequestered by induction of invaginations of the lysosomal membrane, similarly to what happens on multivesicular endosomes. These invaginations elongate and form autophagic tubes. At their extremity vesicles are formed, a split occurs, thus liberating the vesicles within the lysosomal light. In some cases, microautophagy could be selective, however this has only been described in yeast.

### **2.1.3 Autophagy Mediated by Chaperones**

In contrast to the two types of autophagy previously described, CMA (Chaperone Mediated Autophagy) is exclusively a selective degradation process (Cuervo and Wong, 2014). Proteins degraded by this autophagic pathway are specifically targeted through the recognition of KFERQ pentapeptide motif localized in the protein sequence (Cuervo and Wong, 2014). The recognition of this motif takes place in the cytoplasm, by the protein of heat shock, hsc70 (heat shock cognate protein of 70 KDa), a cytosolic chaperone. Once recognized by hsc70, the target protein is delivered to the surface of the lysosome and translocated into the lysosome lumen using LAMP-2A protein. LAMP-2A is present on the surface of the lysosome as a monomer and the combination of several monomers leads to the formation of a LAMP-2 multi-complex required for translocation of the substrate (Gradilone *et al.*, 2007).

CMA is generally involved in the degradation of proteins with structural or peroxidated abnormalities which contributes to the regulation of intracellular levels of certain enzymes and transcription factors. The role of CMA is crucial for amino acid recycling after a prolonged period of nutrient deficiency (Cuervo and Dice, 2000).

## **2.2 Regulation of Autophagy**

The formation of the autophagosome is orchestrated by a set of proteins called ATG for "AuTophagy related" proteins (Meijer and Codogno, 2004). More than thirty genes coding for ATG proteins have been identified by genetic screening in yeast. Eighteen of these ATGs are known to be recruited during isolation of the autophagosome membrane. The formation of the autophagosome can be divided into three stages: initiation, nucleation and elongation. Initiation is the transmission of the signal to the membrane source necessary for the genesis of the phagophore, the nucleation leads to the isolation of this membrane and finally the isolation takes place until the autophagosome is totally formed (E. Morel, 2017).

## 2.2.1 Initiation of autophagosome biogenesis

In yeast, when autophagy is induced, ATG1 serine / threonine kinase protein forms a complex with ATG13, ATG17, ATG29, and ATG31 (Klionsky *et al.*, 2016). In mammals, this complex is composed of ULK-ATG13-FIP200-ATG101 proteins (Figure 11). The formation of these complexes in both yeast and mammals is essential for the initiation of autophagy and under nutrient rich conditions ULK1 and Atg13 are phosphorylated and the complex is inactivated by mammalian target of rapamycin complex 1 (mTORC1). The mammalian homologues of ATG1 are 5 members ULK-1, ULK-2, ULK-3, ULK-4, and STK36/ ULK5. ULK1 and ULK2 have a very strong homology with ATG1 while ULK3, ULK4 and STK36 retain only its kinase domain. Although ULK1, ULK2 and ULK3 seem to contribute to the autophagic process, only ULK1 and ULK2 play an important role in the induction of autophagy (Boukhalifa *et al.*, 2019).

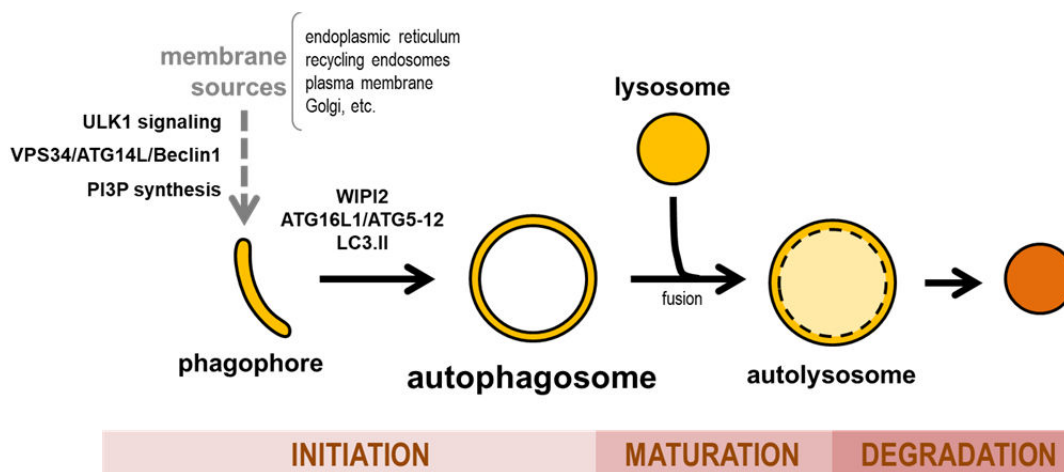


**Figure 11: The formation of the autophagosome**

The autophagic pathway requires three different steps: 1) Initiation in which the cytosolic substrates are sequestered within a double membrane vesicle called phagophore or pre-autophagosome 2) Maturation that is characterized by the elongation and the closure of phagophore forming an autophagosome 3) Degradation that includes the fusion of autophagosome-lysosome to form an autolysosome in which the cargo is degraded and recycled.

Adapted from (Boukhalifa *et al.*, 2019)

Within the mammalian complex, ATG101 stabilizes the expression of ATG13, and stably interacts with the ULK1 and FIP200 complex, regardless of the energy conditions of the cell (Mercer, Kaliappan and Dennis, 2009; Mackeh *et al.*, 2013). Although there is no human ortholog of ATG29 and ATG31, nor a yeast ortholog of ATG101, one nevertheless observes a similarity in the composition of these complexes, suggesting similar functionalities. On the other hand, the membrane localization of the complex remains the same, being located at the level of the phagophore in mammals and its equivalent in yeast, PAS. The C-terminal domain of ULK1, called Early Autophagy Targeting / tethering (EAT), appears to be essential for the recruitment of the phagophore complex (Joachim *et al.*, 2015). In addition, a positively charged amino acid set located at the N-terminus of ATG13 (protein member of the ULK1 complex) allows the interaction with negatively charged phospholipids present in the membranes which leads to the translocation of the ULK1 complex and the recruitment of ATG14, a protein belonging to the Beclin1-PI3KC3 complex, to the omegasome (Karanasios *et al.*, 2016), considered as the cradle of the future phagophore and then the main site for autophagosomal membranes assembly (Molino, Nascimbeni, *et al.*, 2017).

Finally, ULK1 is essential for the induction of autophagy since the simple decrease of its expression is able to inhibit this process and this in different contexts (Razi, Chan and Tooze, 2009). On the other hand and unlike mice invalidated for ATG5 and ATG3 autophagy genes, ULK1<sup>-/-</sup> and ULK2<sup>-/-</sup> mice are born viable and are able to survive the postnatal period (Cheong *et al.*, 2014). They nevertheless have defects in the mitochondrial elimination during the maturation of reticulocytes, indicating a specific role of ULK1 in the selective degradation of mitochondria (mitophagy) especially during erythropoiesis (Kundu *et al.*, 2008).

### **2.2.2 Nucleation of autophagosomal membranes**

In addition to these preferred partners mentioned above, Beclin1 can also interact with other proteins including Bif-1, AMBRA1, PINK1 and VMP1. AMBRA1 has been identified to promote the interaction between Beclin1 and PI3KC3 inducing autophagosome nucleation and acting as an essential factor of autophagy (Figure 12).

Under basal conditions, AMBRA1 is microtubule-sequestered with Beclin1, but when autophagic stress is induced, ULK1 phosphorylates AMBRA1. This phosphorylation disrupts its interaction with dynein, which allows translocation of the complex to the phagophore initiation site (usually the Endoplasmic Reticulum) (Di Bartolomeo *et al.*, 2010).

PINK1 is a serine threonine kinase which is located at the level of the mitochondria, it is involved in the regulation of mitophagy. Its C-terminal domain is able to interact with Beclin1 to induce autophagy (Geisler *et al.*, 2010).

Finally, VMP1, a transmembrane protein of the endoplasmic reticulum, which is strongly expressed in case of pancreatitis, can also interact with Beclin1, notably at ER-plasma membrane contact sites (Nascimbeni, Codogno and Morel, 2017). In non-pathological condition, its C-terminal region is essential for its interaction with Beclin1 and its recruitment at the level of the membrane. Indeed, the mutation of this domain prevents the formation of the complex but also the recruitment of LC3 to the autophagosome (Ropolo *et al.*, 2007). During the formation of the phagophore, the Beclin1-PI3KC3-VPS15 complex is recruited at the site of nucleation of the phagophore to produce and phosphorylate the PI allowing the production of PI3Ps, which will recruit factors necessary for the establishment of the membrane structure of the phagophore. In addition to their contribution to phagophore formation, PI3Ps have been shown to be necessary for the stabilization of ULK1 and the omega-some. Thus, once recruited on its activation site and stabilized, the complex ULK1 phosphorylates Beclin1 which increases the activity of the Beclin1-hVps34 complex (Russell *et al.*, 2013). The PI3KC3 and ULK1 complexes are recruited to the membranes where they act synergistically to stimulate PI3P production and to facilitate the isolation of the phagophore membrane. On the other hand, the ATG13 protein, which belongs to the ULK1 complex, is able to bind PI3P indicating that the ULK1 complex also plays an important role in the stabilization of PI3P in the phagophore (Karanasios *et al.*, 2016).

All these events lead to nucleation of the phagophore membrane and recruitment of other ATG proteins to the omegasome (Figure 12).

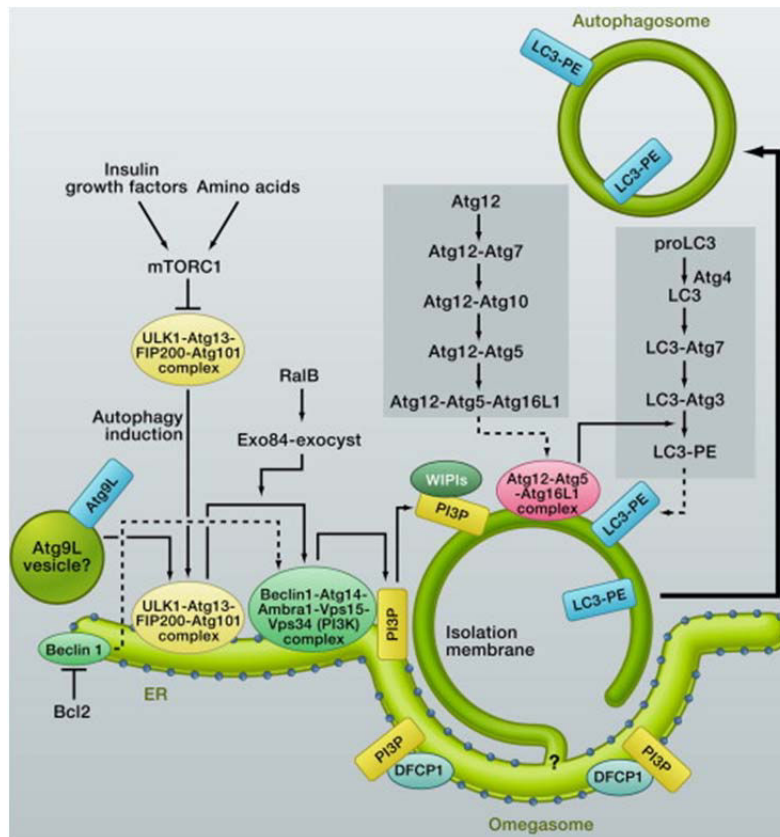


**Figure 12: Early steps of autophagy machinery**

There are three important stages in autophagic machinery: 1. Initiation and nucleation (formation of the phagophore); 2. Vesicle elongation (growth and closure of autophagosome); 3. Maturation into autolysosomes. These stages depend on different core Atg proteins which are recruited to the autophagosome assembly site: Atg1/ULK complex, the class III phosphatidylinositol 3-kinase (PI3K) (Beclin-1-PtdIns3KC3-Atg14L) complex, the WIPI complex, the Atg12-Atg5-Atg16L1 conjugation system, the Atg8/LC3 conjugation system, and Atg9 vesicles.

Adapted from (Mizushima and Komatsu, 2011)

### 2.2.3) Elongation and final maturation

In both yeast and mammalian cells, covalent binding or conjugation between certain ATG proteins is necessary for their function and their role in inducing the autophagic process. Thus, of the thirty ATG genes identified as controlling autophagy, eight are directly involved in the ATG5-ATG12 and LC3-PE conjugation systems. The enzymatic process involved in this ATG protein conjugation action is a system similar to that of ubiquitination and is referred to as

"ubiquitination-like" system. We thus speak of "ubiquitination-like" because it shares many similarities with the mechanism of ubiquitination of proteins destined for degradation by the proteasome. During autophagy, we observe a similar mechanism of cascade transfer, not of ubiquitin, but of ATG proteins. The two conjugation systems described in autophagy are ATG5-ATG12 and LC3, which are necessary for elongation and closure of the autophagosome (Geng *et al.*, 2010).

#### **2.2.4) The ATG5--ATG12 conjugation system and its partners**

ATG7 is the enzyme E1 like which allows the activation of ATG12 protein. Indeed, ATG12 is activated by the formation of a thioester bond between its terminal residue, glycine 186 and cysteine 507 of ATG7 (Tanida *et al.*, 2005). After its activation, ATG12 is transferred to ATG10, an E2-type enzyme and is conjugated to its ATG5 target protein via a peptide linkage. (Reggiori *et al.*, 2003). In contrast to ubiquitin, which may be conjugated to multiple targets, ATG5 appears to be the only substrate of ATG12. Moreover, this conjugation is constitutive and irreversible. Subsequently, the ATG12--ATG5 system interacts with ATG16L1, a small coiled coil protein, leading to the formation of the ATG12--ATG5-ATG16L1 complex.

To date no E3-like ligase has been identified as implicated in the ATG5--ATG12 conjugation system. On the other hand, this complex alone can have an E3 ligase-like activity because it is involved in the LC3 conjugation system by catalyzing the transfer of PE on LC3 (LC3) by means of ATG3. Thus, it promotes the lipidation of LC3, leading to its anchoring to the membrane (Hanada *et al.*, 2009).

#### **2.2.5) The LC3-PE conjugation system**

Another conjugation system is necessary for elongation of the phagophore and future maturation of autophagosome membrane: the LC3 system (Figure 15), which is defined by lipidated form of LC3 (LC3-PE or PC3.II). To play its role in the elongation, LC3 must undergo

several biochemical modifications. The Arg117 (J. Geng and D. Klionsky., 2008) residue present at the C-terminal of pro-LC3 will be removed by the action of a cysteine protease ATG4, which will result in the exposure of a glycine residue. This glycine will thus be able to form a thioester bridge with cysteine 507 of the ATG7 protein (a site also involved in the ATG12-ATG5 conjugation system). The LC3 protein (LC3.I), deleted from its arginine, will be transferred to an E2 type enzyme, ATG3. Finally, the final step of the lipidation of LC3 is the addition of a phosphatidylethanolamine (LC3-PE or LC3.II) at the glycine residue 116 (Matsunaga *et al.*, 2009). This step allows the binding of LC3 to the future autophagosomal membrane.

In contrast to the ATG12 to ATG5 conjugation, LC3 lipidation is reversible. Thus, LC3-PE/LC3.II can be cleaved by ATG4 to generate free LC3.I (Kabeya *et al.*, 2000). There are several homologs of LC3 identified in mammals, they are grouped into two subfamilies, LC3 (LC3A, B, B2, and C) and GABARAP (GABARAP, -L1, - L2 or GATE16). All undergo the same modifications catalyzed by ATG4B, ATG3 and ATG7. These proteins allow the lipidation of LC3, and the transformation of LC3-I (the cytosolic LC3) in LC3-II (or LC3-PE), which is bound to membrane. The members of the LC3 family help to elongate and close the phagophore. The combination of these cytosolic proteins and the protein complexes already present in the membranes allow elongation of the phagophore membrane. Before closing the membrane creating an autophagosome, the ATG present dissociate and only members of the same family LC3 remain associated. After closure of the autophagosome, only LC3-II remains present on the surface of the autophagosome.

It is widely accepted that ATG5 and ATG7 are key proteins for autophagy. However mice deficient for these two genes are still able to form certain kind of autophagosomes / autolysosomes (Nishida *et al.*, 2009). Although the lipidation of LC3-II is generally an excellent autophagy marker, it is absent when inducing this alternative autophagy, independent of ATG5 and ATG7. This atypical autophagy, however, is regulated by ULK1 and Beclin1. In contrast to conventional autophagy, autophagosomes appear to be Rab9 dependent. The newly isolated membrane fuses with trans-Golgi-derived vesicles or late endosomes (Nishida *et al.*, 2009). Thus in this new model, many "certainties" are shaken, since even this ATG5-independent autophagy has been detected in

embryonic tissues, where it also plays an important role in the mitochondria degradation during the Erythrocyte differentiation via ULK1 (Koyama-Honda *et al.*, 2013).

In mammals, there are different ways of inducing autophagy: the conventional or canonical and non-canonical ways. During the latter, the formation of the double-membrane-bound autophagosome does not require the hierarchical intervention of all the ATG proteins, whereas canonical autophagy does. Furthermore, the double membrane does not necessarily elongate from a single source (Dupont and Codogno, 2013). Finally, once the autophagosome is formed, it can merge directly with a lysosome to form an autolysosome. The fusion of the autophagosome with the lysosome is facilitated by microtubules.

## **2.3 ATG16L1: roles and functions**

### **2.3.1) ATG16L1: a platform of the phagophore membrane**

Autophagy-related 16-like 1 (ATG16L1) is a protein is encoded by *ATG16L1* human gene present on chromosome 2. This protein is one of the most described in canonical autophagy. Classically, ATG16L1 is described to be required in the formation of ATG5-ATG12-ATG16 complex, involved in the elongation of the autophagic membrane and is therefore considered as a master regulator of autophagy initiation. More in details, ATG16L1 canonical role in autophagy is referred to target the ATG12-ATG5 conjugate to pre-autophagic membranes to ensure localized proper LC3-lipidation and thus to ensure proper “tagging” of autophagosomal membranes (Fujita N *et al.*, 2008). Pre-autophagosomes are positive for phosphatidylinositol-3-phosphate (PI3P), the key lipid in autophagosome biogenesis sequence and synthesized by the class 3 PI3Kinase VPS34 lipid enzyme. Presence of PI3P allows notably the specific recruitment of the WIPI2 protein which is able to bind to PI3P and to ATG16L1, thus allowing to recruit the ATG12-5 conjugate to the proper membrane and the local LC3 lipidation (Figure 13).

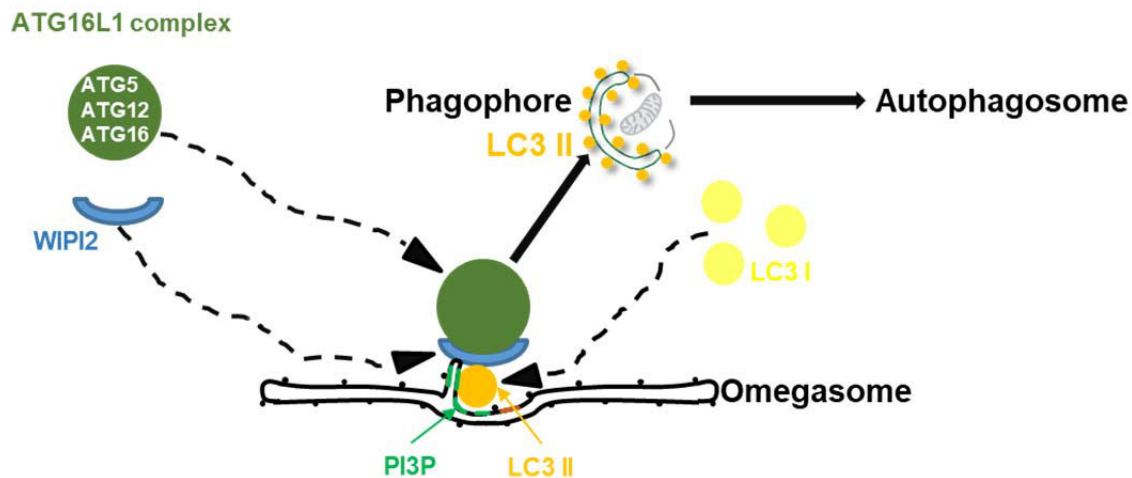


**Figure 13: ATG16L1 and partners in autophagosome biogenesis**

During autophagy initiation the synthesis of a local pool of PI3P (phosphatidylinositol-3-phosphate) at the level of the endoplasmic reticulum located omegasome occurs. Subsequently, the WIPI2 protein (WD repeat domain phosphoinositide-interacting protein 2) (which can associate specifically with PI3P) is also recruited to the omegasome where it allows the addressing of the ATG16L1 complex (ATG16L1, ATG5, ATG12) which participates in the key steps of lipidation - and therefore of membrane addressing - of the LC3 protein. This is then concentrated at the level of the phagophore and then the autophagosome.

Adapted from (Etienne Morel, 2017)

The mammalian ATG16L1 protein harbors three distinct regions: N-terminal portion which is the ATG5-binding site, followed by a coiled-coiled domain (CCD) which is a dimerization domain, and seven tryptophan-aspartic acid repeats called WD40 repeats in the C-terminus part. Interestingly, the N-terminal part and the CCD domain of ATG16L1 is present in yeast ATG16 homologue and essential for bulk and starvation induced autophagy (see discussion, Figure 17). However the c-terminal WD40 domain, an important domain involved in the context of alternative functions of autophagy, such as inflammatory control and xenophagy, is absent in yeast ATG16.

Each domain has its distinct binding partners, which mediate specific functions. In particular, the WD40 repeats domain, which folds into a  $\beta$ -propeller structure, is considered as being a hub for protein-protein interactions. Consequently, many proteins that interact with ATG16L1 WD40

repeats have been identified so far in different screens (Figure 14). These interactions appear to be crucial for autophagy-dependent or -independent functions of ATG16 and will be dealt with below.

Interacting Protein	Binding Region of ATG16	Function
ATG5	N-terminal AFIM	Essential for ATG16 complex localization to PAS and ATG8/LC3 lipidation
FIP200	Between CCD and WD40 repeat domain	Promotes the specific targeting of ATG16L1 to the isolation membrane
WIPI2b	CCD	Promotes the recruitment of ATG16 to the isolation membrane
TMEM166	WD40 repeat domain	Promotes the recruitment of ATG16L1 complex to the autophagosome membrane
Rab33B	CCD	Transport of Golgi-derived membrane to autophagosome
Clathrin	N-terminal region	Transport of plasma membrane to autophagosome
Annexin A2	ND	Promotes the formation of phagophore structures
Connexin 43	WD40 repeat domain	Inhibits autophagosome formation
TMEM59	WD40 repeat domain	Xenophagy
NOD1	WD40 repeat domain	Xenophagy
NOD2	WD40 repeat domain	Xenophagy
T3JAM	WD40 repeat domain	ND
DEDD2	WD40 repeat domain	ND
Ubiquitin	WD40 repeat domain	Xenophagy
PCM1	ND	Antigen presentation
Rab33A	CCD	Hormone secretion
TRIM20	WD40 repeat domain	Autophagic degradation of inflammasome components
PSMD1	N-terminal half; WD40 repeat domain	Autophagic degradation of PSMD1
PSMD2	WD40 repeat domain	Autophagic degradation of PSMD2

The proteins were listed according the order of appearance in this paper. ND: not determined

**Figure 14: ATG16L1 interacting proteins, binding regions, and functions of interactions**

Adapted from (Xiong *et al.*, 2018)

As mentioned above, ATG16L1 has a crucial role in autophagosome formation, by leading the ATG5—12-ATG16L1 complex formation on PI3P positive membranes through WIPI2B protein interaction with ATG16L1 (Dooley *et al.*, 2014), which is currently considered to be crucial to pre-autophagosome assembly via its Rab11 interaction.

Different studies showed also that ATG16L1 can interact with others autophagy related proteins such as FIP200, via the FIP200-binding domain (FBD). Furthermore, the transmembrane protein 166 (TMEM166) (Figure 14) was also suggested to facilitate the recruitment of ATG5—12-ATG16L1 to the autophagosome membrane to promote the formation of the autophagosome.

ATG16L1 also interacts with Rab33B a Rab-type small GTPase localized at cis-Golgi that functions in intra-Golgi trafficking and retrograde Golgi-ER trafficking (Xiong *et al.*, 2018).

Finally, a recent study from Pascale Bomont's lab, showed that, in primary neurons, the E3 ubiquitin ligase Gigaxonin (GAN) interacts with ATG16L1 via the WD40 domain and that ATG16L1 is aggregated in absence of GAN. This work suggests that GAN-E3 ligase controls in turn the production of autophagosomes (Scrivo, Codogno and Bomont, 2019).

### **2.3.2) recently proposed alternative functions and characteristics of ATG16L1**

Recently, ATG16L1 has also been shown to play a role in bacterial sequestration via the seven c-terminal WD40 repeats that is unessential domain for canonical autophagy. Furthermore, this WD40 domain seems to be important for xenophagy. Travassos and colleagues indeed showed that NOD1 and NOD2 are involved in bacterial sensing through recognition of peptidoglycan which make a link to autophagy by recruiting ATG16L1 to the entry site of *Shigella Flexneri* (Travassos *et al.*, 2010). Other studies showed that ATG16L1 was required for the defense of intestinal epithelial cells against *Salmonella Typhimurium* (Conway *et al.*, 2013). Interestingly, a specific motif composed of 19 amino acids was recently identified and seems to be sufficient for a direct binding to the WD40 repeat domain of ATG16L1. This domain was first found at a human transmembrane protein TMEM59 which localizes to the Golgi apparatus, and it has also been found in the N-terminal caspase recruitment domain of NOD2. Both NOD1 and NOD2 thus bind directly to the WD40 of ATG16L1 even if NOD1 lacks the motif of 19 amino acids.

Dudley and colleagues (Dudley *et al.*, 2019) showed that conserved residues inside the CCD domain of ATG16 mediate direct binding to phosphoinositides, such as phosphatidylinositol 3-Phosphate (PI3P) which indicates that ATG16L1 has, in parallel of its WIPI2/PI3P association, an intrinsic ability to bind lipids that plays an essential role during LC3 lipidation and autophagosome maturation (Figure 15). Furthermore, through this region, ATG16L1 was found to interact with several additional phosphoinositides, including PI4.5P2 and PI4P, possibly explaining how ATG16L1 could be recruited to other cellular compartments (Dudley *et al.*, 2019). In addition a

very recent work from Anne Simonsen's lab (Lystad *et al.*, 2019), identified two distinct membrane-binding regions in ATG16L1: N-terminal required for LC3B lipidation upon different conditions tested and C-terminal region dispensable for canonical autophagy and essential for VPS34-independent LC3 lipidation at perturbed endosomes. These results suggest that ATG16L1 isoforms mechanistically distinguish between different LC3 lipidation mechanisms under different cellular conditions.

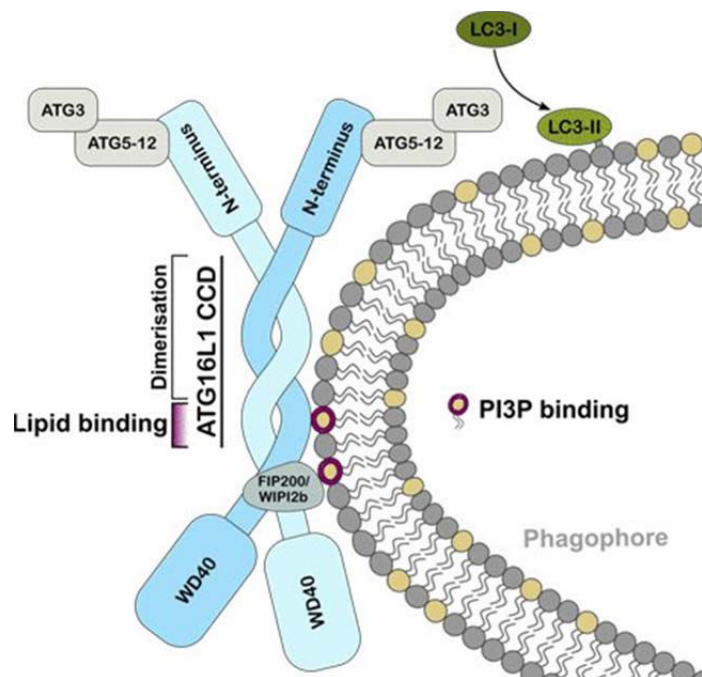


**Figure 15. Interaction between ATG16L1 and PI3P**

The coiled-coil domain (CCD) of ATG16L1 interacts with phosphatidylinositol-3-phosphate and other phosphoinositides. CCD-lipid interaction is required for efficient recruitment of ATG16L1 to the phagophore.

Adapted from (Dudley *et al.*, 2019)

## **2.4) Interrelation between primary cilium and autophagy**

Only very recently, a functional and molecular interaction between PC and autophagy has been identified (Pampliega *et al.*, 2013; Tang *et al.*, 2013). Indeed, several studies describe that different stress conditions (such as serum deprivation, confluence of cell culture, shear stress, etc.) promote the formation of the PC and are associated with an activation of autophagic processes. In an original way, ciliogenesis and autophagy are closely linked since there is a fine regulation between the two mechanisms. Indeed, the basal autophagy induced (by serum deprivation) or

sustained (prolonged serum deprivation) differently control ciliogenesis. Similarly, the activation of autophagy requires the presence of the functional PC (Tang *et al.*, 2013; Wang *et al.*, 2018). All of these new concepts are presented in this section.

#### **2.4.1) Autophagy as a new modulator of ciliogenesis?**

Under basal autophagy (non-stress induced), two major mechanisms regulate ciliogenesis. IFT20 (Intraflagellar transport protein 20), an essential component of ciliogenesis, is degraded by autophagy (Pampliega *et al.*, 2013) and OFD1 (Oral Facial Digital 1), a negative regulator of ciliogenesis, is localized at the level of the centriolar satellites following its sequestration by BBS4 and prevents ciliary biogenesis (Tang *et al.*, 2013). When autophagy is induced by stress, OFD1 is degraded by autophagy and IFT20 contributes to ciliary traffic to ensure ciliogenesis. Similarly Pampliega *et al.* have shown many components of the autophagic machinery (but not Beclin1 or ULK1 for instance) are located at the level of the basal body and the axoneme of the PC in this context (Pampliega *et al.*, 2013). The authors describe in particular that the autophagic ATG16L1 protein is transported on the same vesicles as IFT20 on the basal body. If the inducing stress of autophagy is prolonged, IFT20 becomes a target of autophagic processes and its degradation allows control of the length of the cilia. Indeed, the invalidation of Atg5, Atg7 or Atg14 in MEFs (Mouse embryonic Fibroblast) cells leads to an accumulation of IFT20, an increase in the percentage of ciliated cells and a formation of longer cilia (Pampliega *et al.*, 2013). In a contradictory way, Wang *et al.* (Wang *et al.*, 2018) demonstrate that ATG7-knocked mouse kidney epithelial cells or ATG5-disabled MEFs have shorter cilia and that the addition of a proteasome inhibitor restores the size of the PC. This work suggests that in the absence of autophagy, the proteasome would be able to degrade a protein necessary for ciliogenesis and add a level of complexity in the regulation of ciliogenesis by autophagy. This balance between basal, induced and prolonged autophagy would therefore be crucial in the control of the expression and localization of ciliary components, and thus on ciliogenesis. Any deregulation in these processes could lead to deleterious consequences on cellular homeostasis.

### **2.4.2) The primary cilia as an essential regulator of autophagy?**

An important aspect described in the work of Pampliega et al. (Pampliega *et al.*, 2013) is that the deletion of the proteins involved in the assembly of the cilia, such as IFT20 or IFT88, prevents the full activation of starvation induced autophagy. The authors suggest that the recruitment of ATG proteins at the base of the PC from the early stages of autophagy could be the signature of an atypical localization of autophagosome formation machinery mobilization. Two arguments are in favor of this hypothesis: several sites of simultaneous biogenesis of autophagosomes already exist in the cell (mitochondria, Endoplasmic Reticulum, etc.) (Hamasaki *et al.*, 2013) and the ciliary pocket is an intense site of endocytic trafficking (Benmerah, 2013). Nevertheless, the type of autophagy modulated by the presence of PC seems to depend on the context. In renal epithelial cells, Wang et al. have shown that basal autophagy is inhibited by lack of PC and that autophagy can be restored by inhibiting the mTOR signaling pathway (Wang *et al.*, 2018). Whereas in a model of fibroblast without PC, the inhibition of mTOR does not restore autophagy (Pampliega *et al.*, 2013). These discrepancies suggest that the molecular mechanisms that control the communication between the cilia and autophagy may be different depending on the type of stimulus, the cell type, or the confluence of the cells.

### **2.4.3) The interaction between primary cilia and autophagy: a necessary dialogue in the context of shear forces.**

The function in maintaining cellular homeostasis of this relationship between primary cilia and autophagy has recently been demonstrated in vitro and in vivo by the team of Dr. P. Codogno in the response to mechanical stress of renal epithelial cells (Orhon *et al.*, 2014)). In particular, the authors observed that epithelial renal cells subjected to a shear force of 1 dyn/cm<sup>2</sup> (physiological value of renal tubular urinary flow) show an increase in autophagosomes contain and a decrease in their cell volume. This ability of renal cells to control their cell volume is abolished in cells where autophagy is blocked by knockout of ATG5 or ATG16L1 or in KEC cells deficient / invalidated for IFT88. These results indicate that the autophagy induced by the shear forces necessary to control the volume of these cells requires the presence of functional PC. The authors then used

different *in vivo* approaches to show the importance of this PC / autophagy crosstalk in the response to mechanical stress. Whether using chloroquine to block autophagic flow, an UUO model, Mice subjected to unilateral ureteral obstruction (or a knockout mouse model for KIF3A to block ciliogenesis, Orhon et al. (Orhon *et al.*, 2016) conclude that autophagy induced urinary flow in renal tubules is required to regulate renal cell size via a functional primary cilia. Recently, Boelke et al (Boehlke *et al.*, 2010) demonstrated that a ciliary signaling pathway involving LKB1 / AMPK and mTOR inhibition would be required to control the cellular size of renal epithelial cells in response to shear forces. From a molecular point of view, Orhon et al (Orhon *et al.*, 2016) reproduced these results and assume that the autophagic process could proceed in two stages:

1 / an early autophagic wave dependent on PC1-PC2 (Polycystine 1 and 2), but dispensable for the regulation of renal cell volume.

2 / a late autophagy wave that activate LKB1-AMPK-mTOR pathways in both the "main" ciliated cells and renal cells called "non-ciliated" interlayers to control cell volume.

Although these suggestions involving ATP in cell communication induced by the PC/autophagy dialogue must be experimentally demonstrated, they definitively bring innovative concepts and add a level of complexity to the importance of this communication in the control of the cellular homeostasis.

## II. AIMS of THE STUDY

The PC is a real external sensory antenna present at the surface of most of the vertebrate cells. PC may be the key or the mediator of the dialog between extracellular signals and the cell.

Previous data obtained in our laboratory highlighted a novel crosstalk between primary cilia (PC) and autophagy. A relation between these two cellular mechanisms was based on the temporal coincidence of serum deprivation stimuli. Serum deprivation induces cilia growth starting in the first hours, up to 24 hours *in vitro*. Autophagy is also induced upon serum starvation in the first hours and maintained during the full duration of starvation.

In the work of Pampliega and collaborators (Pampliega *et al.*, 2013), a specific role of autophagy during ciliogenesis was suggested. On the other hand, the PC itself seems to participate in the regulation of autophagic activity in response to extracellular inputs. Finally, under serum starvation and also in response to mechanical stress (Orhon *et al.*, 2016) our lab demonstrated that ATG16L1 is transported to the primary cilium with the ciliary protein IFT20.

In the present work, I have investigated the molecular and the functional relationship between ATG16L1 and IFT20, in the perspective to better understand the dialog between autophagic and PC associated machineries during stress sensing. The precise aim of the actual study was to decipher the crosstalk between these two keys proteins during serum starvation, thus in pro-ciliogenesis and pro-autophagic conditions, in fibroblasts. We chose mouse embryonic fibroblasts as a model of induced ciliogenesis, since these cells are not ciliated until they are cultured in absence of serum.

The first part of our study focused on several questions in order to determine:

- The biological condition(s) of IFT20/ATG16L1 crosstalk and putative partners
- The regulation of IFT20/ATG16L1 crosstalk by testing interaction domains
- The importance of IFT20/ATG16L1 crosstalk during stress sensing

Then, following the obtained results (and shown in the RESULTS section), we focused on the deciphering of a non-canonical role of ATG16L1 in ciliogenesis and PC associated vesicular trafficking, which could shed light on a yet non-reported implication of autophagy and PC associated proteins dialog in cellular stress sensing and regulation of homeostasis.

More precisely, experimental data were collected and analyzed to unravel:

- the molecular link between ATG16L1 and phosphoinositides dynamics at PC membrane
- the molecular link between ATG16L1 and a phosphoinositides associated phosphatase
- the subsequent link between ATG16L1 and Hh signalling pathway in response to serum deprivation associated stress.

The results obtained, as well as the biological implications of these data are discussed in the DISCUSSION section.

### III. RESULTS

#### **“The autophagy protein ATG16L1 cooperates with IFT20 and INPP5E to regulate the turnover of phosphoinositides at the primary cilium”**

In line with the aims of the PhD project described above, I present the results I obtained during the course of my PhD training which directly concerned the ins and outs of ATG16L1 (a key autophagy regulator) crosstalk with IFT20 (a crucial protein associated with ciliary trafficking) in the complex relationship that exists between autophagy and primary cilium. As detailed below, I obtained evidences that ATG16L1, which interacts with IFT20 via its WD40 domain and a Y-E-F-I (Tyr – Glu – Phe – Ile) motif we found in IFT20, is a pivotal player in the vesicular targeting of IFT20 at the primary cilium. Moreover, my data show that ATG16L1 is required for the proper trafficking of INPP5E, a key lipid phosphatase required for the PI4P/PI4.5P2 turnover of PC associated membranes and thus for PC functions regulation. Importantly, ATG16L1 was found to be associated with INPP5E, and able to interact with both PI4.5P2 and PI4P. In turn, the importance of ATG16L1 in primary cilium membrane identity is demonstrated by the aberrant (and non-functional) giant cilium that I observed in ATG16L1 deficient cells.

This study is here presented as a scientific manuscript and will be submitted for publication very soon.

In addition, data obtained on side projects in the lab are presented, together with a recent review on autophagy interplay with primary cilium (Boukhalifa *et al.*, 2019), in the appendix section. One manuscript concerns the role of the PI3KC2alpha in the PI3P synthesis associated with autophagy and primary cilium interplay in response to shear stress (Boukhalifa\*, Nascimbeni\*, et al. in revision) and the second one aimed at clarifying the function(s) of FLCN protein in the dialog between autophagy and primary cilium during shear stress situation (Zemirli\*, Boukhalifa\* *et al.*, 2019).



**The autophagy protein ATG16L1 cooperates with IFT20 and INPP5E to regulate the turnover of phosphoinositides at the primary cilium**

Asma Boukhalifa<sup>1</sup>, Nicolas Dupont<sup>1</sup>, Patrice Codogno<sup>#,1</sup>, Etienne Morel<sup>#,1</sup>

<sup>1</sup>Institut Necker-Enfants Malades (INEM), INSERM U1151-CNRS UMR 8253, Université Paris Descartes-Sorbonne Paris Cité, Paris, France.

# Corresponding Authors:

Patrice Codogno, patrice.codogno@inserm.fr

Etienne Morel, etienne.morel@inserm.fr

**Abstract** (150 words)

The primary cilium (PC) is a plasma membrane located and microtubule-based structure that regulate different signal transduction cascades related to external stress sensing. Previous works established a functional interplay between PC and autophagic machinery. Under serum starvation, a situation that promotes ciliogenesis, we show that ATG16L1 is transported to the PC together with the ciliary protein IFT20. Our results demonstrate that IFT20 and ATG16L1 are part of the same complex and that this interaction is mediated by the ATG16L1 WD40 domain and by a Y-E-F-I motif newly identified in IFT20 protein. We show that ATG16L1 deficient cells exhibit aberrant ciliary structures, in which phosphatidylinositol-4,5-bisphosphate (PI4,5P2) accumulates at PC, while phosphatidylinositol-4-phosphate (PI4P), a lipid normally concentrated in the PC, is excluded. Finally, we demonstrate that INPP5E, a phosphoinositide associated phosphatase responsible for PI4P synthesis, is a partner of ATG16L1 and that perturbation of ATG16L1/IFT20 complex alters its trafficking to the ciliary membrane. Altogether, our results reveal an unidentified function of ATG16L1 in ciliary lipids and proteins trafficking, thus directly contributing to proper PC dynamics and functions.

## Introduction

The primary cilium (PC) is a microtubule-based antenna present at the surface of many cell types that serves as an environmental sensor to integrate chemical (such as hormones and nutrients), morphogens and physical (mucus flow and fluid flow) stimuli (Goetz and Anderson, 2010; Satir, Pedersen and Christensen, 2010; Malicki and Johnson, 2017; Nachury and Mick, 2019). The PC is itself organized with three substructures: the basal body that matures from the mother centriole, the axoneme that protrudes from the cell surface and the transitory zone that allows proteins to be transported into the axoneme from the cytosol (Satir, Pedersen and Christensen, 2010). The dynamics of the PC is closely related to cell cycle progression since it is built up in cells that exit the cell cycle whereas it disappears when cells enter the cell cycle (Izawa *et al.*, 2015; Wang and Dynlacht, 2018). Ciliogenesis depends as well on intraflagellar transport (IFT) particles (Goetz and Anderson, 2010; Satir, Pedersen and Christensen, 2010; Malicki and Johnson, 2017; Nachury and Mick, 2019). IFTB complex, composed of 14 subunits proteins, transports cargoes to the tip of the axoneme in a kinesin 2-dependent manner while IFTA, composed of 6 subunits proteins, transports cargo from the tip of the axoneme to the cytoplasm in a dynein 2-dependent manner (He, Agbu and Anderson, 2017). Defects in PC functioning is the cause of many human diseases known as ciliopathies. These disease can target several organs and many ciliopathy-related syndromes are developmental disorders (Braun and Hildebrandt, 2017; Reiter and Leroux, 2017).

Recent studies illuminate the dialog between the PC and macroautophagy (hereafter refers to as autophagy), a major lysosomal degradative pathway for intracellular material (Boya, Reggiori and Codogno, 2013; Bento *et al.*, 2016; Levine and Kroemer, 2019). PC-dependent autophagy is stimulated by different stimuli including growth factor and nutrient deprivation (Pampliega *et al.*, 2013; Tang *et al.*, 2013), differentiation (Pampliega *et al.*, 2013), mechanical stress in chondrocytes (Pampliega *et al.*, 2013) and fluid flow-induced shear stress in the kidney (Orhon

*et al.*, 2014, 2016; Zemirli *et al.*, 2019). Reciprocally many studies showed that autophagy is able to control ciliary length and PC dynamics (Pampliega *et al.*, 2013; Orhon *et al.*, 2014; Cao and Zhong, 2016; Boukhalfa *et al.*, 2019; Morleo and Franco, 2019; Zemirli *et al.*, 2019).

Autophagy has been shown to control the turnover of ciliary proteins including IFT20 and OFD1 (Lam *et al.*, 2013; Pampliega *et al.*, 2013; Tang *et al.*, 2013) and the term “ciliophagy” has been proposed for the degradation of ciliary proteins by autophagy (Cloonan *et al.*, 2014). However further studies should be addressed to clarify the role of autophagic machinery in the regulation of ciliogenesis and in the selectivity of ciliary proteins degradation.

During the induction of PC-dependent autophagic pathway most of the Autophagy-related (ATG) proteins engaged in the autophagosome formation to sequester cytosolic cargo are recruited at the vicinity of the PC (Pampliega *et al.*, 2013). Notably the protein ATG16L1, a key protein in the regulation of autophagy sequence (Fujita *et al.*, 2008), accumulates both at the basal body and in the axoneme (Pampliega *et al.*, 2013; Orhon *et al.*, 2016). Moreover ATG16L1 is present with the ciliary protein IFT20 in the same vesicular compartment en route to the primary cilium and the deletion of IFT20 protein impairs the formation of autophagosomes (Pampliega *et al.*, 2013). Interestingly IFT20 controls the autophagy lysosomal process in relation with ATG16L1 or not in different modes and at different steps of the process (Finetti *et al.*, 2019).

The aim of the present study was to investigate the functional role of the molecular dialog between IFT20 and ATG16L1. Here we show that ATG16L1 is associated with IFT20 and the phosphoinositide phosphatase INPP5E, which produces PI4P by hydrolyzing PI(4,5)P<sub>2</sub>, and which was shown to be associated with the Joubert syndrome (Bielas *et al.*, 2009). The homeostasis of PI4P at PC is a key feature of ciliary identity, as illustrated notably by controlling the recruitment of tau-tubulin kinase-2 at the basal body (Xu *et al.*, 2016). The presence of PI4P in the membrane of the axoneme is also required the trafficking of PC associated signaling

proteins (Chávez *et al.*, 2015; Garcia-Gonzalo *et al.*, 2015). We showed here that ATG16L1 is a PI4P-interacting protein and that, in the absence of ATG16L1, PI(4,5)P2 accumulates at the expense of PI4P and ciliogenesis, characterized by a giant cilium, as well as ciliary signaling functions are severely affected. We show that the proper trafficking of INPP5E is dependent on the interaction between ATG16L1 and IFT20. The WD domain of ATG16L1 is important for the interaction as well as an IFT20 motif previously shown to be an ATG16L1 binding domain (Boada-Romero *et al.*, 2013). Interestingly the WD domain of ATG16L1 is not required for starvation-induced autophagy (Boada-Romero *et al.*, 2013; Fletcher *et al.*, 2018). Following on with this observation we showed that the function of ATG16L1 is independent of its role in canonical autophagy.

In conclusion our study demonstrates a novel function for the protein ATG16L1 in ciliary trafficking and PC membrane turnover. The study also underlines the intricate relation between the autophagy and the ciliary machineries.

## Results

### **IFT20 and ATG16L1 are part of the same complex from Golgi to primary cilium**

To study dynamically the interplay of IFT20 and ATG16L1 in the context of ciliogenesis, we chose to analyze the behavior of our proteins of interest in an inducible model of cilia biogenesis. Serum deprivation is known to induce ciliogenesis and autophagy in Mouse embryonic fibroblasts (MEFs) (Pampliega *et al.*, 2013; Orhon *et al.*, 2014). Importantly in regards to our study IFT20 is mostly associated with Golgi apparatus and centrosome in full medium conditions culture MEFs (Sup Figure 1a, serum condition). As expected, the protein is relocalized at the PC under serum deprivation, which leads to ciliogenesis as confirmed by axoneme staining with ARL13B ciliary protein (Sup Figure 1a, minus serum condition). PC associated IFT20 is mostly present at axoneme membrane (Sup Figure 1b, 3D acquisition) but it is important to notify that this peculiar localization is only detected with a methanol-based fixation (which is not compatible with some other proteins), since classical paraformaldehyde fixation does not allow to detect properly the intra-axonemal pool of IFT20, but only IFT20 present at the base of the cilium (Sup Figure 1c). Serum starvation induces not only ciliogenesis, but also autophagy, as assessed by LC3 lipidation (Sup Figure 1f) and we did observed a stabilization of IFT20 protein amount in the same condition (Sup Figure 1f, 1g), as previously observed (Pampliega *et al.*, 2013), which make sense with the ciliated status of the cell. Importantly, the localization of IFT20 in non-ciliated MEFs is similar to that observed in cells which are not prone to natural ciliogenesis, such as hepatocytes (De La Iglesia and Porta, 1967; Wheatley, 1969), as we show by IFT20 colocalization with centrosomal and Golgi markers in HepG2 cells (Sup Figure 1d). As another relationship with PC associated autophagy, IFT20 is also addressed to PC axoneme in epithelial cells submitted to mechanical stress and shown in

kidney polarized HK2 cells cultured in 1 dyn/cm<sup>2</sup> shear fluid flow inducing shear stress conditions (Sup Figure 1e).

IFT20, as being part of the IFTB protein family, has been described as essential for ciliogenesis and Golgi-ciliary trafficking (Follit *et al.*, 2006). Accordingly, we showed that IFT20<sup>-/-</sup> MEFs cells (Sup Figure 2a and 2b) are not able to protrude a ciliary structure in absence of serum anymore (Sup Figure 2c). Interestingly, we showed as well that the Golgi apparatus structure is altered in cells lacking IFT20 (Sup Figure 2d) which makes sense with IFT20 Golgian localization (Sup Figure 1a) and highlights the crucial importance of Golgi-to-plasma membrane trafficking required for the growing of the PC structure at the surface of the cell (Kim and Dynlacht, 2013).

Previous data from our lab report a specific connection in between IFT20 and autophagic regulator ATG16L1 protein (Pampliega *et al.*, 2013). In MEFs cultured in presence of serum (thus non ciliated), a pool of ATG16L1 and IFT20 co-distributes at Golgi vicinity (Figure 1a), but we do observe a striking ATG16L1/IFT20 colocalization at the PC in serum deprivation induced ciliogenesis state (Figure 1b). To test the biochemical interaction between the two proteins we used ATG16L1 and IFT20 knock-out/rescued experimental models to enable biochemical and fluorescence based read-outs analyzes with cells expressing ATG16L1<sup>GFP</sup> and/or IFT20<sup>mCherry</sup>. Re-expression of fluorescent tagged version of ATG16L1 and IFT20 in knock-down for endogenous proteins allowed us to maintain an equilibrated ratio of proteins, since overexpression of ATG16L1 leads to alteration of biological functions, probably because ATG16L1 containing complexes deregulation. This was notably observed in wild-type MEFs cells transfected with ATG16L1<sup>GFP</sup>, in which we observed GFP positive puncta at subcellular localizations in which endogenous ATG16L1 was absent (Figure Sup 3a), as reported in autophagy related studies (Li *et al.*, 2017), and which did not displayed PC localization anymore (Fig Sup 3b). This double experimental set-up (*i.e.* IFT20<sup>-/-</sup> MEFs transfected with IFT20<sup>mCherry</sup> and ATG16L1<sup>-/-</sup> MEFs transfected with ATG16L1<sup>GFP</sup>) allowed us to confirm the presence of

IFT20 and ATG16L1 in the same complex by GFP and mCherry driven co-immunoprecipitation, as previously suggested (Pampliega *et al.*, 2013), in presence of serum (Figure 1c and 1e) or in induced ciliogenesis situation (Figure 1d and 1f).

ATG16L1 is a central protein in autophagosome biogenesis sequence initiation, and it is well established that its autophagy associated main function, which is dedicated to LC3 lipidation/targeting to autophagosomal membrane, requires the association of ATG16L1 with ATG5 and ATG12 (Fujita *et al.*, 2008). To test whether the IFT20 association with ATG16L1 was dependent on autophagy and ATG16L1 autophagy partners, we tested the ability of endogenous ATG16L1 to interact with endogenous IFT20 protein using anti-ATG16L1 antibodies in MEFs knock-out for ATG3, a key regulator of LC3 lipidation and autophagy initiation (Tanida *et al.*, 2006) and in MEFs knock-out for ATG5, the key partner of ATG16L1 in autophagy. Interestingly we show that IFT20 and ATG16L1 still interact one with each other in absence of either ATG3 or ATG5 (Figure 1g), suggesting that the ATG16L1/IFT20 dialog we were interested in is not dependent on classical autophagic machinery. We checked presence of some key proteins of the autophagy initiation in the IFT20/ATG16L1 complex and we notably report that both Vps34 and Beclin1, responsible for local synthesis of PI3P at autophagosomal membrane (Nascimbeni, Codogno and Morel, 2017), were not associated with ATG16L1 complex (Sup Figure 4).

### **Exocyst component Sec8 is a partner of ATG16L1 and IFT20 during ciliogenesis**

Interestingly, IFT20 was recently reported to be associated with subunits of the exocyst complex, function of which is directly connected to post-Golgi trafficking (Nachury, 2011; Wu and Guo, 2015), such complex being as well associated with both autophagy regulation (Joffre *et al.*, 2015; Nishida-Fukuda, 2019) and PC turnover (Nachury, 2011). Interestingly, we show

that the exocyst Sec8 protein interacts with IFT20, but only in ciliated cells (Figure 2a). As expected, the siRNA mediated knock-down of Sec8 led to exocyst destabilization (as assessed by SEC10 levels, Figure 2b) and to ciliogenesis abrogation, but also promotes IFT20 relocalization on intracellular structures (Figure 2c) which were mostly identified as Golgi vesicles (Figure 2d). Altogether, these data demonstrates that ATG16L1 and IFT20 are part of a complex which does not rely on autophagy machinery but which handle exocyst subunits in ciliated cells only, which suggest a role of this complex in Golgi to plasma membrane trafficking, which participates in proper ciliogenesis regulation.

### **WD40 domain of ATG16L1 and a “YEFI” motif of IFT20 are required for ATG16L1/IFT20 interaction**

To further characterize the molecular dialog of ATG16L1 and IFT20, we analyzed the putative binding domains which could afford for their interaction. ATG16L1 WD40 repeat domain, which is not required for starvation associated autophagy (Boada-Romero *et al.*, 2013; Zavodszky, Vicinanza and Rubinsztein, 2013; Fletcher *et al.*, 2018), has been reported to be crucial for protein/protein interactions. We thus tested whether this domain could be required for ATG16L1 interaction with IFT20. We compared the ability of wild-type ATG16L1<sup>GFP</sup> and  $\Delta$ WD40-ATG16L1<sup>GFP</sup>, in which the 336 to 623 amino acids sequence was removed, to co-immunoprecipitate endogenous IFT20 in ATG16L1<sup>-/-</sup> MEFs (Figure 3a). Interestingly, we show that IFT20 is no longer co-immunoprecipitated in  $\Delta$ WD40-ATG16L1<sup>GFP</sup> rescued cells (Figure 3b), suggesting that the ATG16L1 WD domain is required for IFT20/ATG16L1 interaction.

A recent paper reported a putative “ATG16L1 binding domain” in the Golgi associate TMEM59 protein (Boada-Romero *et al.*, 2013). By sequence analysis, we found a similar domain in human IFT20 protein and we mutated the essential amino acids reported to be crucial in this

domain, namely Tyr111 (Y), Glu118 (E), Phe124 (F) and Ile129 (I). We replaced these amino acids by 4 alanines, and we reported this IFT20 version as “YEFI mutant” (Figure 3c).

Interestingly, while rescuing absence of endogenous IFT20 by wild type IFT20<sup>mCherry</sup> allowed the detection of endogenous ATG16L1 in the co-immunoprecipitate, this was not the case anymore with the YEFI-IFT20 mutant (Figure 3d and 3e), showing for the first time that this IFT20 domain was required for ATG16L1 binding.

We then investigated the phenotype associated with YEFI-IFT20 mutant and wondered if the absence of IFT20 binding to ATG16L1 could have consequences on ciliogenesis. As expected (supplementary Figure 2c), the ciliogenesis was inhibited in IFT20<sup>-/-</sup> MEFs cells and expression of wild type IFT20 rescued this phenotype, with the associated ATG16L1 recruitment at PC (Figure 4a, upper and middle channel, and 4c). However, in IFT20<sup>-/-</sup> MEFs transfected with the ATG16L1-non-binding version of IFT20 YEFI mutant, ciliogenesis was not rescued (Figure 4a, lower channel, and 4c). This show that simply deleting the ATG16L1 binding motif of IFT20 is sufficient to abrogate IFT20 PC associated function in ciliogenesis and strengthens the importance of ATG16L1 and IFT20 dialog during ciliogenesis regulation. Interestingly and accordingly, we finally showed that the YEFI IFT20 mutant was no longer colocalized with ATG16L1 and present in Golgi structures (Figure 4b and 4d).

### **Absence of ATG16L1 alters ciliogenesis and IFT20 trafficking**

To go further we questioned the effect of ATG16L1 knock out (using ATG16L1<sup>-/-</sup> MEFs) on IFT20 subcellular localization and associated functions at PC. Unexpectedly, we noticed that total absence of ATG16L1 leads to PC overgrowth, as measured by ciliary length (Figure 5a and 5b), and produced a giant PC, which was confirmed by normal ciliogenesis rescue through expression of wild type ATG16L1 in ATG16L1<sup>-/-</sup> MEFs (Figure 5a and 5b). These intriguing

results suggested that ATG16L1 could be directly required for the regulation of ciliogenesis. In line with this hypothesis we observed that IFT20 subcellular pattern was different in serum starved ATG16L1<sup>-/-</sup> MEFs compared to wild type cells, with a significant increase of vesicular IFT20 positive structures (Supplementary Figure 5a), which could account for a defect in vesicular trafficking of the protein, since IFT20 was massively colocalized with Golgi structures (Supplementary Figure 5b), as we classically observed in non-ciliated cells (Supplementary Figure 1). More importantly, IFT20 was absent from giant cilia observed in ATG16L1<sup>-/-</sup> cells (Figure 5c).

We next focused on the Hedgehog (Hh) signaling pathway because of its dependence on the PC and intact IFT trafficking (Rohatgi, Milenkovic and Scott, 2007; Liem *et al.*, 2012). We first showed that Gli1, a downstream factor of Hh associated with PC, stability was affected in ATG16L1<sup>-/-</sup> MEFs cultured in absence of serum (Figure 5d and 5e). Activation of Hh signaling can be as well monitored by transcriptional regulation and local recruitment of Smoothened (SMO) receptor at the axoneme (Chávez *et al.*, 2015). Treatment of serum-starved control MEFs with the SMO agonist purmorphamine leads, as expected, to an increase of SMO mRNA level in wild-type MEFs (Figure 5f). However purmorphamine failed to induce similar increase in ATG16L1<sup>-/-</sup> cells (Figure 5g), suggesting that the Hh signaling response is deficient in absence of ATG16L1, even in presence of the giant cilia associated structures we observed in ATG16L1<sup>-/-</sup> cells. Finally we showed that while SMO was indeed recruited massively to PC in wild-type cells, the giant PC produced in ATG16L1<sup>-/-</sup> MEFs were deprived of SMO (Figure 5h and 5i), confirming the inefficient PS associated Hh signaling in absence of ATG16L1.

Our results indicate a yet unreported function for ATG16L1 in PC regulation and in ciliary associated trafficking, notably via its partnership with IFT20. The giant, but nonfunctional, cilia obtained in ATG16L1 depleted cells questions directly the identity of ciliary components and membrane in this specific situation. One of the key-feature of ciliary structure and functions

regulation is the precise phosphoinositides equilibrium established at the interface of axonemal membrane and plasma membrane, at the base of the PC (Shewan, Eastburn and Mostov, 2011; Fry, Leaper and Bayliss, 2014; Nakatsu, 2015; Schink, Tan and Stenmark, 2016). Indeed, it is clearly established that axonemal membrane is positive for PI4P (which is as well present on some Golgian subdomains), while PI4,5P2 is totally excluded from axoneme, but present at the base of the PC (Nakatsu, 2015). We thus tested the PI4P and PI4,5P2 relative distribution in ATG16L1 depleted cells at PC. Interestingly, we show that giant cilia observed in ATG16L1<sup>-/-</sup> cells were devoided of PI4P (Figure 6a and 6b) while they show aberrant accumulation of PI4,5P2 in the axoneme (Figure 6c and 6d). Moreover we show that recombinant purified human ATG16L1 was able to bind to purified PI4P and PI4,5P2 from in vitro lipid strips experiments (Figure 6e and 6f), suggesting a direct association of membrane bound ATG16L1 on PI4,5P2 and PI4P positive vesicles *in vivo*.

### **The phosphoinositides turnover at the PC depends on ATG16L1/INPP5E dialog**

To go further, we wondered if the altered PI4P/PI4,5P2 equilibrium observed at the PC of ATG16L1 knocked out cells was related to INPP5E, a crucial phosphatase implicated in cilia membrane turnover (Jacoby *et al.*, 2009; Luo, Lu and Sun, 2012; Xu *et al.*, 2016) and mutated in the Joubert syndrome ciliopathy (Bielas *et al.*, 2009). Interestingly, INPP5E is required to dephosphorylate the PI4,5P2 at the 5<sup>th</sup> position and promotes PI4P increase concomitantly with PI4,5P2 decrease. In serum deprived ATG16L1<sup>-/-</sup> MEFs the total cellular amount of INPP5E was not affected (Figure 7a and 7b). However we show that its subcellular targeting was affected in absence of ATG16L1: while a pool of INPP5E is classically addressed at PC in wild type cells (Figure 7c, upper panels, and 7d), the giant cilia observed in ATG16L1 knock-out cells are

devoided of INPP5E (Figure 7c, lower panels, and 7d), which suggest that proper INPP5E trafficking to PC was affected in these cells.

We thus wondered if INPP5E could be a partner of ATG16L1 and IFT20 along the vesicular trafficking en route from the Golgi to the PC. Indeed, we showed by co-immunoprecipitation, using ATG16L1<sup>-/-</sup> cells and ATG16L1<sup>GFP</sup>, that INPP5E was a partner of ATG16L1 (Figure 7e). Finally and importantly, we showed that IFT20 and ATG16L1 proper interaction was required to stabilize INPP5E in the ATG16L1 complex, since INPP5E was not co-immunoprecipitated from ATG16L1<sup>-/-</sup> MEFs expressing  $\Delta$ WD40 ATG16L1 (Figure 7f).

Altogether our results suggest that ATG16L1 interacts with INPP5E and that the ATG16L1/INPP5E/IFT20 complex is required at dedicated membranes, presumably Golgian vesicles (notably suggested by presence of Sec8 during ciliogenesis situation), to ensure membrane depletion of PI4,5P2 and PI4P synthesis en route to the PC.

## Discussion

The interconnection between PC and autophagic machinery has been highlighted since 2013 (Pampliega *et al.*, 2013; Tang *et al.*, 2013) and raised up several questions about the ins and outs of such functional crosstalk with direct implication(s) in both autophagy and ciliogenesis processes. Here we confirmed the interaction between IFT20 and ATG16L1 in both ciliated and non-ciliated conditions (Pampliega *et al.*, 2013). We show that while CCD domain of ATG16L1 are essential for autophagy related functions (such as ATG5 interaction), the WD40 domain of ATG16L1, a seven repetitions of WD motif suggested to be important in protein-protein interactions (Xu and Min, 2011) but not essential for classical autophagy, was required for the interaction with IFT20. Reciprocally, we identified an “ATG16L1 putative domain” on the Cter of IFT20 (notably 4 essential amino acids which constitute what we reported as a YEFI motif (Tyr – Glu – Phe – Ile)), that was previously reported for the binding of ATG16L1 with TMEM59 and which is crucial in the interaction between IFT20 and ATG16L1 proteins. In our model, the absence of the YEFI motif of IFT20 is sufficient to alter the ciliogenesis and IFT20 is then blocked at Golgi. Our results indicate that the IFT20/ATG16L1 complex is trafficking in response to serum starvation conditions and suggest for the first time a role of the WD40-ATG16L1 and YEFI-IFT20 domains as regulators of ciliogenesis and probably required for the proper intracellular targeting of the protein complex to the PC, together with the exocyst protein SEC8.

Very surprisingly and unexpectedly, absence of ATG16L1 protein leads to an abnormal and giant cilia in nutritional stress conditions, with altered PC Hedgehog associated signaling functions. It was an interesting and surprising observation that required clarification, notably with contradictory reports of cilia length regulation in autophagy deficient MEFs (Tang *et al.*, 2013). This discrepancy could be explained first by the difference of cells type used in Tang and colleagues paper, which are MCF7 different from MEFs and non-ciliated in serum starvation conditions except when OFD1 level is decreased. Altogether, previous results and our own observation clearly questions the

canonical nature of the pathway mobilized in cilia-dependent autophagy induction. This is notably strengthened by the fact that ATG16L1 and IFT20 interact independently of presence of ATG5 and ATG3, thus presumably in absence of canonical autophagic efficient machinery. In this way, we probably revealed a non-classical autophagy related role of ATG16L1. Whether this is related to *bona fide* autophagy-associated functions of ATG16L1 is a central and intriguing question. Importantly, we show that both Beclin-1 and VPS34, key regulators of the autophagy associated PI3P synthesis were not found at the base of the PC (Pampliega *et al.*, 2013) and that we report that Beclin1 is not present in the IFT20 and ATG16L1 complex that we studied, whatever the ciliogenesis status.

Interestingly, we found that ATG16L1 was required for PC-associated trafficking of IFT20 in ciliated condition. Absence of IFT20 at giant cilia observed in ATG16L1 knock-out cells could explain, even partially, the aberrant cilia features of these ciliary structures. Phosphoinositides are key regulators of cellular organelles identity (Di Paolo and De Camilli, 2006). The PC membrane is indeed characterized by absence of PI4,5P2 and presence of PI4P (Chávez *et al.*, 2015; Nakatsu, 2015; Phua, Nihongaki and Inoue, 2018). Here we reported for the first time that purified ATG16L1 interacts with phosphoinositides like PI4P and, in a lesser extent, with PI(4.5)P2 making sense with recent results of Gammoh lab (Dudley *et al.*, 2019), which reported ability of ATG16L1 to bind PI3P, PI4P and PI4,5P2. This could suggest that different pools of ATG16L1 coexist at different trafficking stations, probably in different protein complexes, supposedly for different stress related processes.

Our study showed that absence of ATG16L1 alters the PC distribution of ciliary phosphoinositides. PI4P is then absent from the giant axoneme and the latter is positive for PI4,5P2, which confirms the altered SMO and Hh signaling observed in ATG16L1 null cells. These results suggest that this proper phosphoinositides equilibrium at PC depends, at least

partially, on ATG16L1. In line with this hypothesis, we showed for the first time that INPP5E, the cilia and Golgi-localized inositol 5-phosphatase associated with Joubert syndrome (Braun and Hildebrandt, 2017) and responsible for PC-PI4P production (Bielas *et al.*, 2009; Xu *et al.*, 2016, 2017) is a partner of ATG16L1/IFT20 complex. Our results suggest that absence of ATG16L1 leads to the blockade of INPP5E trafficking to PC membrane. It is thus very tempting to explain the PI4,5P2 axonemal accumulation that we observed in ATG16L1 knock-out cells giant cilia is in fact directly connected to alteration of IFT20/INPP5E vesicular trafficking to the proper subcellular localization (*i.e.* the site of PC biogenesis).

Our data highlights for the first time the importance of ATG16L1 in the stress associated trafficking of INPP5E, which is directly connected to the PC membrane identity regulation. The relationship to bona-fide autophagy associated functions of ATG16L1 is of course puzzling in this situation. One hypothesis to explain how the giant cilia of ATG16L1 knocked out cells forms, is to speculate this structure originates directly from the plasma membrane itself (and not “fed” by Golgian trafficking) as illustrated by the phosphoinositides equilibrium alteration that we reported. Further experiments must clarify the likely other differences in membrane composition and/or dynamics between wild type and ATG16L1 KO cells, in response to serum deprivation.

Altogether, our results suggest a new role for ATG16L1 in lipids dynamic, ciliary protein trafficking, in which the protein directly participates into ciliogenesis regulation and identity in response to stress sensing.

## Material and Methods

**Cell culture, transfection and constructions:** Mouse Embryonic Fibroblasts (MEFs) IFT20<sup>-/-</sup> were kindly provided by A.M.Cuervo (Albert Einstein College of Medicine, New York, USA) and were generated by G.J. Pazour (University of Massachusetts, Worcester, Massachusetts, USA). The ATG16L1<sup>-/-</sup> MEFs were a kind gift from S. Tooze (Francis Crick Institute, London, UK). ATG3<sup>-/-</sup> and ATG5<sup>-/-</sup> MEFs were kindly provided by M. Komatsu (Tokyo Metropolitan Institute of Medical Science, Tokyo, Japan) and N. Mizushima (Tokyo Medical and Dental University, Tokyo, Japan) respectively. HK2 and HEPG2 cells (ATCC) and MEFs were cultured in Dulbecco's Modified Eagle Medium (DMEM), supplemented with 10% FCS at 37°C and 5% CO<sub>2</sub>. For the serum deprivation experiments, cells were incubated with DMEM without serum for 24h. When indicated, MEFs were treated by 5µm Smoothed (SMO) agonist purmorphamine (Calbiochem) or DMSO under serum starvation condition during 24 hours.

The cDNA transfections were performed using lipofectamine 2000 according to the manufacturer's instructions. SiRNA transfections were performed using Lipofectamine RNAi Max (Invitrogen, Life Technologies) according to the manufacturer's instructions and two siRNA primers were used for each target at a final concentration of 20nM. All siRNAs were purchased from Qiagen and the references are as follows: Control siRNA (SI1027281); SEC8 (SI00040894 and SI00040901); RFP-Sec61β was a kind gift from T. Rapoport (Harvard University, Cambridge, MA, USA). Human GFP-ATG16L1 and IFT20-mcherry constructs were from X.M. Yin (Indianapolis, IN, USA) and Genecopoeia respectively. To generate mutants of GFP-Atg16L1 and mcherry-IFT20, we performed site-directed mutagenesis using a quick change kit (Stratagene), according to the manufacturer's instructions. The sequences of the primers used were as follows.

For IFT20 YEFI mutant:

1) Y►A (TAT ► GCU):

5'-cagctagaaaggtatcgggtgaagctgaagctttgtgtaaagtaga-3' (sense) and

5'-tctactttacacaaagcttcagcttcaacccgatacctttctagctg-3' (anti-sense)

2) E►A (GAA►GCA):

5'-gctgaagctttgtgtaaagtagcagcagaacaaaatgaagctatt-3' (sense) and

5'-aatagcttcattttgttctgctgctactttacacaaagcttcagc-3' (antisense)

3) F►A (TTT►GCU):

5'-gtgtaaagtagaagcagaacaaaatgaagctattgaccaattgcttttcagaaatac-3' (sense) and

5'-gtatttctgaaaagcaaattggtaaatagcttcattttgttctgcttctactttacac-3' (antisense)

4) I►A (ATT►GCU):

5'-gaacaaaatgaattattgaccaattgcttttcagaaatacctcgagtgcgg-3' (sense) and

5'-ccgactcgaggtatttctgaaaagcaaattggtaataaattcattttgttc-3' (antisense)

For ATG16L1 ΔWD40 mutant:

5'-cttccgcagcagagcgttggtggtggtggc-3' and 5'-tcccggttactggcctaaggaggcatggaccgc-3'

a958t c959a t960a: 5'-tcccggttactggcctaaggaggcatggaccgc-3' (sense)

a958t c959a t960a: 5'-gctggtccatgcctccttaggccagtaaccggga-3' (antisense)

**Protein extraction, western blotting analysis and antibodies:** Cells in 6 wells plates were washed twice with ice-cold PBS and lysed in ice with 200 µl of 1X Laemmli buffer (60mM Tris-HCL pH=6.8, 2% SDS, 10% Glycerol, bromophenol blue, supplemented with 100mM DTT) for 30min. Samples were boiled for 10min at 95°C, separated by SDS/PAGE and then transferred

onto Nitrocellulose or PVDF membranes. Western blot analysis was performed with specific antibodies and the antigen–antibody complexes were visualized by chemiluminescence (Immobilon Western, Merck Millipore). The following antibodies were used for western blotting: rabbit-anti LC3 (Sigma, Cat#L7543); mouse-anti-actin (Millipore, Cat#1501); mouse-anti-Beclin1 (BD Biosciences, Cat#612113); Rabbit-anti-IFT20 (Proteintech Cat#13615-1-AP); rabbit- Anti-ATG16L1 (MBL, Cat#PM040); mouse-anti-sec8 (Enzo Cat#814G1); rabbit anti mCherry/RFP (Rockland Cat#600401379), mouse anti-GFP (Roche Cat#11814460001), rabbit anti-Sec 10 (Proteintech, cat#17593-1-AP), rabbit anti-INPP5E (proteintech Cat#77797-1-AP), mouse anti-GLI1 (Novus, Cat#Nb600600), rabbit anti-VPS34 (Zymed, Cat#382100), rabbit anti-INPP5E (proteintech Cat#77797-1-AP). Secondary HRP conjugate anti-rabbit IgG and HRP conjugate anti-mouse IgG were from GE Healthcare and Bio-Rad, respectively.

**Immunofluorescence microscopy and antibodies:** Cells were fixed either with 4% paraformaldehyde (PFA) for 20min or with cold methanol for 5min at -20°C for proper PC axoneme proteins detection. Cells were then washed and incubated for 30min in blocking buffer (10% FCS or 5% bovine serum albumine in PBS) followed by incubation with primary antibodies diluted in blocking buffer supplemented with 0.05% saponin for 1h at room temperature or overnight at 4°C. Cells were washed 3 times, and then incubated for 1h with fluorescent Alexa-Fluor secondary antibodies. For HK2 cells cultured in microchambers at 1dyn/cm<sup>2</sup> fluid flow (for shear stress experiments with Ibidi fluidic pumps), 150µl of DAPI-Fluoromount were added after washing into the Luer chamber (Southern Biotech). Images were acquired with a Zeiss Apotome.2 fluorescence microscope or Zeiss LSM700 confocal microscope both equipped with 63x oil immersion fluorescence objectives. Number of ciliated cells and length of cilia were quantified using Zen Software (Zeiss). The following antibodies were used for immunofluorescence: mouse anti-ARL13B (Santa Cruz, Cat#515784); rabbit anti-ARL13B

(Proteintech, Cat#515784); rabbit anti-ATG16L1 (MBL, Cat#PM040); mouse anti- $\gamma$ -Tubulin (Sigma; Cat#T5326); rabbit anti-acetylated Tubulin (Sigma, Cat#T7451); rabbit- anti IFT20 (Proteintech, Cat#13615-1-AP); mouse anti-GM130 (BD, Cat# 610823); rabbit anti-INPP5E (Proteintech Cat#77797-1-AP); rabbit anti-PI4P (Echelon Cat#Z-P004); rabbit antiPI4,5P2 (Echelon Cat#Z-P045); goat anti-SMO (AbCam, Cat#ab38686), mouse anti-sec8 (Enzo, Cat#814G1) mouse acetylated tubulin (Sigma-Aldrich, Cat# T7451), mouse anti GM130 (BD, Cat#610823); Alexa Fluor-conjugated secondary antibodies (donkey anti-mouse IgG and donkey anti-Rabbit IgG, Life Technologies).

**Real Time Quantitative PCR.** RNA was extracted from cells using the NucleoSpin RNA kit (Macherey-Nagel). Reverse transcriptase PCR and qRT-PCR were performed using “Power Sybr green cells to CT” kit (Thermo Fisher Scientific) according to manufacturer’s instructions. Actin was used as reference gene and relative quantification was calculated using the  $\Delta\Delta CT$  method. Primers sequences are as followed:

SMO-forward: 5'-ATCGCTACCCTGCGGTTATT-3';

SMO-reverse: 5'-CCAGACTACTCCAGCCATCAA-3'

Actin-forward: 5'-GGCCAACCGTGAAAAGATGA-3';

Actin-reverse: 5'-ACCAGAGGCATACAGGGACAG-3'

**GFP-trap and RFP-trap assays.** For immunoprecipitation with GFP-ATG16L1 wt and GFP-ATG16L1  $\Delta$ WD40, MEF ATG16<sup>-/-</sup> cells were transiently transfected with plasmids expressing GFP, GFP-ATG16 wt and GFP-ATG16L1  $\Delta$ WD40 constructs. For immunoprecipitation with RFP trap, wt IFT20-RFP or YEF1 mutant IFT20 RFP plasmids were transfected in IFT20<sup>-/-</sup> cells. 24h

post transfection, in addition to 24h of complete medium or medium without serum, cells were collected and proteins extracted in lysis buffer (10 mM Tris, pH 7.5, 150 mM NaCl, 0.5 mM EDTA, 0.5% NP-40) complemented with protease and phosphatase inhibitor cocktail (Pierce). Cell lysates were centrifuged at 15,000rpm for 10 min at 4°C. The resulting supernatant was diluted with the dilution buffer (10 mM Tris, pH 7.5, 150 mM NaCl, 0.5mM EDTA) to NP-40final concentration of 0.1%. The protein extracts were incubated with anti-GFP and anti-RFP beads (GFP-Trap Chromotek) for 2 h at 4°C. Beads were collected by centrifugation and washed six times, the protein complexes were eluted by boiling the beads in 1×SDS-sample buffer for 10 minutes.

**Lipid overlay assay.** Membrane Lipid strip (Echelon, Cat# P-6001) were used. The human recombinant ATG16L1 (Addgene) was detected on the strips using the protocol stated by the manufacturer. In brief, the strips were blocked using a solution PBS with 3% BSA without fatty acids/ overnight at 4°C, incubated with the recombinant ATG16L1 or as a positive control the PI4,5P2-GRIP protein 1h at room temperature, washed 6 times for 10 min in washing buffer containing PBS plus 0.1% Tween-20 and detected by chemiluminescence using an anti-rabbit IgG-HRP (Sigma, Spain) or anti GST-HRP antibody (REF) and ECL Detection reagent (Amersham, GE Healthcare, Spain). The concentration of the peptides in the solution was 20µg/ml.

**Statistical analysis.** Data are presented as means ± SD or SEM. Statistical analyses were performed by unpaired, two-tailed Student's t-test, using GraphPad Prism7 (\*p < 0.005, \*\*p < 0.001, and \*\*\*p < 0.0001). Images showing Western blotting or immunofluorescence analysis are representative of three independent experiments unless otherwise stated.

## Figures legends

### **Figure 1. ATG16L1 is present at PC in ciliated cells and interacts with IFT20.**

**a, b.** confocal analysis of MEFs cells cultured in presence (**a**) or 24h absence of serum (**b**) and processed for immunofluorescence using DAPI, anti-IFT20, anti-ATG16L1 and anti-GM130 (**a**) or anti-ARL13B (**b**) antibodies. Arrowheads show ATG16L1/IFT20 codistribution at Golgi structures positive for GM130 (**a**) and at the base of the primary cilium (PC) in (**b**). Scale bars: 10 $\mu$ m. **c, d.** IFT20<sup>-/-</sup> MEFs were transiently transfected with IFT20<sup>mCherry</sup> expression vector, cultured in presence (**c**) or 24h absence of serum (**d**) and processed for co-immunoprecipitations analysis. Total lysates (input) were subjected to immunoprecipitation (IP) with mCherry/RFP-trap beads. Samples were analyzed by SDS-PAGE and western blotting with anti-mCherry and anti-ATG16L1 antibodies. **e, f.** ATG16L1<sup>-/-</sup> MEFs were transiently transfected with ATG16L1<sup>GFP</sup> expression vector, cultured in presence (**e**) or 24h absence of serum (**f**) and processed for co-immunoprecipitations analysis. Total lysates (input) were subjected to immunoprecipitation (IP) with GFP-trap beads. Samples were analyzed by SDS-PAGE and western blotting with anti-GFP and anti-IFT20 antibodies. **g.** Wild type (WT), ATG3<sup>-/-</sup> and ATG5<sup>-/-</sup> MEFs were cultured during 24h in absence of serum and processed for co-immunoprecipitations analysis. Total lysates (input) were subjected to immunoprecipitation (Co-IP) using anti-ATG16L1 antibodies. Samples were analyzed by SDS-PAGE and western blotting with anti-ATG16L1 and anti-IFT20 antibodies.

**Figure 2. The exocyst Sec8 component is present in the ATG16L1/IFT20 complex only in ciliated cells**

**a.** IFT20<sup>-/-</sup> MEFs were transiently transfected with IFT20<sup>mCherry</sup> expression vector, cultured in presence (+ serum) or 24h absence of serum (- serum) and processed for co-immunoprecipitations analysis. Total lysates (input) were subjected to immunoprecipitation (IP) with mCherry/RFP-trap beads. Samples were analyzed by SDS-PAGE and western blotting with anti-mCherry, anti-ATG16L1 and anti-SEC8 antibodies. **b.** MEFs cells were transfected with SEC8 siRNA or control siRNA (siCTRL), cultured during 24h in absence of serum and processed for western blotting analysis with anti-SEC8, anti-SEC10 and anti-actin antibodies. **c.** Confocal analysis of MEFs cells transfected with SEC8 siRNA or control siRNA (siCTRL), cultured during 24h in absence of serum and processed for immunofluorescence using anti-IFT20 and ARL13B antibodies. **d.** Confocal analysis of MEFs cells transfected with SEC8 siRNA, cultured during 24h in absence of serum and processed for immunofluorescence using anti-IFT20 and anti-GM130 antibodies. Scale bars: 10µm.

**Figure 3. ATG16L1/IFT20 interacting domains.**

**a, b.** ATG16L1<sup>-/-</sup> MEFs were transiently transfected with empty GFP, wild-type (WT) ATG16L1<sup>GFP</sup> and  $\Delta$ WD40-ATG16L1<sup>GFP</sup> expression vectors, cultured during 24h in absence of serum and processed for western blotting analysis (**a**) and for co-immunoprecipitations analysis (**b**). Total lysates (input) were subjected to immunoprecipitation (IP) with GFP-trap beads and samples were analyzed by SDS-PAGE and western blotting with anti-GFP and anti-IFT20 antibodies. **c.** 111 to 130 amino acids sequence of human IFT20 protein. The key residues mutated (Y, E, F and I) in the putative ATG16L1 binding sequence are highlighted in red and “YEFI mutant” version of IFT20 is shown (lower sequence, with alanines replacing the YEFI

residues). **d, e.** IFT20<sup>-/-</sup> MEFs were transiently transfected with empty mCherry, wild-type (WT) IFT20<sup>mCherry</sup> and YEFI mutant of IFT20<sup>GFP</sup> expression vectors, cultured during 24h in absence of serum and processed for western blotting analysis (**d**) and for co-immunoprecipitations analysis (**e**). Total lysates (input) were subjected to immunoprecipitation (IP) with mCherry/RFP-trap beads and samples were analyzed by SDS-PAGE and western blotting with anti-mCherry and anti-ATG16L1 antibodies. OVX: overexposed.

**Figure 4. Loss of ATG16L1 binding motif in IFT20 leads to IFT20 Golgi retention and ciliogenesis defect.**

**a.** IFT20<sup>-/-</sup> MEFs were transiently transfected with wild-type (WT) IFT20<sup>mCherry</sup> (middle panel) and YEFI mutant of IFT20<sup>mCherry</sup> (lower panel) expression vectors or not (mock, upper panel), cultured during 24h in absence of serum and processed for immunofluorescence analysis using anti-acetylated tubulin and anti-ATG16L1. Arrowheads show WT-IFT20<sup>mCherry</sup> colocalization with endogenous ATG16L1 at the base of PC (**a**, middle panel). **b.** IFT20<sup>-/-</sup> MEFs were transiently transfected with YEFI mutant of IFT20<sup>mCherry</sup> (lower panel) expression vectors cultured during 24h in absence of serum and processed for immunofluorescence analysis using anti-GM130 and anti-ATG16L1. Arrowheads show YEFI mutant of IFT20<sup>mCherry</sup> colocalization with GM130 and absence of colocalization with ATG16L1. **c.** Bar diagram showing the quantification of ciliogenesis (as expressed by the percentage of ciliated cells) in wild-type (WT) IFT20<sup>mCherry</sup> and YEFI mutant of IFT20<sup>mCherry</sup> conditions. **d.** Bar diagram showing the quantification of endogenous ATG16L1/IFT20<sup>mCherry</sup> colocalization area (as expressed by percentage of total IFT20<sup>mCherry</sup> signal) in wild-type (WT) IFT20<sup>mCherry</sup> and YEFI mutant of IFT20<sup>mCherry</sup> conditions. Values denote means ± S.E.M. \*\*\*P-values<0.001 using Student's t-test.

**Figure 5. ATG16L1 knockout promotes aberrant ciliogenesis and alters ciliary signaling.**

**a.** Wild type (WT) or ATG16L1<sup>-/-</sup> MEFs transiently transfected (or not) with wild-type (WT) ATG16L1<sup>GFP</sup> expression vectors were cultured during 24h in absence of serum and processed for immunofluorescence analysis using DAPI and anti-ARL13B antibody. **b.** Bar graphs showing the quantification of PC axoneme length measured via ARL13B staining (as shown in **(a)**) in wild type (WT) MEFs or in ATG16L1<sup>-/-</sup> MEFs transfected with wild-type (WT) ATG16L1<sup>GFP</sup>. Values denote means ± S.E.M. \*\*\*P-values<0.001 and \*\*P-values<0.01, using Student's t-test. **c.** Wild type (WT) or ATG16L1<sup>-/-</sup> MEFs were cultured during 24h in absence of serum and processed for immunofluorescence analysis using DAPI and anti-ARL13B and anti-IFT20 antibodies. **d, e.** Wild type (WT) or ATG16L1<sup>-/-</sup> MEFs were cultured during 24h in absence of serum and processed for western blotting analysis using anti-ATG16L1, anti GLI1 and anti-actin antibodies (**d**). **e.** Bar diagram showing the quantification of relative GLI1 protein levels shown in **(d)** in wild type (WT) or ATG16L1<sup>-/-</sup> MEFs. A.U.: arbitrary units. Values denote means ± S.E.M. \*\*\*P-values<0.001 using Student's t-test. **f, g.** Wild type (WT, **(f)**) or ATG16L1<sup>-/-</sup> (**(g)**) MEFs were cultured during 24h in absence of serum, stimulated (or not, DMSO) with 5µM of Smoothed (SMO) agonist purmorphamine and processed for SMO mRNA quantification. **h, i.** Wild type (WT) or ATG16L1<sup>-/-</sup> MEFs were cultured during 24h in absence of serum and processed for immunofluorescence analysis using DAPI, anti-ARL13B and anti-SMO antibodies. **i.** Bar diagram showing the quantification of SMO presence at PC (as a percentage of wild-type (WT) condition, as illustrated in **(h)**) in wild type (WT) or ATG16L1<sup>-/-</sup> MEFs. Values denote means ± S.E.M. \*\*\*P-values<0.001 using Student's t-test.

**Figure 6. PC associated PI4P and PI4,5P2 turnover is altered in absence of ATG16L1**

**a, b.** Wild type (WT) or ATG16L1<sup>-/-</sup> MEFs were cultured during 24h in absence of serum and processed for immunofluorescence analysis using DAPI, anti-ARL13B and anti-PI4P antibodies. Arrowheads denote codistribution of PI4P positive *punctae* with PC (only in wild type (WT) condition). **b.** Bar diagram showing the quantification of PI4P positive axoneme (as expressed as a percentage of total cilia), as illustrated in (**a**), in wild type (WT) or ATG16L1<sup>-/-</sup> MEFs. Values denote means ± S.E.M. \*\*\*P-values<0.001 using Student's t-test. **c, d.** Wild type (WT) or ATG16L1<sup>-/-</sup> MEFs were cultured during 24h in absence of serum and processed for immunofluorescence analysis using DAPI, anti-ARL13B and anti-PI4,5P2 antibodies. Arrowheads denote localization of PI4,5P2 only at the base PC (in the wild type cells) or in the axoneme (in ATG16L1<sup>-/-</sup> MEFs). **d.** Bar diagram showing the quantification of PI4,5P2 positive axoneme (as expressed as a percentage of total cilia), as illustrated in (**c**), in wild type (WT) or ATG16L1<sup>-/-</sup> MEFs. Values denote means ± S.E.M. \*\*\*P-values<0.001 using Student's t-test. **e, f.** Lipid strip probed with Gip<sup>TM</sup> protein positive control for PI4,5P2 (upper panel) and with human recombinant ATG16L1, followed by secondary antibody conjugated with peroxidase for visualization. **f,** Bar diagram showing the quantification of recombinant ATG16L1 binding on lipid strip with positive values: PI4P, PI4,5P2, phosphatidic acid (PA) and cardiolipin (CL).

### **Figure 7. The INPP5E phosphatase is a key partner of ATG16L1 during ciliogenesis**

**a, b.** Wild type (WT) or ATG16L1<sup>-/-</sup> MEFs were cultured during 24h in absence of serum and processed for western blotting analysis using anti-INPP5E and anti-actin antibodies. **b.** Bar diagram showing the quantification of relative INPP5E protein levels shown in (**a**) in wild type (WT) or ATG16L1<sup>-/-</sup> MEFs. A.U.: arbitrary units. Values denote means ± S.E.M. NS for not significant. **c, d.** Wild type (WT) or ATG16L1<sup>-/-</sup> MEFs were cultured during 24h in absence of serum and processed for immunofluorescence analysis using DAPI, anti-ARL13B and anti-

INPP5E antibodies. Arrowheads denote codistribution of INPP5E positive *punctae* with PC (only in wild type (WT) condition). **b.** Bar diagram showing the quantification of INPP5E positive axoneme (as expressed as a percentage of total cilia), as illustrated in **(c)**, in wild type (WT) or ATG16L1<sup>-/-</sup> MEFs. Values denote means  $\pm$  S.E.M. \*\*\*P-values<0.001 using Student's t-test. **e, f.** ATG16L1<sup>-/-</sup> MEFs were transiently transfected with wild-type (WT) ATG16L1<sup>GFP</sup> **(e)** or  $\Delta$ WD40-ATG16L1<sup>GFP</sup> **(f)** expression vectors, cultured during 24h in absence of serum and processed for co-immunoprecipitations analysis. Total lysates (input) were subjected to immunoprecipitation (IP) with GFP-trap beads and samples were analyzed by SDS-PAGE and western blotting with anti-GFP and anti-INPP5E antibodies. OVX: overexposed.

### **Supplementary Figure 1. IFT20 subcellular localization in ciliated and non-ciliated cells**

**a.** confocal analysis of MEFs cells cultured in presence (+ serum) or 24h absence of serum (- serum) and processed for immunofluorescence using DAPI, anti-IFT20, anti-GM130 (Golgi marker, upper panel), anti-CEP63 (centrosomal marker, middle panel) and anti-ARL13B (primary cilium (PC) marker, lower panel). **b.** 3D confocal acquisition of MEFs cells cultured during 24h in absence of serum and processed for immunofluorescence using DAPI, anti-IFT20, and anti-ARL13B. **c.** Comparison of IFT20 subcellular pattern, using DAPI, anti-IFT20 and anti-ARL13B antibodies, in MEFs cells cultured during 24h in absence of serum and fixed with paraformaldehyde (PFA) or cold methanol (MetOH), showing IFT20 at base of PC in PFA fixation and IFT20 in the PC axoneme in MetOH fixation. **d.** confocal analysis of HEPG2 cells processed for immunofluorescence using DAPI, anti-IFT20, anti-GM130 (Golgi marker, right panel) and anti-CEP63 (centrosomal marker, right panel). **e.** confocal analysis of HEK2 cells cultured for 96h in presence of 1dyn/cm<sup>2</sup> fluid flow inducing shear stress and processed for immunofluorescence using DAPI, anti-IFT20, and anti-ARL13B. Scale bars (**a – e**): 10µm. **f.** MEFs cells were cultured in presence (+ serum) or 24h absence of serum (- serum) and processed for analysis by SDS-PAGE and western blotting using anti-IFT20, anti-LC3 and anti-actin antibodies. **g.** Bar diagram showing the quantification of relative IFT20 levels shown in (**f**) in presence (+ serum) or in absence (- serum) or serum. A.U.: arbitrary units. Values denote means ± S.E.M. \*\*\*P-values<0.001 using Student's t-test.

### **Supplementary Figure 2. IFT20 knockdown alters ciliogenesis and Golgi morphology**

**a.** Wild type (WT) and IFT20<sup>-/-</sup> MEFs cells were processed for analysis by SDS-PAGE and western blotting using anti-IFT20 and anti-actin antibodies. **b.** Bar diagram showing the quantification of relative IFT20 levels shown in (**a**). A.U.: arbitrary units. Values denote means ±

S.E.M. \*\*\*P-values<0.001 using Student's t-test. **c, d.** Confocal analysis of wild type (WT) and IFT20<sup>-/-</sup> MEFs cells cultured during 24h in absence of serum and processed for immunofluorescence using DAPI, anti-ARL13B (**c**) and anti-GM130 (**d**) antibodies. Scale bars: 10µm.

### **Supplementary Figure 3. ATG16L1 does not phenocopy endogenous ATG16L1**

**a.** Confocal analysis of MEFs cells transiently transfected with ATG16L1<sup>GFP</sup> expression vector, cultured during 24h in absence of serum and processed for immunofluorescence using anti-ATG16L1 antibody. **b.** Confocal analysis of MEFs cells transiently transfected with ATG16L1<sup>GFP</sup> and Endoplasmic Reticulum marker Sec61β<sup>RFP</sup> expression vectors, cultured during 24h in absence of serum and processed for immunofluorescence using DAPI and anti-acetylated tubulin antibody as marker of PC. Scale bar: 10µm.

### **Supplementary Figure 4. Endogenous IFT20 interacts with ATG16L1, but not with VPS34 and Beclin1 autophagy regulators**

MEFs cells were cultured in presence (+ serum) or 24h in absence of serum (- serum) and processed for co-immunoprecipitations analysis. Total lysates (input) were subjected to immunoprecipitation (IP) using anti-ATG16L1 antibodies. Samples were analyzed by SDS-PAGE and western blotting with anti-ATG16L1, anti-IFT20, anti-VPS34 and anti-Beclin1 antibodies. OVX: overexposed.

**Supplementary Figure 5. ATG16L1 knockout promotes retention of IFT20 at Golgi**

**a.** Wild type (WT) or ATG16L1<sup>-/-</sup> MEFs were cultured during 24h in absence of serum and processed for immunofluorescence analysis using DAPI and anti-IFT20 antibody. **b.** ATG16L1<sup>-/-</sup> MEFs were cultured during 24h in absence of serum and processed for immunofluorescence analysis using DAPI, anti-IFT20 and anti-GM130 antibodies. Scale bars: 10µm.

## References

- Bento, C. F. *et al.* (2016) 'Mammalian Autophagy: How Does It Work?', *Annual review of biochemistry*, 85(1), pp. 685–713. doi: 10.1146/annurev-biochem-060815-014556.
- Bielas, S. L. *et al.* (2009) 'Mutations in INPP5E, encoding inositol polyphosphate-5-phosphatase E, link phosphatidyl inositol signaling to the ciliopathies.', *Nature genetics*, 41(9), pp. 1032–6. doi: 10.1038/ng.423.
- Boada-Romero, E. *et al.* (2013) 'TMEM59 defines a novel ATG16L1-binding motif that promotes local activation of LC3.', *The EMBO journal*, 32(4), pp. 566–82. doi: 10.1038/emboj.2013.8.
- Boukhalifa, A. *et al.* (2019) 'Interplay between Primary cilia, Ubiquitin-Proteasome system and Autophagy', *Biochimie*. doi: 10.1016/j.biochi.2019.06.009.
- Boya, P., Reggiori, F. and Codogno, P. (2013) 'Emerging regulation and functions of autophagy', *Nat Cell Biol*, 15(7), pp. 713–720. Available at: [http://www.ncbi.nlm.nih.gov/entrez/query.fcgi?cmd=Retrieve&db=PubMed&dopt=Citation&list\\_uids=23817233](http://www.ncbi.nlm.nih.gov/entrez/query.fcgi?cmd=Retrieve&db=PubMed&dopt=Citation&list_uids=23817233).
- Braun, D. A. and Hildebrandt, F. (2017) 'Ciliopathies.', *Cold Spring Harbor perspectives in biology*, 9(3), p. a028191. doi: 10.1101/cshperspect.a028191.
- Cao, M. and Zhong, Q. (2016) 'Cilia in autophagy and cancer', *Cilia*. BioMed Central, 5, p. 4. doi: 10.1186/S13630-016-0027-3.
- Chávez, M. *et al.* (2015) 'Modulation of Ciliary Phosphoinositide Content Regulates Trafficking and Sonic Hedgehog Signaling Output.', *Developmental cell*, 34(3), pp. 338–50. doi: 10.1016/j.devcel.2015.06.016.
- Cloonan, S. M. *et al.* (2014) "Ciliophagy", *Autophagy*, 10(3), pp. 532–534. doi:

10.4161/auto.27641.

Dudley, L. J. *et al.* (2019) 'Intrinsic lipid binding activity of ATG16L1 supports efficient membrane anchoring and autophagy.', *The EMBO journal*, 38(9). doi: 10.15252/emj.2018100554.

Finetti, F. *et al.* (2019) 'The intraflagellar transport protein IFT20 controls lysosome biogenesis by regulating the post-Golgi transport of acid hydrolases.', *Cell death and differentiation*. doi: 10.1038/s41418-019-0357-y.

Fletcher, K. *et al.* (2018) 'The WD 40 domain of ATG 16L1 is required for its non-canonical role in lipidation of LC 3 at single membranes', *The EMBO Journal*, 37(4). doi: 10.15252/emj.201797840.

Follit, J. A. *et al.* (2006) 'The Intraflagellar Transport Protein IFT20 Is Associated with the Golgi Complex and Is Required for Cilia Assembly □ V', *Molecular Biology of the Cell*, 17, pp. 3781–3792. doi: 10.1091/mbc.E06.

Fry, A. M., Leaper, M. J. and Bayliss, R. (2014) 'The primary cilium', *Organogenesis*, 10(1), pp. 62–68. doi: 10.4161/org.28910.

Fujita, N. *et al.* (2008) 'The Atg16L Complex Specifies the Site of LC3 Lipidation for Membrane Biogenesis in Autophagy', *Molecular Biology of the Cell*. Edited by H. Riezman, 19(5), pp. 2092–2100. doi: 10.1091/mbc.e07-12-1257.

Garcia-Gonzalo, F. R. *et al.* (2015) 'Phosphoinositides Regulate Ciliary Protein Trafficking to Modulate Hedgehog Signaling', *Developmental Cell*. Cell Press, 34(4), pp. 400–409. doi: 10.1016/J.DEVCEL.2015.08.001.

Goetz, S. C. and Anderson, K. V (2010) 'The primary cilium: a signalling centre during

vertebrate development.', *Nature reviews. Genetics*, 11(5), pp. 331–44. doi: 10.1038/nrg2774.

He, M., Agbu, S. and Anderson, K. V (2017) 'Microtubule Motors Drive Hedgehog Signaling in Primary Cilia.', *Trends in cell biology*, 27(2), pp. 110–125. doi: 10.1016/j.tcb.2016.09.010.

Izawa, I. *et al.* (2015) 'Current topics of functional links between primary cilia and cell cycle.', *Cilia*, 4(1), p. 12. doi: 10.1186/s13630-015-0021-1.

Jacoby, M. *et al.* (2009) 'INPP5E mutations cause primary cilium signaling defects, ciliary instability and ciliopathies in human and mouse', *Nature Genetics*, 41(9), pp. 1027–1031. doi: 10.1038/ng.427.

Joffre, C. *et al.* (2015) 'The Pro-apoptotic STK38 Kinase Is a New Beclin1 Partner Positively Regulating Autophagy.', *Current biology : CB*, 25(19), pp. 2479–92. doi: 10.1016/j.cub.2015.08.031.

Kim, S. and Dynlacht, B. D. (2013) 'Assembling a primary cilium', *Current Opinion in Cell Biology*, 25(4), pp. 506–511. doi: 10.1016/j.ceb.2013.04.011.

De La Iglesia, F. A. and Porta, E. A. (1967) 'Ciliated biliary epithelial cells in the livers of non-human primates.', *Experientia*, 23(1), pp. 49–51. doi: 10.1007/bf02142263.

Lam, H. C. *et al.* (2013) 'Histone deacetylase 6-mediated selective autophagy regulates COPD-associated cilia dysfunction', *J Clin Invest.* 2013/11/10, 123(12), pp. 5212–5230. doi: 69636 [pii]10.1172/JCI69636.

Levine, B. and Kroemer, G. (2019) 'Biological Functions of Autophagy Genes: A Disease Perspective.', *Cell*, 176(1–2), pp. 11–42. doi: 10.1016/j.cell.2018.09.048.

Li, J. *et al.* (2017) 'Transiently expressed ATG16L1 inhibits autophagosome biogenesis and aberrantly targets RAB11-positive recycling endosomes.', *Autophagy*, 13(2), pp. 345–358. doi:

10.1080/15548627.2016.1256521.

Liem, K. F. *et al.* (2012) 'The IFT-A complex regulates Shh signaling through cilia structure and membrane protein trafficking', *The Journal of Cell Biology*, 197(6), pp. 789–800. doi: 10.1083/jcb.201110049.

Luo, N., Lu, J. and Sun, Y. (2012) 'Evidence of a role of inositol polyphosphate 5-phosphatase INPP5E in cilia formation in zebrafish', *Vision Research*, 75, pp. 98–107. doi: 10.1016/j.visres.2012.09.011.

Malicki, J. J. and Johnson, C. A. (2017) 'The Cilium: Cellular Antenna and Central Processing Unit.', *Trends in cell biology*, 27(2), pp. 126–140. doi: 10.1016/j.tcb.2016.08.002.

Morleo, M. and Franco, B. (2019) 'The Autophagy-Cilia Axis: An Intricate Relationship', *Cells*, 8(8), p. 905. doi: 10.3390/cells8080905.

Nachury, M. V (2011) 'Trafficking to the ciliary membrane', *Annual Review of Cell and Developmental Biology*, 26, pp. 59–87. doi: 10.1146/annurev.cellbio.042308.113337.Trafficking.

Nachury, M. V and Mick, D. U. (2019) 'Establishing and regulating the composition of cilia for signal transduction.', *Nature reviews. Molecular cell biology*, 20(7), pp. 389–405. doi: 10.1038/s41580-019-0116-4.

Nakatsu, F. (2015) 'A Phosphoinositide Code for Primary Cilia.', *Developmental cell*, 34(4), pp. 379–80. doi: 10.1016/j.devcel.2015.08.008.

Nascimbeni, A. C., Codogno, P. and Morel, E. (2017) 'Phosphatidylinositol-3-phosphate in the regulation of autophagy membrane dynamics', *The FEBS Journal*, 284(9), pp. 1267–1278. doi: 10.1111/febs.13987.

Nishida-Fukuda, H. (2019) 'The Exocyst: Dynamic Machine or Static Tethering Complex?',

*BioEssays*, 41(8), p. 1900056. doi: 10.1002/bies.201900056.

Orhon, I. *et al.* (2014) 'Autophagy and regulation of cilia function and assembly', *Cell Death and Differentiation*. Nature Publishing Group, 22(3), pp. 389–397. doi: 10.1038/cdd.2014.171.

Orhon, I. *et al.* (2016) 'Primary-cilium-dependent autophagy controls epithelial cell volume in response to fluid flow.', *Nature cell biology*, 18(6), pp. 657–67. doi: 10.1038/ncb3360.

Pampliega, O. *et al.* (2013) 'Functional interaction between autophagy and ciliogenesis.', *Nature*, 502(7470), pp. 194–200. doi: 10.1038/nature12639.

Di Paolo, G. and De Camilli, P. (2006) 'Phosphoinositides in cell regulation and membrane dynamics', *Nature*, 443(7112), pp. 651–657. doi: 10.1038/nature05185.

Phua, S. C., Nihongaki, Y. and Inoue, T. (2018) 'Autonomy declared by primary cilia through compartmentalization of membrane phosphoinositides.', *Current opinion in cell biology*, 50, pp. 72–78. doi: 10.1016/j.ceb.2018.01.008.

Reiter, J. F. and Leroux, M. R. (2017) 'Genes and molecular pathways underpinning ciliopathies.', *Nature reviews. Molecular cell biology*, 18(9), pp. 533–547. doi: 10.1038/nrm.2017.60.

Rohatgi, R., Milenkovic, L. and Scott, M. P. (2007) 'Patched1 Regulates Hedgehog Signaling at the Primary Cilium', *Science*, 317(5836), pp. 372–376. doi: 10.1126/science.1139740.

Satir, P., Pedersen, L. B. and Christensen, S. T. (2010) 'The primary cilium at a glance.', *Journal of cell science*, 123(Pt 4), pp. 499–503. doi: 10.1242/jcs.050377.

Schink, K. O., Tan, K.-W. and Stenmark, H. (2016) 'Phosphoinositides in Control of Membrane Dynamics.', *Annual review of cell and developmental biology*. doi: 10.1146/annurev-cellbio-111315-125349.

Shewan, A., Eastburn, D. J. and Mostov, K. (2011) 'Phosphoinositides in cell architecture', *Cold Spring Harbor Perspectives in Biology*, 3(8), pp. 1–17. doi: 10.1101/cshperspect.a004796.

Tang, Z. *et al.* (2013) 'Autophagy promotes primary ciliogenesis by removing OFD1 from centriolar satellites', *Nature*. 2013/10/04, 502(7470), pp. 254–257. doi: 10.1038/nature12606.

Tanida, I. *et al.* (2006) 'Atg8L/Apg8L is the fourth mammalian modifier of mammalian Atg8 conjugation mediated by human Atg4B, Atg7 and Atg3', *FEBS Journal*, 273(11), pp. 2553–2562. doi: 10.1111/j.1742-4658.2006.05260.x.

Wang, L. and Dynlacht, B. D. (2018) 'The regulation of cilium assembly and disassembly in development and disease', *Development*, 145(18), p. dev151407. doi: 10.1242/dev.151407.

Wheatley, D. N. (1969) 'Cilia in cell-cultured fibroblasts. I. On their occurrence and relative frequencies in primary cultures and established cell lines.', *Journal of anatomy*, 105(Pt 2), pp. 351–62. Available at: <http://www.ncbi.nlm.nih.gov/pubmed/4308456> (Accessed: 24 September 2019).

Wu, B. and Guo, W. (2015) 'The Exocyst at a Glance', *Journal of Cell Science*, 128(16), pp. 2957–2964. doi: 10.1242/jcs.156398.

Xu, C. and Min, J. (2011) 'Structure and function of WD40 domain proteins.', *Protein & cell*, 2(3), pp. 202–14. doi: 10.1007/s13238-011-1018-1.

Xu, Q. *et al.* (2016) 'Phosphatidylinositol phosphate kinase PIPK1γ and phosphatase INPP5E coordinate initiation of ciliogenesis.', *Nature communications*, 7(1), p. 10777. doi: 10.1038/ncomms10777.

Xu, W. *et al.* (2017) 'The Joubert Syndrome Protein Inpp5e Controls Ciliogenesis by Regulating Phosphoinositides at the Apical Membrane', *Journal of the American Society of Nephrology*,

28(1), pp. 118–129. doi: 10.1681/ASN.2015080906.

Zavodszky, E., Vicinanza, M. and Rubinsztein, D. C. (2013) 'Biology and trafficking of ATG9 and ATG16L1, two proteins that regulate autophagosome formation', *FEBS Letters*, 587(13), pp. 1988–1996. doi: 10.1016/j.febslet.2013.04.025.

Zemirli, N. *et al.* (2019) 'The primary cilium protein folliculin is part of the autophagy signaling pathway to regulate epithelial cell size in response to fluid flow', *Cell Stress*. Shared Science Publishers, 3(3), pp. 100–109. doi: 10.15698/cst2019.03.180.

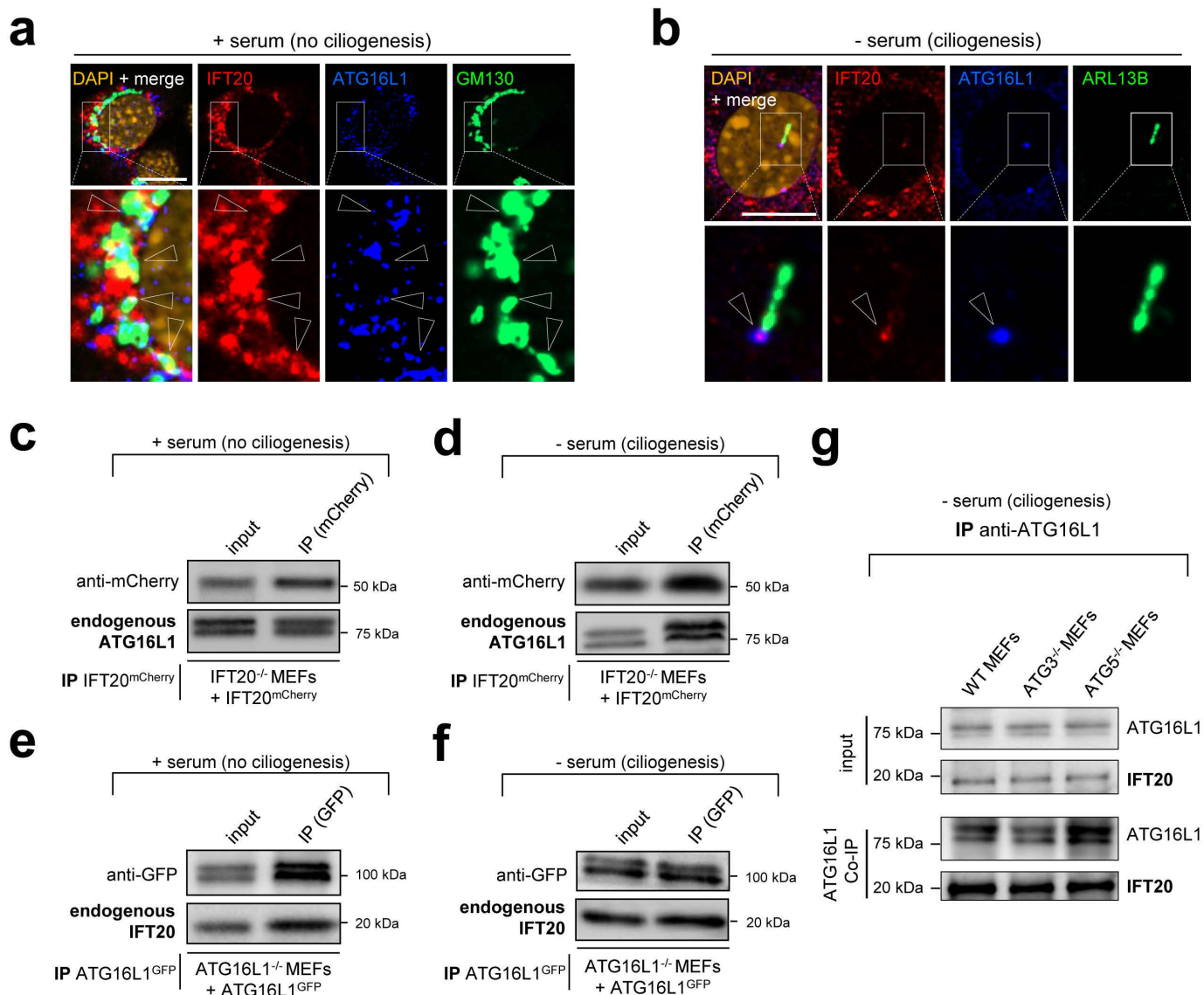


**Figure 1. ATG16L1 is present at PC in ciliated cells and interacts with IFT20.**

**a, b.** confocal analysis of MEFs cells cultured in presence **(a)** or 24h absence of serum **(b)** and processed for immunofluorescence using DAPI, anti-IFT20, anti-ATG16L1 and anti-GM130 **(a)** or anti-ARL13B **(b)** antibodies. Arrowheads show ATG16L1/IFT20 codistribution at Golgi structures positive for GM130 **(a)** and at the base of the primary cilium (PC) in **(b)**. Scale bars: 10 $\mu$ m. **c, d.** IFT20<sup>-/-</sup> MEFs were transiently transfected with IFT20<sup>mCherry</sup> expression vector, cultured in presence **(c)** or 24h absence of serum **(d)** and processed for co-immunoprecipitations analysis. Total lysates (input) were subjected to immunoprecipitation (IP) with mCherry/RFP-trap beads. Samples were analyzed by SDS-PAGE and western blotting with anti-mCherry and anti-ATG16L1 antibodies. **e, f.** ATG16L1<sup>-/-</sup> MEFs were transiently transfected with ATG16L1<sup>GFP</sup> expression vector, cultured in presence **(e)** or 24h absence of serum **(f)** and processed for co-immunoprecipitations analysis. Total lysates (input) were subjected to immunoprecipitation (IP) with GFP-trap beads. Samples were analyzed by SDS-PAGE and western blotting with anti-GFP and anti-IFT20 antibodies. **g.** Wild type (WT), ATG3<sup>-/-</sup> and ATG5<sup>-/-</sup> MEFs were cultured during 24h in absence of serum and processed for co-immunoprecipitations analysis. Total lysates (input) were subjected to immunoprecipitation (Co-IP) using anti-ATG16L1 antibodies. Samples were analyzed by SDS-PAGE and western blotting with anti-ATG16L1 and anti-IFT20 antibodies.

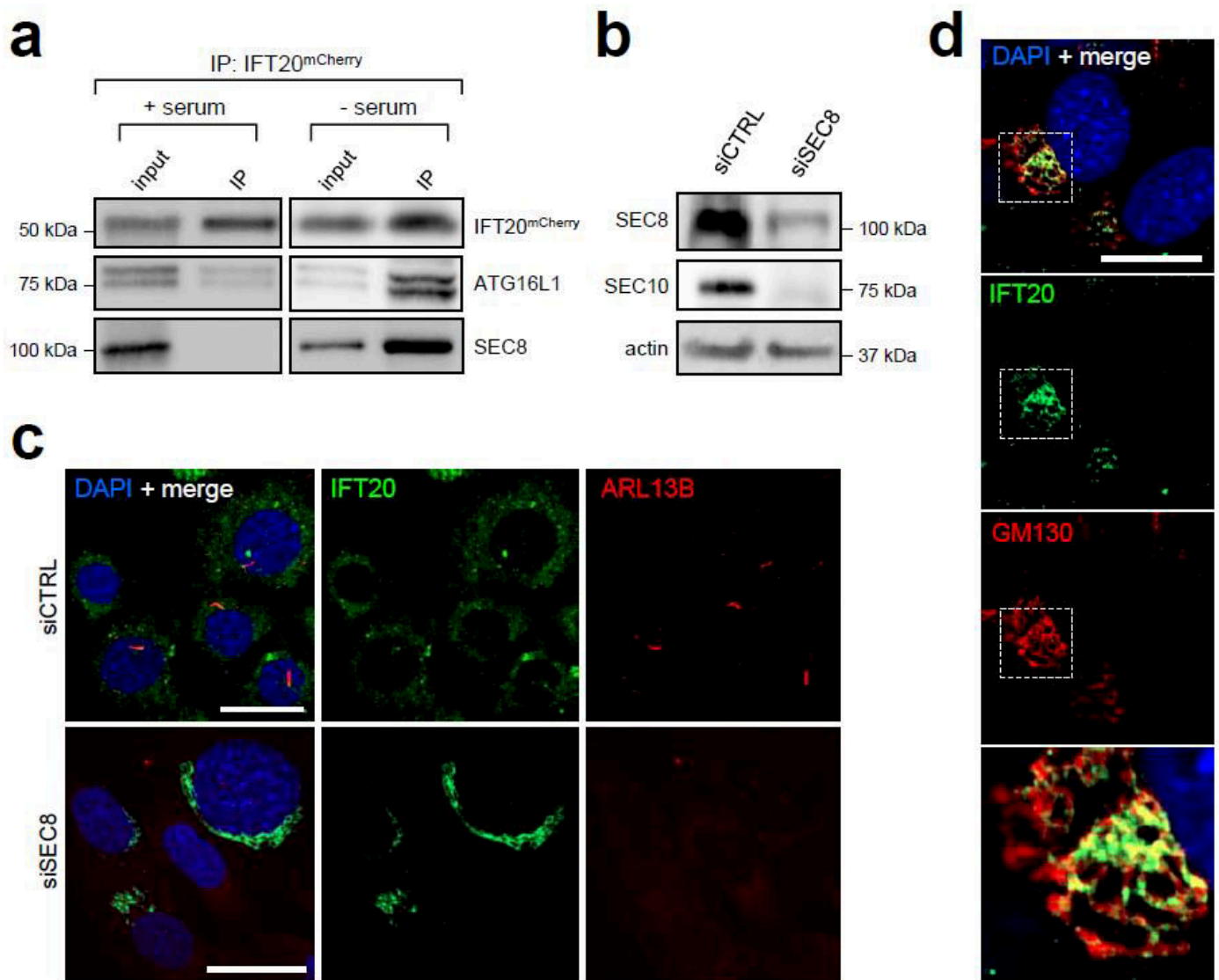


**Figure 2. The exocyst Sec8 component is present in the ATG16L1/IFT20 complex only in ciliated cells**

**a.** IFT20<sup>-/-</sup> MEFs were transiently transfected with IFT20<sup>mCherry</sup> expression vector, cultured in presence (+ serum) or 24h absence of serum (- serum) and processed for co-immunoprecipitations analysis. Total lysates (input) were subjected to immunoprecipitation (IP) with mCherry/RFP-trap beads. Samples were analyzed by SDS-PAGE and western blotting with anti-mCherry, anti-ATG16L1 and anti-SEC8 antibodies. **b.** MEFs cells were transfected with SEC8 siRNA or control siRNA (siCTRL), cultured during 24h in absence of serum and processed for western blotting analysis with anti-SEC8, anti-SEC10 and anti-actin antibodies. **c.** Confocal analysis of MEFs cells transfected with SEC8 siRNA or control siRNA (siCTRL), cultured during 24h in absence of serum and processed for immunofluorescence using anti-IFT20 and ARL13B antibodies. **d.** Confocal analysis of MEFs cells transfected with SEC8 siRNA, cultured during 24h in absence of serum and processed for immunofluorescence using anti-IFT20 and anti-GM130 antibodies. Scale bars: 10 μm.

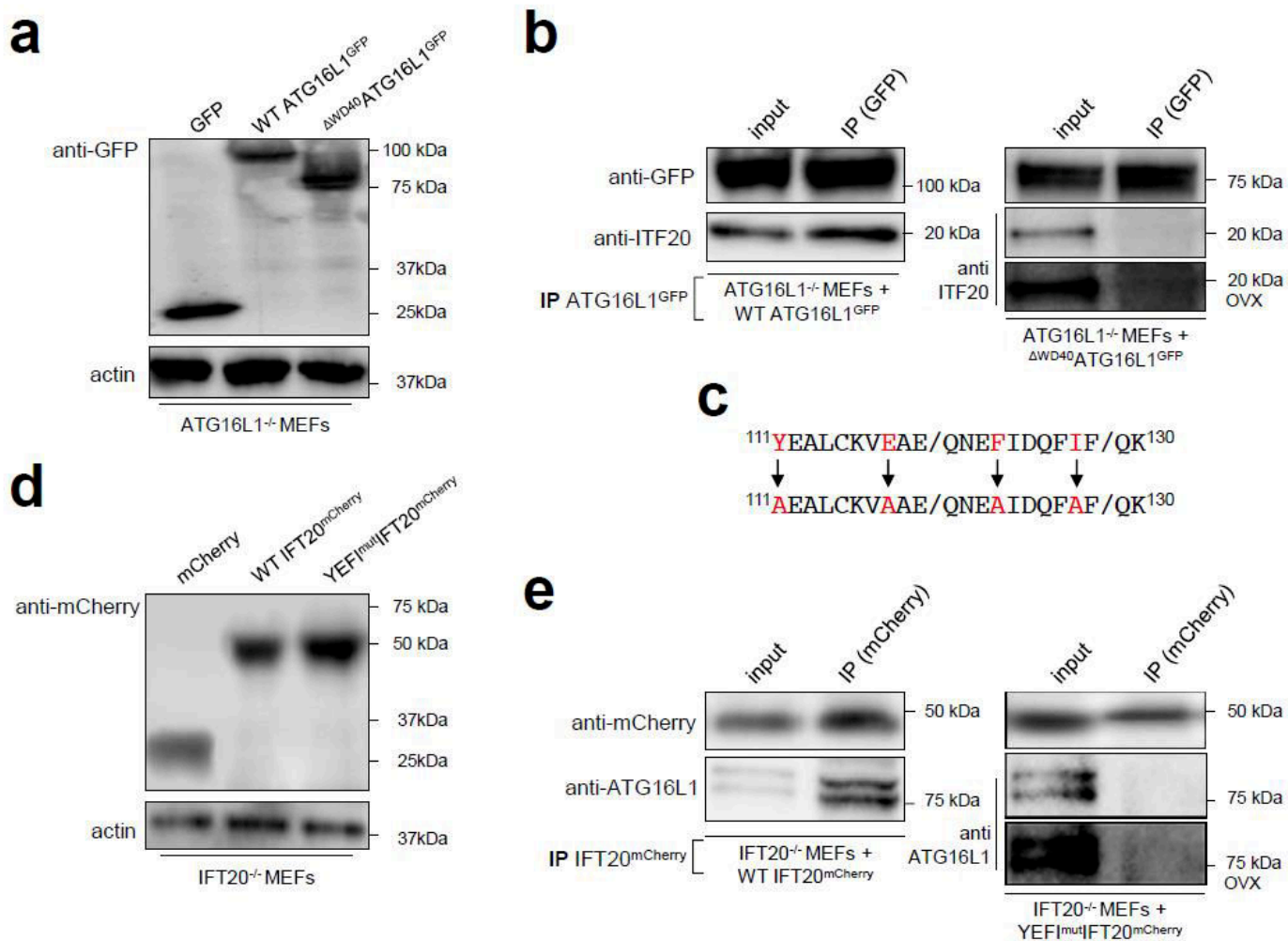


**Figure 3. ATG16L1/IFT20 interacting domains.**

**a, b.** ATG16L1<sup>-/-</sup> MEFs were transiently transfected with empty GFP, wild-type (WT) ATG16L1<sup>GFP</sup> and ΔWD40-ATG16L1<sup>GFP</sup> expression vectors, cultured during 24h in absence of serum and processed for western blotting analysis (**a**) and for co-immunoprecipitations analysis (**b**). Total lysates (input) were subjected to immunoprecipitation (IP) with GFP-trap beads and samples were analyzed by SDS-PAGE and western blotting with anti-GFP and anti-IFT20 antibodies. **c.** 111 to 130 amino acids sequence of human IFT20 protein. The key residues mutated (Y, E, F and I) in the putative ATG16L1 binding sequence are highlighted in red and “YEF1 mutant” version of IFT20 is shown (lower sequence, with alanines replacing the YEFI residues). **d, e.** IFT20<sup>-/-</sup> MEFs were transiently transfected with empty mCherry, wild-type (WT) IFT20<sup>mCherry</sup> and YEF1 mutant of IFT20<sup>GFP</sup> expression vectors, cultured during 24h in absence of serum and processed for western blotting analysis (**d**) and for co-immunoprecipitations analysis (**e**). Total lysates (input) were subjected to immunoprecipitation (IP) with mCherry/RFP-trap beads and samples were analyzed by SDS-PAGE and western blotting with anti-mCherry and anti-ATG16L1 antibodies. OVX: overexposed.

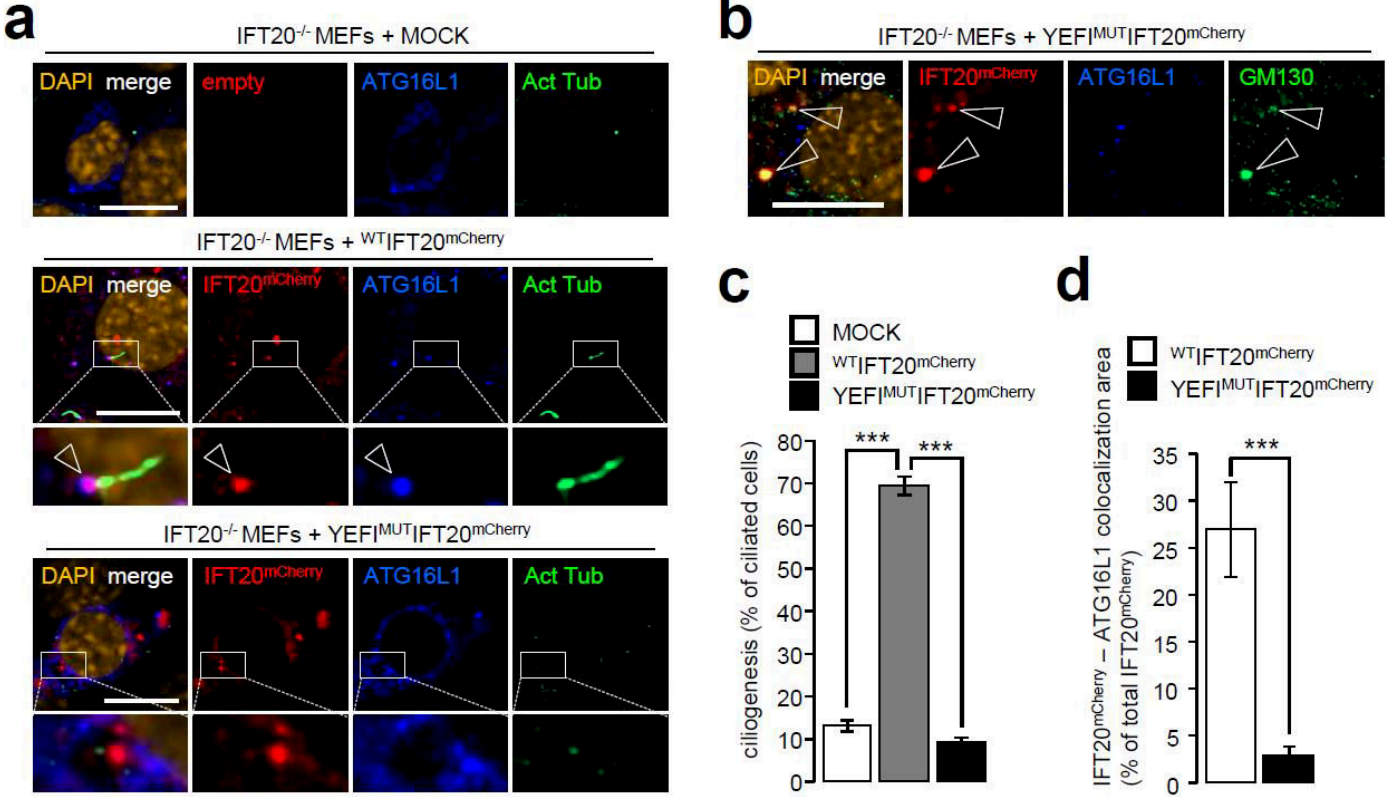


**Figure 4. Loss of ATG16L1 binding motif in IFT20 leads to IFT20 Golgi retention and ciliogenesis defect.**  
**a.** IFT20<sup>-/-</sup> MEFs were transiently transfected with wild-type (WT) IFT20<sup>mCherry</sup> (middle panel) and YEF1 mutant of IFT20<sup>mCherry</sup> (lower panel) expression vectors or not (mock, upper panel), cultured during 24h in absence of serum and processed for immunofluorescence analysis using anti-acetylated tubulin and anti-ATG16L1. Arrowheads show WT-IFT20<sup>mCherry</sup> colocalization with endogenous ATG16L1 at the base of PC (**a**, middle panel). **b.** IFT20<sup>-/-</sup> MEFs were transiently transfected with YEF1 mutant of IFT20<sup>mCherry</sup> (lower panel) expression vectors cultured during 24h in absence of serum and processed for immunofluorescence analysis using anti-GM130 and anti-ATG16L1. Arrowheads show YEF1 mutant of IFT20<sup>mCherry</sup> colocalization with GM130 and absence of colocalization with ATG16L1. **c.** Bar diagram showing the quantification of ciliogenesis (as expressed by the percentage of ciliated cells) in wild-type (WT) IFT20<sup>mCherry</sup> and YEF1 mutant of IFT20<sup>mCherry</sup> conditions. **d.** Bar diagram showing the quantification of endogenous ATG16L1/IFT20<sup>mCherry</sup> colocalization area (as expressed by percentage of total IFT20<sup>mCherry</sup> signal) in wild-type (WT) IFT20<sup>mCherry</sup> and YEF1 mutant of IFT20<sup>mCherry</sup> conditions. Values denote means  $\pm$  S.E.M. \*\*\*P-values<0.001 using Student's t-test.

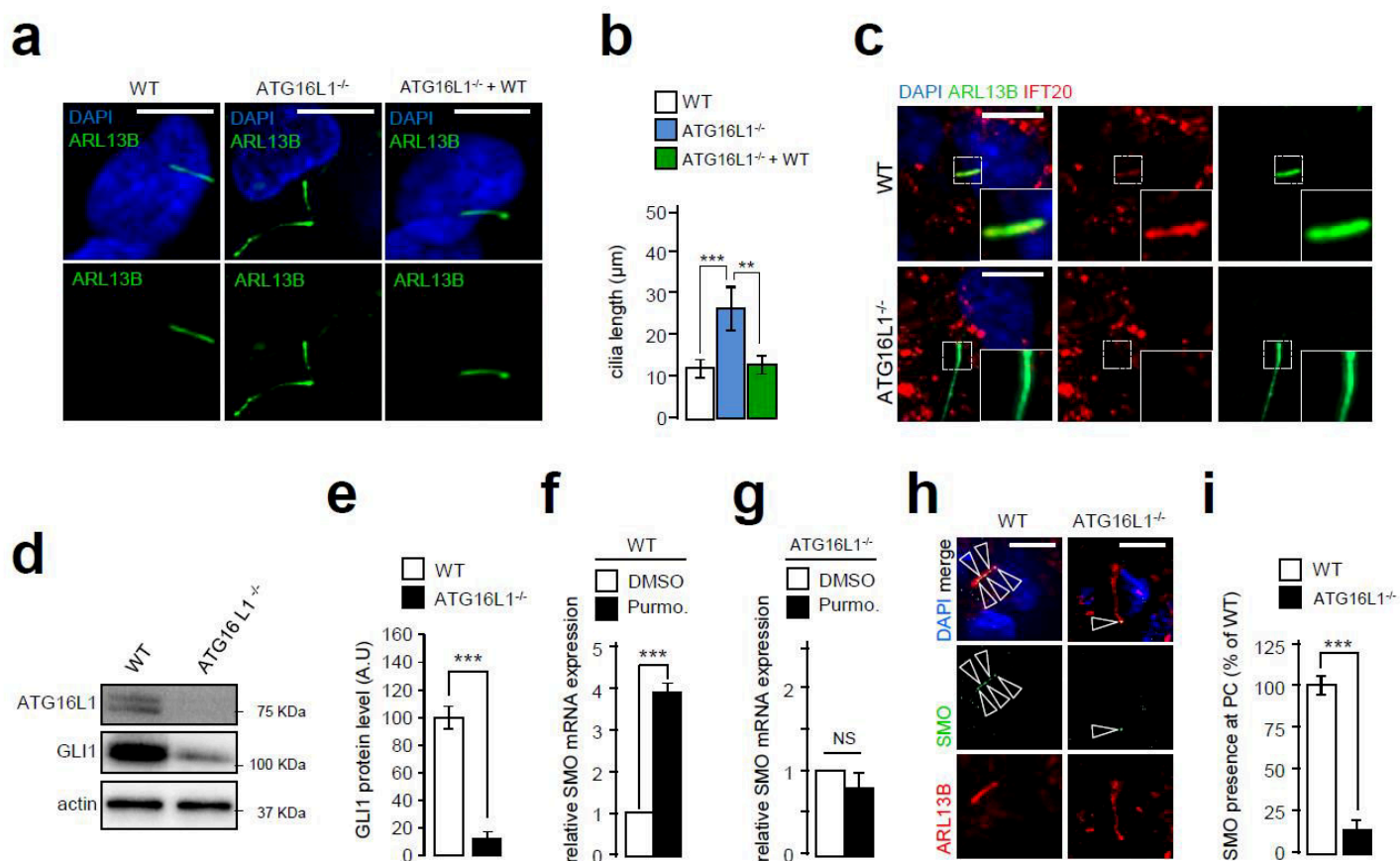


**Figure 5. ATG16L1 knockout promotes aberrant ciliogenesis and alters ciliary signaling.**

**a.** Wild type (WT) or ATG16L1<sup>-/-</sup> MEFs transiently transfected (or not) with wild-type (WT) ATG16L1<sup>GFP</sup> expression vectors were cultured during 24h in absence of serum and processed for immunofluorescence analysis using DAPI and anti-ARL13B antibody. **b.** Bar graphs showing the quantification of PC axoneme length measured via ARL13B staining (as shown in **a**) in wild type (WT) MEFs or in ATG16L1<sup>-/-</sup> MEFs transfected with wild-type (WT) ATG16L1<sup>GFP</sup>. Values denote means  $\pm$  S.E.M. \*\*\*P-values<0.001 and \*\*P-values<0.01, using Student's t-test. **c.** Wild type (WT) or ATG16L1<sup>-/-</sup> MEFs were cultured during 24h in absence of serum and processed for immunofluorescence analysis using DAPI and anti-ARL13B and anti-IFT20 antibodies. **d, e.** Wild type (WT) or ATG16L1<sup>-/-</sup> MEFs were cultured during 24h in absence of serum and processed for western blotting analysis using anti-ATG16L1, anti GLI1 and anti-actin antibodies (**d**). **e.** Bar diagram showing the quantification of relative GLI1 protein levels shown in (**d**) in wild type (WT) or ATG16L1<sup>-/-</sup> MEFs. A.U.: arbitrary units. Values denote means  $\pm$  S.E.M. \*\*\*P-values<0.001 using Student's t-test. **f, g.** Wild type (WT, (**f**) or ATG16L1<sup>-/-</sup> (**g**) MEFs were cultured during 24h in absence of serum, stimulated (or not, DMSO) with 5µM of Smoothened (SMO) agonist purmorphamine and processed for SMO mRNA quantification. **h, i.** Wild type (WT) or ATG16L1<sup>-/-</sup> MEFs were cultured during 24h in absence of serum and processed for immunofluorescence analysis using DAPI, anti-ARL13B and anti-SMO antibodies. **i.** Bar diagram showing the quantification of SMO presence at PC (as a percentage of wild-type (WT) condition, as illustrated in (**h**)) in wild type (WT) or ATG16L1<sup>-/-</sup> MEFs. Values denote means  $\pm$  S.E.M. \*\*\*P-values<0.001 using Student's t-test.

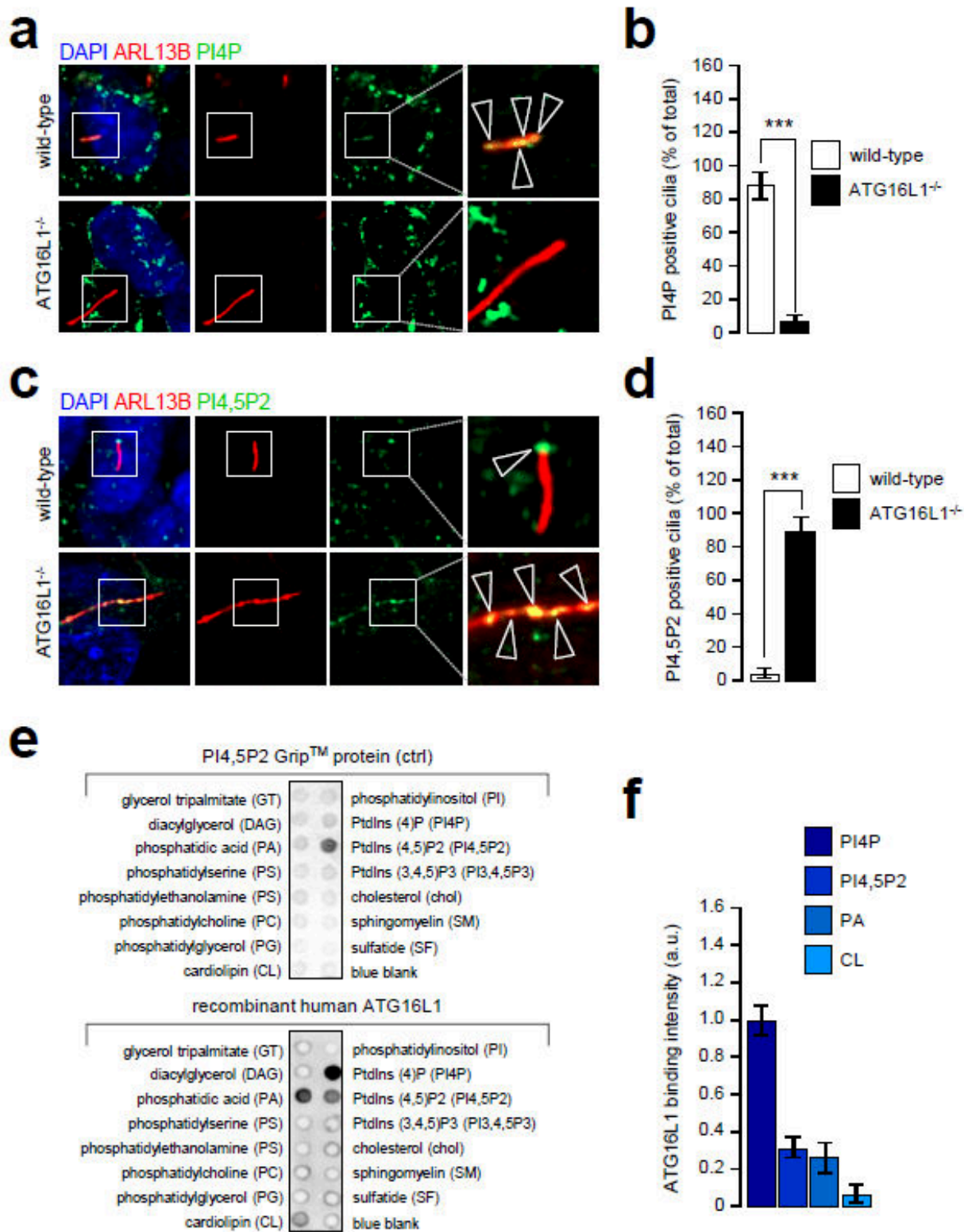


**Figure 6. PC associated PI4P and PI4,5P2 turnover is altered in absence of ATG16L1**

**a, b.** Wild type (WT) or ATG16L1<sup>-/-</sup> MEFs were cultured during 24h in absence of serum and processed for immunofluorescence analysis using DAPI, anti-ARL13B and anti-PI4P antibodies. Arrowheads denote codistribution of PI4P positive *punctae* with PC (only in wild type (WT) condition). **b.** Bar diagram showing the quantification of PI4P positive axoneme (as expressed as a percentage of total cilia), as illustrated in **(a)**, in wild type (WT) or ATG16L1<sup>-/-</sup> MEFs. Values denote means  $\pm$  S.E.M. \*\*\*P-values<0.001 using Student's t-test. **c, d.** Wild type (WT) or ATG16L1<sup>-/-</sup> MEFs were cultured during 24h in absence of serum and processed for immunofluorescence analysis using DAPI, anti-ARL13B and anti-PI4,5P2 antibodies. Arrowheads denote localization of PI4,5P2 only at the base PC (in the wild type cells) or in the axoneme (in ATG16L1<sup>-/-</sup> MEFs). **d.** Bar diagram showing the quantification of PI4,5P2 positive axoneme (as expressed as a percentage of total cilia), as illustrated in **(c)**, in wild type (WT) or ATG16L1<sup>-/-</sup> MEFs. Values denote means  $\pm$  S.E.M. \*\*\*P-values<0.001 using Student's t-test. **e, f.** Lipid strip probed with Gip<sup>TM</sup> protein positive control for PI4,5P2 (upper panel) and with human recombinant ATG16L1, followed by secondary antibody conjugated with peroxidase for visualization. **f.** Bar diagram showing the quantification of recombinant ATG16L1 binding on lipid strip with positive values: PI4P, PI4,5P2, phosphatidic acid (PA) and cardiolipin (CL).

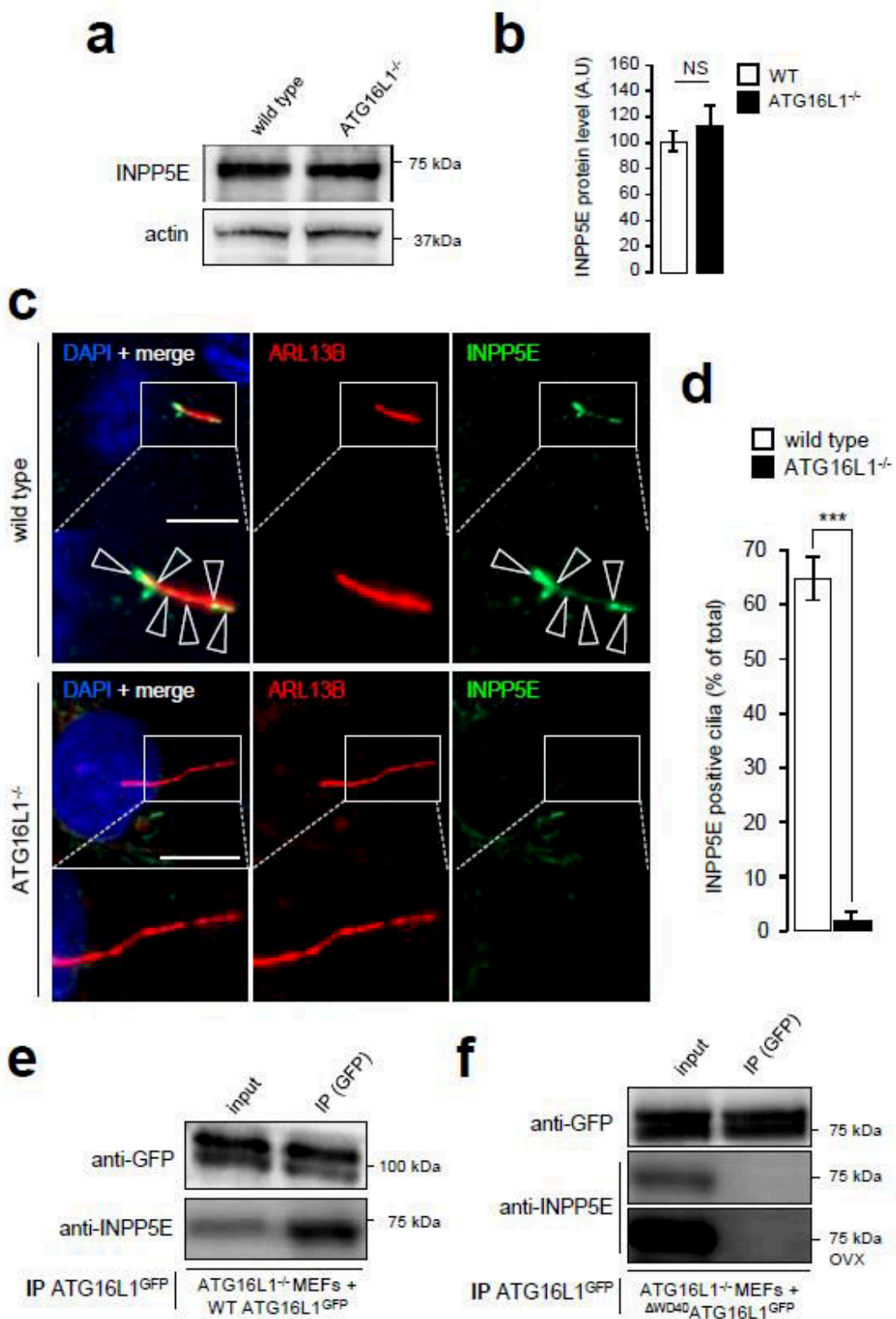
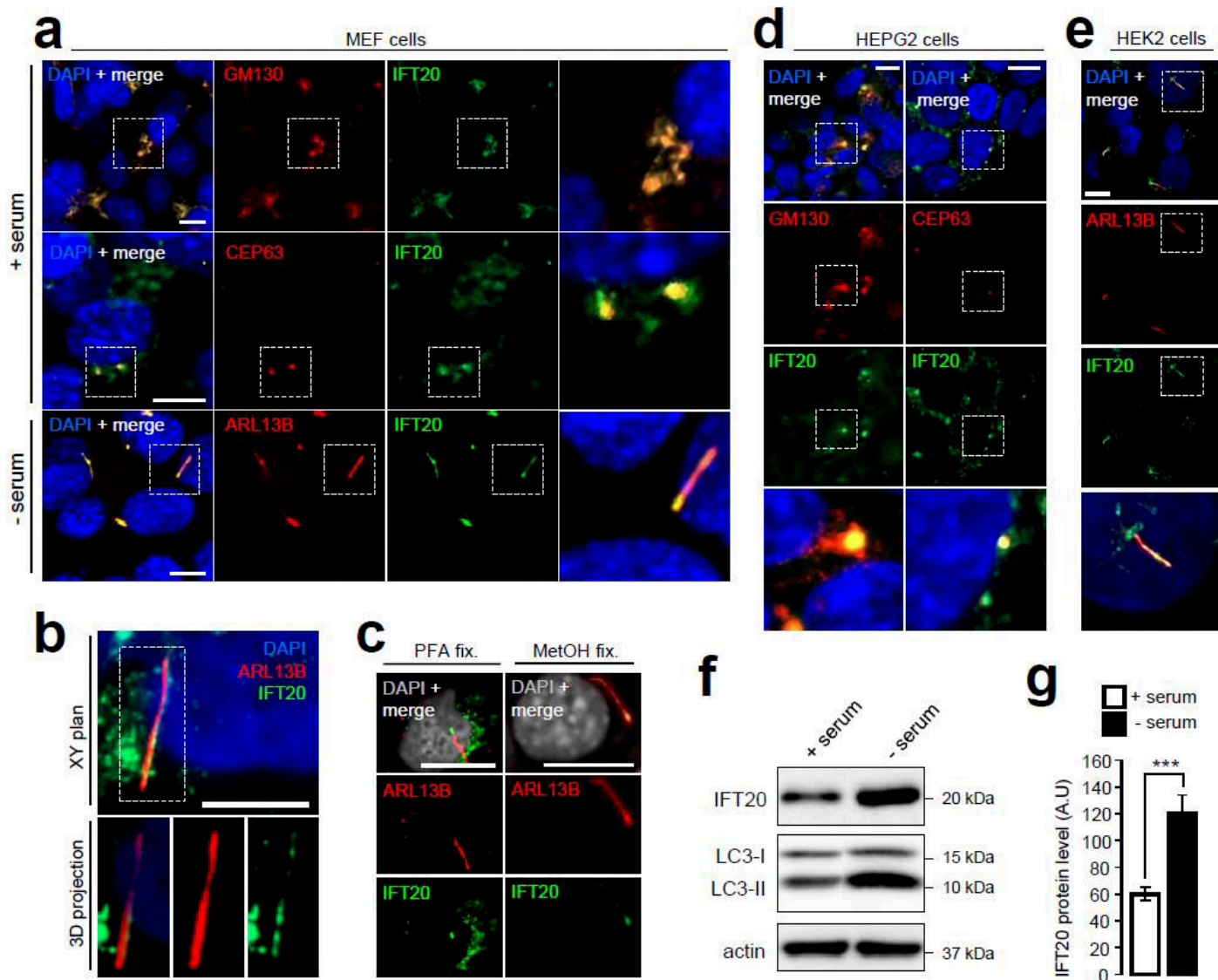


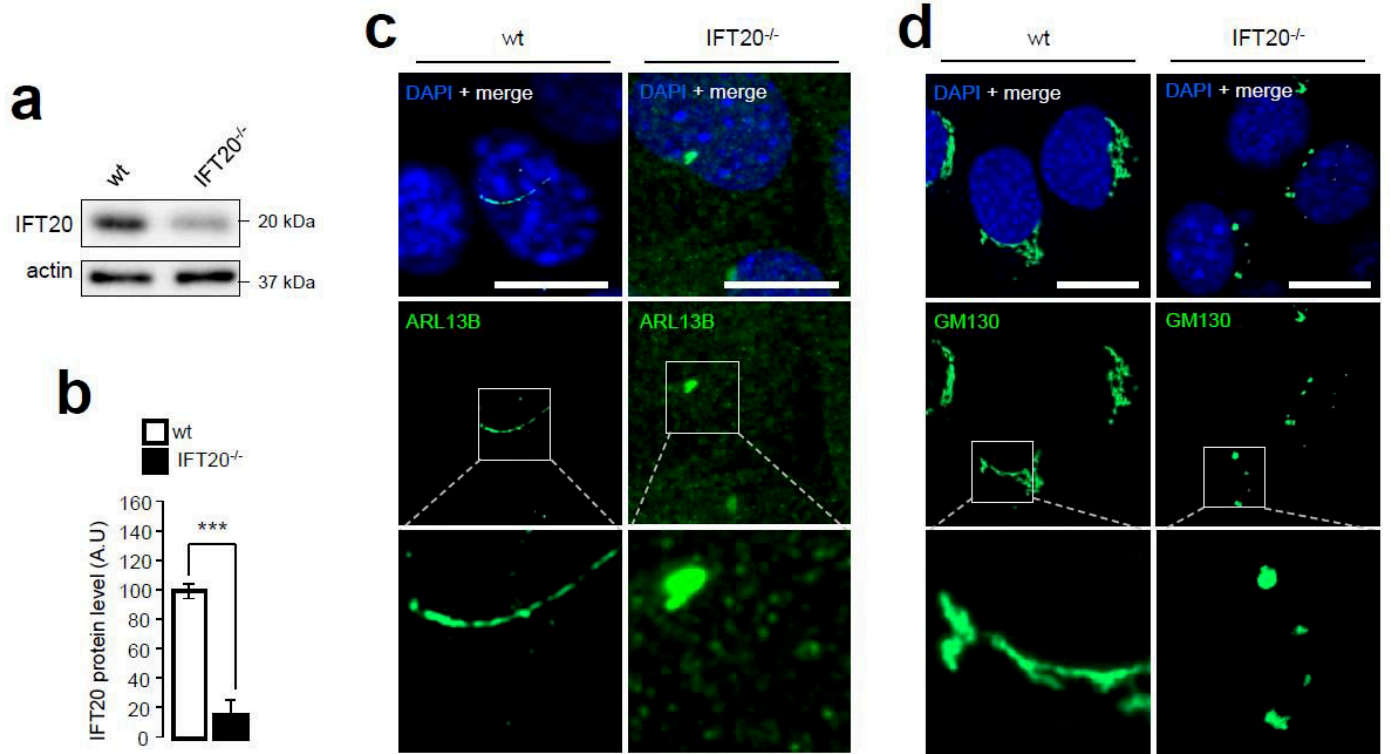
**Figure 7. The INPP5E phosphatase is a key partner of ATG16L1 during ciliogenesis**

**a, b.** Wild type (WT) or ATG16L1<sup>-/-</sup> MEFs were cultured during 24h in absence of serum and processed for western blotting analysis using anti-INPP5E and anti-actin antibodies. **b.** Bar diagram showing the quantification of relative INPP5E protein levels shown in **(a)** in wild type (WT) or ATG16L1<sup>-/-</sup> MEFs. A.U.: arbitrary units. Values denote means  $\pm$  S.E.M. NS for not significant. **c, d.** Wild type (WT) or ATG16L1<sup>-/-</sup> MEFs were cultured during 24h in absence of serum and processed for immunofluorescence analysis using DAPI, anti-ARL13B and anti-INPP5E antibodies. Arrowheads denote codistribution of INPP5E positive *punctae* with PC (only in wild type (WT) condition). **b.** Bar diagram showing the quantification of INPP5E positive axoneme (as expressed as a percentage of total cilia), as illustrated in **(c)**, in wild type (WT) or ATG16L1<sup>-/-</sup> MEFs. Values denote means  $\pm$  S.E.M. \*\*\*P-values < 0.001 using Student's t-test. **e, f.** ATG16L1<sup>-/-</sup> MEFs were transiently transfected with wild-type (WT) ATG16L1<sup>GFP</sup> **(e)** or  $\Delta$ WD40-ATG16L1<sup>GFP</sup> **(f)** expression vectors, cultured during 24h in absence of serum and processed for co-immunoprecipitations analysis. Total lysates (input) were subjected to immunoprecipitation (IP) with GFP-trap beads and samples were analyzed by SDS-PAGE and western blotting with anti-GFP and anti-INPP5E antibodies. OVX: overexposed.



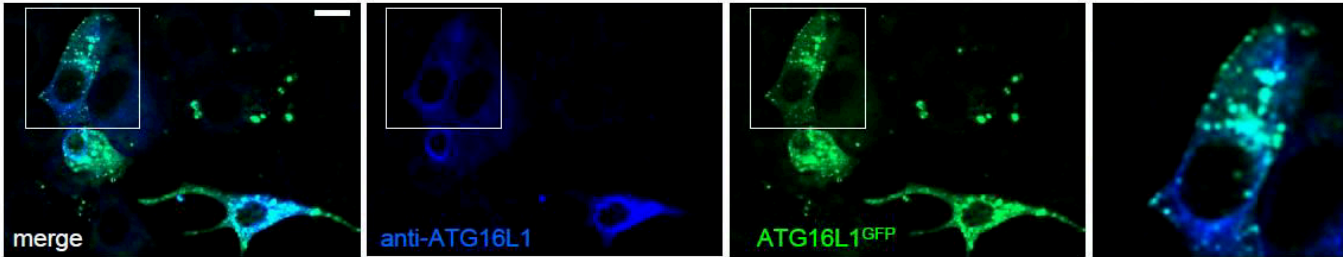
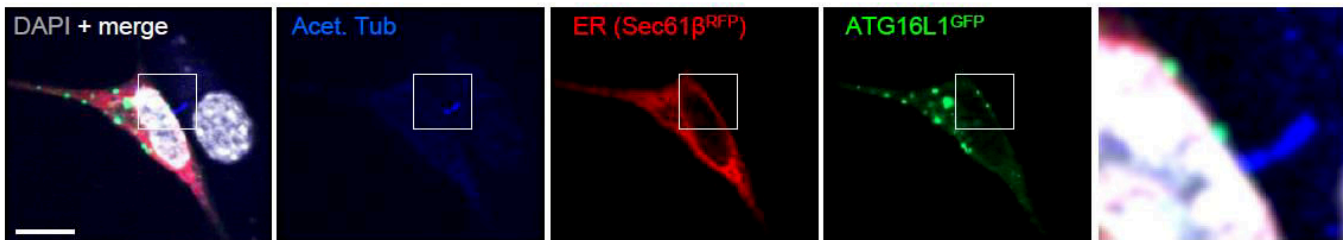
### Supplementary Figure 1. IFT20 subcellular localization in ciliated and non-ciliated cells

**a.** confocal analysis of MEFs cells cultured in presence (+ serum) or 24h absence of serum (- serum) and processed for immunofluorescence using DAPI, anti-IFT20, anti-GM130 (Golgi marker, upper panel), anti-CEP63 (centrosomal marker, middle panel) and anti-ARL13B (primary cilium (PC) marker, lower panel). **b.** 3D confocal acquisition of MEFs cells cultured during 24h in absence of serum and processed for immunofluorescence using DAPI, anti-IFT20, and anti-ARL13B. **c.** Comparison of IFT20 subcellular pattern, using DAPI, anti-IFT20 and anti-ARL13B antibodies, in MEFs cells cultured during 24h in absence of serum and fixed with paraformaldehyde (PFA) or cold methanol (MetOH), showing IFT20 at base of PC in PFA fixation and IFT20 in the PC axoneme in MetOH fixation. **d.** confocal analysis of HEPG2 cells processed for immunofluorescence using DAPI, anti-IFT20, anti-GM130 (Golgi marker, right panel) and anti-CEP63 (centrosomal marker, right panel). **e.** confocal analysis of HEK2 cells cultured for 96h in presence of 1dyn/cm<sup>2</sup> fluid flow inducing shear stress and processed for immunofluorescence using DAPI, anti-IFT20, and anti-ARL13B. Scale bars (**a – e**): 10µm. **f.** MEFs cells were cultured in presence (+ serum) or 24h absence of serum (- serum) and processed for analysis by SDS-PAGE and western blotting using anti-IFT20, anti-LC3 and anti-actin antibodies. **g.** Bar diagram showing the quantification of relative IFT20 levels shown in (**f**) in presence (+ serum) or in absence (- serum) or serum. A.U.: arbitrary units. Values denote means ± S.E.M. \*\*\*P-values<0.001 using Student's t-test.

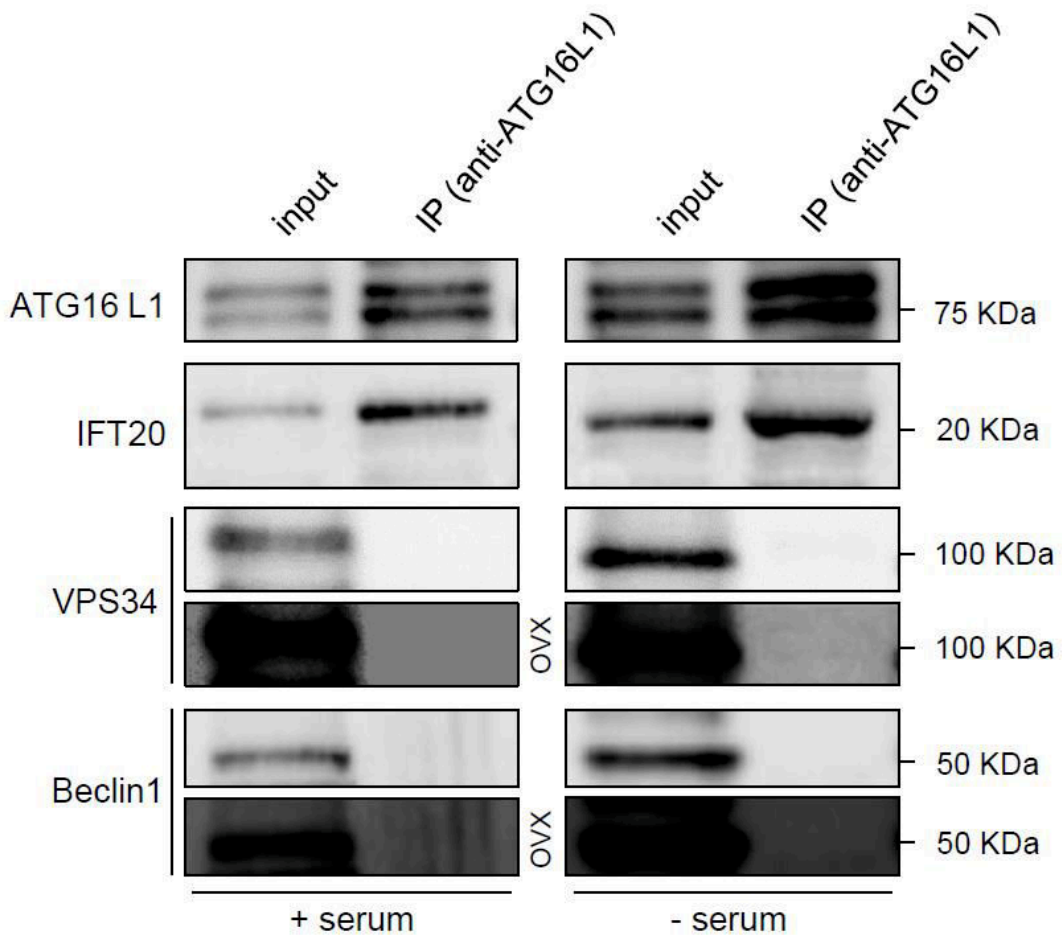


### Supplementary Figure 2. IFT20 knockdown alters ciliogenesis and Golgi morphology

**a.** Wild type (WT) and IFT20<sup>-/-</sup> MEFs cells were processed for analysis by SDS-PAGE and western blotting using anti-IFT20 and anti-actin antibodies. **b.** Bar diagram showing the quantification of relative IFT20 levels shown in **(a)**. A.U.: arbitrary units. Values denote means  $\pm$  S.E.M. \*\*\*P-values<0.001 using Student's t-test. **c, d.** Confocal analysis of wild type (WT) and IFT20<sup>-/-</sup> MEFs cells cultured during 24h in absence of serum and processed for immunofluorescence using DAPI, anti-ARL13B (**c**) and anti-GM130 (**d**) antibodies. Scale bars: 10 $\mu$ m.

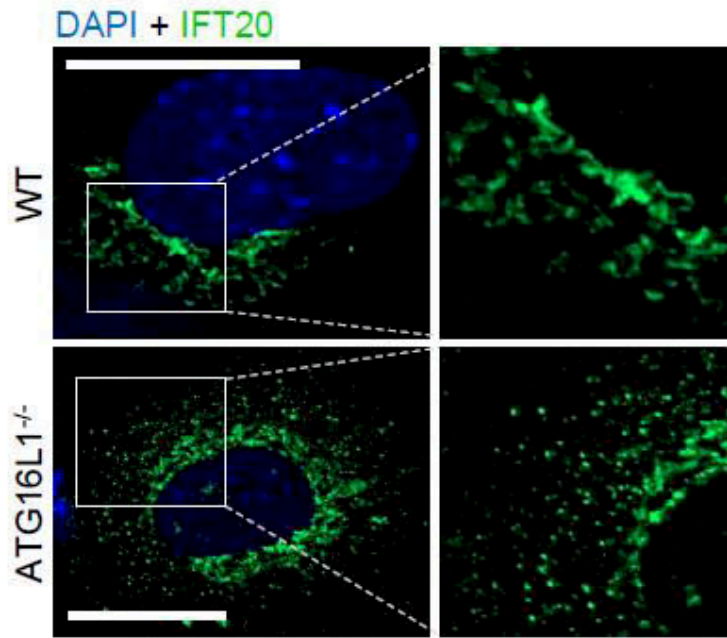
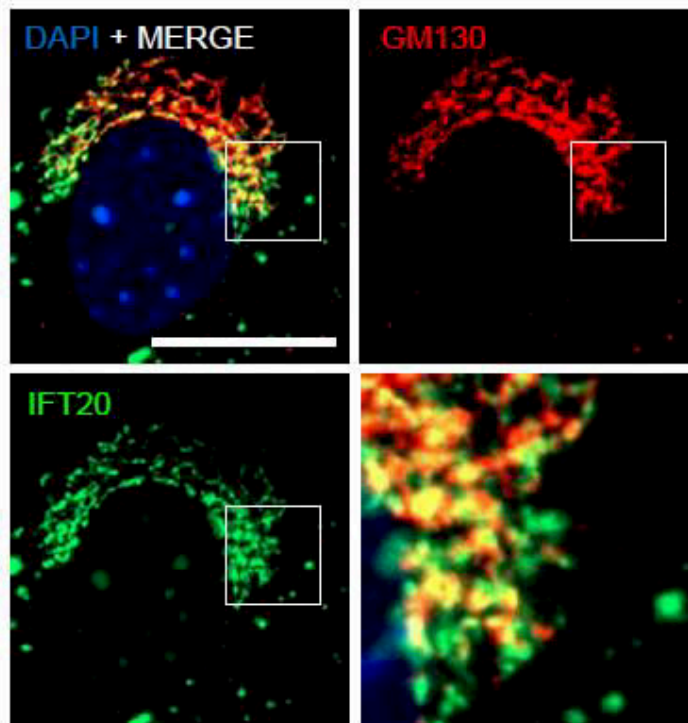
**a**wild type MEFs + ATG16L1<sup>GFP</sup>**b**wild type MEFs + ATG16L1<sup>GFP</sup>**Supplementary Figure 3. ATG16L1 does not phenocopy endogenous ATG16L1**

**a.** Confocal analysis of MEFs cells transiently transfected with ATG16L1<sup>GFP</sup> expression vector, cultured during 24h in absence of serum and processed for immunofluorescence using anti-ATG16L1 antibody. **b.** Confocal analysis of MEFs cells transiently transfected with ATG16L1<sup>GFP</sup> and Endoplasmic Reticulum marker Sec61β<sup>RFP</sup> expression vectors, cultured during 24h in absence of serum and processed for immunofluorescence using DAPI and anti-acetylated tubulin antibody as marker of PC. Scale bar: 10μm.



**Supplementary Figure 4. Endogenous IFT20 interacts with ATG16L1, but not with VPS34 and Beclin1 autophagy regulators**

MEFs cells were cultured in presence (+ serum) or 24h in absence of serum (- serum) and processed for co-immunoprecipitations analysis. Total lysates (input) were subjected to immunoprecipitation (IP) using anti-ATG16L1 antibodies. Samples were analyzed by SDS-PAGE and western blotting with anti-ATG16L1, anti-IFT20, anti-VPS34 and anti-Beclin1 antibodies. OVX: overexposed.

**a****b**

**Supplementary Figure 5. ATG16L1 knockout promotes retention of IFT20 at Golgi**

**a.** Wild type (WT) or ATG16L1<sup>-/-</sup> MEFs were cultured during 24h in absence of serum and processed for immunofluorescence analysis using DAPI and anti-IFT20 antibody. **b.** ATG16L1<sup>-/-</sup> MEFs were cultured during 24h in absence of serum and processed for immunofluorescence analysis using DAPI, anti-IFT20 and anti-GM130 antibodies. Scale bars: 10 $\mu$ m.



## IV DISCUSSION

A functional crosstalk between PC and autophagy has been established since 2013 after the publication of the two *princeps* papers, by Pampliega et al. 2013 and Tang et al. 2013 (Pampliega *et al.*, 2013; Tang *et al.*, 2013) and this molecular dialog was the basis of my PhD project when I joined the lab.

In the first paper, (Pampliega *et al.*, 2013), the authors identified a novel reciprocal relationship between PC and autophagic machinery. Authors showed also that the induction of autophagosome formation depends on serum availability, functional PC and the ciliary Hedgehog pathway. They demonstrated that most of the components of the autophagic machinery is located at the PC vicinity, or directly associated with axoneme and basal body. The localization of autophagy initiating ATG proteins at the base of the cilium suggests that the sensing of nutrient deficiency by the PC machinery or activation of signaling from this organelle could initiate a specific cilia mediated autophagic induction mechanism. This hypothesis is consistent with the reduced autophagy in cells with compromised ciliogenesis, and with the recruitment of one of the early markers of autophagy, Atg16L1 to the basal body upon starvation. As another connecting clue, the IFT20 ciliary protein, which delivery to the cilia is crucial for cilia assembly and proper localization of various ciliary proteins including polycystin 2 (PC2), is also delivered to the ciliary axoneme from the Golgi apparatus in Atg16L1-containing vesicles. Interestingly authors showed that the PC associated Hh signaling triggers the Golgi-to-cilia shuttling of the IFT20 and Atg16L1 positive vesicles. Finally, the serum dependent relocation of specific ATG proteins to pre-existing basal bodies leads to maximal activation of autophagy (Pampliega *et al.*, 2013).

In the second paper, the authors showed that negative regulators of ciliogenesis such as the centriolar satellite protein OFD1 can be degraded by serum starvation induced-autophagy. Moreover, upon serum starvation the ciliogenesis is concomitantly induced with the degradation of OFD1 by autophagy in an IFT20 dependent status (Tang *et al.*, 2013).

In my PhD work, we confirmed the interaction between IFT20 and ATG16L1 in both ciliated and non-ciliated conditions, which was previously suggested from Pampliega and coll (Pampliega *et al.*, 2013). More importantly, we show that while CCD domain of ATG16L1 is essential for autophagy related functions (such as ATG5 interaction), the WD40 domain of ATG16L1, a seven repetitions of WD motif suggested to be important in protein-protein interactions (Xu and Min, 2011) but not essential for autophagy, was required for the interaction with IFT20. Reciprocally, we identified an “ATG16L1 putative domain” on the Cter of IFT20, that was previously reported for the binding of ATG16L1 with TMEM59 (Boada-Romero *et al.*, 2013), and more precisely 4 essential amino acids in this domain, that constitute what we reported as a YEFI motif (Tyr – Glu – Phe – Ile), which are crucial in the interaction between the IFT20 and ATG16L1 proteins.

Furthermore, we found that IFT20 and ATG16L1 colocalized at different organelles and endomembranes: the Golgi, the basal body and axoneme in nutritional stress conditions; this make sense with results from Pazour lab, who previously reported that IFT20 is localized at *cis* and *trans* Golgi and that is an important protein for Golgi structure (Follit *et al.*, 2006). However, in our model, the absence of YEFI domain of IFT20 is sufficient to alter the ciliogenesis and we observed that IFT20 is blocked at Golgi. Thus, our results let us speculate that this IFT20/ATG16L1 complex is trafficking between Golgi and PC in response to serum starvation conditions which suggest a role of the WD40 and YEFI domains as important actors in the regulation of ciliogenesis and that are essential for the proper intracellular targeting of the protein complex to the PC, in addition to the exocyst protein SEC8.

In contrast, the complete absence of ATG16L1 protein leads to an increase of cilia length in nutritional stress conditions, with alters PC signaling functions. It was an interesting and surprising observation that required clarification, notably with contradictory reports of cilia length in autophagy deficient MEFs (Tang *et al.*, 2013). This discrepancy could be explained first by the difference of cells type used in Tang and colleagues paper, which are MCF7 different from MEFs and non-ciliated in serum starvation conditions except when OFD1 level is decreased. Moreover, the ATG16L1 was not tested in this study. Thus, our results led us hypothesize that a specific pool of this ATG16L1/IFT20 complex moves between Golgi and PC in nutritional stress sensing situation and that ATG16L1 could be important for the regulation of cilia length by helping and/or

regulating this trafficking. Whether this is related to autophagy-associated functions of ATG16L1 is a central question. It is noteworthy to precise that Beclin-1, a core component of the autophagic machinery associated with PI3P synthesis in the VPS34 complex (see autophagy section in the introduction) was not found at the base of the PC (Pampliega *et al.*, 2013) and that we report that Beclin1 is not present in the IFT20 and ATG16L1 complex that we studied, whatever is the ciliogenesis status. Altogether, previous results and our own observation clearly questions the canonical nature of the pathway mobilized in cilia-dependent autophagy induction. This is notably strengthened by the fact that ATG16L1 and IFT20 interact one with each other independently of presence of ATG5 and ATG3 (two key regulators of canonical autophagy, ATG5 being a direct partner of ATG16L1). In this way, we probably revealed a non-autophagy related role of ATG16L1.

### **ATG16L1, IFT20 and phosphoinositides**

In an intriguing manner, we found that ATG16L1 absence led to mis-trafficking of IFT20 in serum starvation conditions, which could account, or participate, to the aberrant ciliogenesis that we did observed in this condition. More specifically, in these conditions, IF20 is present at both Golgi structures and intracellular trafficking vesicles. Phosphoinositides confer identity to trafficking organelles and their distribution serves as a membrane code to spatially and temporally control numerous cellular processes (Di Paolo and De Camilli, 2006). For example, early endosomes and Golgi membranes are associated with PI3P and PI4P, respectively, whereas late endosomes are positive for PI3,5P2 and the plasma membrane possesses both PI4P and PI4,5P2. Accordingly, the PC membrane identity is mostly regulated by absence of PI4,5P2 and presence of PI4P (Chávez *et al.*, 2015; Nakatsu, 2015; Phua, Nihongaki and Inoue, 2018).

From our experimental data we found that purified ATG16L1 interacts with phosphoinositides like PI4P and, in a lesser extent, with PI4,5P2, which make sense with recent results of Gammoh lab (Edinburgh, UK), who identified conserved residues within the CCD domain of ATG16L1 that mediate direct binding to phosphoinositides such as PI3P, PI4P and PI4,5P2 (Dudley *et al.*, 2019). Interestingly, they showed that mutating putative lipid binding residues abrogated the localization of ATG16L1 to pre-autophagosomal membranes and inhibited LC3 lipidation. On the other hand, enhancing lipid binding of ATG16L1 by mutating negatively charged residues adjacent to the lipid

binding motif also resulted in autophagy inhibition, suggesting that regulated recruitment, via phosphoinositides, of ATG16L1 to future autophagosome is required for its autophagic activity (Dudley *et al.*, 2019). We thus postulated that different pools of ATG16L1 coexist at different trafficking stations, probably in different protein complexes.

Interestingly, our study showed that absence of ATG16L1 alters the PC distribution of ciliary phosphoinositides: the axonemal membrane is then negative for PI4P and positive for PI4,5P2, which confirms somehow the altered SMO and Hh signaling observed in this conditions and lead to postulate that the giant ciliary structure, positive for PI4,5P2, we observed in absence of ATG16L1 is non-functional. These results, in addition to the interaction between PI4P and ATG16L1, suggest that this proper phosphoinositides equilibrium at PC depends, at least partially, on ATG16L1.

### **ATG16L1 and INPP5E: a ciliogenesis associated partnership**

In line with our hypothesis, we finally showed for the first time that INPP5E, the cilia and Golgi-localized inositol 5-phosphatase phosphatase responsible for PI4P production (from PI4,5P2), was a partner of ATG16L1/IFT20 complex. INPP5E is crucial for PC associated membrane related signaling and is notably associated with the Joubert syndrome, which is classified as a ciliopathy (Braun and Hildebrandt, 2017). Notably, a Zebrafish study demonstrated that INPP5E was directly responsible for the fine-tuned turnover of PI4P/PI4,5P2 levels at ciliary membrane (Luo, Lu and Sun, 2012) (Figure 16). In parallel, a recent study suggests that INPP5E could be required for autophagy process completion, notably during the autophagosome/lysosome fusion (Hasegawa *et al.*, 2016). Interestingly, we show that absence of ATG16L1 blocked the INPP5E trafficking to PC membrane. It is thus very tempting to explain the PI4,5P2 axonemal accumulation that we observed in giant cilia from ATG16L1 KO cells is in fact directly connected to alteration of IFT20/INPP5E vesicular trafficking to the proper subcellular localization (*i.e.* the site of PC biogenesis). Thus, our study highlights for the first time the importance of ATG16L1 in the stress associated trafficking of the gatekeeper INPP5E, which is directly connected to the PC membrane identity regulation and thus to proper ciliary signaling functions. The relationship to bona-fide autophagy associated functions of ATG16L1 is of course puzzling in this situation.

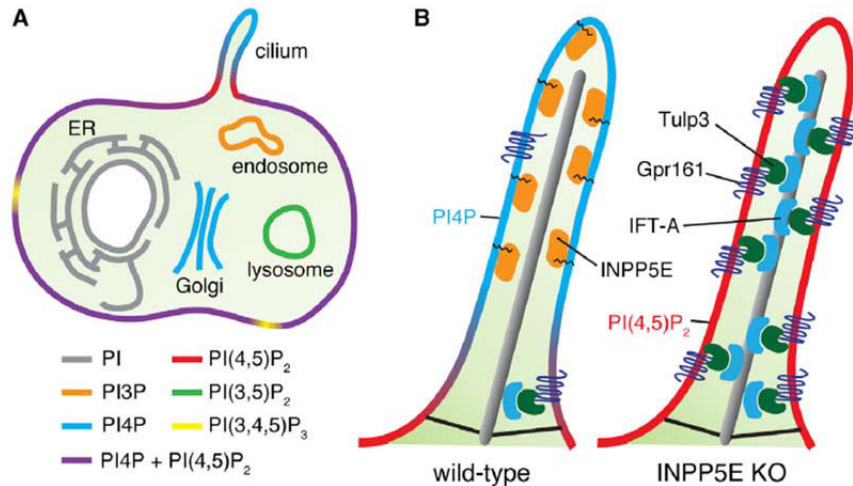


**Figure 16. Phosphoinositide Regulation at Distinct Cellular Membranes**

(A) Phosphoinositides known to localize at distinct cellular membranes are depicted. Note that both PI4P and PI(4,5)P<sub>2</sub> are concentrated throughout the plasma membrane. (B) Model for regulation of Hh signaling proteins by phosphoinositide metabolism at PC. Normally, INPP5E keeps PI(4,5)P<sub>2</sub> levels low or at a minimum to tightly control the trafficking of Hh proteins at PC (left). In INPP5E-deficient PC, a PI(4,5)P<sub>2</sub>-effector, Tulp3, and its binding partners Gpr161 and IFT-A accumulate upon PI(4,5)P<sub>2</sub> buildup, leading to impairment of Hh signaling (right).

Adapted from (Nakatsu, 2015)

All these results suggest a link between, ATG16L1, IFT20, INPP5E and a ciliopathy (Joubert Syndrome) and this relationship appears to be complex.

It will be interesting to determine whether INPP5E shares this function with other ciliary phosphoinositide phosphatases, such as OCRL or INPP5B ((Chávez *et al.*, 2015)). It should be noted that the mechanistic insights into how INPP5E (and other 5-phosphatases) controls cilia physiology still remained elusive.

In an intriguing manner, IFT20 is not localized at the axoneme in ATG16L1 KO fibroblasts, but remains in intracellular vesicles and at Golgi. It was previously shown that IFT machinery is required for the regulation of PC length in order to deliver additional axonemal subunits at the distal tip (Scholey, 2008). This vision does not correlate with our results, especially because cilia length increases in ATG16L1KO, which suggest that aberrant cilia formation is not disturbed by the alteration of IFT associated post-Golgi trafficking. One speculation for this is that ciliary

proteins (but not IFT20) may gain access to the cilium by lateral diffusion after reaching the plasma membrane. One other possibility, is that in absence of ATG16L1, the giant cilia observed is originated directly from the plasma membrane itself (and not “fed” by Golgian trafficking) and by the way the cilia is not considered as a bona-fide PC by the cells, as illustrated by the phosphoinositides equilibrium alteration that we reported. Further experiments must clarify the likely other differences in membrane composition between wild type and ATG16L1 KO cells, in response to serum deprivation.

Finally, it is tempting to hypothesize that ATG16L1 “alone” (independently of ATG5 and ATG12, engaged in canonical autophagy processes) is, at least in part, associated with its partners IFT20 and SEC8 in PI4P (and/or PI4.5P2 to PI4P) positive vesicles, moving between Golgi and PC in nutritional stress conditions which is important for cilia length regulation, activation of Hh signaling and of course for the composition of the ciliary membrane by phosphoinositides (Figure 17 and Figure 18).

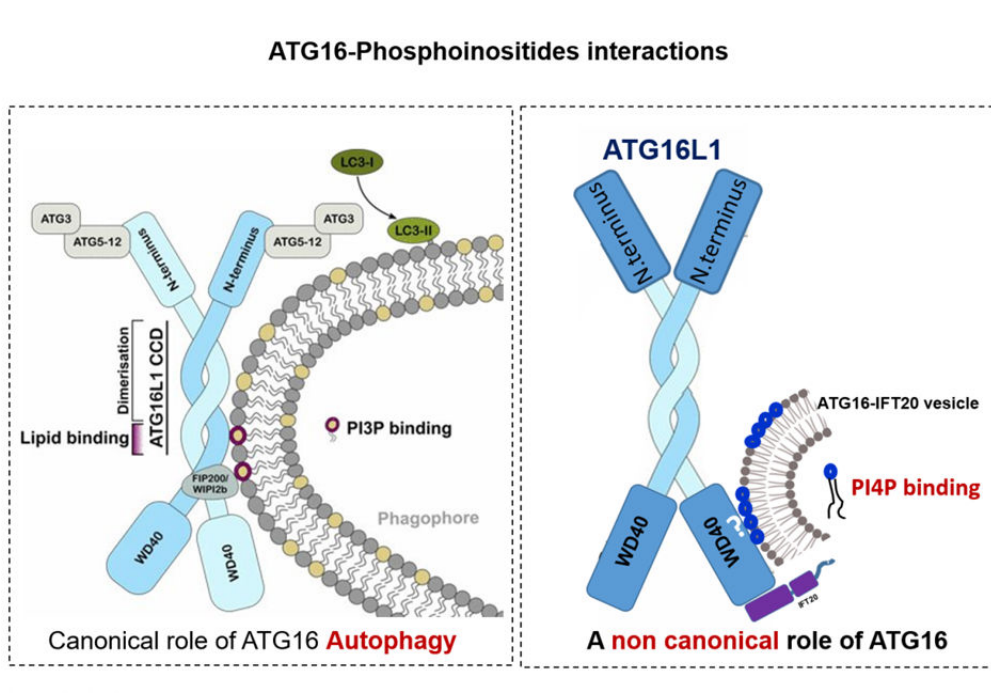


**Figure 17: ATG16L1 and phosphoinositides membranes dialog**

Our results led us hypothesize that ATG16 could be in different vesicles, in interaction with different phosphoinositides like PI3P or PI4P and by the way, the vesicles labeled PI3P or PI4P have different destination (autophagic membrane in the case of PI3P) and cilia in the case of PI4P.

On the other side one can imagine that, when ATG16L1 is engaged with its “classical” partners ATG5 and ATG12 (for canonical autophagy) it could benefit from its ability to binds PI3P (Dudley *et al.*, 2019) to coordinates membrane delivery at specialized sites of autophagosome biogenesis.

Altogether, these results suggest a new role for ATG16L1 in lipids dynamic, ciliary protein trafficking, in which the protein directly participates into ciliogenesis regulation and identity in response to stress sensing.

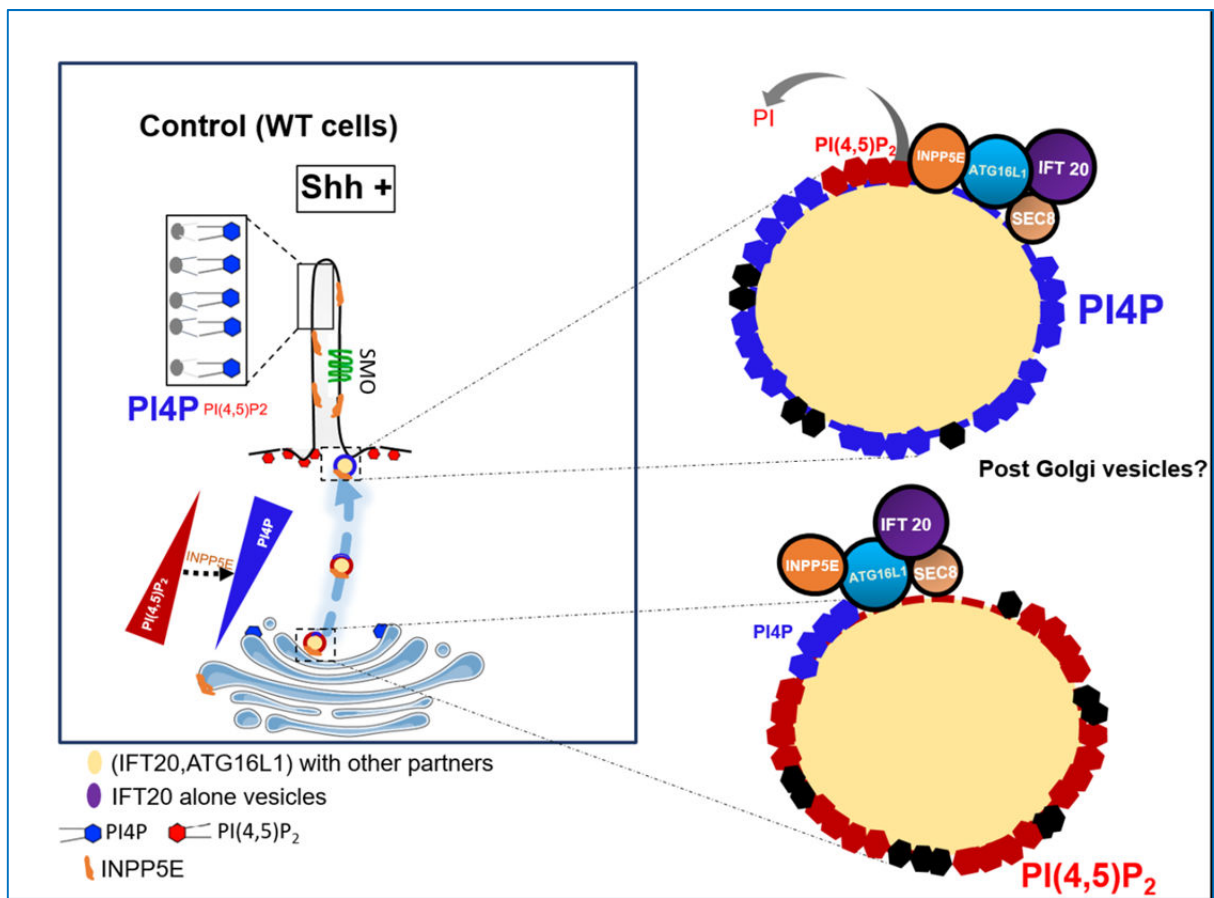


**Figure 18. A specific post-Golgian trafficking to PC for phosphoinositides turnover?**

The scheme highlights our hypothesis about presence of ATG16L1 and IFT20 positive Golgian vesicles which target INPP5E and produce PI4P from PI4.5P2 en route and/or at the PC terminal station.

One might speculate that regarding the kind of stress situation and the nature of the involved partners, ATG16L1 could be seen as a membrane sorting organizer, which could directly (via phosphoinositides binding and also via membrane protein interaction(s)) manage a “membrane reservoir” which the cell could use to deal with the membrane dynamics required to adapt to stresses, from autophagosome formation to ciliogenesis regulation. It is thus an open question to correlates or not the previously reported “non-canonical autophagy” associated functions of ATG16L1 (Figure 19), such as membrane repair during microbial infection (Tan *et al.*, 2018), with the one we describe here in relationship with membrane trafficking regulation.

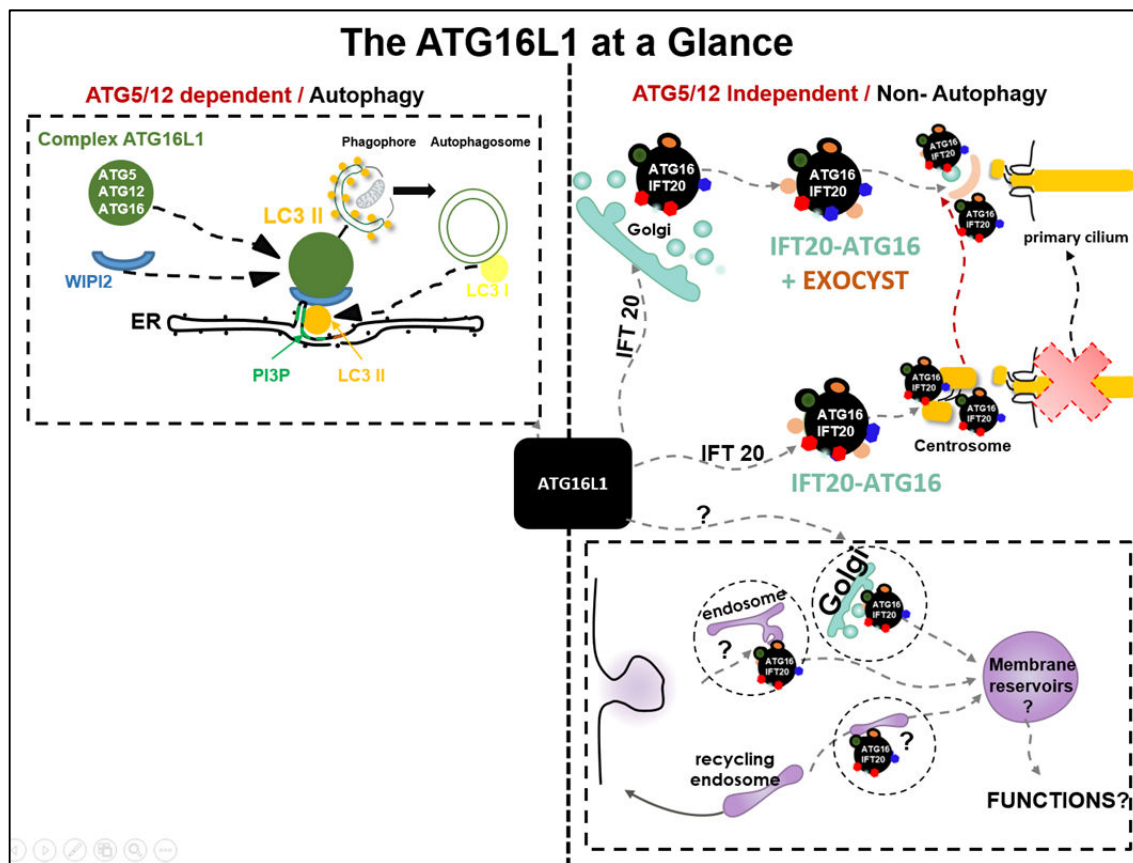


**Figure 19: The ATG16L1 partners and functions at a glance**

ATG16 has an important partner (IFT20 protein) in ciliogenesis conditions and before ciliogenesis. It has also other partner from multiple origins, like Golgi and post-Golgi (Sec8), autophagic machinery (ATG16, Vps15, GABARAP, LC3, AMBRA) and notably endosomes. These different kind of organelles and membrane-associated complexes could form an intermediate organelle “membrane reservoir” that participate in different functions like: bringing membranes to make different structure, a cilium, a phagophore, and autophagosome, or other functions not related to ciliogenesis and autophagic machineries.



## **V. APPENDIX**

### **1) PI3KC2 $\alpha$ -dependent and VPS34-independent generation of PI3P to regulate primary cilium-mediated autophagy in response to shear stress**

Asma Boukhalfa\*, Anna Chiara Nascimbeni\*, Damien Ramel, Nicolas Dupont, Emilio Hirsch, Stephanie Gayral, Muriel Laffargue#, Patrice Codogno#, Etienne Morel#

(Currently in revision)

### **2) Folliculin regulates primary cilium-dependent autophagy and epithelial cell size in response to fluid flow**

Naïma Zemirli\*, Asma Boukhalfa\*, Nicolas Dupont, Joëlle Botti, Patrice Codogno#, Etienne Morel#

(Published in Cell Stress, 2019)

### **3) Interplay between Primary cilia, Ubiquitin-Proteasome system and Autophagy**

Asma Boukhalfa\*, Caterina Miceli\*, Yennifer Ávalos, Etienne Morel#, Nicolas Dupont#

(Published in Biochimie, 2019 (REVIEW))

**PI3KC2 $\alpha$ -dependent and VPS34-independent generation of PI3P controls primary cilium-mediated autophagy in response to shear stress in epithelial cells**

Asma Boukhalfa<sup>\*,1</sup>, Anna Chiara Nascimbeni<sup>\*,1</sup>, Damien Ramel<sup>2</sup>, Nicolas Dupont<sup>1</sup>, Emilio Hirsch<sup>3</sup>, Stephanie Gayral<sup>2</sup>, Muriel Laffargue<sup>#,2</sup>, Patrice Codogno<sup>#,1</sup>, Etienne Morel<sup>#,1</sup>

<sup>1</sup>Institut Necker-Enfants Malades (INEM), INSERM U1151-CNRS UMR 8253, Université Paris Descartes-Sorbonne Paris Cité, Paris, France.

<sup>2</sup>Institute of Metabolic and Cardiovascular Diseases, INSERM UMR 1048, University of Toulouse, UMR1048, Paul Sabatier University, Toulouse, France.

<sup>3</sup>Molecular Biotechnology Center, Department of Molecular Biotechnology and Health Sciences, University of Torino, Turin, Italy

\* These authors contributed equally to this work

# Corresponding Authors:

Etienne Morel, [etienne.morel@inserm.fr](mailto:etienne.morel@inserm.fr)

Patrice Codogno, [patrice.codogno@inserm.fr](mailto:patrice.codogno@inserm.fr)

Muriel Laffargue, [muriel.laffargue@inserm.fr](mailto:muriel.laffargue@inserm.fr)

## ABSTRACT

Cells subjected to stress situations mobilize specific membranes and protein complexes to initiate the formation of autophagosomes, the main organelle of autophagic pathway. Phosphatidylinositol-3-phosphate (PI3P), a crucial lipid in membrane dynamics and identity, is known to be essential in this context. In addition to nutrients deprivation, autophagy is also triggered by fluid-flow induced shear stress in polarized epithelial cells, and this specific autophagic response depends on primary cilium (PC) signaling and leads to cell size regulation. Here we report that PI3KC2 $\alpha$ , a lipid enzyme required for ciliogenesis and the proper functioning of the PC, promotes the synthesis of a local pool of PI3P upon fluid flow-induced shear stress. We show that PI3KC2 $\alpha$  depletion in epithelial cells subjected to shear stress remarkably abolishes ciliary formation as well as the autophagic response and related cell size regulation *in vitro* and *in vivo*. We finally show that PI3KC2 $\alpha$  and VPS34, the two main enzymes responsible for PI3P synthesis, have different roles during autophagy, depending on the type of cellular stress: while VPS34 is clearly required for starvation-induced autophagy, PI3KC2 $\alpha$  participates only in shear stress-dependent autophagy.

## INTRODUCTION

In the phosphoinositides family, the phosphatidylinositol-3-phosphate (PI3P) is a central lipidic player in membrane dynamics and trafficking regulation in eukaryotic cells<sup>1,2</sup>. PI3P is mainly synthesized by the class 3 PI3 Kinase (PI3KC3, also known as VPS34) and is associated with the autophagic machinery<sup>3-6</sup> and the endosomal functions<sup>7,8</sup>, both systems being connected with the lysosome, the acidic degradative organelle in eukaryotes. While the endosomal system is mostly responsible for sorting, recycling and degradation of plasma membrane components and external material<sup>9,10</sup>, autophagic membranes and their associated machinery are mobilized during stress situations to ensure the degradation of intracellular components by triggering the formation of autophagosomes, which capture cytoplasmic material and subsequently lead it to degradation upon fusion with lysosomes<sup>11-13</sup>. The formation of these double membrane organelle is initiated by two ATG (autophagy-related) containing complexes: the ULK signaling complex and the PIK3C3 complex I. The core of the latter is composed by Beclin1, ATG14L, VPS15 and the lipid kinase VPS34. When associated with the above mentioned partners, VPS34 produces PI3P at autophagosomal membrane source sites allowing the recruitment of autophagy-associated PI3P-binding proteins such as DFCP1 and WIPI-2, and thus directly participates in the activation of the downstream ATG machinery, including the lipidated LC3 (LC3.II), which leads to the nucleation of the autophagosomal membrane<sup>14</sup>. Among other cellular structures that participate to external stress sensing, the primary cilium (PC), an essential microtubule-based organelle located at the apical side of most epithelial cells<sup>15</sup>, triggers a signaling cascade upon sensing extracellular chemical and mechanical stimuli<sup>16</sup>, including shear stress. Interestingly, we have recently shown that autophagic machinery is also stimulated in response to fluid flow - induced shear stress in kidney epithelial cells, a situation that requires primary cilium (PC) signaling and leads to cell size regulation<sup>17,18</sup>. Finally, the PI3KC2 $\alpha$  lipid kinase, considered as an alternative source of PI3P, has been shown to participate in the regulation of PC biogenesis and PC associated signaling via specific PI3P synthesis in embryonic fibroblasts

and renal epithelial cells<sup>19,20</sup>. Altogether, these observations combining PC, PI3P and PI3KC2 $\alpha$ , highlight a putative role for this kinase in the intriguing connection between autophagy and PC function in response to mechanical stimulation.

Here we demonstrate that the lipid enzyme PI3KC2 $\alpha$ , whose expression is increased during shear stress, is responsible for the synthesis of a specific pool of PI3P at the vicinity of the PC in response to fluid flow in kidney epithelial cells. We show that the knockdown of PI3KC2 $\alpha$  not only abrogates shear stress-induced PI3P production, but also abolishes autophagy as well as cell volume adaptation to shear stress. Similar data were observed in PI3KC2 $\alpha$ <sup>+/-</sup> mice epithelial kidney cells *in vivo*. The specific need for PI3P production in response to shear stress was further demonstrated in cells lacking a functional PC in which the autophagy program associated with shear stress was restored upon artificial delivery of exogenous PI3P. We finally show that while PI3KC3/VPS34 is, as expected, required for starvation-induced autophagy, it is not involved in shear stress -associated autophagy. In sharp contrast, PI3KC2 $\alpha$  is specifically required for the autophagic program associated with mechanical stimulation relayed by the PC, but not essential for nutritional stress response, suggesting that a selective pool of PI3P is generated during shear stress.

## RESULTS

### **A PI3KC2 $\alpha$ -associated PI3P pool appears at the base of the primary cilium in response to shear stress stimulation**

We previously reported that a constant laminar fluid flow on mouse proximal tubule kidney epithelial cells induces primary cilium (PC)-dependent autophagy activation and cell size regulation<sup>17</sup>. Similar results were obtained using human HK2 cells (proximal tubule kidney cells) (Sup Figure 1 and<sup>18</sup>). We indeed show that, compared to a static cell culture situation, a 4 days-long 1dyn/cm<sup>2</sup> laminar fluid flow induces an autophagic response, as shown by an increase in LC3-II (Sup Figure 1a) and in the number of LC3-positive structures in polarized cells during 4 days (Sup Figure 1b and 1c). Moreover shear stress induces a decrease in cell size (Sup Figure 1b and 1d) as previously shown in mice kidney epithelial cells and MDCK cells<sup>17,21</sup>. We observed as well that shear stress increases PI3KC2 $\alpha$  stability at the protein level (Figure 1a and 1b) and mRNA level (Figure 1c). It also leads to a direct and local mobilization of PI3KC2 $\alpha$  at the PC (Figure 1d and 1e), indicating that PI3KC2 $\alpha$  and the autophagic machinery (Sup Figure 1) are both reactive to shear stress in ciliated cells. As the main known enzymatic function of PI3KC2 $\alpha$  is to synthesize PI3P<sup>22</sup>, we tested whether the shear stress response could also mobilize a dedicated pool of PI3P membranes at the PC vicinity. We thus monitored and quantified the local changes in PI3P-positive structures at the PC basal body area (see scheme on Figure 1f) in fixed cells using indirect fluorescent recombinant FYVE dye to avoid overexpression of PI3P-binding domains<sup>23</sup> and ARL13B as a specific marker for PC axoneme. In accordance with PI3KC2 $\alpha$  mobilization upon fluid flow stimulation, we show that shear stress also induces the appearance of a local pool of PI3P at the base of the PC (Figure 1g and 1h).

## PI3KC2 $\alpha$ knock-down affects shear stress-associated PI3P synthesis

We analyzed next the effect of PI3KC2 $\alpha$  knock-down (PI3KC2 $\alpha$  siRNA, Sup Figure 2a) on polarized epithelial cells submitted to shear stimulation. While the siRNA mediated knock-down (Sup Figure 3a) of VPS34, the other major enzyme responsible for PI3P synthesis, has no effect on PC (Sup Figure 3b and 3c) we show that PI3KC2 $\alpha$  depletion abrogates ciliogenesis (Sup Figure 2b, 2c and 2d), as previously reported<sup>19</sup>. Moreover, we show that the AMPK/LKB1 signaling cascade<sup>21,24</sup>, which is associated with fluid flow sensing by the PC<sup>17,18</sup>, is abolished in PI3KC2 $\alpha$  KD cells, since p-AMPK (Sup Figure 4a and 4b) and LKB1 (Sup Figure 4c and 4d) recruitment to PC are compromised in the absence of PI3KC2 $\alpha$ . To analyze precisely the dynamics of the PI3P present in the basal body area (see Figure 1g), we systematically quantified the PI3P-positive structures in a 150 $\mu$ m<sup>2</sup> circular area close to the nucleus (corresponding to the PC basal body location, Figure 2a and 2b) in control cells and in PI3KC2 $\alpha$  KD cells, in which PC presence was inhibited (Sup Figure 2). Interestingly, while absence of PI3KC2 $\alpha$  has no consequences on the number of PI3P structures in the PC area in static culture situation, the pool of PI3P-positive membranes drops by approximately 50% in cells lacking PI3KC2 $\alpha$  during shear stress treatment (Figure 2a and 2c).

Importantly, the amount of autophagy-associated WIPI2 PI3P-binding protein<sup>25</sup> was increased upon shear stress but reduced in PI3KC2 $\alpha$  KD cells (Figure 2d), as well as WIPI2 mRNA levels (Figure 2e), arguing for a specific autophagic response mediated by a PI3KC2 $\alpha$  synthesized pool of PI3P in shear stress treatment. Importantly, a pool of WIPI2 protein is associated with the PI3P observed at the base of PC in response to shear stress (figure 2f). Moreover, the small GTPase Rab11a, a key partner of WIPI2 in autophagy<sup>26,27</sup> and PI3P-positive membranes in relationship with PC and endocytosis turnover regulation<sup>19,28</sup>, was increased by shear stress stimulation (Sup Figure 5a and 5b). In addition, we observed that the GTP bound (*i.e.* activated) form of Rab11a was partially addressed to the cilium axoneme in the same situation (<sup>GTP</sup>Rab11, Sup Figure 5c). Interestingly, the knock down of PI3KC2 $\alpha$  inhibits this Rab11a behavior in response to fluid flow, as revealed by

biochemical analysis (Sup Figure 5a and 5b) and immunofluorescence (Sup Figure 5c). Finally, in conditions of PI3KC2 $\alpha$  depletion, we analyzed the behavior of ATG16L1, a crucial regulator of early autophagic processes, notably as a key partner of WIPI2 and PI3P in autophagy regulation<sup>29,30</sup>, and known to be recruited to the basal body in PC associated autophagy<sup>31</sup> during shear stress<sup>18</sup>. Importantly we showed that, as observed for Rab11a and WIPI2, ATG16L1 was mobilized by shear stress but not in siPI3KC2 $\alpha$  transfected cells (Sup Figure 6a and 6b). The local recruitment of ATG16L1 at the base of PC observed in control cells was no longer detectable in PI3KC2a knock-down cells (Sup Figure 6c and 6d), highlighting the crucial role of the autophagy-related PI3P-associated machinery in response to shear stress.

Altogether, these results suggest that shear stress induced PI3P mobilization and autophagy both depend on PI3KC2 $\alpha$  lipid kinase.

### **PI3KC2 $\alpha$ , but not VPS34, regulates shear stress-associated autophagy and cell size regulation**

As shown in supplementary Figure 1, shear stress treatment of polarized epithelial cells leads to autophagy induction and cell size decrease. PI3P measurements by fluorescence (Figure 2) suggest that PI3KC2 $\alpha$  is responsible for shear stress-induced PI3P synthesis. However, VPS34 (also known as PI3KC3) has been described as the canonical lipid kinase regulating PI3P-associated autophagy<sup>14,32</sup>. To decipher the precise function(s) of PI3KC2 $\alpha$  in our experimental system, we thus compared autophagy elicited by shear stress in cells KD for PI3KC2 $\alpha$  or PI3KC3/VPS34.

Interestingly, we observe that LC3 lipidation induced by shear stress is blocked by PI3KC2 $\alpha$  KD but not by VPS34 KD (Sup Figure 7a and 7b), suggesting that shear stress-associated autophagy is solely dependent on PI3KC2 $\alpha$ , and not VPS34. Next we compared the number of LC3-positive endomembranes in cells KD for VPS34 or PI3KC2 $\alpha$  and subjected to either 24h shear stress or 24h

nutritional stress (starvation), both situations inducing autophagy. Surprisingly, and in accordance with western blot data, we show that the presence of PI3KC2 $\alpha$  was necessary for membrane LC3 mobilization upon shear stress, but not upon starvation (Figure 3a and 3b, siPI3KC2 $\alpha$  conditions). On the contrary, while VPS34 is required for starvation-induced LC3 mobilization, its depletion had no consequence on the shear stress-induced LC3 membrane mobilization (Figure 3a and 3b, siVPS34 conditions). Similar results were obtained when we quantified the total number of PI3P-positive cellular structures (*i.e.* early endosomal and autophagosomal membranes), in the very same conditions: while VPS34 is required for PI3P synthesis at steady state and during starvation-induced autophagy, absence of PI3KC2 $\alpha$  is only deleterious for shear stress-induced autophagy (Sup Figure 7c and 7d), confirming the above mentioned LC3 data and illustrating the importance of PI3KC2 $\alpha$  in shear stress-associated autophagic machinery mobilization.

Finally, we show that starvation-induced autophagy has no effect on the cell size decrease observed upon fluid flow treatment and, more interestingly, that PI3KC2 $\alpha$  KD completely abolishes this cell size adaptation while VPS34 KD has no effect on it (Figure 3c and 3d). To confirm the non-involvement of the PI3KC3 complex in shear stress-associated autophagy, we investigated Beclin1 behavior in response to mechanical stress, since it is a master regulator of VPS34 activity regulation in autophagy-associated PI3P synthesis<sup>33</sup>. Interestingly, while PI3KC2 $\alpha$  protein stability is associated with shear stress response (Figure 1a and 1b), Beclin1 turnover was not affected either by shear stress or by PI3KC2 $\alpha$  knock-down (Sup Figure 8a). In cells lacking Beclin1 (BECN1 siRNA, Sup Figure 8b), LC3 lipidation induced by shear stress is comparable to the control cells (Sup Figure 8c), illustrating that the absence of Beclin1 protein has no deleterious effect on shear stress-associated autophagy. This was confirmed, in cells subjected to shear stress, by the absence of a Beclin1 knock-down effect on quantifications of LC3-positive structures (Sup Figure 8d and 8e) and on cell volume regulation (Sup Figure 8f and 8g). Similar results were obtained when we questioned the involvement of FIP200, a key protein in starvation induced autophagy, which regulates

VSP34/Beclin1 activity with its partners ULK1/2 and ATG101<sup>34,35</sup>. We show that FIP200 amount was not affected by shear stress (Sup Figure 9a, siCTRL conditions), unlike PI3KC2 $\alpha$  and WIPI2.

Moreover, the siRNA-mediated knock down of FIP200 has no effect either on LC3 lipidation (Sup Figure 9a and 9b) or LC3 dots numbers (Sup Figure 9c and 9d) and cell size regulation (Sup Figure 9e and 9f) during shear stress. These observations confirm that the classical physical and functional partners of VPS34 activity during starvation induced autophagy are not required in shear stress associated autophagy.

Finally, our *in vitro* observations about PI3KC2 $\alpha$  implication in fluid flow-associated autophagy were confirmed *in vivo* by comparing wild type (WT) and PI3KC2 $\alpha$ <sup>+/-</sup> mice in the cortex zone of kidneys. We observe a decrease in the LC3-positive structures number in the PI3KC2 $\alpha$ <sup>+/-</sup> mice (Figure 3e and 3g) as well as an increase in the cell surface compared to wild type (Figure 3f and 3h). Altogether, these results show that PI3KC2 $\alpha$  is required for autophagy induction and cell size regulation in cells subjected to shear stress.

### **Exogenous PI3P delivery rescues autophagy in cells deprived of primary cilium**

Our results indicate that fluid flow mediates PI3KC2 $\alpha$  mobilization to induce PI3P synthesis at the vicinity of PC basal body (Figure 1). We thus wondered whether artificial delivery of PI3P could counteract the absence of the PC (see experimental set-up in Figure 4a), considered as the central signaling structure that triggers the response to shear stress<sup>16</sup>. To do this, we knocked down the PC associated IFT88 protein<sup>36</sup> (Figure 4b) and we showed, as expected, that IFT88 siRNA transfected cells displayed altered ciliogenesis (sup Figure 10a and 10b), similarly to what we can observed for other IFT protein, such as IFT20 (sup Figure 10c, 10d and 10e). IFT88 knock down cells failed to induce proper autophagic response to shear stress (Sup Figure 10f and 10g) and interestingly, absence of IFT88 also alters PI3KC2 $\alpha$  stability (Sup Figure 10h and 10i). Finally, and making sense

with alteration of PI3KC2 $\alpha$  stability, we show that IFT88 knock-down cells failed to induce local and shear stress associated PI3P synthesis as we observed in control cells (Sup Figure 10j and 10k). As expected IFT88 knock-down leads to the abolition of cellular adaptation to fluid flow induced shear stress, demonstrated by the lack of LC3-positive structures increase (Figure 4c and 4d, siCTRL and siIFT88 + lipid carrier conditions) compared to control cells, and the lack of cell volume regulation (Figure 4e and 4f, siCTRL and siIFT88 + lipid carrier conditions). Interestingly, external delivery of increasing doses of purified DiC16.PI3P (0.1  $\mu$ M and 1 $\mu$ M, during the 3 last hours of the fluid flow treatment) overcame the absence of IFT88, as both readouts were partially recovered (Figure 4c, 4d, 4e and 4f, siIFT88 + PI3P condition), further demonstrating the crucial role of PI3P in the autophagic response induced by shear stress on epithelial cells.

### **Overexpression of wild type PI3KC2 $\alpha$ , but not kinase-inactive mutant, rescues absence of PC for shear stress induced autophagy**

Our artificial PI3P delivery experiments showed that presence of PI3P is directly responsible for re-engagement of autophagic program in response to fluid flow induced shear stress (Figure 4). To go further and to connect these data with our observations concerning PI3KC2 $\alpha$  mobilization (Figure 1), requirement for autophagy (Figure 3) and PI3P associated autophagy (Figure 2) during shear stress sensing, we overexpressed the human PI3KC2 $\alpha$  protein in IFT88 siRNA transfected cells submitted to fluid flow. Interestingly we show that while presence of wild type (WT) PI3KC2 $\alpha$  is able to rescue LC3 mobilization as monitored by LC3 lipidation (Sup Figure 11a and 11b, wild type condition) and puncta quantification (Sup Figure 11c and 11d, wild type condition), the kinase-inactive PI3KC2 $\alpha$  (PI3KC2 $\alpha$  K<sub>inact</sub>), which lacks the ability to produce PI3P<sup>22,37</sup>, was unable to do so (Sup Figure 11 a, 11b, 11c and 11d, PI3KC2 $\alpha$  K<sub>inact</sub> condition), illustrating the crucial importance of PI3KC2 $\alpha$  associated PI3P synthesis in response to shear stress.

## DISCUSSION/CONCLUSION

The metabolism of phosphoinositides is central to cellular homeostasis regulation in eukaryotic cell. As a prototypical example, PI3P, one of the most abundant lipids of the family, is a central player in endosomal and autophagosomal membrane dynamics<sup>4-6,23</sup>, as well as required for PC functions and regulation<sup>19</sup>. PI3P is synthesized by PI3KC3/VPS34, PI3KC2 $\alpha$ , PI3KC2 $\beta$  and PI3KC2 $\gamma$ <sup>38</sup> and despite significant advances in the field, it is still unclear how, where and why these enzymes contribute to different PI3P pools dedicated to specific cellular processes. Here we show that PC-mediated response to mechanical stimulation triggers specific PI3KC2 $\alpha$ -dependent PI3P synthesis which participates in autophagic machinery mobilization and in turn in cell volume regulation. More importantly, our data suggest for the first time that two distinct PI3P synthesizing lipid kinases are differentially mobilized, according to the stress type: while PI3KC3/VPS34 is – as expected – crucial for nutritional stress-induced autophagy<sup>11</sup>, it is not necessary for the shear stress-induced autophagic program, which requires instead PI3KC2 $\alpha$  activity.

PI3KC2 $\alpha$  was reported to be a key regulator of PC functions via the synthesis of a pool of PI3P, which in turn is crucial for Rab11a membrane mobilization and activation<sup>19,28</sup>. Here we demonstrate that PI3KC2 $\alpha$  knock-down not only affects ciliogenesis, but also has severe consequences on PC-associated functions and signaling in cells subjected to shear stress, a situation known to activate the autophagic program via the PC machinery<sup>17</sup>. Indeed, we show that Rab11a is stabilized by shear stress in ciliated cells, and that its mobilization is affected upon PI3KC2 $\alpha$  knock-down, presumably as a consequence of the PI3KC2 $\alpha$  dependent PI3P pool depletion. Our data linking Rab11a activation to shear-stress associated PI3P further confirm recent report supporting an essential role for Rab11a, PI3P-binding protein WIPI2 and associated PI3P-positive recycling endosomal membranes in autophagosome biogenesis<sup>27</sup>.

We observe that PI3KC2 $\alpha$  stability is strongly increased by shear stress and that artificial delivery of PI3P, or overexpression of PI3KC2 $\alpha$  (but not the PI3KC2 $\alpha$  kinase-inactive mutant), on PC deprived polarized cells, compensate for the PC role and is sufficient to reboot the autophagic response associated with shear stress sensing. Our observation that PI3KC2 $\alpha$  is not essential for starvation-induced (VPS34 dependent) autophagy, could explain why the knockdown of Beclin1, the key partner of VPS34 in starvation-associated PI3P synthesis<sup>33</sup>, or the knockdown of VPS34 itself, have no deleterious effect on the shear stress-associated response. Thus, our results make sense with previous observation of absence of Beclin1 recruitment at the basal body during PC associated autophagy<sup>31</sup>. We therefore propose that class 3 and class 2 PI3kinases are involved in different kinds of autophagic response. Thus, it can be postulated that cellular adaptation to shear stress mobilizes PI3KC2 $\alpha$ -dependent PI3P synthesis without depending on VPS34, which in turn is available for endosomal trafficking regulation, as a putative consequence of previously reported increase in shear stress-induced endocytosis<sup>39,40</sup>, as well for autophagic response to other stimuli.

Our findings open up the question of canonical *versus* non-canonical autophagy discrimination in the mechanical stimulation of epithelial ciliated cells. It is indeed tempting to hypothesize that, while PI3P is essential for autophagy-machinery mobilization (notably in the autophagosome biogenesis sequence), the source of PI3P can differ from one stress situation to another, with, at least in our experimental data, exclusive PI3KC2 $\alpha$  lipid enzyme mobilization upon shear stress conditions in relation with the PC. In this context, we would like to emphasize that the low shear stress used in this study (*i.e.* 1 dyn/cm<sup>2</sup>) reflects the primary urine flow in normal kidney epithelium, thus suggesting that *in vitro* studies like the present one contribute to reveal the importance of PI3KC2 $\alpha$  activity in a still poorly studied, despite being physiological, situation. In this regard, it is tempting to hypothesize that a specific mobilization of the PI3P-dependent autophagic program may directly participate in the PI3KC2 $\alpha$ -mediated prevention of renal cysts formation<sup>20</sup>, highlighting the protective role of the autophagy and PC dialog in kidney epithelium homeostasis. PI3KC2 $\alpha$  activity

is known to be involved in many physiological processes beyond its role in kidney physiology, by notably controlling mast cells degranulation, angiogenesis, thrombosis and systemic glucose homeostasis (reviewed in<sup>41</sup>). Whether shear stress autophagy is a downstream effector of PI3KC2 $\alpha$  in these activities remains to be investigated.

## FIGURES LEGENDS

**Fig. 1 Shear stress induces PI3KC2 $\alpha$  expression and a local pool of PI3P at the primary cilium.** **a, b** Western blot analysis of LC3-I, LC3-II and PI3KC2 $\alpha$  and quantification of PI3KC2 $\alpha$  protein (**b**) and mRNA levels (**c**) in lysates of polarized HK2 cells subjected to shear stress for 96 hours, compared to static cultured cells (ctrl, 96 hours). Bar graphs denote average protein levels normalized to actin (**b**) (mean  $\pm$  SEM, from 3 independent experiments) and fold increase of average mRNA levels (**c**) relative to ctrl and normalized to actin mRNA (mean  $\pm$  SEM, from 3 independent experiments). \*\*\* $p < 0.001$  in two-tailed Student's t test. **d, e** Representative 3D confocal acquisitions (**d**) and quantification (**e**) of polarized HK2 cells subjected to shear stress (96 hours), compared to static cultured cells (ctrl, 96 hours), immunostained for PI3KC2 $\alpha$ , ARL13B (primary cilium (PC) marker) and DAPI, showing increased PI3KC2 $\alpha$  expression at the PC upon shear stress (N = 40 cells, from 3 independent experiments). Scale bar, 10 $\mu$ m. **f** Schematic representation of PC structure and zone (150 $\mu$ m<sup>2</sup> circular area) of PI3P positive structures quantification. **g, h** Representative 3D confocal acquisitions and related PI3P quantification of polarized HK2 cells subjected to shear stress (96 hours), compared to static cultured HK2 cells (ctrl, 96 hours), immunostained for the primary cilia (PC) axoneme marker ARL13B and for PI3P (using indirect FYVE-GST recombinant peptide), showing PI3P-positive structures at the base of PC area (mean  $\pm$  SEM, N = 100 cells, from 3 independent experiments). \*\*\* $p < 0.001$  in two-tailed Student's t test. Scale bar, 10 $\mu$ m.

**Fig. 2 Shear stress-induced PI3P synthesis at the PC depends on PI3KC2 $\alpha$ .** **a** Representative confocal images upon shear stress conditions of PI3KC2 $\alpha$  knocked down HK2 cells (siPI3KC2 $\alpha$ ), compared to control cells (siCTRL), immunostained for ARL13B, PI3P (using FYVE-GST indirect recombinant peptide) and DAPI (N = 80 cells, from 5 independent experiments). Scale bar, 10 $\mu$ m. **b**

Schematic drawing showing the 150  $\mu\text{m}^2$  circular area centred at the cell nucleus used as identifier of the PC basal body area. **c** Quantification of the PI3P-positive structures at the PC area, as defined in **b** and shown in **a**, in siCTRL or siPI3KC2 $\alpha$  HK2 cells, upon static (ctrl) and shear stress (96 hours) conditions (mean  $\pm$  SEM, N = 80 cells, from 5 independent experiments). NS: not significant, \*\*\*p < 0.001 in two-tailed Student's t test. **d** Western blot analysis and quantification of WIPI2 protein levels in lysates of polarized siCTRL or siPI3KC2 $\alpha$  HK2 cells, upon static (ctrl) and shear stress (96 hours) conditions. Bar graph denotes average protein levels normalized to actin (mean  $\pm$  SEM, from 3 independent experiments). NS: not significant, \*\*\*p < 0.001 in two-tailed Student's t test. **e** WIPI2 mRNA levels quantifications from total lysates of polarized siCTRL or siPI3KC2 $\alpha$  HK2 cells, upon static (ctrl) and shear stress (96 hours) conditions. Bar graphs denote fold change of average mRNA levels relative to ctrl and normalized to actin mRNA (mean  $\pm$  SEM, from 3 independent experiments). \*\*\*p < 0.001 in two-tailed Student's t test. **f** Representative confocal acquisition of WIPI2<sup>GFP</sup> transfected HK2 cells upon shear stress conditions immunostained for ARL13B, PI3P (using FYVE-GST indirect recombinant peptide) and DAPI showing PI3P and WIPI2<sup>GFP</sup> colocalization at the base of PC (arrowhead). Scale bar, 10 $\mu\text{m}$ .

**Fig. 3 Shear stress-induced autophagy and cell size regulation depend on PI3KC2 $\alpha$ , but not on PI3KC3/VPS34.** **a, c** Representative confocal images of polarized HK2 cells (siCTRL), compared to PI3KC2 $\alpha$  knocked down cells (siPI3KC2 $\alpha$ ) and PI3KC3/VPS34 knocked down cells (siVPS34), upon static (ctrl, 24 hours), shear stress (24 hours) and starvation conditions (24 hours, see Methods section for more details), immunostained for LC3, F-actin and DAPI. Scale bar, 10 $\mu\text{m}$ . **b, d** Quantifications of **a** and **c**. Bar graphs denote average number of LC3 puncta and average cell areas (mean  $\pm$  SEM, N = 100 cells, from 3 independent experiments). NS: not significant, \*\*\*p < 0.001 in two-tailed Student's t test. **e, g** Cortex zone of kidneys from wild type (WT) and PI3KC2<sup>+/-</sup> mice, immunostained for LC3, LTL (*Lotus Tetragonolobus* Lectin) and DAPI, and quantification of LC3

puncta (mean  $\pm$  SEM, from 3 independent experiments). Scale bar, 10 $\mu$ m. \*p < 0.05 in two-tailed Student's t test. **f, h** PAS (Periodic Acid Schiff) staining of the cortex zone of kidneys from wild type and PI3KC2<sup>+/-</sup> mice and quantification of tubular cell area (mean  $\pm$  SEM, from 3 independent experiments). Scale bar, 50 $\mu$ m. \*p < 0.05 in two-tailed Student's t test.

**Fig. 4 Exogenous PI3P delivery restores autophagy and cell size regulation upon shear stress in PC-deprived cells.**

**a** Schematic display of the experimental design; all cells were analyzed after 96 hours of fluid flow. We added to IFT88 knock down (siIFT88) HK2 cells two different concentrations of exogenous PI3P (DiC16.PI3P, in lipid carrier vehicle, at 0.1 and 1  $\mu$ M) during the last 3 hours of fluid flow treatment and compared them to control cells (siCTRL) and to siIFT88 cells added with carrier alone, as a negative control. **b** Western blot analysis of IFT88 in lysates of HK2 cells (siCTRL) and IFT88 knocked down cells (siIFT88). **c, e** Representative confocal images of HK2 cells (siCTRL), compared to siIFT88, supplemented with exogenous PI3P (0.1 and 1  $\mu$ M) or with carrier only, upon shear stress (96 hours) conditions, immunostained for LC3 and DAPI or F-actin and DAPI, respectively. Scale bar, 10 $\mu$ m. **d, f** Quantifications of **c** and **e**. Bar graphs denote average number of LC3 puncta per 200  $\mu$ m<sup>2</sup> area and average cell surface, respectively (mean  $\pm$  SEM, N = 70, from 3 independent experiments). \*\*p < 0.01, \*\*\*p < 0.001 in two-tailed Student's t test.

**Supplementary Fig. 1 Shear stress induces autophagy and regulates cell size in kidney**

**epithelial cells. a** Western blot analysis and quantification of LC3-I and LC3-II levels in lysates of polarized HK2 cells subjected to shear stress for 4 and 96 hours, compared to static cultured HK2 cells (ctrl). Bar graph denotes average protein levels normalized to ctrl (mean  $\pm$  SEM, from 3 independent experiments). LC3 levels were normalized to actin levels (lysate total protein). \* $p < 0.05$ , \*\*\* $p < 0.001$  in two-tailed Student's t test. **b** Representative confocal images of cells subjected to shear stress (96 hours), compared to static cultured cells (ctrl, 96 hours), immunostained for LC3 and  $\beta$ -catenin. Dashed white lines are used to better show the cell boundary. Scale bar, 10 $\mu$ m. **c, d** Bar graphs indicate average number of LC3 puncta per 500  $\mu$ m<sup>2</sup> cellular area and average cell area in cells subjected to shear stress for 96 hours, compared to static condition (ctrl, 96 hours) (mean  $\pm$  SEM, N = 70 cells, from 3 independent experiments). \*\*\* $p < 0.001$  in two-tailed Student's t test.

**Supplementary Fig. 2 PI3KC2 $\alpha$  knockdown affects ciliogenesis. a** Western blot analysis and quantification of PI3KC2 $\alpha$  levels in lysates of HK2 cells (siCTRL), compared to PI3KC2 $\alpha$  knocked down cells (siPI3KC2 $\alpha$ ), upon static (ctrl, 96 hours) and shear stress (96 hours) conditions. Bar graph denotes average protein levels normalized to actin (mean  $\pm$  SEM, from X independent experiments). \*\*\* $p < 0.001$  in two-tailed Student's t test. **b, c** Representative confocal images of ciliogenesis (percentage of ciliated cells) in HK2 cells (siCTRL), compared to PI3KC2 $\alpha$  knocked down cells (siPI3KC2 $\alpha$ ), by immunostaining of ARL13B,  $\gamma$ -tubulin and DAPI, showing decreased ciliogenesis at the PC in the latter ones, calculated as a percentage of ciliated cells (mean  $\pm$  SEM, N = 50 cells, from 3 independent experiments). \*\*\* $p < 0.001$  in two-tailed Student's t test. Scale bar, 10 $\mu$ m. **d** Representative confocal images of HK2 cells (siCTRL), compared to PI3KC2 $\alpha$  knocked down cells (siPI3KC2 $\alpha$ ), by immunostaining of acetylated tubulin (Act-tubulin),  $\gamma$ -tubulin and DAPI. Scale bar, 10 $\mu$ m.

**Supplementary Fig. 3 PI3KCIII/VPS34 knockdown has no effect on ciliogenesis.** **a** Western blot analysis of VPS34 levels in lysates of HK2 cells (siCTRL), compared to VPS34 knocked down cells (siVPS34), upon shear stress (96 hours) conditions. **b, c** Representative confocal images of HK2 cells (siCTRL), compared to VPS34 knocked down cells (siVPS34), by immunostaining of ARL13B,  $\gamma$ -tubulin and DAPI, showing no effect on primary cilium length (mean  $\pm$  SEM, N = 50 cells, from 3 independent experiments). \*\*\*p < 0.001 in two-tailed Student's t test. Scale bar, 10 $\mu$ m.

**Supplementary Fig. 4 PI3KC2 $\alpha$  knockdown affects AMPK/LKB1 signalling.** **a, b** representative confocal images and related quantification of TYR172-phospho-AMPK (P-AMPK) recruitment to PC area in HK2 cells (siCTRL), compared to PI3KC2 $\alpha$  knocked down cells (siPI3KC2 $\alpha$ ), by immunostaining of ARL13B, P-AMPK and DAPI, showing recruitment of P-AMPK in shear stress conditions in siCTRL but not in siPI3KC2 $\alpha$  cells (mean  $\pm$  SEM, N = 40 cells, from 3 independent experiments). \*\*\*p < 0.001 in two-tailed Student's t test. Scale bar, 10 $\mu$ m. **c, d**, representative confocal images and related quantification of LKB1 recruitment to PC area in HK2 cells (siCTRL), compared to PI3KC2 $\alpha$  knocked down cells (siPI3KC2 $\alpha$ ), by immunostaining of ARL13B, LKB1 and DAPI, showing recruitment of LKB1 in shear stress conditions in siCTRL but not in siPI3KC2 $\alpha$  cells (mean  $\pm$  SEM, N = 40 cells, from 3 independent experiments). \*\*\*p < 0.001 in two-tailed Student's t test. Scale bar, 10 $\mu$ m.

**Supplementary Fig. 5 Shear stress induces PI3KC2 $\alpha$ -dependent Rab11a activation at the PC.** **a, b** Western blot analysis and quantification of Rab11a levels in lysates of HK2 cells (siCTRL), compared to PI3KC2 $\alpha$  knocked down cells (siPI3KC2 $\alpha$ ), upon static (ctrl) and shear stress (96 hours) conditions. Bar graph denotes average protein levels normalized to actin (mean  $\pm$  SEM, from 3 independent experiments). \*\*\*p < 0.001 in two-tailed Student's t test. **c** Representative confocal

images of HK2 cells (siCTRL), compared to PI3KC2 $\alpha$  knocked down cells (siPI3KC2 $\alpha$ ), upon static (ctrl, 96 hours) and shear stress (96 hours) conditions, immunostained for GTP bound form of Rab11 (<sup>GTP</sup>Rab11), ARL13B and DAPI (N = 60 cells, from 3 independent experiments). White arrowheads indicate active GTP-bound Rab11 at the basal body of PC and empty arrowheads indicate active GTP-bound Rab11 at the axoneme of PC. Scale bar, 10 $\mu$ m.

**Supplementary Fig. 6 Shear stress induces PI3KC2 $\alpha$  dependent ATG16L1 recruitment at the**

**PC. a, b** Western blot analysis and quantification of ATG16L1 levels in lysates of HK2 cells (siCTRL), compared to PI3KC2 $\alpha$  knocked down cells (siPI3KC2 $\alpha$ ), upon static (ctrl) and shear stress (96 hours) conditions. Bar graph denotes average protein levels normalized to actin (mean  $\pm$  SEM, from 3 independent experiments). \*\*\*p < 0.001 in two-tailed Student's t test. **c, d** Representative confocal acquisitions, and quantifications (**d**), of HK2 cells (siCTRL), compared to PI3KC2 $\alpha$  knocked down cells (siPI3KC2 $\alpha$ ), upon static (ctrl, 96 hours) and shear stress (96 hours) conditions, immunostained for ATG16L1, ARL13B and DAPI (N = 60 cells, from 3 independent experiments). Arrowheads indicate ATG16L1 recruitment at the basal body of PC. Scale bar, 10 $\mu$ m.

**Supplementary Fig. 7 Shear stress-induced PI3P synthesis and autophagy depend on**

**PI3KC2 $\alpha$  but not on VPS34. a, b** Western blot analysis and quantification of PI3KC2 $\alpha$ , VPS34, LC3-I and LC3-II levels in lysates of HK2 cells (siCTRL), compared to PI3KC2 $\alpha$  knocked down cells (siPI3KC2 $\alpha$ ), upon static (ctrl, 96 hours) and shear stress (96 hours) conditions. Bar graph denotes average LC3-II protein levels normalized to actin and compared to ctrl (mean  $\pm$  SEM, from 3 independent experiments). \*\*\*p < 0.001 in two-tailed Student's t test. **c, d** Representative confocal images and related quantification of PI3P-positive structures in HK2 cells (siCTRL), compared to PI3KC2 $\alpha$  knocked down cells (siPI3KC2 $\alpha$ ), upon static (ctrl, 96 hours) and shear stress (96 hours)

conditions, immunostained for total PI3P-positive intracellular structures and DAPI (mean  $\pm$  SEM, N = 60 cells, from 3 independent experiments). Bar graph denotes average number of PI3P-positive structures per 200  $\mu\text{m}^2$  area (mean  $\pm$  SEM, N = 60, from 3 independent experiments). \*\*\*p < 0.001 in two-tailed Student's t test. Scale bar, 10 $\mu\text{m}$ .

**Supplementary Fig. 8 Shear stress-induced autophagy is independent of Beclin1.** **a** Western blot analysis and quantification of Beclin1 and actin levels in lysates of HK2 cells (siCTRL), compared to PI3KC2 $\alpha$  knocked down cells (siPI3KC2 $\alpha$ ), upon static (ctrl, 96 hours) and shear stress (96 hours) conditions. Bar graph denotes average Beclin1 protein levels normalized to actin and compared to ctrl (mean  $\pm$  SEM, from 3 independent experiments). **b** Western blot representative picture of Beclin1 siRNA (siBECN1) efficiency in HK2 cells. Bar graph denotes average Beclin1 protein levels normalized to actin and compared to ctrl (mean  $\pm$  SEM, from 3 independent experiments). **c** Western blot analysis and quantification of LC3.I, LC3.II and actin levels in lysates of HK2 cells (siCTRL), compared to Beclin1 knocked down cells (siBECN1), upon static (ctrl, 96 hours) and shear stress (96 hours) conditions. Bar graph denotes average LC3.II protein levels normalized to actin and compared to ctrl (mean  $\pm$  SEM, from 3 independent experiments). \*\*p < 0.05 in two-tailed Student's t test **d, e, f, g** Representative confocal images and related quantification of HK2 cells (siCTRL), compared to Beclin1 knocked down cells (siBECN1), upon shear stress (96 hours) conditions, immunostained for LC3 (in d) and  $\beta$ -catenin (in f) and DAPI (mean  $\pm$  SEM, N = 60 cells, from 3 independent experiments). Bar graph denotes average number of LC3 puncta (in e) per 200  $\mu\text{m}^2$  area (mean  $\pm$  SEM, N = 60, from 3 independent experiments) and cell area (mean  $\pm$  SEM, N = 40, from 3 independent experiments). \*\*\*p < 0.001 in two-tailed Student's t test. Scale bars, 10 $\mu\text{m}$ .

**Supplementary Fig. 9 Shear stress-induced autophagy is independent of FIP200.** **a, b** Western blot analysis and quantification of FIP200, LC3 and actin levels in lysates of HK2 cells (siCTRL), compared to FIP200 knocked down cells (siFIP200), upon static (ctrl, 96 hours) and shear stress (96 hours) conditions. Bar graph (**b**) denotes average FIP200 protein levels normalized to actin and compared to ctrl (mean  $\pm$  SEM, from 3 independent experiments). \*\*\* $p < 0.05$  in two-tailed Student's t test. **c, d, e, f** Representative confocal acquisitions and related quantifications (**d** and **f**) of HK2 cells (siCTRL), compared to FIP200 knocked down cells (siFIP200), upon shear stress (96 hours) conditions, immunostained for LC3 (**c**) and  $\beta$ -catenin (**e**) and DAPI (mean  $\pm$  SEM, N = 60 cells, from 3 independent experiments). Bar graph denotes average number of LC3 puncta (**d**) per 200  $\mu\text{m}^2$  area (mean  $\pm$  SEM, N = 60, from 3 independent experiments) and cell area (**e**, mean  $\pm$  SEM, N = 40, from 3 independent experiments). \*\*\* $p < 0.001$  in two-tailed Student's t test. Scale bars, 10 $\mu\text{m}$ .

**Supplementary Fig. 10 characterisation of IFT88 knockdown HK2 cells.** **a, b** Representative confocal acquisitions, and quantifications (**b**) of ciliogenesis (percentage of ciliated cells), in HK2 cells (siCTRL), compared to IFT88 knocked down cells (siIFT88), by immunostaining of ARL13B,  $\gamma$ -tubulin and DAPI, showing decreased ciliogenesis at the PC in siIFT88 cells, calculated as a percentage of ciliated cells (mean  $\pm$  SEM, N = 50 cells, from 3 independent experiments). \*\*\* $p < 0.001$  in two-tailed Student's t test. Scale bar, 10 $\mu\text{m}$ . **c** Western blot analysis of IFT20 and actin levels in lysates of HK2 cells (siCTRL), compared to IFT20 knocked down cells (siIFT20), upon shear stress (96 hours) conditions. **d, e** Representative confocal acquisitions, and quantifications (**e**) of ciliogenesis (percentage of ciliated cells), in HK2 cells (siCTRL), compared to IFT88 knocked down cells (siIFT88) and IFT20 knocked down cells (siIFT20), by immunostaining of ARL13B,  $\gamma$ -tubulin and DAPI, showing decreased ciliogenesis at the PC in siIFT88 and siIFT20 cells, calculated as a percentage of ciliated cells (mean  $\pm$  SEM, N = 50 cells, from 3 independent experiments). \*\*\* $p < 0.001$  in two-tailed Student's t test. Scale bar, 10 $\mu\text{m}$ . **f, g** Western blot analysis and quantification of LC3 and actin levels in lysates of HK2 cells (siCTRL), compared to IFT88 knocked down cells

(silFT88) and IFT20 knocked down cells (silFT20) upon shear stress (96 hours) conditions. Bar graph (g) denotes average LC3.II protein levels normalized to actin and compared to ctrl (mean  $\pm$  SEM, from 3 independent experiments). \*\*\* $p < 0.05$  in two-tailed Student's t test. h, i Western blot analysis and quantification of PI3KC2 $\alpha$  and actin levels in lysates of HK2 cells (siCTRL), compared to IFT88 knocked down cells (silFT88) upon static (ctrl, 96 hours) and shear stress (96 hours) conditions. Bar graph (i) denotes average PI3KC2 $\alpha$  protein levels normalized to actin and compared to ctrl (mean  $\pm$  SEM, from 3 independent experiments). \*\*\* $p < 0.05$  in two-tailed Student's t test. j Representative confocal acquisition upon shear stress conditions of IFT88 knocked down HK2 cells (silFT88), compared to control cells (siCTRL), immunostained for ARL13B, PI3P (using FYVE-GST indirect recombinant peptide),  $\gamma$ -tubulin and DAPI. Scale bar, 10 $\mu$ m. k Quantification of the PI3P-positive structures at the PC area, as shown in j, in HK2 cells (siCTRL), compared to IFT88 knocked down cells (silFT88), upon shear stress (96 hours) conditions (mean  $\pm$  SEM, N = 60 cells, from 3 independent experiments). NS: not significant, \*\*\* $p < 0.001$  in two-tailed Student's t test.

**Supplementary Fig. 11 the kinase-inactive PI3KC2 $\alpha$  mutant does not rescue autophagy in IFT88 knocked-down cells.** a, b Western blot analysis of GFP-PI3KC2 $\alpha$  variants, LC3 and actin levels in lysates of IFT88 knocked down cells transfected with wild-type PI3KC2 $\alpha$  (WT PI3KC2 $\alpha$ ), kinase-inactive mutant of PI3KC2 $\alpha$  (PI3KC2 $\alpha$  K<sub>inact</sub>) or mock transfected (mock), upon shear stress (96 hours) conditions. Bar graph (b) denotes average LC3.II protein levels normalized to actin and compared to mock condition (mean  $\pm$  SEM, from 3 independent experiments). \*\*\* $p < 0.05$  in two-tailed Student's t test. c, d Representative confocal acquisition of IFT88 knocked down cells, transfected with wild-type PI3KC2 $\alpha$  (WT PI3KC2 $\alpha$ ), kinase-inactive mutant of PI3KC2 $\alpha$  (PI3KC2 $\alpha$  K<sub>inact</sub>) or mock transfected (mock), upon shear stress (96 hours) conditions, and immunostained for LC3 and DAPI. Scale bar, 10 $\mu$ m. d Bar graphs denote average number of LC3 puncta per 200  $\mu$ m<sup>2</sup>

area (mean  $\pm$  SEM, N = 60, from 3 independent experiments). \*\*p < 0.01, \*\*\*p < 0.001 in two-tailed Student's t test.

## MATERIALS and METHODS

**Animals and in vivo samples analysis:** PI3KC2 $\alpha^{+/-}$  mice were described in Franco *et al.*<sup>19</sup>. Briefly, a *lacZ* (bacterial  $\beta$ -galactosidase)-*neoR* cassette was inserted in-frame with the ATG start codon of *Pik3c2a* via bacterial recombination. Constructs were electroporated in ES cells and chimeras obtained by standard procedures. Mice were backcrossed for eight generations in the C57Bl/6J. Wild-type littermates from heterozygous crosses were used as controls. Mice were from the breeding facility of CREFRE (US006, Toulouse, France) and maintained under SPF conditions at the animal facility of Ranguel (Anexplo platform, US06, Toulouse, France). All animal experimental procedures were conducted in accordance with institutional guidelines on animal experimentation approved by the local ethical committee of animal care and are conformed to the guidelines from Directive 2010/63/EU of the European Parliament on the protection of animals used for scientific purposes or the NIH guidelines. For morphological analysis and immunohistochemistry, mouse kidneys were fixed in 4% paraformaldehyde and paraffin embedded. For surface quantification, four-micrometer kidney sections were stained with Periodic Acid Schiff (PAS) and at least 50 tubular sections were measured for each mouse using Calopix software (TRIBVN). Briefly, the area of external profile of the tubule and the area of the lumen were measured and epithelial surface was calculated as the difference between the two areas. For autophagy quantification, four-micrometers kidney sections were incubated with anti-LC3 (MBL, PM036) antibody, followed by fluorophore-conjugated secondary antibody (Molecular Probes). Kidney sections were incubated with biotinylated-Lotus tetragonolobus lectin (LTL) (AbCys biology) followed by Alexa Fluor® 555 streptavidin (Molecular Probes) to stain proximal kidney tubules. DAPI was used to stain nuclei. Whole kidney sections were scanned using a nanozoomer 2.0 HT (Hamamatsu) with a 40X oil immersion objective. LC3 *punctae* were quantified using Calopix software (TRIBVN) in all the microscopic cortical fields of the kidney section.

**Cell culture and transfections:** HK2 cells (ATCC) were cultured in Dulbecco's Modified Eagle Medium (DMEM), supplemented with 10% FCS at 37°C and 5% CO<sub>2</sub>. For the starvation experiments, cells were incubated with Earle's balanced salt solution (EBSS) for the indicated times. Confluent HK2 cells were transfected with GFP-WIPI2 (a kind gift from Tassula Proikas-Cezanne), GFP-PI3KC2 $\alpha$  and GFP- PI3KC2 $\alpha$  kinase inactive (previously described in Franco *et al*<sup>19</sup>) cDNAs using Lipofectamine 2000 (Invitrogen, Life Technologies) according to the manufacturer's instructions. SiRNA transfections were performed using Lipofectamine RNAi Max (Invitrogen, Life Technologies) according to the manufacturer's instructions and two siRNA primers were used for each target at a final concentration of 20nM. All siRNAs were purchased from Qiagen and the references are as follows: Control siRNA (SI1027281); BECN1 (Beclin1) siRNA (SI00055580 and SI00055573); VPS34/PIK3C3 siRNA (SI00040950 and SI00040971); PIK3C2 $\alpha$  (SI00040894 and SI00040901); IFT88 (SI04374552, SI04294416, SI03180065 and SI00752374); FIP200 (SI02664578, SI03036194, SI02664571 and SI00108122); IFT20 (SI04132919 and SI03134355).

**Shear stress induction:** HK2 cells were seeded ( $2.25 \times 10^5$  in 150 $\mu$ l of medium) into a microslide "10.6 Luer" chamber (channel dimensions: 50 x 5 x 0.4mm, Ibidi) and cultured for 96h to allow proper polarization and epithelial differentiation. The microslides were connected to a fluid flow system, which contains an air-pressure pump and a two-way switch valve that pumps the culture medium unidirectionally between two reservoirs through the flow chamber at a rate corresponding to a shear stress of 1 dyn/cm<sup>2</sup>. The control cells (static) were set up in the same microslide Luer chambers and maintained in culture as long as the flow-subjected cells.

**Protein extraction, western blotting analysis and antibodies:** Cells in microslides were washed twice with ice-cold PBS and lysed in ice with 150 $\mu$ l of 1X Laemmli buffer (60mM Tris-HCL pH=6.8, 2% SDS, 10% Glycerol, bromophenol blue, supplemented with 100mM DTT) for 30min. Samples were boiled for 10min at 95°C, separated by SDS/PAGE and then transferred onto Nitrocellulose

membranes. Western blot analysis was performed with specific antibodies and the antigen–antibody complexes were visualized by chemiluminescence (Immobilon Western, Merck Millipore). The following antibodies were used in immunoblotting: rabbit-anti LC3 (Sigma, Cat#L7543); mouse-anti-actin (Millipore, Cat#1501); mouse-anti-Beclin1 (BD Biosciences, Cat#612113); rabbit-anti-IFT88 (Proteintech, Cat#13967-1-AP); rabbit-anti-PIK3C2 $\alpha$  (Novus, Cat#NBP2-19829); mouse-anti-Wipi2 (2A2) (AbD Serotec, Cat#MCA5780GA); rabbit-anti-Rab11 (Cell Signaling, Cat#2413S); rabbit-anti-VPS34 (d9A5) (Cell Signaling, Cat#4263); rabbit-anti-LKB1 (Cell signaling, Cat#3050); rabbit-anti-FIP200 (Sigma, Cat#SAB4200135); mouse-anti-ATG16L1 (MBL, Cat#PM040); rabbit-anti-IFT20 (Proteintech, Cat#13615). Secondary HRP conjugate anti-rabbit IgG (GE Healthcare) and HRP conjugate anti-mouse IgG (Bio-Rad).

**Immunofluorescence and microscopy:** Cells were fixed either with 4% paraformaldehyde (PFA) for 20min or with cold methanol for 5min at -20°C for proper PC axoneme proteins detection. Cells were then washed and incubated for 30min in blocking buffer (10% FCS in PBS) followed by incubation with primary antibodies diluted in blocking buffer supplemented with 0.05% saponin for 1h at room temperature or overnight at 4°C. Cells were washed 3 times, and then incubated for 1h with fluorescent Alexa-Fluor secondary antibodies. After washing, 150 $\mu$ l of DAPI-Fluoromount were added into the Luer chamber (Southern Biotech). For the labeling of PI3P with FYVE-FYVEGST, cells were fixed and incubated for 1h with purified FYVE-FYVEGST recombinant protein (20 $\mu$ g/ml final concentration), washed with PBS, and labeled with a FITC-conjugated anti-GST antibody (Rockland) as previously described<sup>23</sup>. Images were acquired with a Zeiss Apotome.2 fluorescence microscope or Zeiss LSM700 confocal microscope both equipped with 63x oil immersion fluorescence objectives. Number of ciliated cells and length of cilia were quantified using Zen Software (Zeiss) or Imaris Software (Bitplane). The following antibodies were used for immunofluorescence: mouse-anti-LC3B (MBL, Cat# M152-3); mouse-anti-ARL13B (C-5) (Santa Cruz, Cat#515784); rabbit-anti-ARL13B (Proteintech, Cat#515784); rabbit-anti-ATG16L1 (MBL,

Cat#PM040); rabbit-anti-p-AMPK (T172) (Cell signaling, Cat#2535); rabbit-anti-PIK3C2A (Novus, Cat#NBP2-19829); mouse-anti-WIP1 (Bio-Rad, Cat#MCA5780GA); rabbit-anti- $\beta$ catenin (Cell Signaling, Cat#8480); mouse-anti- $\gamma$ -Tubulin (Sigma; Cat#T5326); rabbit-anti- $\gamma$ -Tubulin (Sigma; Cat#T5192); mouse-anti-acetylated Tubulin (Sigma; Cat#T7451); rabbit-anti-LKB1 (Cell signaling, Cat#3050); mouse-anti- Rab11-GTP (New East Biosciences; Cat#26919); Phalloidin (Cat# A34055). Alexa Fluor-conjugated secondary antibodies (donkey anti-mouse IgG and donkey anti-Rabbit IgG, Life Technologies).

**External delivery of purified PI3P:** DiC16.PI3P ( $C_{41}H_{77}Na_3O_{16}P_2$ , Echelon) and lipid carrier (shuttle PIP<sup>TM</sup>, Echelon) were reconstituted in H<sub>2</sub>O separately following the manufacturer's instructions and then mixed to prepare stock solution (0.5mM DiC16PI3P). Final mixture was diluted in fresh media for the indicated final concentrations (0.1 $\mu$ M and 1 $\mu$ M) and used on microslide chambers connected to the fluid flow system and pumps for the 3 last hours of shear stress treatment. Carrier only was used as a negative control on siFT88 transfected HK2 cells.

**Real Time Quantitative PCR:** RNA was extracted from cells using the NucleoSpin RNA kit (Macherey-Nagel). Reverse transcriptase PCR and qRT-PCR were performed using "Power Sybr green cells to CT" kit (Thermo Fisher Scientific) according to manufacturer's instructions. Actin was used as reference gene and relative quantification was calculated using the  $\Delta\Delta$ CT method. Primers sequences are as follow:

PIK3C2 $\alpha$  -forward: 5'- TGAATAGTTCATTAGTGCAATTCCTT-3';

PIK3C2 $\alpha$  –reverse: 5'- GGCATCTTTGAGAAGCCAAT-3'

WIP1 -forward: 5'- ACTGGCTACTTTGGGAAGGTTCT-3';

WIP1 –reverse: 5'- AGATGCAGAGTCTACGAT-3'

Actin-forward: 5'-GGCCAACCGTGAAAAGATGA-3';

Actin-reverse: 5'-ACCAGAGGCATACAGGGACAG-3'

**Statistical analysis:** Data are presented as means  $\pm$  SD or SEM. Statistical analyses were performed by unpaired, two-tailed Student's t-test, using GraphPad Prism7 (\*p < 0.005, \*\*p < 0.001, and \*\*\*p < 0.0001). Images showing Western blotting or immunofluorescence analysis are representative of three independent experiments unless otherwise stated.

## REFERENCES

1. De Craene, J.-O., Bertazzi, D., Bär, S. & Friant, S. Phosphoinositides, Major Actors in Membrane Trafficking and Lipid Signaling Pathways. *Int. J. Mol. Sci.* **18**, 634 (2017).
2. Di Paolo, G. & De Camilli, P. Phosphoinositides in cell regulation and membrane dynamics. *Nature* **443**, 651–657 (2006).
3. Petiot, A., Ogier-Denis, E., Blommaert, E. F., Meijer, A. J. & Codogno, P. Distinct classes of phosphatidylinositol 3'-kinases are involved in signaling pathways that control macroautophagy in HT-29 cells. *J. Biol. Chem.* **275**, 992–8 (2000).
4. Marat, A. L. & Haucke, V. Phosphatidylinositol 3-phosphates-at the interface between cell signalling and membrane traffic. *EMBO J.* (2016). doi:10.15252/embj.201593564
5. Nascimbeni, A. C., Codogno, P. & Morel, E. Phosphatidylinositol-3-phosphate in the regulation of autophagy membrane dynamics. *FEBS J.* **284**, 1267–1278 (2017).
6. Shatz, O., Holland, P., Elazar, Z. & Simonsen, A. Complex Relations Between Phospholipids, Autophagy, and Neutral Lipids. *Trends Biochem. Sci.* **41**, 907–923 (2016).
7. Lindmo, K. & Stenmark, H. Regulation of membrane traffic by phosphoinositide 3-kinases. *J Cell Sci* **119**, 605–614 (2006).
8. Schink, K. O., Tan, K.-W. & Stenmark, H. Phosphoinositides in Control of Membrane Dynamics. *Annu. Rev. Cell Dev. Biol.* (2016). doi:10.1146/annurev-cellbio-111315-125349
9. Platta, H. W. & Stenmark, H. Endocytosis and signaling. *Curr Opin Cell Biol* **23**, 393–403 (2011).
10. Gruenberg, J. The endocytic pathway: a mosaic of domains. *Nat Rev Mol Cell Biol* **2**,

- 721–730 (2001).
11. Boya, P., Reggiori, F. & Codogno, P. Emerging regulation and functions of autophagy. *Nat Cell Biol* **15**, 713–720 (2013).
  12. Mizushima, N. & Komatsu, M. Autophagy: renovation of cells and tissues. *Cell* **147**, 728–741 (2011).
  13. Dikic, I. & Elazar, Z. Mechanism and medical implications of mammalian autophagy. *Nat. Rev. Mol. Cell Biol.* **19**, 349–364 (2018).
  14. Lamb, C. a, Yoshimori, T. & Tooze, S. A. The autophagosome: origins unknown, biogenesis complex. *Nat Rev Mol Cell Biol* **14**, 759–774 (2013).
  15. Whewey, G., Nazlamova, L. & Hancock, J. T. Signaling through the Primary Cilium. *Front. Cell Dev. Biol.* **6**, 8 (2018).
  16. Orhon, I., Dupont, N., Pampliega, O., Cuervo, a M. & Codogno, P. Autophagy and regulation of cilia function and assembly. *Cell Death Differ.* **22**, 389–397 (2014).
  17. Orhon, I. *et al.* Primary-cilium-dependent autophagy controls epithelial cell volume in response to fluid flow. *Nat. Cell Biol.* **18**, 657–67 (2016).
  18. Zemirli, N. *et al.* The primary cilium protein folliculin is part of the autophagy signaling pathway to regulate epithelial cell size in response to fluid flow. *Cell Stress* **3**, 100–109 (2019).
  19. Franco, I. *et al.* PI3K class II  $\alpha$  controls spatially restricted endosomal PtdIns3P and Rab11 activation to promote primary cilium function. *Dev. Cell* **28**, 647–658 (2014).
  20. Franco, I. *et al.* Phosphoinositide 3-Kinase-C2 Regulates Polycystin-2 Ciliary Entry and Protects against Kidney Cyst Formation. *J. Am. Soc. Nephrol.* **27**, 1135–1144 (2016).

21. Boehlke, C. *et al.* Primary cilia regulate mTORC1 activity and cell size through Lkb1. *Nat. Cell Biol.* **12**, 1115–1122 (2010).
22. Gulluni, F., De Santis, M. C., Margaria, J. P., Martini, M. & Hirsch, E. Class II PI3K Functions in Cell Biology and Disease. *Trends Cell Biol.* (2019).  
doi:10.1016/j.tcb.2019.01.001
23. Nascimbeni, A. C., Codogno, P. & Morel, E. Local detection of PtdIns3P at autophagosome biogenesis membrane platforms. *Autophagy* **13**, 1602–1612 (2017).
24. Bays, J. L., Campbell, H. K., Heidema, C., Sebbagh, M. & DeMali, K. A. Linking E-cadherin mechanotransduction to cell metabolism through force-mediated activation of AMPK. *Nat. Cell Biol.* **19**, 724–731 (2017).
25. Polson, H. E. J. J. *et al.* Mammalian Atg18 (WIPI2) localizes to omegasome-anchored phagophores and positively regulates LC3 lipidation. *Autophagy* **6**, 506–522 (2010).
26. Vicinanza, M., Puri, C. & Rubinsztein, D. C. Coincidence detection of RAB11A and PI(3)P by WIPI2 directs autophagosome formation. *Oncotarget* **10**, 2579–2580 (2019).
27. Puri, C. *et al.* The RAB11A-Positive Compartment Is a Primary Platform for Autophagosome Assembly Mediated by WIPI2 Recognition of PI3P-RAB11A. *Dev. Cell* **45**, 114-131.e8 (2018).
28. Campa, C. C. *et al.* Rab11 activity and PtdIns(3)P turnover removes recycling cargo from endosomes. *Nat. Chem. Biol.* **14**, 801–810 (2018).
29. Dudley, L. J. *et al.* Intrinsic lipid binding activity of ATG16L1 supports efficient membrane anchoring and autophagy. *EMBO J.* **38**, (2019).
30. Dooley, H. C. *et al.* WIPI2 links LC3 conjugation with PI3P, autophagosome formation,

- and pathogen clearance by recruiting Atg12-5-16L1. *Mol Cell* **55**, 238–252 (2014).
31. Pampliega, O. *et al.* Functional interaction between autophagy and ciliogenesis. *Nature* **502**, 194–200 (2013).
  32. Simonsen, A. & Tooze, S. A. Coordination of membrane events during autophagy by multiple class III PI3-kinase complexes. *J Cell Biol* **186**, 773–782 (2009).
  33. Liang, X. H. *et al.* Induction of autophagy and inhibition of tumorigenesis by beclin 1. *Nature* **402**, 672–6 (1999).
  34. Hara, T. *et al.* FIP200, a ULK-interacting protein, is required for autophagosome formation in mammalian cells. *J. Cell Biol.* **181**, 497–510 (2008).
  35. Mizushima, N. The role of the Atg1/ULK1 complex in autophagy regulation. *Curr. Opin. Cell Biol.* **22**, 132–139 (2010).
  36. Pazour, G. J. *et al.* *Chlamydomonas* IFT 88 and Its Mouse Homologue, Polycystic Kidney Disease Gene *Tg* 737, Are Required for Assembly of Cilia and Flagella. *J. Cell Biol.* **151**, 709–718 (2000).
  37. Gaidarov, I., Zhao, Y. & Keen, J. H. Individual phosphoinositide 3-kinase C2alpha domain activities independently regulate clathrin function. *J. Biol. Chem.* **280**, 40766–72 (2005).
  38. Vanhaesebroeck, B., Guillermet-Guibert, J., Graupera, M. & Bilanges, B. The emerging mechanisms of isoform-specific PI3K signalling. *Nat. Rev. Mol. Cell Biol.* **11**, 329–341 (2010).
  39. Long, K. R. *et al.* Proximal tubule apical endocytosis is modulated by fluid shear stress via an mTOR-dependent pathway. *Mol. Biol. Cell* **28**, 2508–2517 (2017).
  40. Raghavan, V. & Weisz, O. a. Flow stimulated endocytosis in the proximal tubule. *Curr.*

*Opin. Nephrol. Hypertens.* **24**, 359–365 (2015).

41. Falasca, M. *et al.* Class II Phosphoinositide 3-Kinases as Novel Drug Targets. *J. Med. Chem.* **60**, 47–65 (2017).

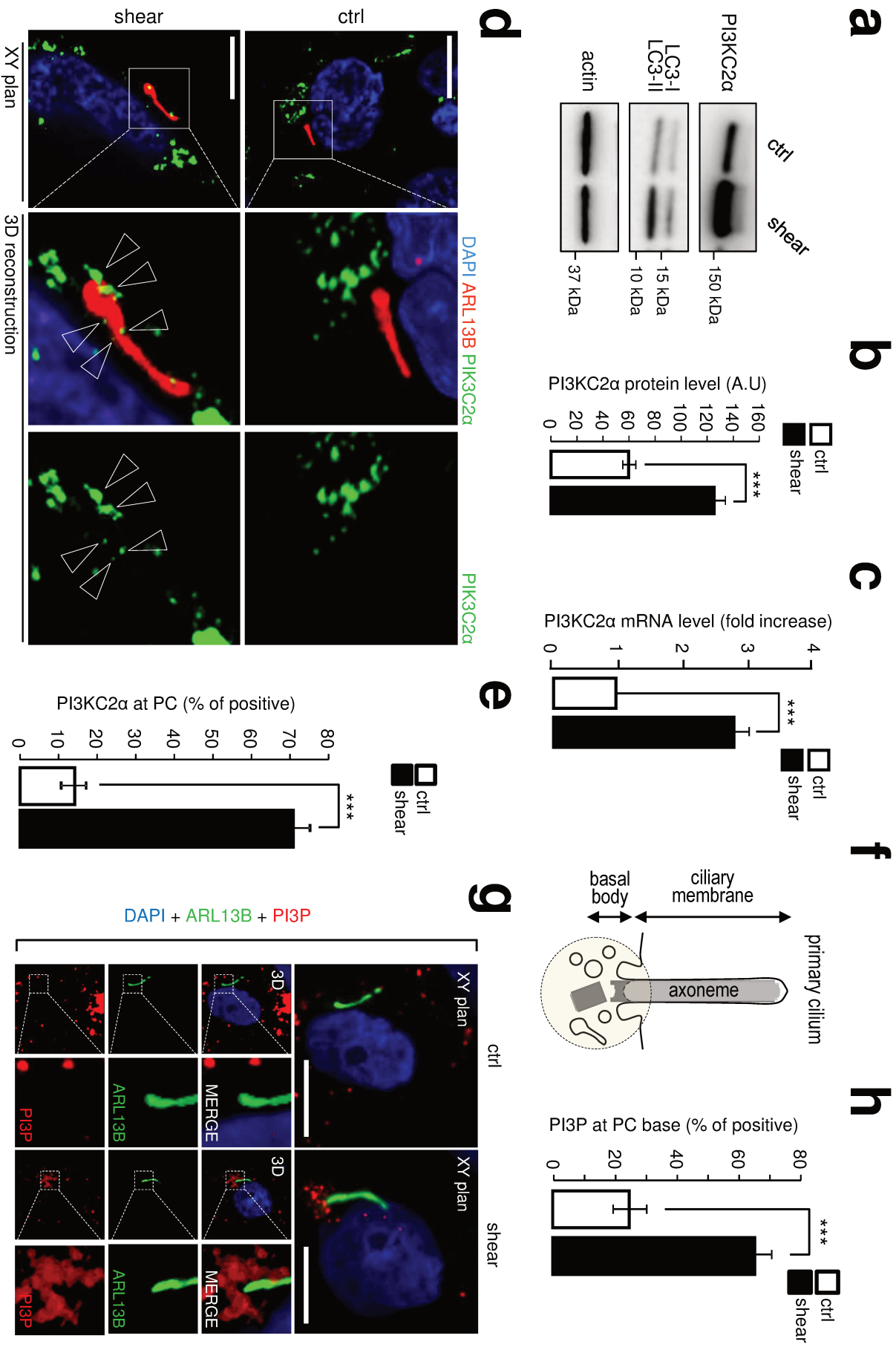


Figure 1

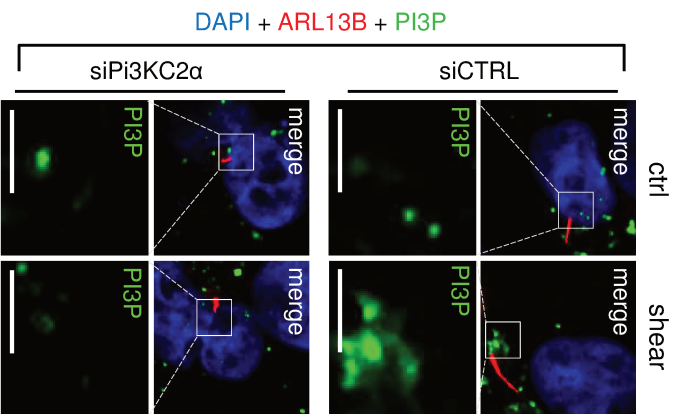
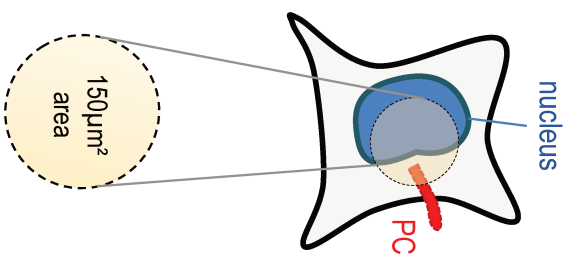
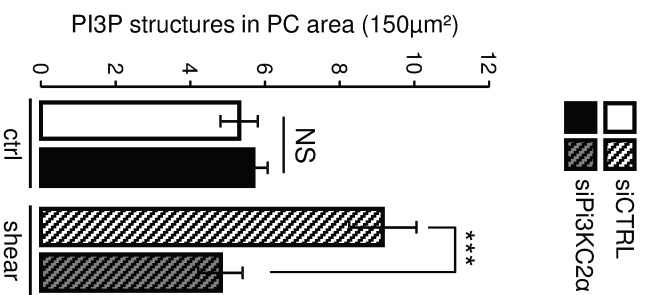
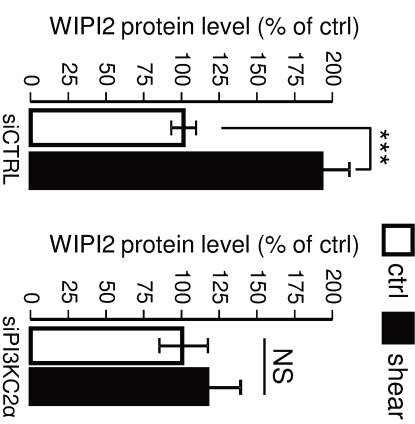
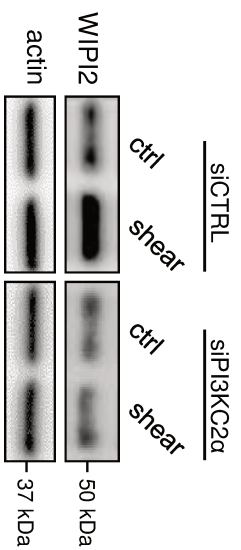
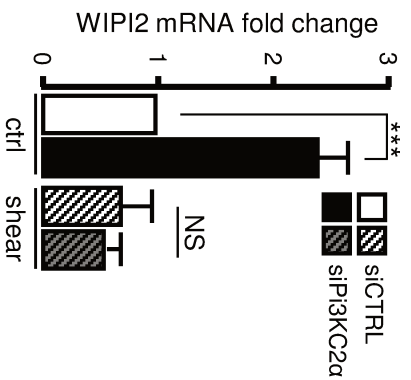
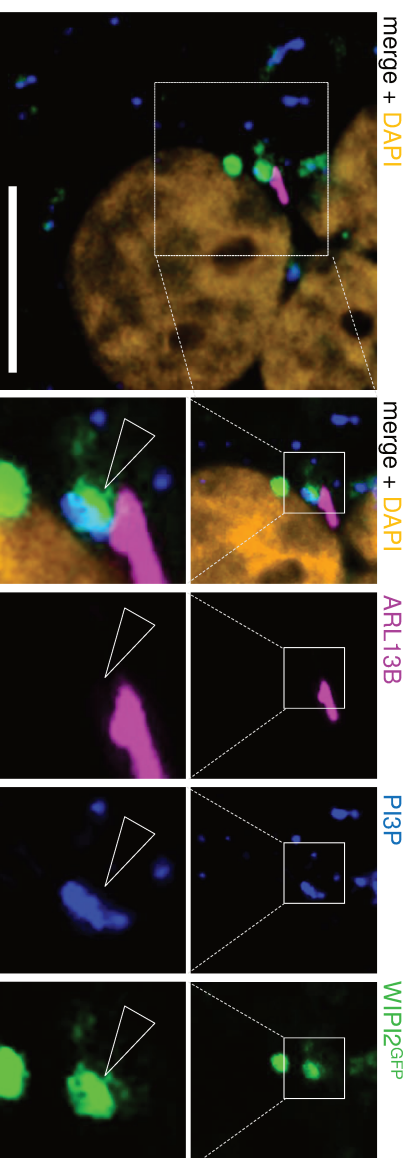
**a****b****c****d****e****f**

Figure 2

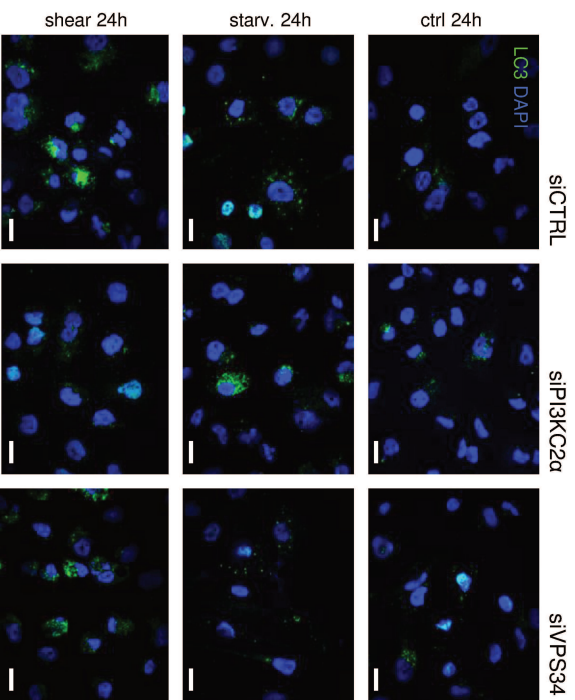
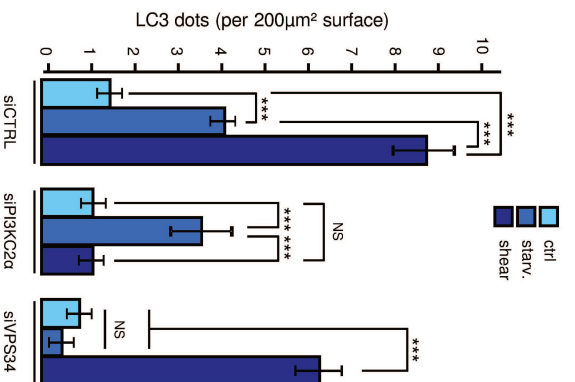
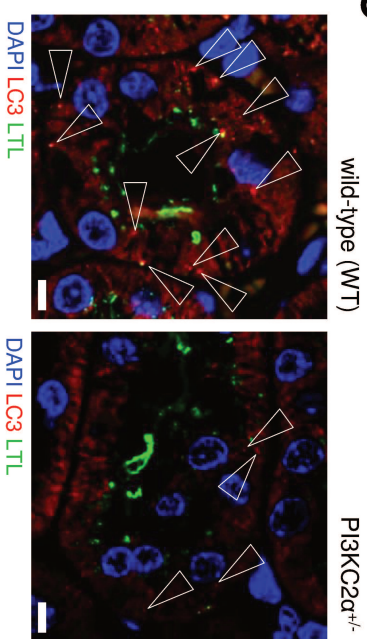
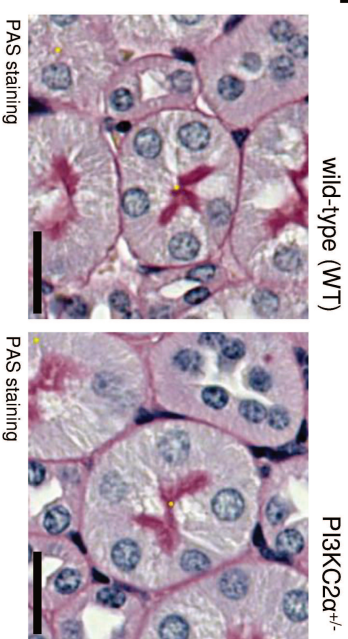
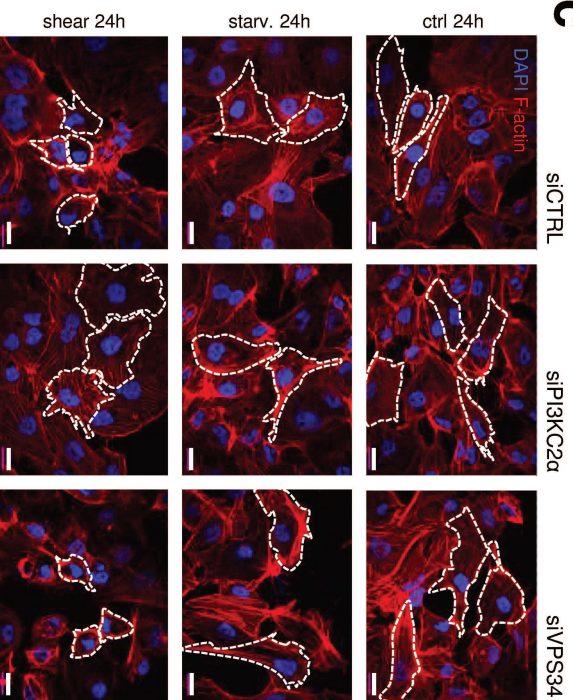
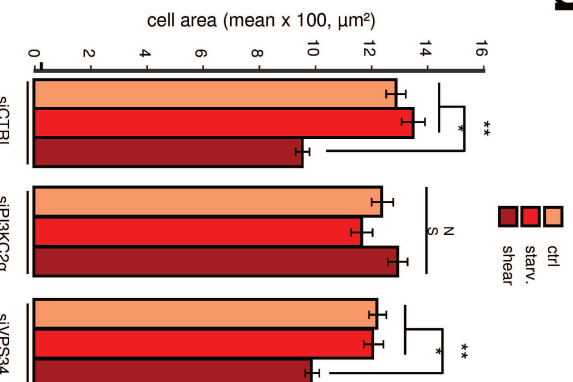
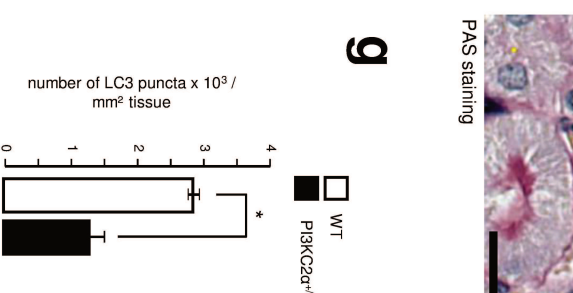
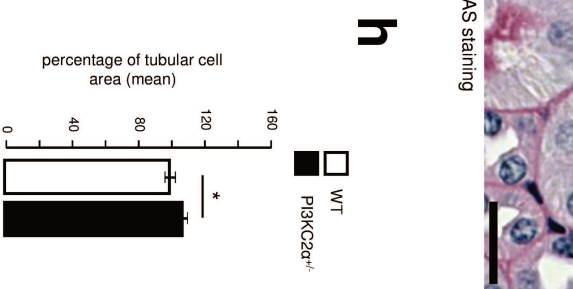
**a****b****e****f****c****d****g****h**

Figure 3

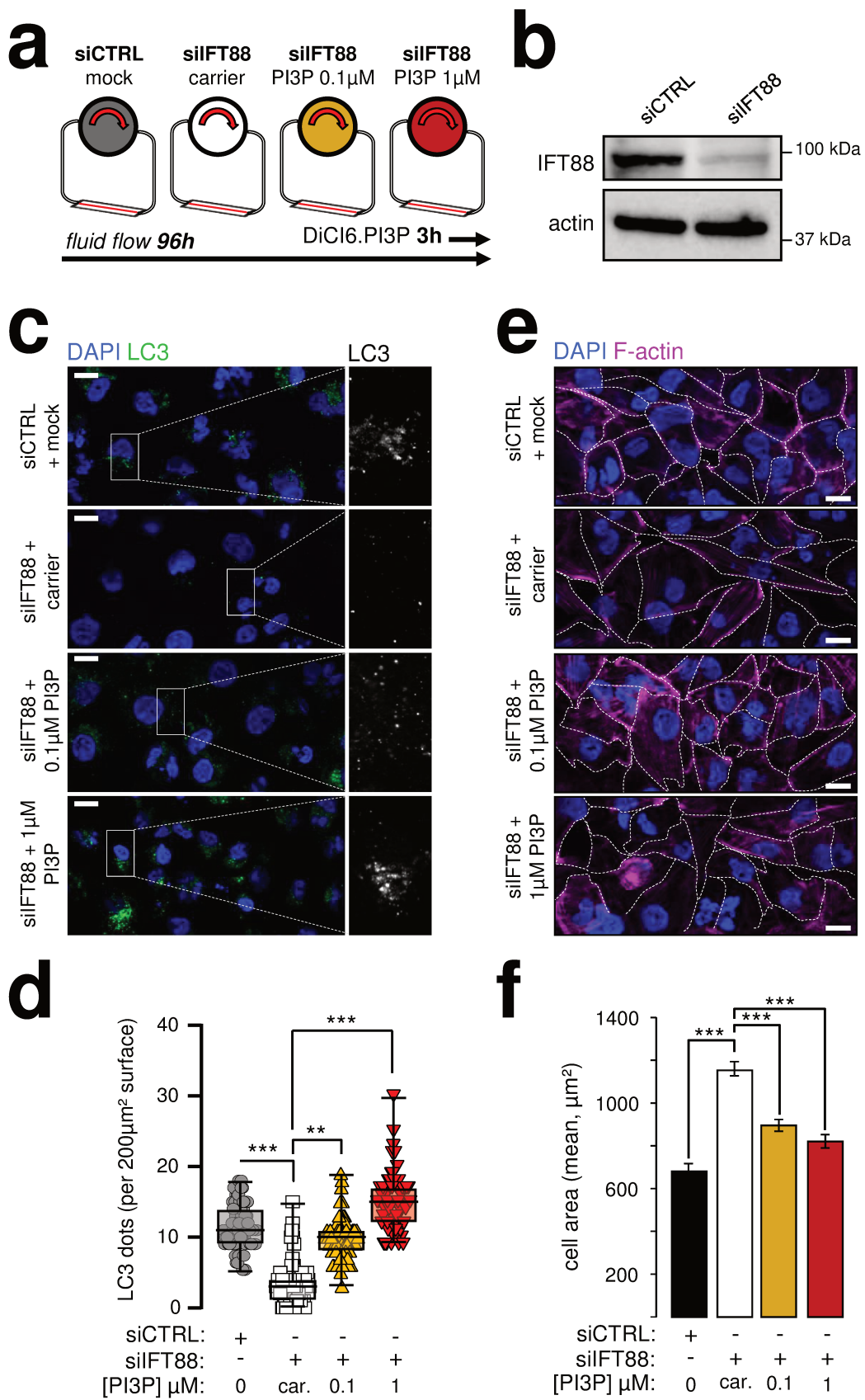
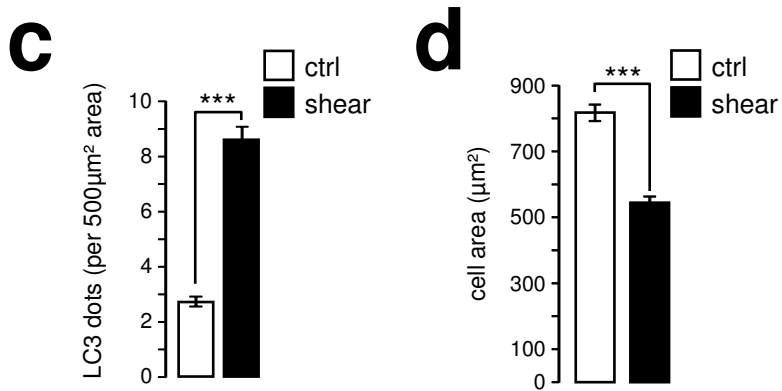
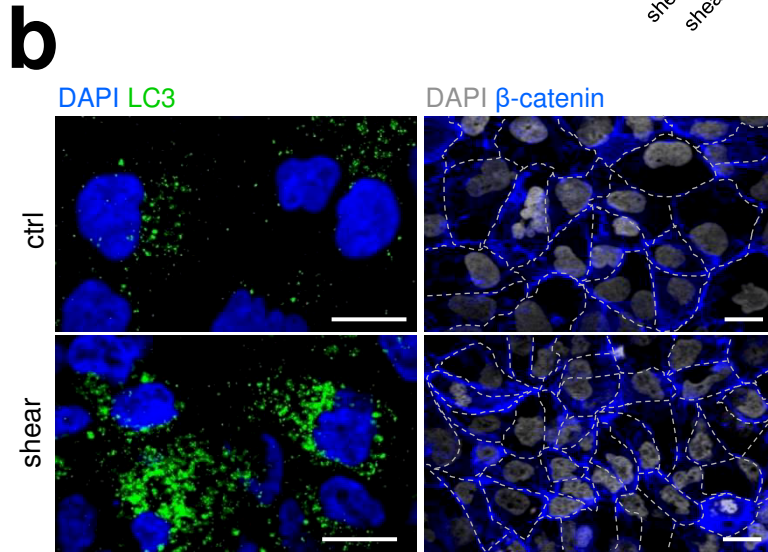
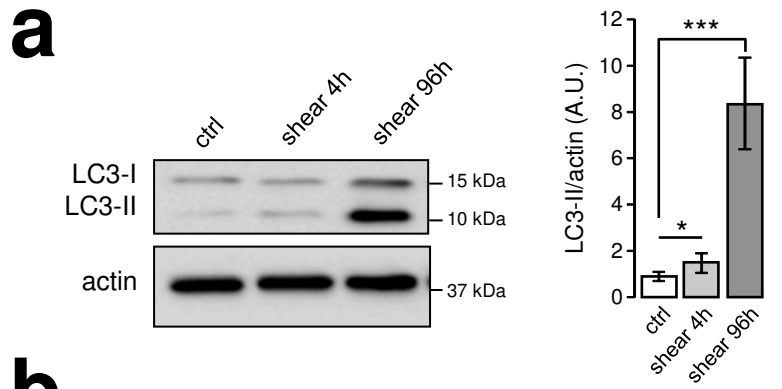
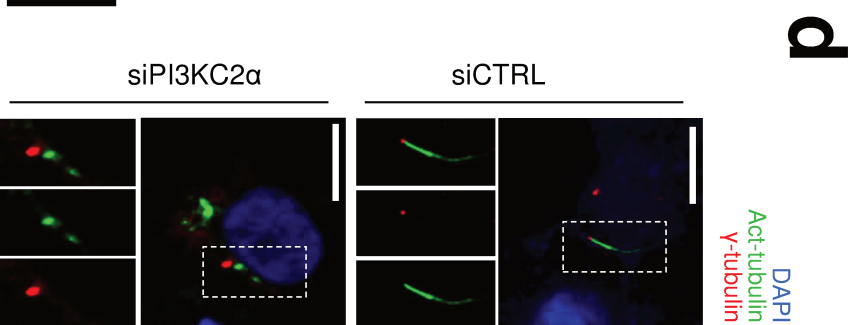
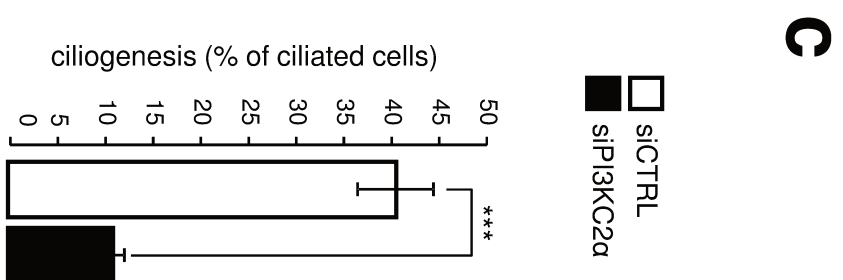
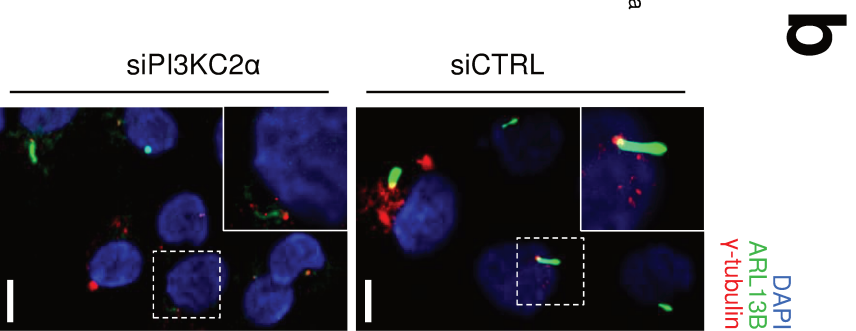
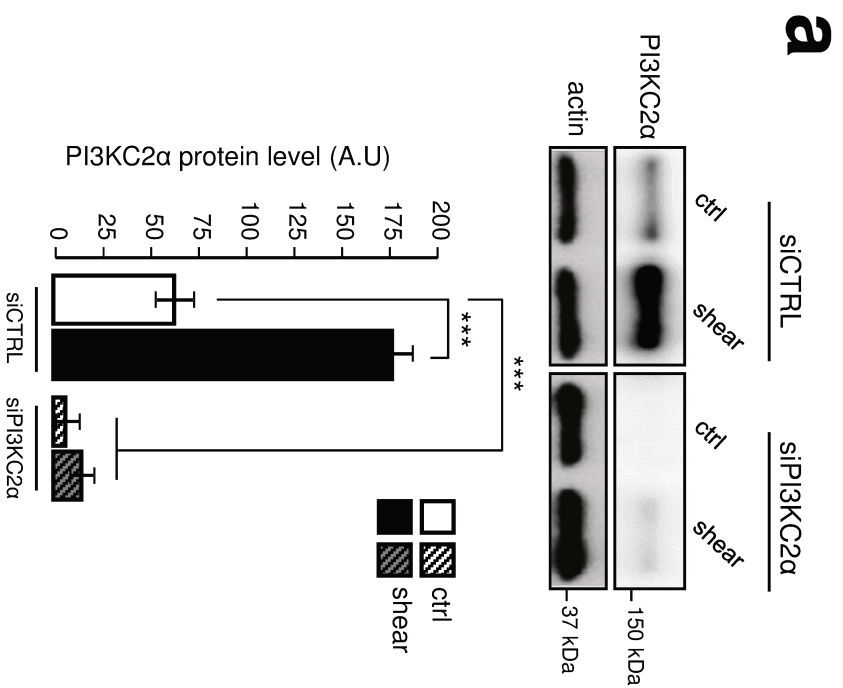


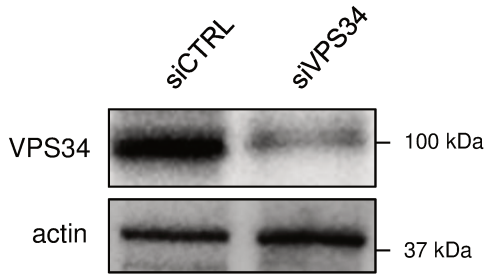
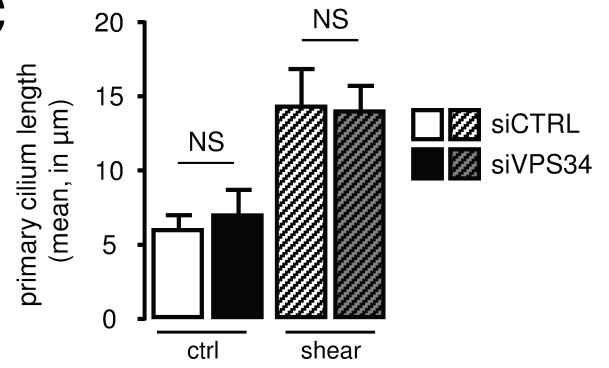
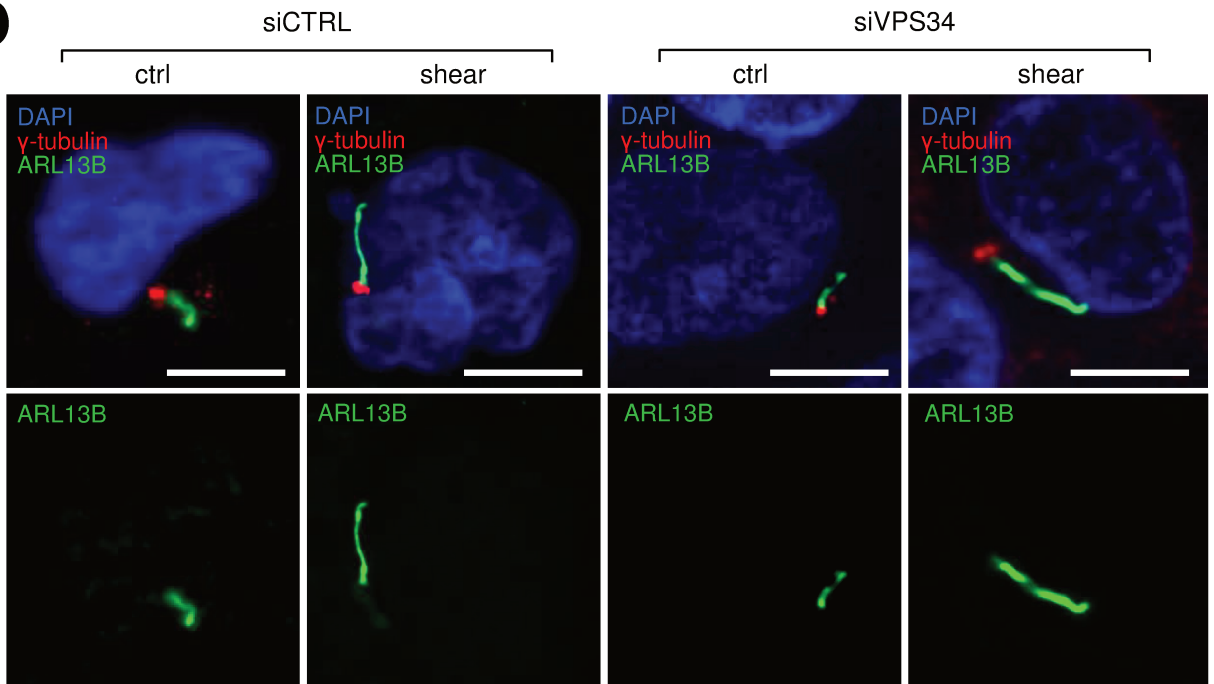
Figure 4



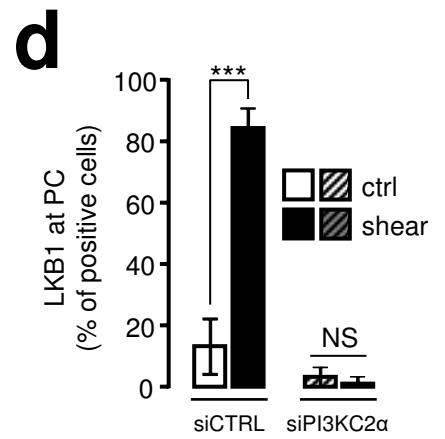
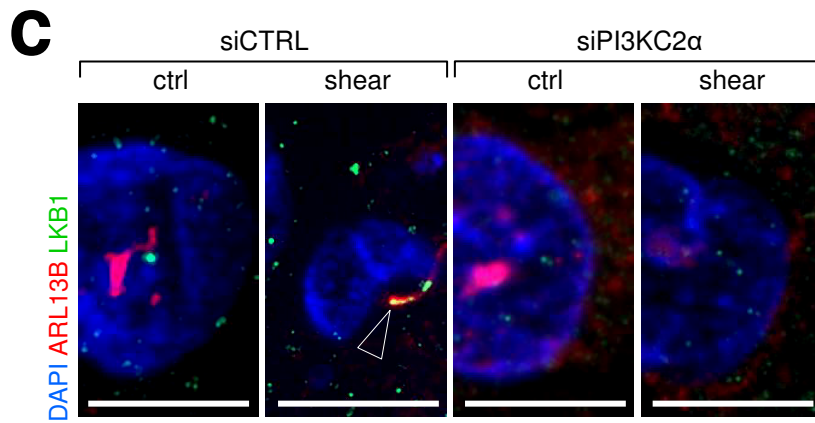
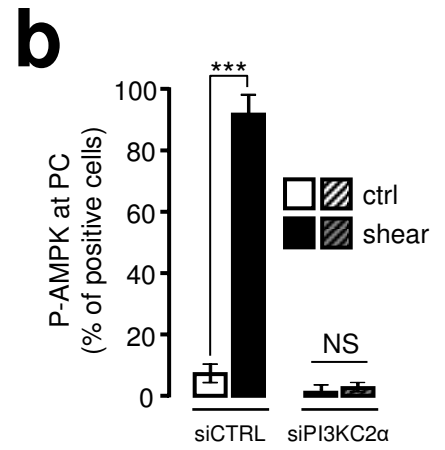
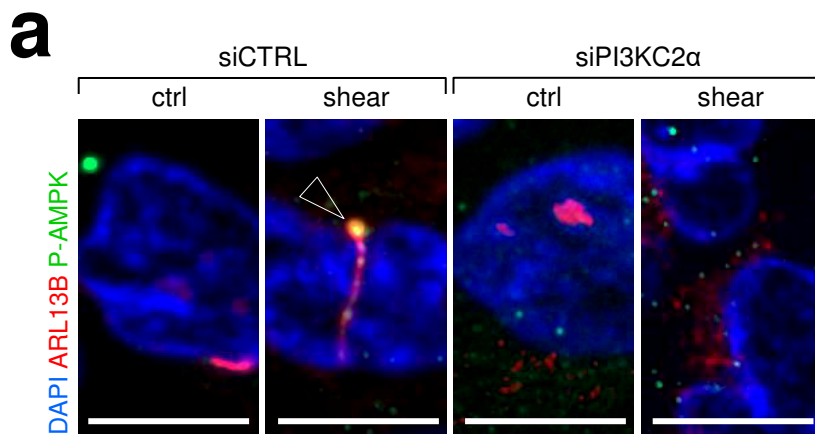
supplementary figure 1



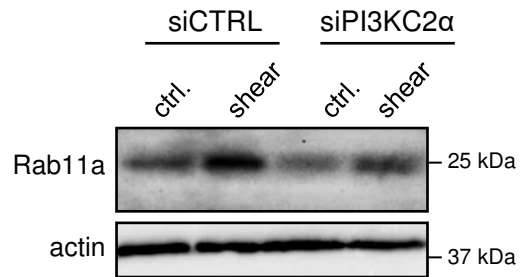
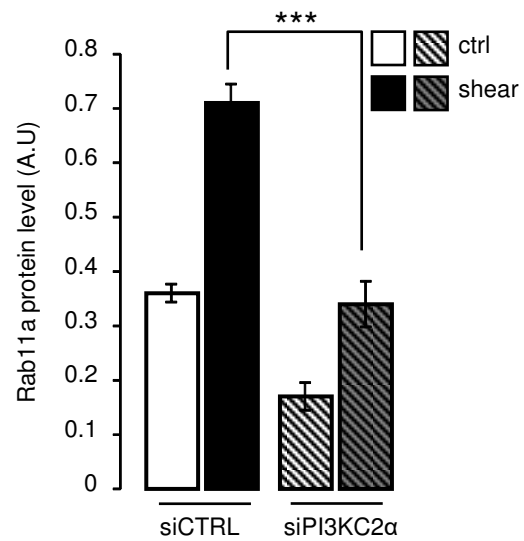
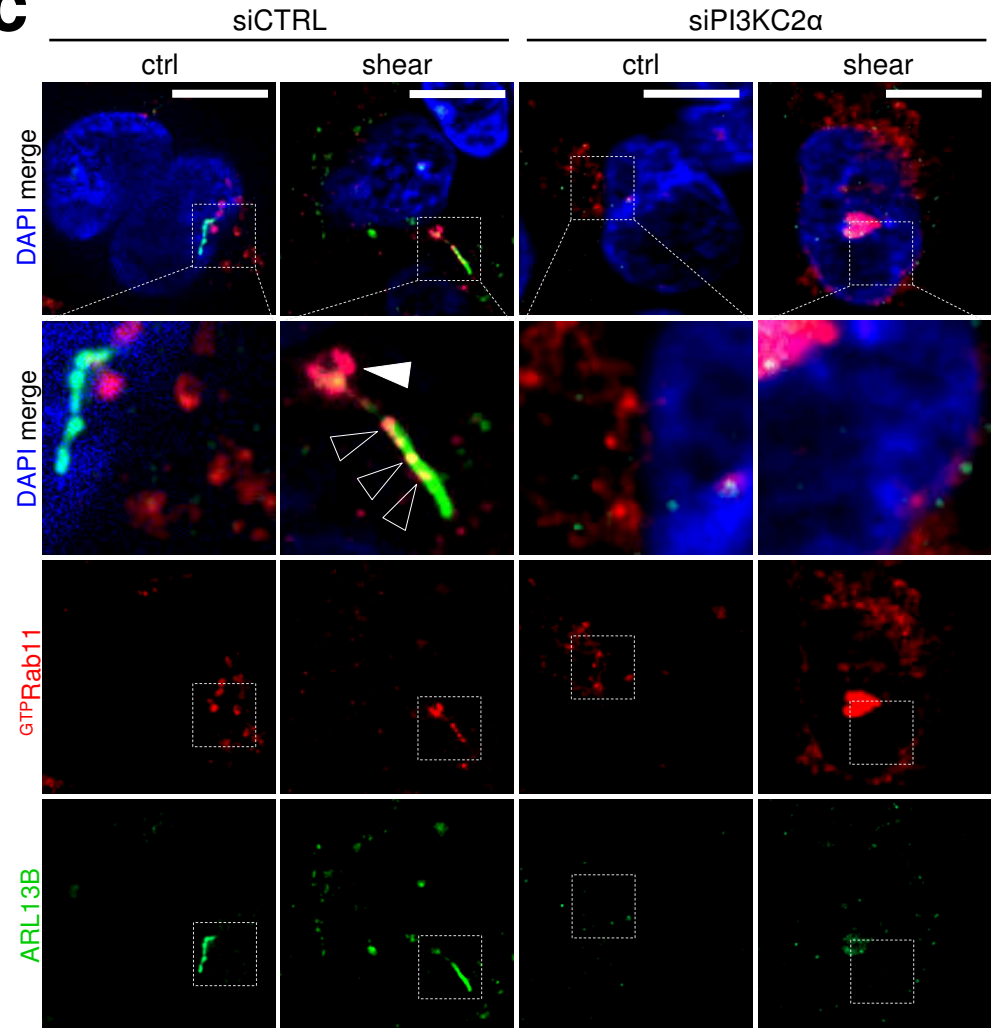
supplementary figure 2

**a****c****b**

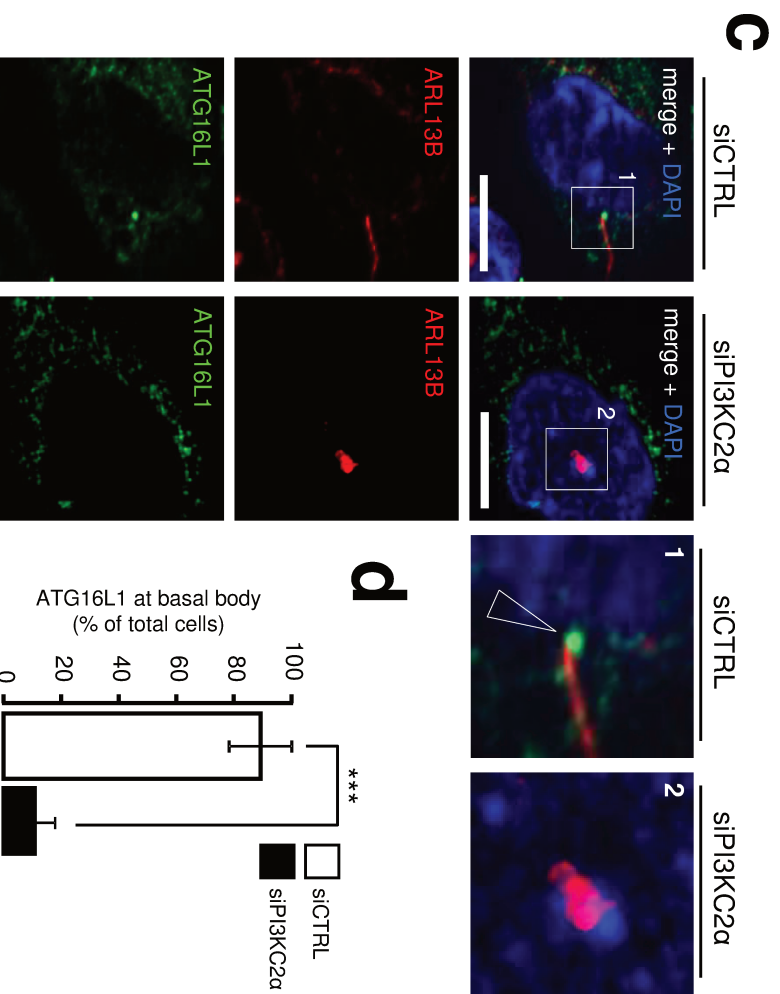
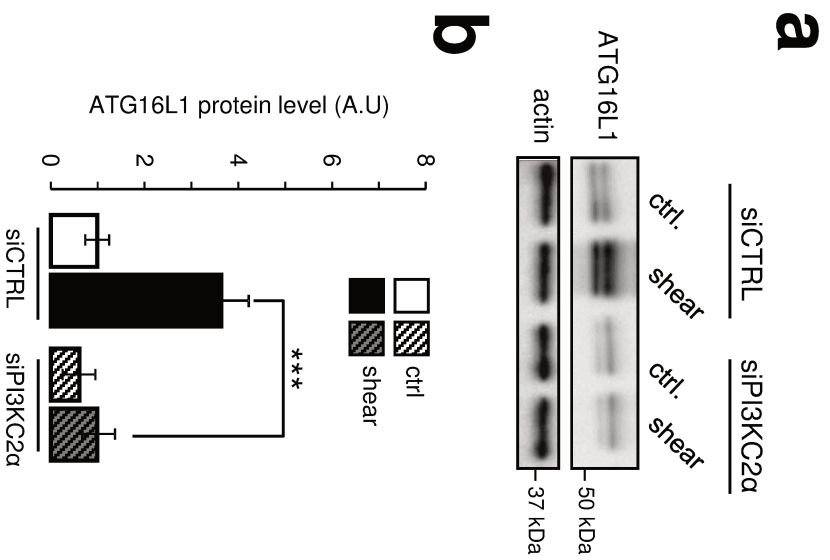
supplementary figure 3



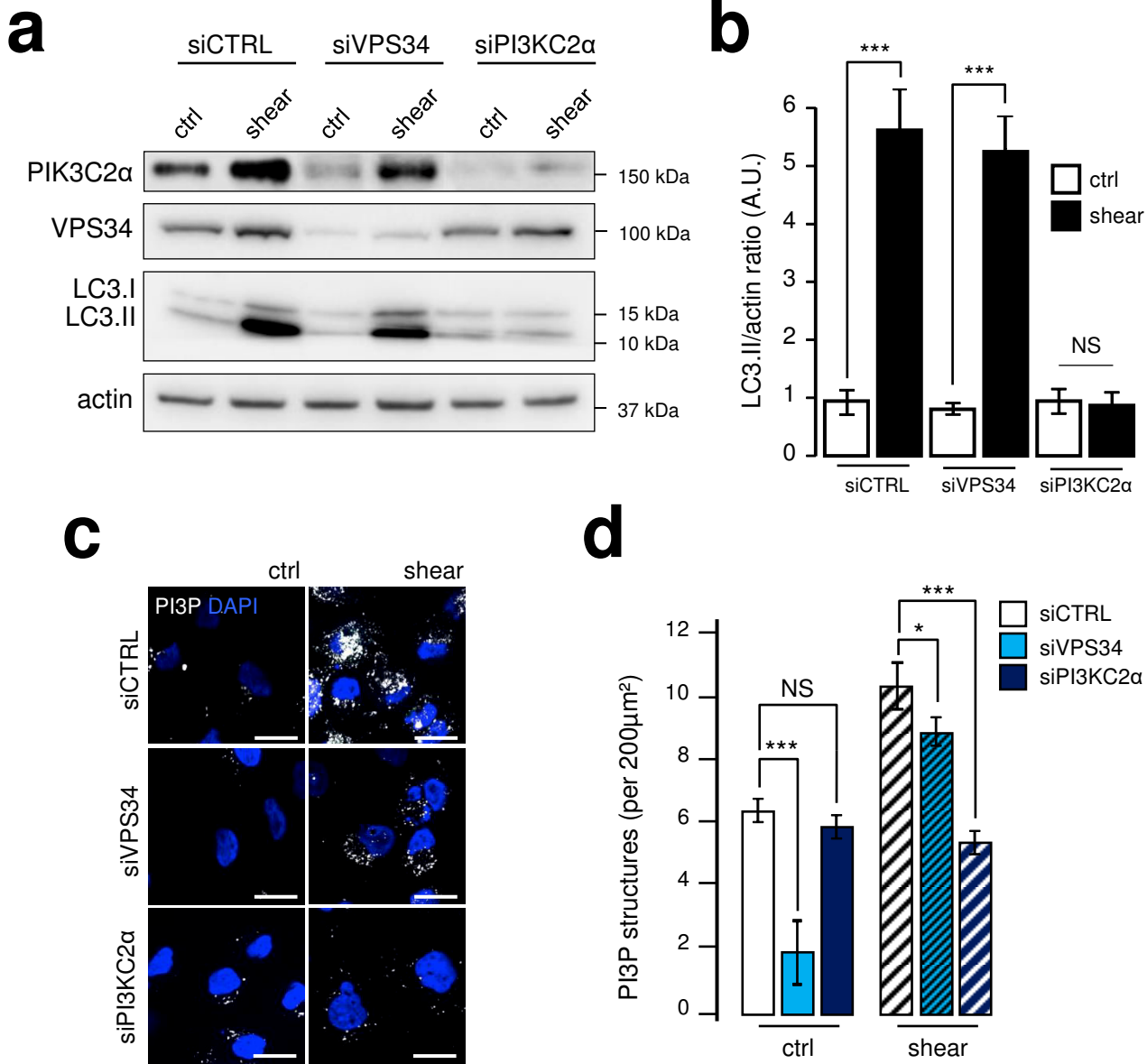
supplementary figure 4

**a****b****c**

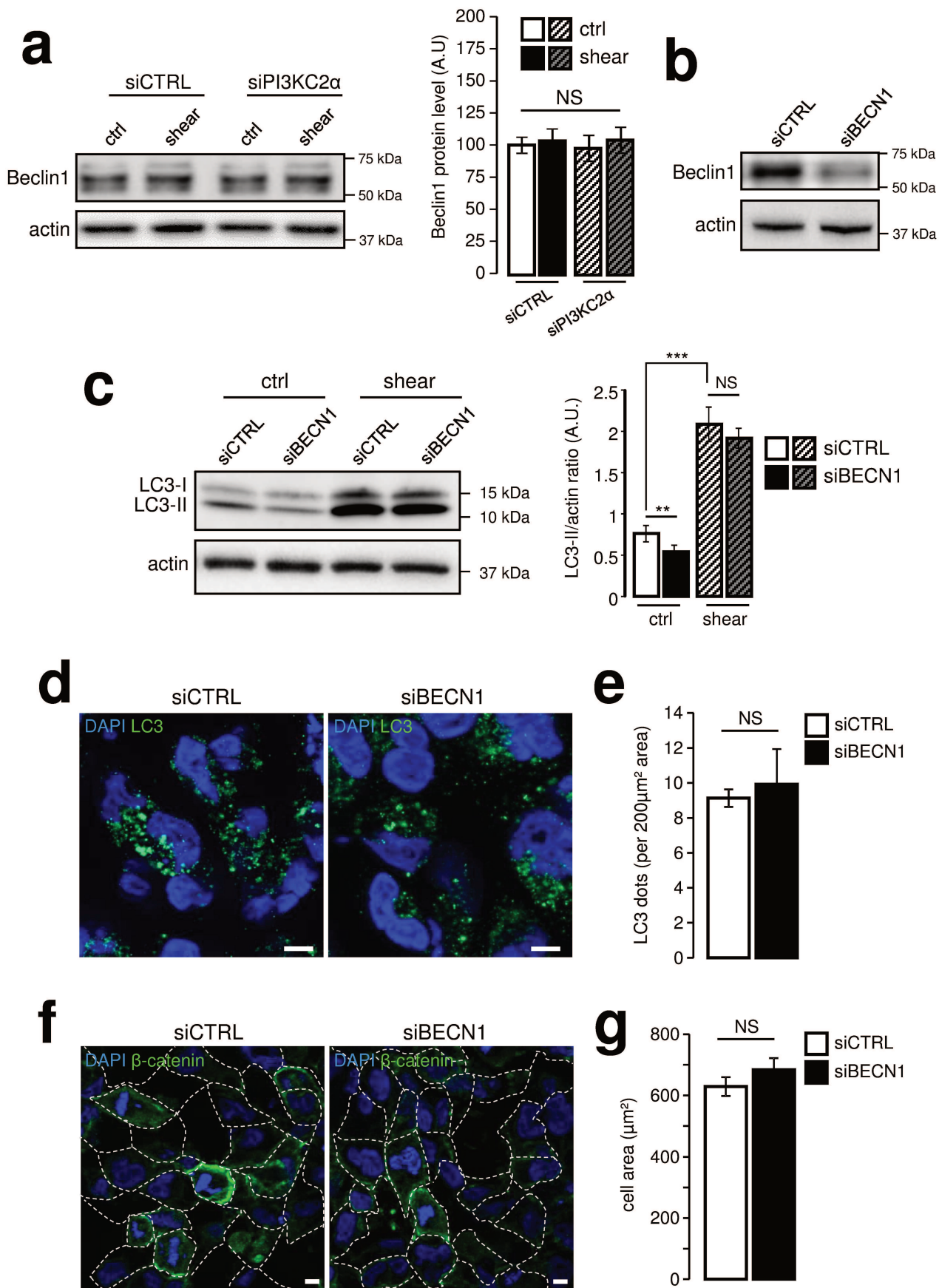
supplementary figure 5



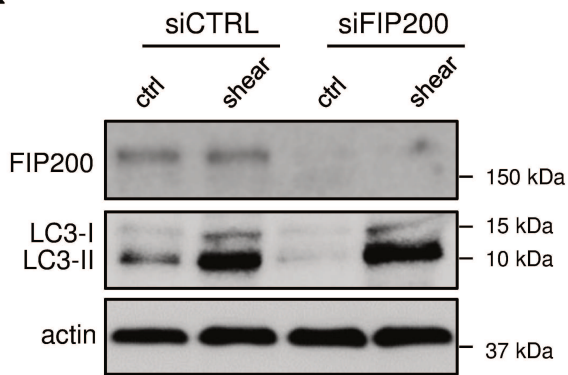
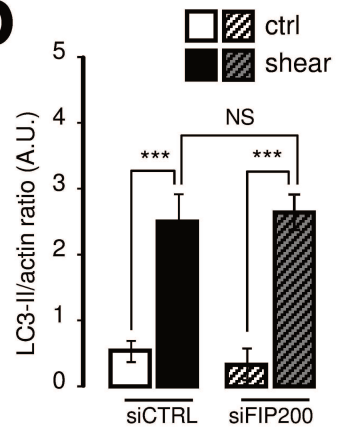
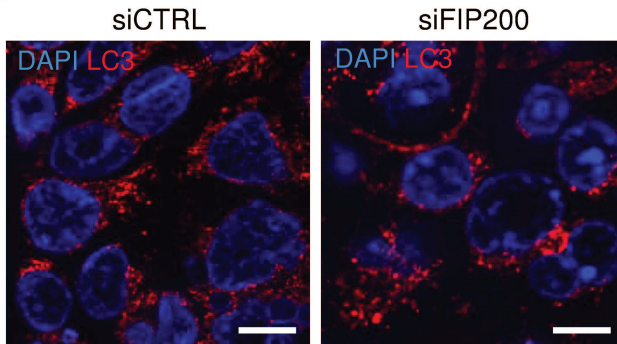
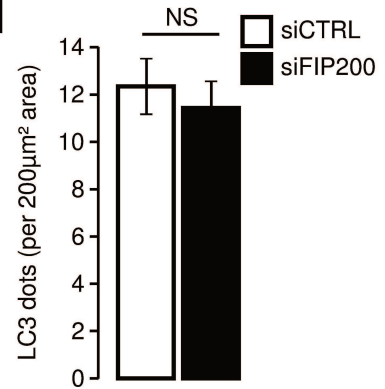
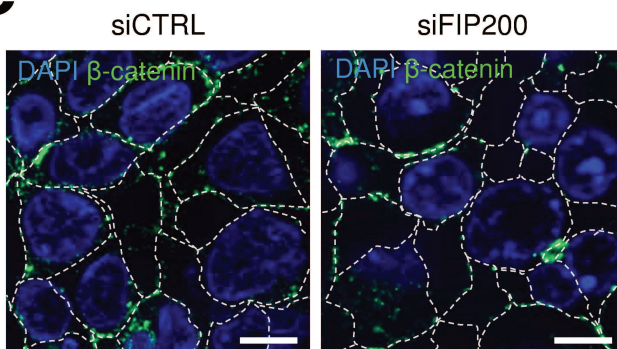
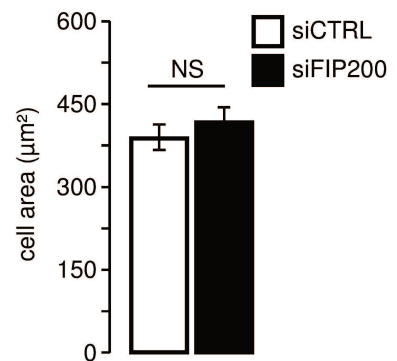
Supplementary Figure 6

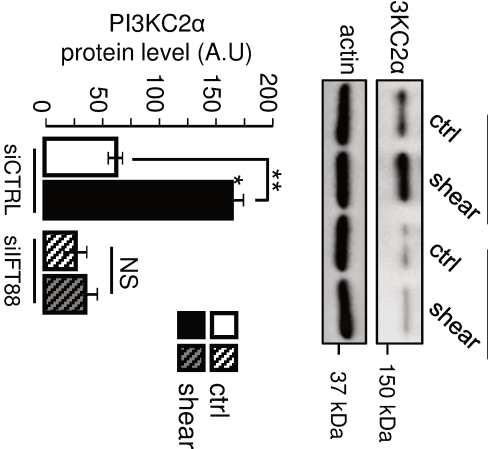
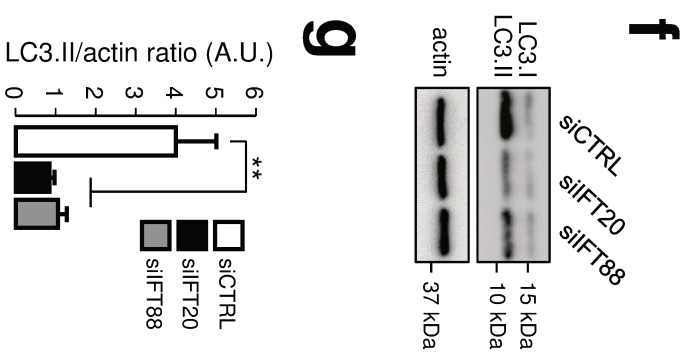
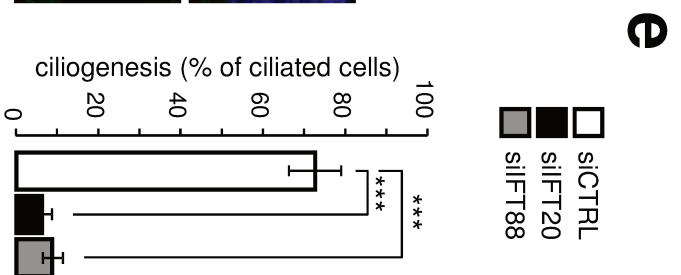
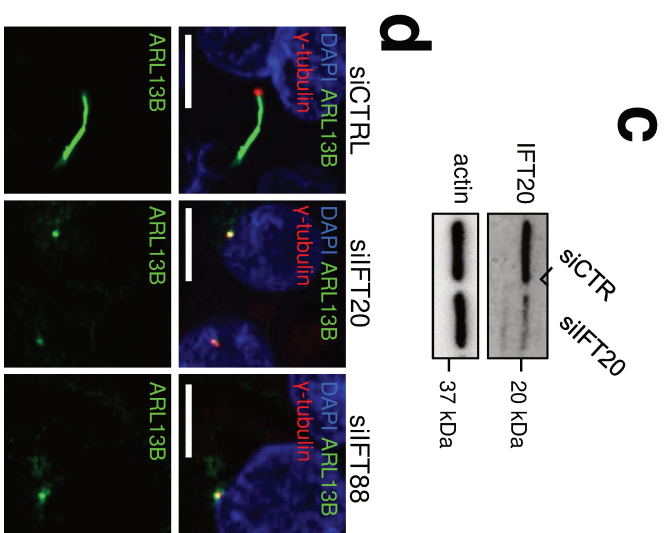
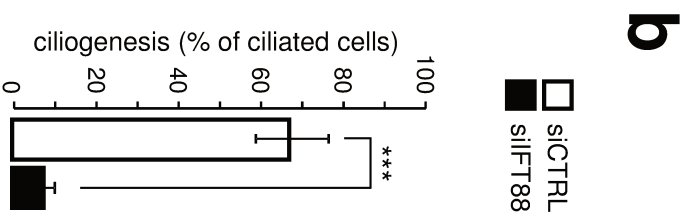
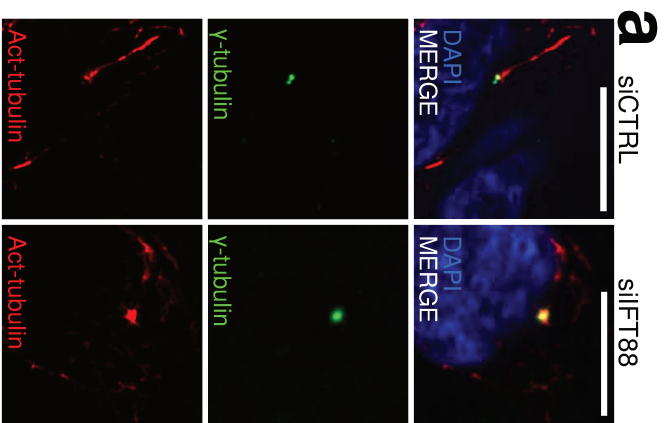


supplementary figure 7

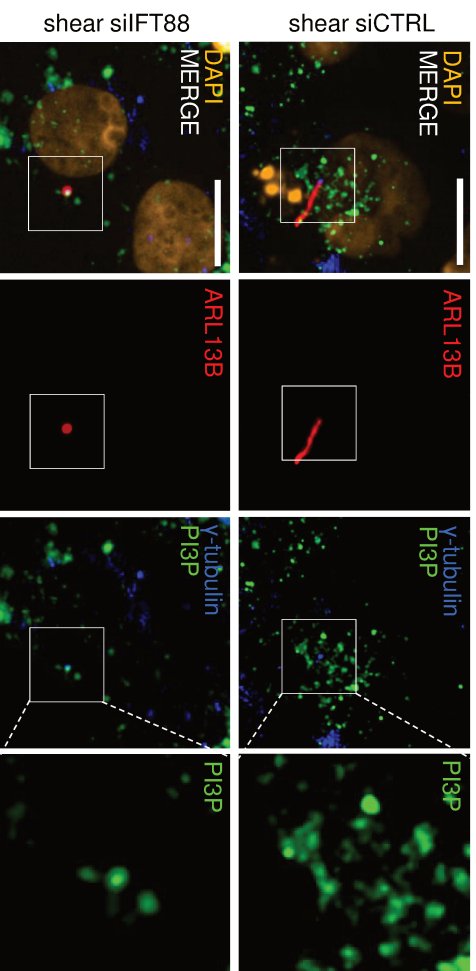


supplementary figure 8

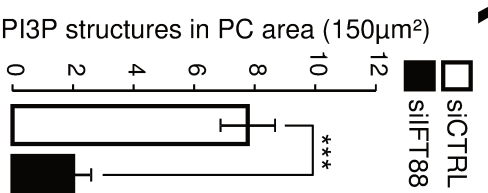
**a****b****c****d****e****f**

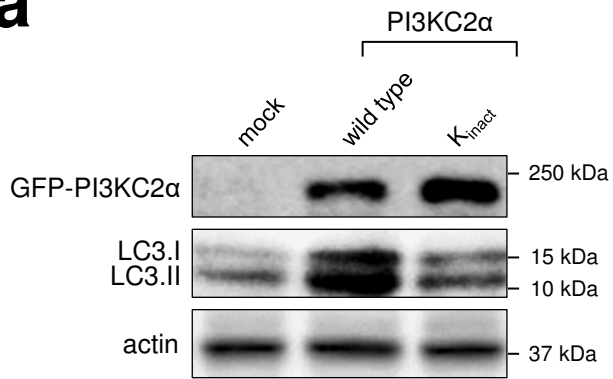
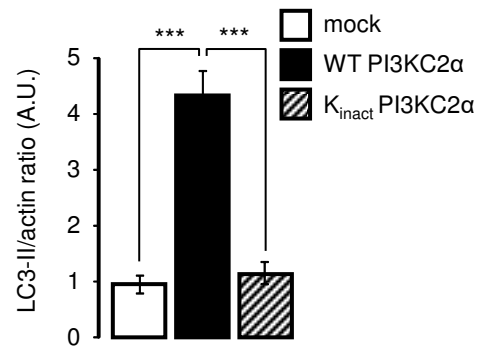
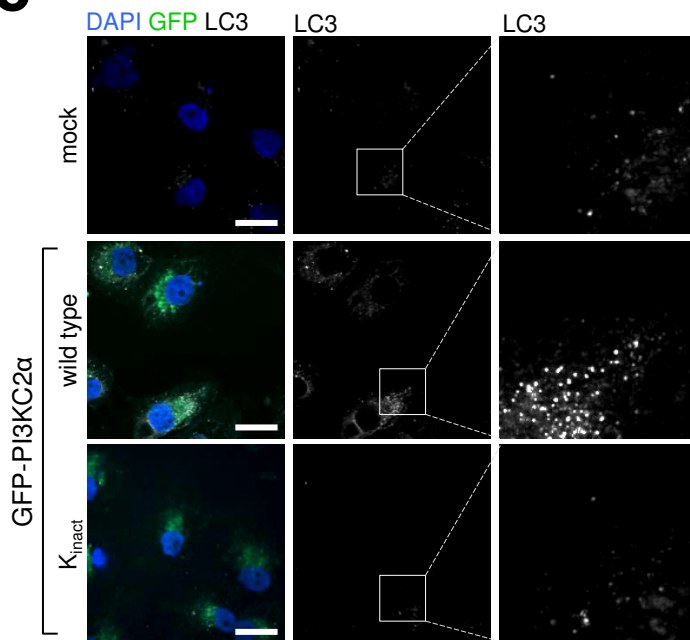
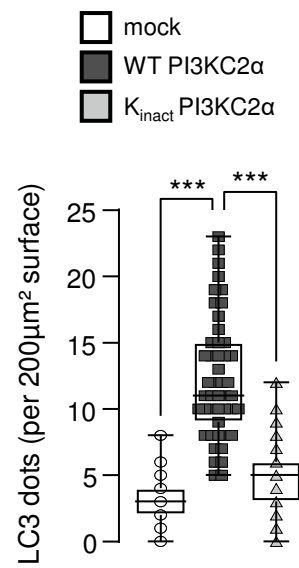


**h**



**i**



**a****b****c****d**

# The primary cilium protein folliculin is part of the autophagy signaling pathway to regulate epithelial cell size in response to fluid flow

Naïma Zemirli<sup>1,2,#</sup>, Asma Boukhalifa<sup>1,2,#</sup>, Nicolas Dupont<sup>1,2</sup>, Joëlle Botti<sup>1,3</sup>, Patrice Codogno<sup>1,2,\*</sup> and Etienne Morel<sup>1,2,\*</sup>

<sup>1</sup>Institut Necker-Enfants Malades (INEM), INSERM U1151-CNRS UMR 8253.

<sup>2</sup> Université Paris Descartes-Sorbonne Paris Cité, F-75993, Paris, France.

<sup>3</sup> Université Paris Denis Diderot Sorbonne Paris Cité, F-75993, Paris, France.

# These authors contributed equally.

\* Corresponding Authors:

Etienne Morel, Institut Necker-Enfants Malades (INEM), INSERM U1151-CNRS 8253 (Cell Biology Department of INEM, 14 rue Maria Helena Viera Da Silva, F-75014 Paris, France); E-mail: etienne.morel@inserm.fr;

Patrice Codogno, Institut Necker-Enfants Malades (INEM), INSERM U1151-CNRS 8253 (Cell Biology Department of INEM, 14 rue Maria Helena Viera Da Silva, F-75014 Paris, France); E-mail: patrice.codogno@inserm.fr

**ABSTRACT** Autophagy is a conserved molecular pathway directly involved in the degradation and recycling of intracellular components. Autophagy is associated with a response to stress situations, such as nutrients deficit, chemical toxicity, mechanical stress or microbial host defense. We have recently shown that primary cilium-dependent autophagy is important to control kidney epithelial cell size in response to fluid flow induced shear stress. Here we show that the ciliary protein folliculin (FLCN) actively participates to the signaling cascade leading to the stimulation of fluid flow-dependent autophagy upstream of the cell size regulation in HK2 kidney epithelial cells. The knock-down of FLCN induces a shortening of the primary cilium, inhibits the activation of AMPK and the recruitment of the autophagy protein ATG16L1 at the primary cilium. Altogether, our results suggest that FLCN is essential in the dialog between autophagy and the primary cilium in epithelial cells to integrate shear stress-dependent signaling.

doi: 10.15698/cst2019.03.180

Received originally: 23.09.2018;

in revised form: 02.02.2019,

Accepted 12.02.2019,

Published 25.02.2019.

**Keywords:** fluid flow, shear stress, autophagy, folliculin, autophagy, primary cilium.

**Abbreviations:**

BHD – Birt-Hogg-Dubé,

FLCN – folliculin,

FNIP – folliculin-interacting protein,

KEC – kidney epithelial cell.

## INTRODUCTION

Autophagy is an evolutionary conserved stress-response process by which cells break down intracellular components, damaged organelles and proteins aggregates or pathogens, to ensure cellular quality control and homeostasis. It is induced in response to various stress types such as nutrient deprivation, cytotoxic agents, and hypoxia. Autophagy involves the sequestration of cytoplasmic material in a double membrane organelle named autophagosome, which subsequently fuses with the lysosome to degrade and recycle autophagosomal cargoes [1]. We have recently shown that in kidney epithelial cells (KECs) autophagy is induced in response to fluid flow-provoked shear stress and that this fluid flow-dependent autophagy regulates cell

volume [2]. We have demonstrated that shear stress-induced autophagy is triggered by a signaling cascade emanating from the primary cilium located at the apical side of epithelial cells [2]. The primary cilium, which is composed of a basal body and an axoneme, is a microtubule-based organelle present at the surface of various cell types [3] and plays a critical role in maintaining tissue homeostasis by sensing extracellular mechanical and chemical stimuli [4].

To better understand the molecular mechanisms of fluid flow-induced autophagic response and cell volume regulation, it is important to identify additional players located at the primary cilium. The folliculin protein (FLCN) presents interesting features in that respect. A pool of FLCN is locat-

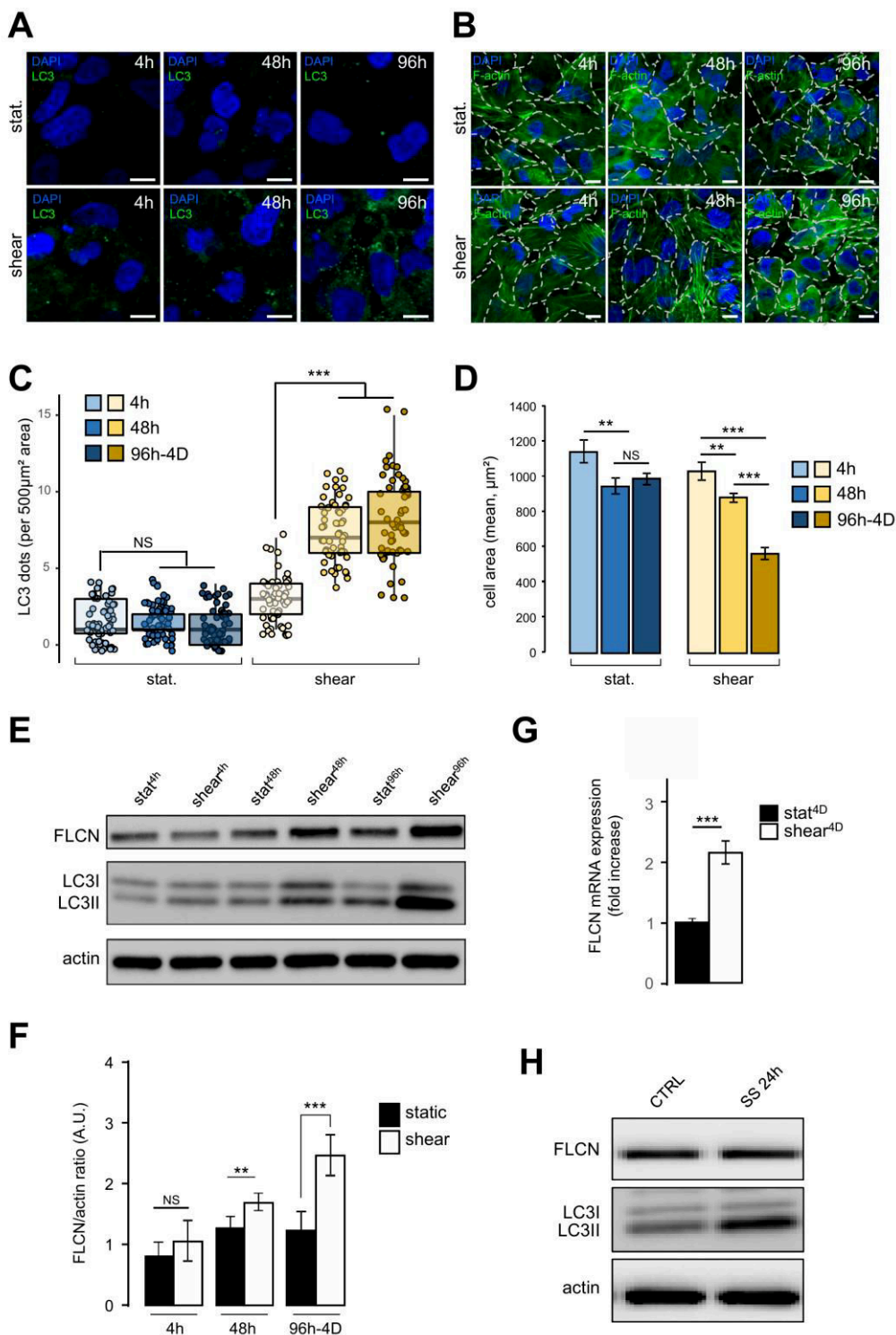


**FIGURE 1: Shear stress induces autophagy, cell size decrease and FLCN expression.** (A-D) HK2 cells were subjected to fluid flow from 4 h to 4 days (shear 4 h, 48 h, 96h-4D), or not (static 4 h, 48 h, 96h-4D). (A) After fluid flow treatment or static culture, cells were fixed, labeled with DAPI and immunostained for the autophagosome marker LC3 or stained with phalloidin to reveal F-actin and cell borders are marked out with white dashes (B) and then analyzed by fluorescence microscopy. (C) Quantification of LC3 puncta (LC3 dots number per 500 μm<sup>2</sup> area) from experiments shown in (A). (D) Quantification of cell area (mean) from experiments shown in (C). (E-F) HK2 cells were subjected to fluid flow from 4 h to 4 days (shear 4 h, 48 h, 96h-4D), or not (static 4 h, 48 h, 96h-4D). (E) Representative western blot analysis of FLCN, LC3I, LC3II and actin in the indicated conditions. (F) Quantification of Western blot shown in (E). (G) HK2 cells were subjected to 4 days (shear 4D) fluid flow or not (static 4D) and FLCN mRNA expression level was determined and quantified by RT-qPCR. (H) HK2 cells were maintained in normal culture condition (CTRL) or subjected to a 24 h serum starvation (SS 24h). Levels of the FLCN, LC3I and LC3II were analyzed by western blot. Scale bars in (A) and (C) = 10 μm.

ed at the primary cilium [5] and regulates the AMPK/mTOR signaling pathway in response to fluid flow [6]. Indeed, FLCN promotes the recruitment of LKB1 kinase to basal bodies where it activates AMPK, which in turn inhibits mTOR activation [6]. FLCN has moreover been associated with autophagy pathway regulation [7–9].

FLCN is a conserved tumor suppressor protein expressed in most cell types. Loss-of-function mutations of the FLCN gene are associated with the autosomal dominant disorder Birt-Hogg-Dubé (BHD) syndrome. It is characterized by benign hair follicle tumors, pneumothorax, cysts and renal cancer occurrence [10], and has an estimated prevalence of 1/200.000. Importantly, considering the abnormal ciliogenesis and canonical Wnt signaling, the BHD syndrome is also considered as a ciliopathy [5]. FLCN can form a complex with its two main partners FNIP1 and FNIP2 (Folliculin interacting protein 1/2). Different studies suggest a role of the FLCN/FNIP complex in multiple signaling pathways (i.e. mTOR/AMPK, TGF-β or Wnt/cadherin),

and cellular processes including cell cycle, cell adhesion and migration, membrane trafficking, cilium and lysosome biogenesis, stress responses, autophagy and several others [5]. Taken together, these data point to a pivotal role of FLCN in cellular homeostasis and raise the interesting possibility that FLCN might be an important actor during fluid flow-induced autophagy and cell volume regulation in epithelial cells.

In the present study we investigated the role of FLCN in the primary cilium-dependent molecular signaling pathway that controls autophagy and cell volume in response to shear stress-induced by fluid flow in human kidney epithelial cells.

**RESULTS**

**Folliculin and autophagy are increased in response to fluid flow in HK2 cells**

We have recently shown that autophagy is induced in response to shear stress in mouse KECs and in Madin-Darby

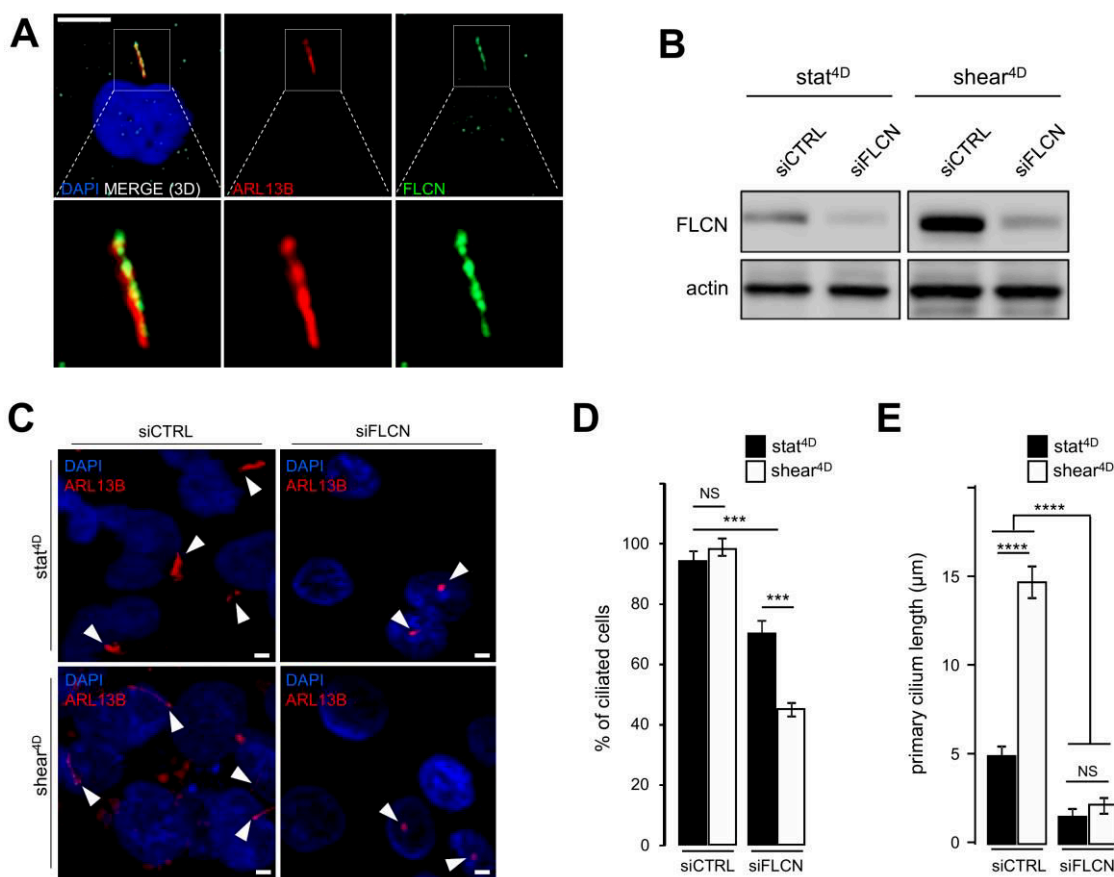


**FIGURE 2: FLCN is associated with primary cilium and ciliogenesis. (A)** HK2 cells grown for 9 6h in static conditions were fixed with methanol, labeled with DAPI, immunostained for FLCN, ARL13B (to reveal primary cilium) and then analyzed by fluorescence microscopy. **(B-E)** HK2 cells were transfected either with siRNA targeting FLCN (siFLCN) or control siRNA (siCTRL). 72 h later they were subjected to 4 days fluid flow (shear 4D) or not (static 4D). **(B)** FLCN downregulation by siRNA efficiency was verified by western blot. **(C)** Cells were fixed with methanol, labeled with DAPI, immunostained for ARL13B (to reveal primary cilium) and then analyzed by fluorescence microscopy. **(D, E)** Quantification of ciliated cells number and cilia length from experiments shown in (C). Scale bars in (A) = 10µm and (C) = 5µm.

canine kidney (MDCK) cells [2]. Similar results were observed in the human kidney proximal tubule HK2 cells (see **Figure 1**). To monitor dynamically the behavior of HK2 cells submitted to shear stress, we analyzed several parameters after 4 h, 48 h and 96 h-4D of fluid flow, and compared them with cells in the same culture chambers for the same periods of time, but without any fluid flow (i.e. under static conditions). As expected, a constant shear stress induced a strong autophagic response, as monitored [11] by an increase in the number of LC3 dots (**Figure 1A** and **1C**) and in the LC3 lipidation status (**Figure 1E**). Cell size was also decreased after shear stress as previously shown in KEC mouse cells [2], notably after 96 h-4D of treatment (**Figure 1B** and **1D**). Interestingly, upon shear stress the amount of FLCN protein increased in time, (**Figure 1E** and **1F**), as was the FLCN mRNA (**Figure 1G**), suggesting that shear stress induction of autophagy leads to a specific upregulation of FLCN expression at the transcriptional level. Remarkably, this was not observed in cells prone to autophagy induced by serum starvation (**Figure 1H**), suggesting that FLCN response to the autophagic machinery and its mobilization are dependent on the stress type.

**Folliculin controls the length of primary cilium in response to shear stress**

In addition to the induction of autophagy and the decrease of the cell size, we show that fluid flow-induced shear stress promotes an increase in the primary cilium length in human HK2 cells (Supplemental Figure S1A and S1B). This is accompanied at the molecular level by the upregulation of the primary cilium regulatory protein IFT20 [3] (Supplemental Figure S1C and S1D) in response to fluid flow. We thus question the relationship between FLCN behavior and primary cilium. We show, as previously reported [6], that FLCN is present at the axoneme of primary cilium (**Figure 2A**). Upon knockdown of FLCN (**Figure 2B**), the number of ciliated cells under shear stress is affected (**Figure 2C** and **2D**) as well as the length of remaining primary cilia (**Figure 2C** and **2E**). At the molecular level, knockdown of FLCN induces a decrease of the IFT20 protein amount in a shear stress situation (Supplemental Figure S2A and S2B), highlighting the key role of FLCN in the primary cilium organelle dynamics.

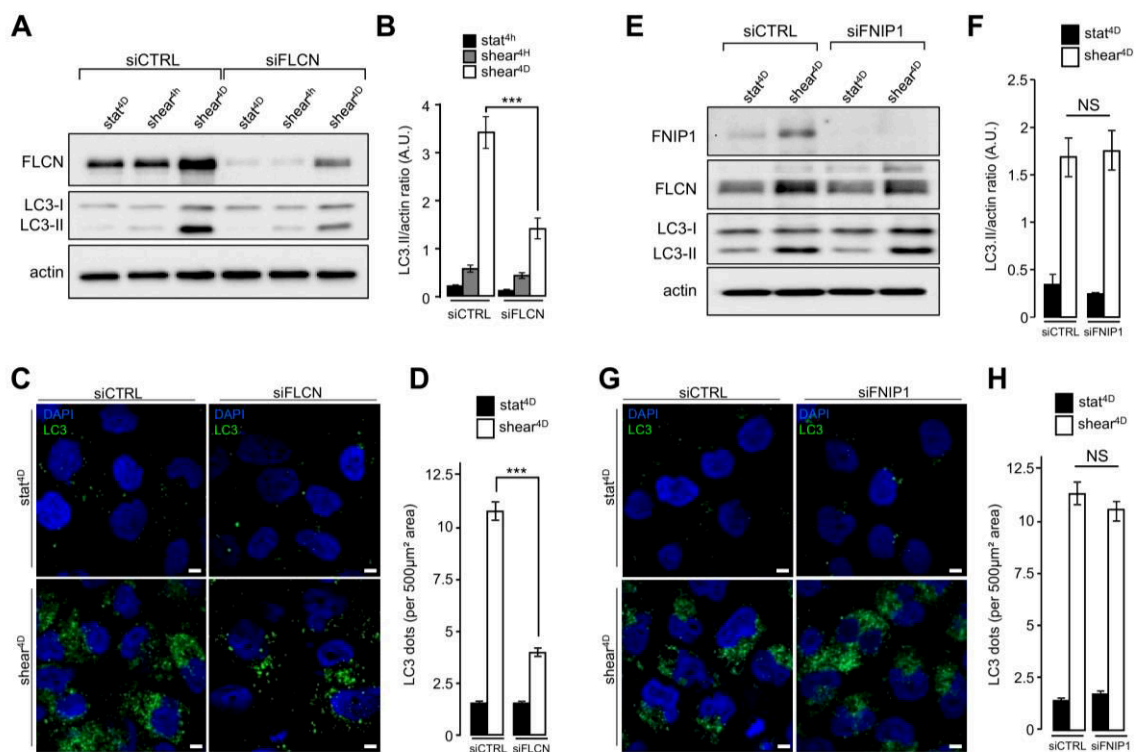


**FIGURE 3: FLCN, but not FNIP1, is required for shear stress-induced autophagy.** (A-D) HK2 cells were transfected either with siRNA targeting FLCN (siFLCN) or control siRNA (siCTRL) 72 h later they were subjected to fluid flow (shear) for the indicated times or not (static). (A) Levels of FLCN, LC3I and LC3II were analyzed by western blot and LC3 II/actin ratio was quantified (B). (C) Cells were fixed, labeled with DAPI, immunostained for LC3 and then analyzed by fluorescence microscopy. (D) LC3 dots were quantified from experiments shown in (C). (E-H) HK2 cells were transfected either with siRNA targeting FNIP1 (siFNIP1) or control siRNA (siCTRL). 72 h later they were subjected to fluid flow for 4 days (shear 4D) or not (static 4D). (E) Levels of FNIP1, FLCN, LC3I and LC3II were analyzed by western blot and LC3 II/actin ratio was quantified (F). (G) Cells were fixed, labeled with DAPI, immunostained for LC3 and then analyzed by fluorescence microscopy. (H) LC3 dots were quantified from experiments shown in (G). Scale bars in (C) and (G) = 5µm.

**Folliculin controls autophagy-dependent cell size regulation in response to shear stress**

We recently reported that primary cilium-dependent autophagy regulates KEC size decrease [2]. To better decipher the role of FLCN localized at the primary cilium in autophagy and cell size regulation, we first analyzed the shear stress-associated autophagic response in FLCN siRNA transfected cells. Lipidation of the LC3 marker in response to shear stress was strongly diminished in siFLCN compared to control cells (Figure 3A and 3B and Supplemental Figure S3A and S3B), suggesting that the autophagy response induced by fluid flow is associated with FLCN, while FLCN knock-down did not affect starvation induced autophagy, as monitored by LC3 lipidation (Supplemental Figure S3C). The reduction of autophagosome biogenesis in siFLCN cells prone to shear stress was confirmed by a decrease of the total number of LC3 positive structures which presumably

correspond to pre-autophagosomes, mature autophagosomes and autophagolysosomes (Figure 3C and 3D). However, downregulation of the folliculin-interacting protein FNIP1 [12], has no effect either on LC3 lipidation (Figure 3E and 3F) or on the number of LC3 positive structures (Figure 3G and 3H) in response to fluid flow, suggesting that FLCN function in shear stress associated autophagy is independent of its FNIP1 partner.

Likewise, knocking down FLCN impairs cell size decrease in response to fluid flow (Figure 4A, 4B), while the knockdown of FNIP1 has no effect on fluid flow-induced cell size decrease (Figure 4C, 4D). In line with cell size regulation and autophagy interplay induced by mechanical stress, we observed defaults in the mTORC1 pathway activation in FLCN knockdown cells, since phosphorylation of TSC2, known to inactivate the mTOR signaling sequence, was strongly diminished in siFLCN cells prone to shear

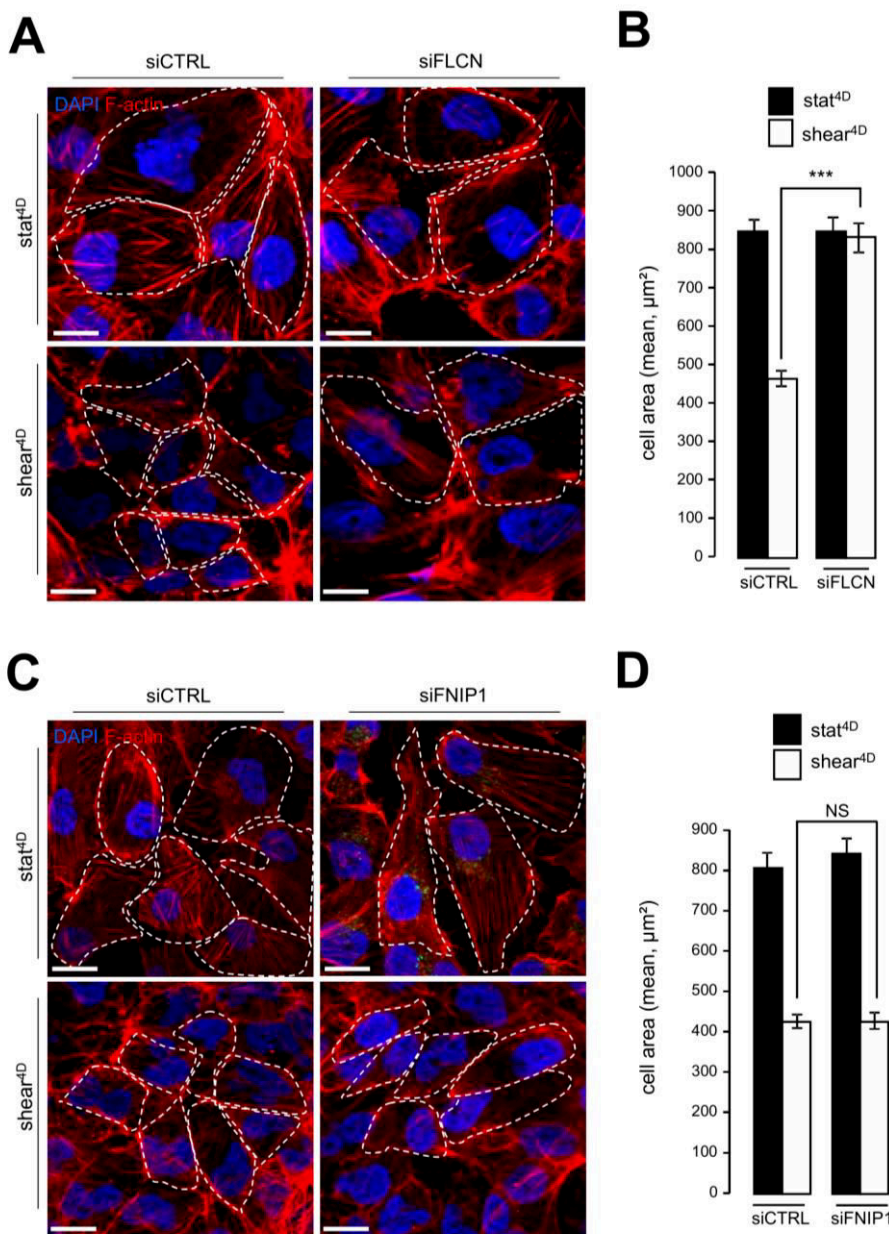


**FIGURE 4: FLCN, but not FNIP1, is required for shear stress-induced cell size regulation.**

(A-B) HK2 cells were transfected either with siRNA targeting FLCN (siFLCN) or control siRNA (siCTRL) 72 h later they were subjected to fluid flow for 4 days (shear 4D) or not (static 4D). (A) Cells were fixed, labeled with DAPI and phalloidin to reveal F-actin and cell boarder and then analyzed by fluorescence microscopy. (B) Cells areas were quantified from experiments shown in (A). (C-D) HK2 cells were transfected with siRNA targeting FNIP1 (siFNIP1) or control siRNA (siCTRL). The experiments were performed and quantified as in (A-B). Scale bars in (A) and (C) = 10μm.

stress (Supplemental Figure S4A and S4B). Moreover, the phosphorylation status of the S6 protein, a downstream target in the mTOR signaling pathway, was strongly increased in FLCN knock-down cells prone to fluid flow compared to control cells (Supplemental Figure S4A and S4C).

We confirmed to importance of FLCN in cell size adaptation and autophagy in response to fluid flow using a Birt–Hogg–Dubé derived FLCN-null cells (UOK 257cells) and FLCN restored companion cells (UOK 257-2 cells) [12, 13]. Indeed, UOK 257cells prone to shear stress did neither display any autophagy change, as monitored by the number of LC3 positive structures (Figure 5A and 5B), nor cell size adaptation to the fluid flow treatment (Figure 5E and 5F). Importantly, UOK 257-2 cells, in which the FLCN expression is restored, display identical features than control HK2 cells (Figure 1) and other kidney cells [2] regarding autophagic machinery mobilization under shear stress (Figure 5C and 5D) and cell size adaptation (Figure 5G and

5H). These data strengthened the hypothesis that FLCN is central for autophagy induced by mechanical stress in kidney epithelial cells.

A hallmark of primary cilium-dependent autophagy is the recruitment of components of the autophagy machinery at the primary cilium [14]. We have previously shown that ATG16L1 is recruited at the basal body in response to shear stress [2]. Interestingly, knocking down FLCN leads to ATG16L1 destabilization (Figure 6A) and impairs its recruitment at the basal body of primary cilium (Figure 6B and 6C), emphasizing the role of FLCN in setting up autophagy upon fluid flow.

Overall these results show that FLCN is a key player in the regulation of fluid flow-induced autophagy and cell size regulation.

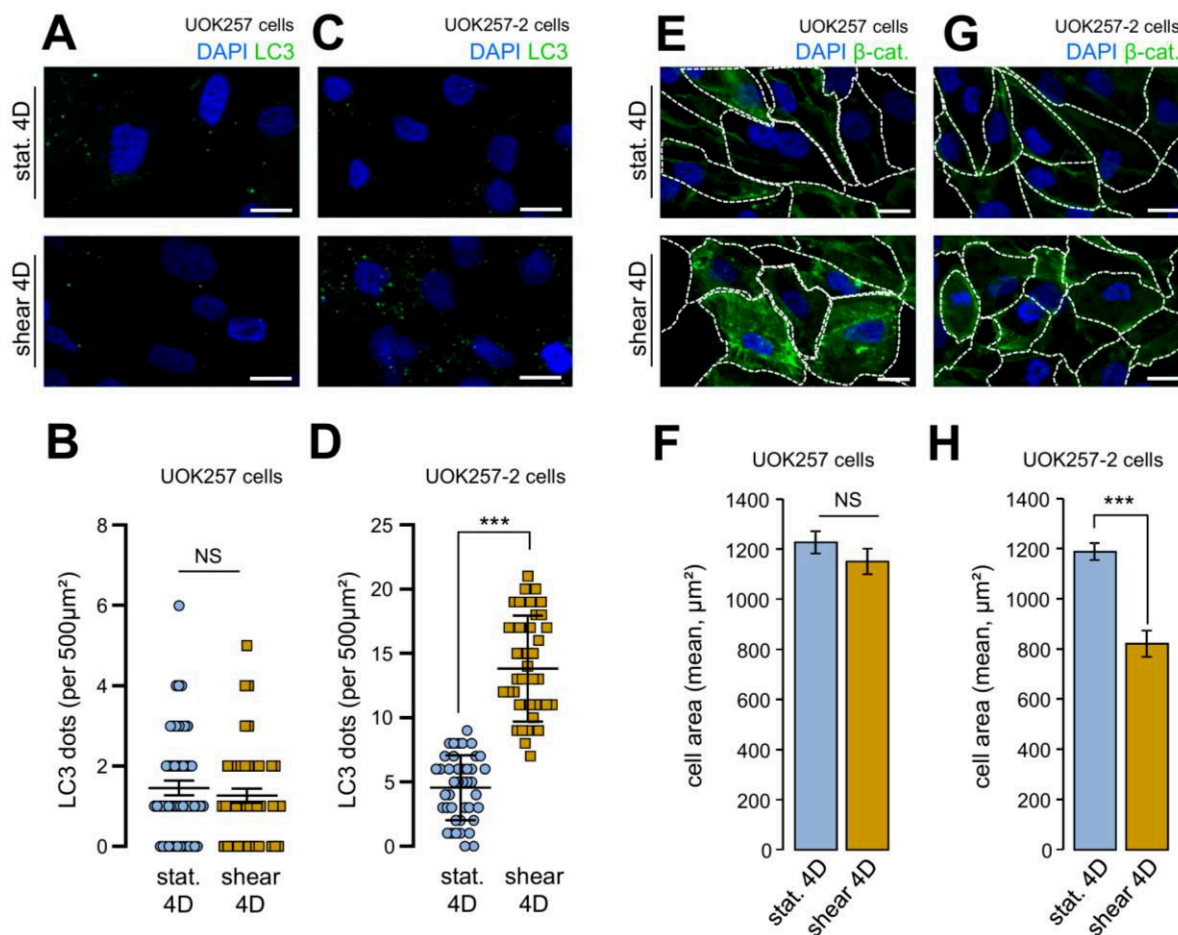


**FIGURE 5: Shear-stress-induced autophagy and cell size regulation are abolished in FLCN-null cells.** UOK 257 FLCN-null cells and UOK 257-2 FLCN restored cells were cultured on microslides and then subjected to fluid flow for 4 days (shear) or not (static 4D). Cells were fixed, labeled with DAPI, immunostained for LC3 (A, C) or labeled with DAPI and immunostained for β-catenin to reveal cell boarder (E, G) and then analyzed by fluorescence microscopy. (B, D) LC3 dots were quantified from experiments shown in (A) (UOK 257cells) and (C) (UOK 257-2 cells). (F, H) cells areas were quantified from experiments shown in (E) (UOK 257cells) and (G) (UOK 257-2 cells). Scale bars in (A, C, E and F) = 10µm.

**Folliculin is upstream of AMPK and LKB1 in the primary cilium signaling cascade**

Stress sensing signalization induced by the bending of primary cilium in epithelial cells has been associated with local recruitment of LKB1 and AMPK at the primary cilium and local phosphorylation of the latter [15, 16]. This signaling cascade controls primary cilium-dependent autophagy [2] and FLCN has been shown to contribute to the recruitment of LKB1 on the primary cilium to regulate activation of AMPK and mTORC1 during shear stress [6]. In our experimental system we observe as well that under shear stress, AMPK phosphorylation depends on the presence of FLCN (Figure 7A and 7B), so does its recruitment to the primary cilium (Figure 7C). Moreover, knocking down FLCN prevents LKB1 targeting to the primary cilium in cells prone to shear stress (Figure 7D). These findings suggest that FLCN orchestrates the AMPK/LKB1 signaling machinery at the primary cilium to regulate autophagy and cell size in kidney epithelial cells.

**DISCUSSION**

In the present work we identify FLCN as a component of the primary cilium signaling cascade that senses fluid flow to regulate autophagy and cell size in kidney epithelial cells. FLCN is upregulated upon shear stress, and it functions in modulating autophagic-dependent cellular size decrease. Ciliary length is also dependent on the levels of FLCN. These findings are in line with the observation that

FLCN level affects the timing of ciliogenesis in HK2 cells [5]. Interestingly, autophagy has been shown to influence the ciliary length as well [14, 17]; whether the implication of FLCN in the control of cilia length is related to its role in autophagy and/or in its regulation of mTOR activity [17] is an open question.

In accordance with the observations of Zhong et al. [6], our study shows that FLCN acts upstream of AMPK and mTOR to control autophagy in response to shear stress. FLCN contributes to the recruitment of LKB1 to the primary cilium, which is important for the activation of AMPK [6]. FLCN-associated proteins FNIP1 and FNIP2 have been shown to be engaged in a complex with AMPK, and the loss of FNIP1 stimulates AMPK and increases autophagy in B cells [18]. However, in our experimental setting, knock-down of FNIP1 does neither impact autophagy nor fluid flow-dependent cell size. Thus, although the implication of FLCN and its associated proteins FNIP1 and 2 in autophagy has been studied in various settings [7, 8, 18], it is difficult to summarize it in a unified picture. It is most probably dependent on the cell type, the stimuli of autophagy and their subcellular localization (e.g., primary cilium vs lysosomal membrane).

Our study adds a new component to the signaling cascade emanating from the primary cilium in response to fluid flow to regulate autophagy. However, the relation between this signaling cascade and the mechanosensor present in the primary cilium associated membrane re-

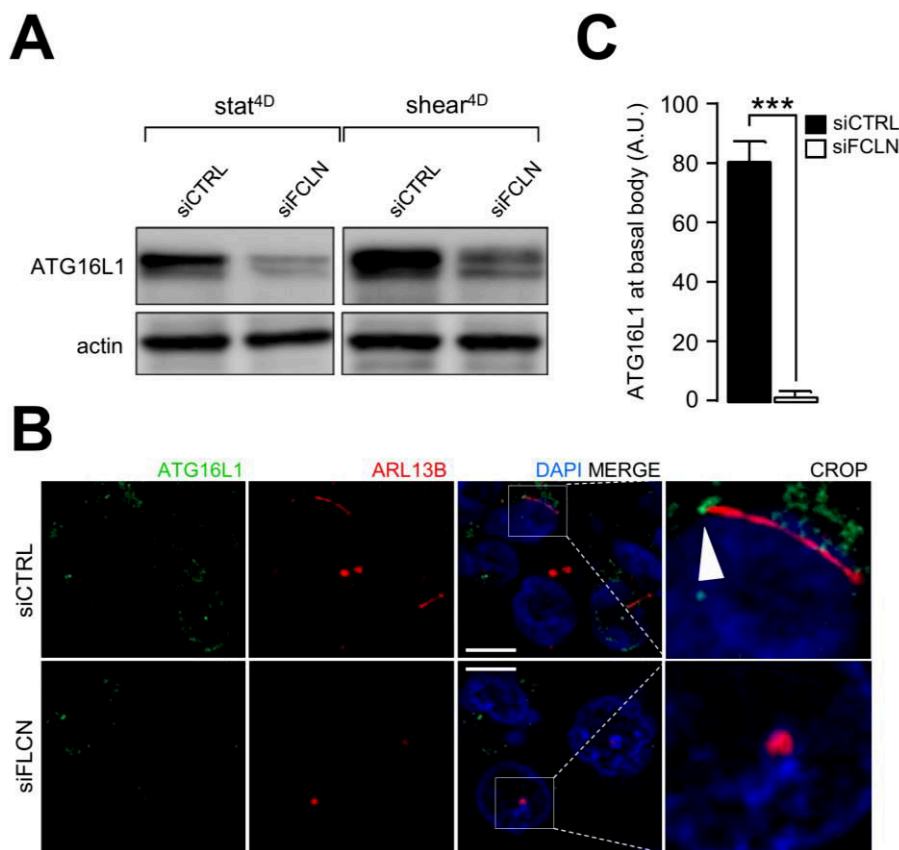


**FIGURE 6: Shear-stress dependent recruitment of ATG16L1 to primary cilium is impaired in FLCN knockdown cells.** HK2 cells were transfected with control siRNA (siCTRL) or with siRNA targeting FLCN (siFLCN). 72 h later, they were subjected to fluid flow for 4 days (shear 4D) or not (static 4D). (A) ATG16L1 and actin levels were analyzed by western blot. (B) Cells prone to fluid flow were fixed with methanol, labeled with DAPI, immunostained for ATG16L1 and ARL13B and then analyzed by fluorescence microscopy. Arrowhead indicates presence of ATG16L1 at the basal body. (C) ATG16L1 positive structures at basal body were quantified from experiments shown in (B). Scale bar = 10µm.

mains to be identified. The complex formed by polycystin 1 (PC1) and polycystin 2 (PC2) functions as a calcium channel at the primary cilium [19, 20]; in this complex PC1 is a mechanosensor [21]. Our previous studies have shown that PC2 is not involved in the autophagy cascade leading to cell size regulation in response to fluid flow [2]. However, it remains a possibility that PC1 is upstream of FLCN to regulate this cascade and cell size in kidney epithelial cells. Further experiments should challenge this hypothesis.

In conclusion we show that FLCN localized at the primary cilium regulates autophagy and cell size in kidney epithelial cells in response to shear stress induced by fluid flow. Our work is in line with the fact that autophagy is inhibited in clear cell tumors from a BHD patient [7]. Further studies should address whether this physiological response is altered in BHD patients.

**MATERIALS AND METHODS**

**Cell culture and siRNA transfection**

Human kidney HK2 cells (from ATCC) and Birt-Hogg-Dube syndrome associated FLCN-null human kidney UOK 257 cells (as well as FLCN-restored UOK257-2 cells) (from Dr Laura Schmidt (National Cancer Institute, NIH, Bethesda)) were cultured in Dulbecco's Modified Eagle Medium (DMEM), supplemented with 10% FCS at 37°C and 5% CO<sub>2</sub>. For the starvation experiments, cells were cultured in Earle's balanced salt solution (EBSS) for the indicated times. siRNA transfections were performed using Lipofectamine RNAi Max (Invitrogen, Life Technologies) according to the manufacturer's instructions. Two siRNA oligomers were used for each target at a final concentration of 20 nM. All siRNAs were purchased from Qiagen and the references are as follows: Control (SI1027281); FLCN (SI05121417 and SI00387660); FNIP1 (a): (SI03222611 and SI05001766).

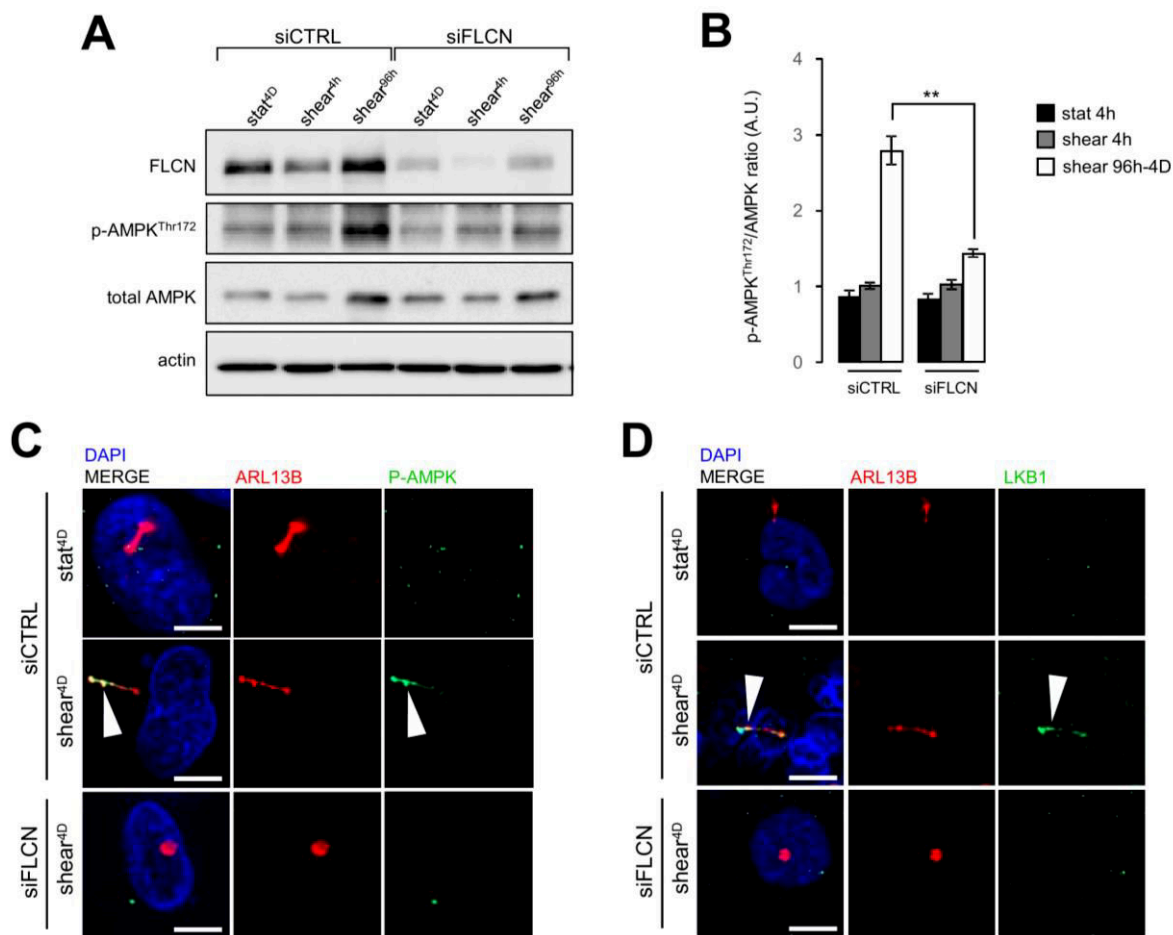


**FIGURE 7: FLCN is associated with phospho-AMPK and LKB1 mobilization during shear stress.** HK2 cells were transfected with control siRNA (siCTRL) or with siRNA targeting FLCN (siFLCN). 72 h later, they were subjected (shear) or not (static) to fluid flow for the indicated times. (A) Phospho-AMPK (Thr172), total AMPK, FLCN and actin levels were analyzed by western blot and quantified (B) in the indicated conditions (A). (C, D) Cells prone to fluid flow (shear 4D) or not (static 4D) were fixed with methanol, labeled with DAPI, immunostained for ARL13B, phospho-AMPK (C), LKB1 (D), ARL13B, and then analyzed by fluorescence microscopy. Arrowheads indicate presence of phospho-AMPK (P-AMPK) or LKB1 at primary cilium. Scale bars in (C) and (D) = 10µm.

### Shear stress induction

HK2 cells were seeded ( $2.25 \times 10^5$  in 150  $\mu$ l of culture medium) into a microslide “10.6 Luer” chamber (channel dimensions: 50 x 5 x 0.4 mm, Ibidi) and cultured for 96 h to allow proper polarization and epithelial differentiation. The microslides were connected to a fluid flow system which contains an air-pressure pump and a two-way switch valve that pumps the culture medium unidirectionally between two reservoirs through the flow chamber at a rate corresponding to a shear stress of 1 dyn/cm<sup>2</sup>. The control cells (static) were set up in the same microslides Luer chambers and maintained in culture as long as the flow-subjected cells.

### Protein extraction, immunoblot analysis and antibodies

Cells in microslides were washed twice with ice-cold PBS and lysed on ice with 150  $\mu$ l of 1X Laemmli buffer (60 mM Tris-HCl pH=6.8, 2% SDS, 10% Glycerol, bromophenol blue, supplemented with 100 mM DTT) for 30 min. Samples were boiled for 10 min at 95°C, separated by SDS/PAGE and then transferred onto Nitrocellulose membranes. Western blot analysis was performed with specific antibodies and the antigen-antibody complexes were visualized by chemiluminescence (Immobilon Western, Merck Millipore). The following antibodies were used in immunoblotting: rabbit-anti LC3 (Sigma, Cat#L7543); rabbit-anti-FLCN (Cell signaling, Cat#3697); rabbit-anti-FNIP1 (Abcam, Cat#ab134969); rabbit-anti-AMPK (Cell signaling, Cat#2532S); rabbit-anti-p-AMPK (T172) (Cell signaling, Cat#2535); mouse-anti-actin (Millipore, Cat#1501); rabbit-anti-ATG16L1 (MBL, Cat#PM040); rabbit-anti-IFT20 (Proteintech, Cat#13615-1-AP); rabbit-anti  $\beta$ -catenin (Cell signaling, Cat#8480); rabbit-anti-LKB1 (Cell signaling, Cat#3050); rabbit-anti-S6 ribosomal protein (Cell signaling, Cat#2217); rabbit-anti-p-S6 ribosomal protein (S240/244) (Cell signaling, Cat#2215); rabbit-anti-Tuberin/TSC2 (Cell signaling, Cat#4308); rabbit-anti-p-Tuberin/TSC2 (T1462) (Cell signaling, Cat#3617). Secondary HRP conjugate anti-rabbit IgG (GE Healthcare) and HRP conjugate anti-mouse IgG (Bio-Rad).

### Immunofluorescence and microscopy

Cells were fixed either with 4% paraformaldehyde (PFA) for 20 min or with cold methanol for 5 min at -20°C for proper axoneme proteins detection [22]. They were then washed and incubated for 30 min in blocking buffer (10% FCS in PBS) followed by incubation with primary antibodies diluted in blocking buffer supplemented with 0.05% saponin for 1 h at room temperature or overnight at 4°C. Cells were washed 3 times, and then incubated for 1 h with fluorescent Alexa-Fluor secondary antibodies. After washing, 150  $\mu$ l of DAPI-Fluoromount were added into the Luer chamber (Southern Biotech). Images were acquired with a Zeiss Apotome.2 fluorescence microscope equipped with a 63x oil immersion fluorescence objective. Number of ciliated cells and length of cilia were quantified using Zen Software (Zeiss) or Imaris Software (Bitplane). The following antibodies were used for immunofluorescence: mouse-anti-LC3B (MBL, Cat# M152-3); rabbit-anti-FLCN (Cell signaling, Cat#3697); mouse-anti-ARL13B (C-5) (Santa Cruz, Cat#515784); rabbit-anti-ATG16 (MBL, Cat#PM040); rabbit-anti IFT20 (Proteintech, Cat#13615-1-AP); rabbit-anti-p-AMPK (T172) (Cell signaling, Cat#2535); Phalloidin (Cat# A34055); Alexa Fluor-conjugated secondary antibodies (donkey anti-mouse IgG and donkey anti-Rabbit IgG, Life Technologies).

### Real Time Quantitative PCR

RNA was extracted from cells using the NucleoSpin RNA kit (Macherey-Nagel). Reverse transcriptase PCR and qRT-PCR were performed using “Power Sybr green cells to CT” kit (Thermo Fisher Scientific) according to manufacturer’s instructions. Actin was used as reference gene and relative quantification was calculated using the  $\Delta\Delta$ CT method. Primers sequences are as followed:

Flcn-forward: 5'-TTCACGCCATTCTACACCAGA-3';  
 Flcn-reverse 5'-GCCACAGGTTGTCATCACTTG-3'  
 Actin-forward 5'-GGCCAACCGTGAAAAGATGA-3';  
 Actin-reverse 5'-ACCAGAGGCATACAGGGACAG-3'

### Statistical analysis

Data are presented as means  $\pm$  SD or SEM. Statistical analyses were performed by unpaired, two-tailed Student’s t-test, using GraphPad Prism7 (\*p < 0.005, \*\*p < 0.001, and \*\*\*p < 0.0001). Images showing Western blotting or immunofluorescence analysis are representative of three independent experiments unless stated otherwise.

### AUTHOR CONTRIBUTIONS

N.Z., A.B. and JB performed most of the biological experiments and analyses, N.D. and J.B. analyzed parts of the cell biological assays, P.C. supervised the project and wrote the paper and E.M. contributes to imaging experiments, analyzed parts of the cell biological assays, supervised the project and wrote the paper.

### ACKNOWLEDGMENTS

We thank Dr Laura Schmidt (NIH, Bethesda) for UOK 257 and UOK 257-2 cell lines. We are grateful to Dr Julien Morel for statistical analysis and Dr Zeina Chamoun for critical reading of the manuscript. This study was supported in part by ANR (agence nationale de la recherche), INSERM (Institut national de la santé et de la recherche médicale), CNRS (Centre national de la recherche scientifique) and IEEP (Institut européen d’expertise en physiologie).

### SUPPLEMENTAL MATERIAL

All supplemental data for this article are available online at [www.cell-stress.com](http://www.cell-stress.com).

### CONFLICT OF INTEREST

The authors declare that there is no conflict of interests.

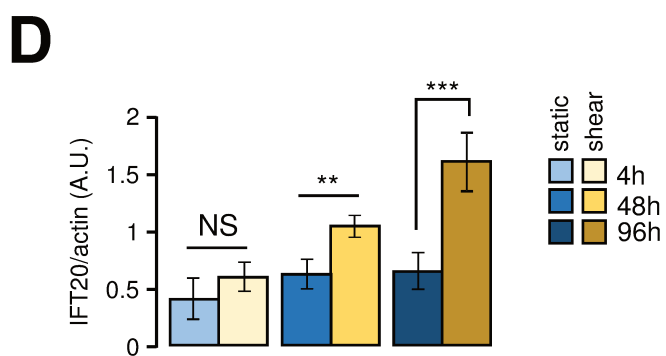
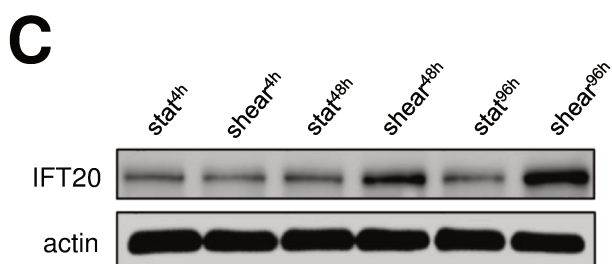
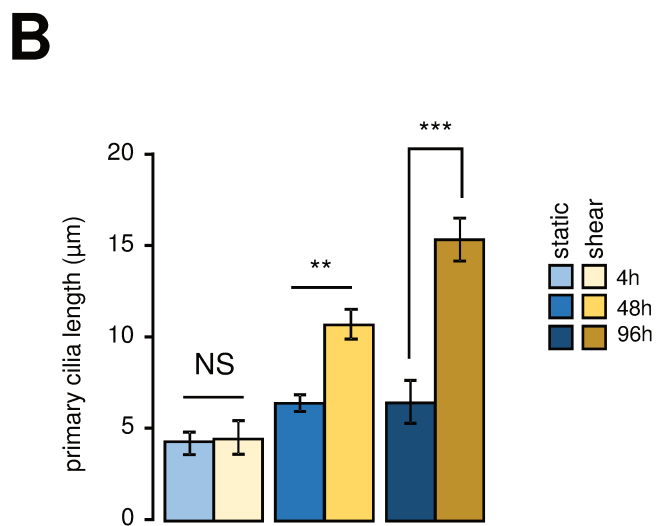
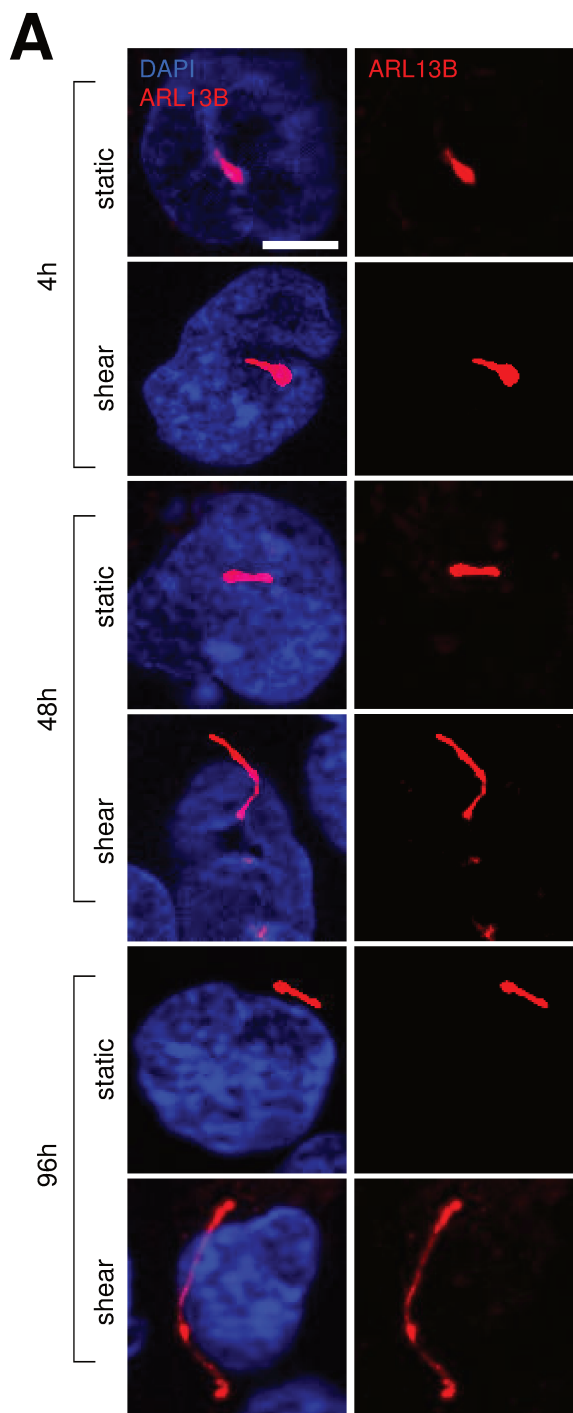
### COPYRIGHT

© 2019 Zemirli *et al.* This is an open-access article released under the terms of the Creative Commons Attribution (CC BY) license, which allows the unrestricted use, distribution, and reproduction in any medium, provided the original author and source are acknowledged.

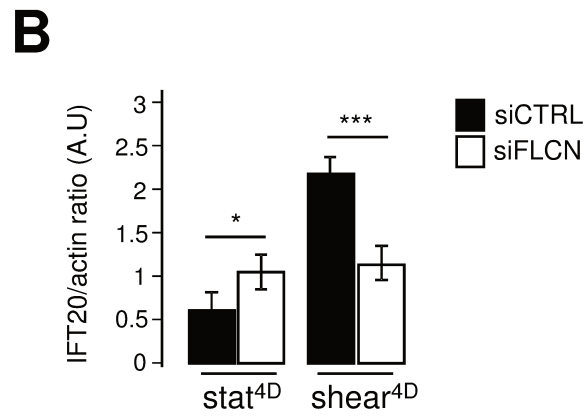
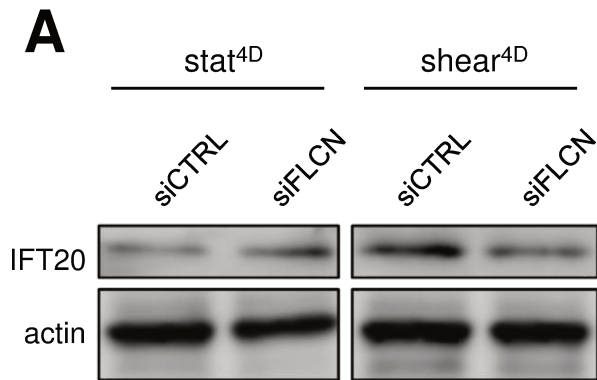
Please cite this article as: Naïma Zemirli, Asma Boukhalfa, Nicolas Dupont, Joëlle Botti, Patrice Codogno and Etienne Morel (2019). The primary cilium protein folliculin is part of the autophagy signaling pathway to regulate epithelial cell size in response to fluid flow. *Cell Stress* 3(3): 100-109. doi: 10.15698/cst2019.03.180

## REFERENCES

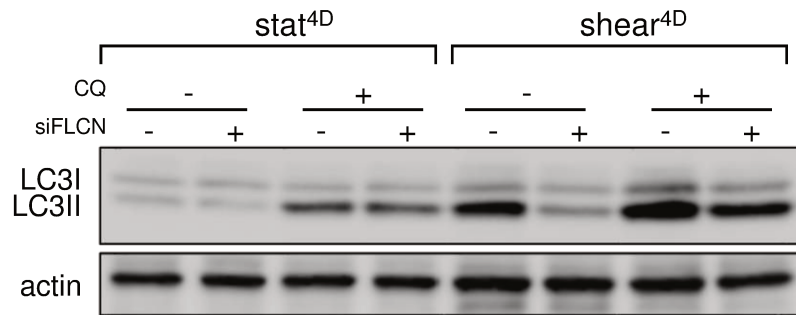
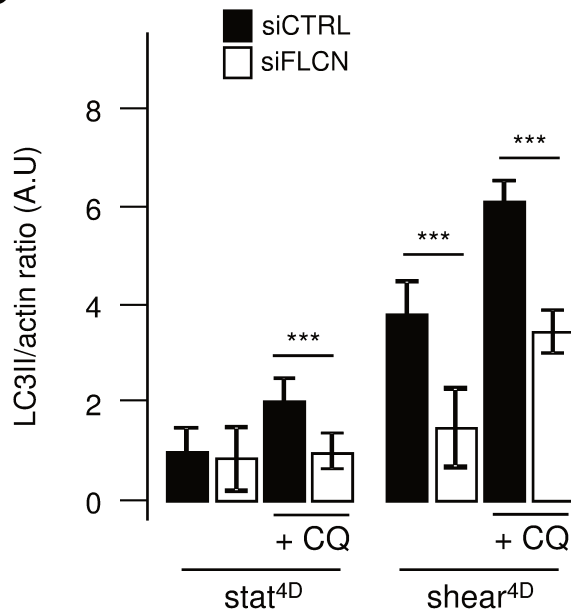
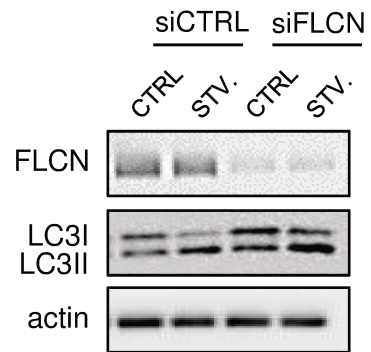
1. Boya P, Reggiori F, and Codogno P (2013). Emerging regulation and functions of autophagy. *Nat Cell Biol* 15(7): 713–720. doi: 10.1038/ncb2788
2. Orhon I, Dupont N, Zaidan M, Boitez V, Burtin M, Schmitt A, Capiod T, Viau A, Beau I, Wolfgang Kuehn E, Friedlander G, Terzi F, and Codogno P (2016). Primary-cilium-dependent autophagy controls epithelial cell volume in response to fluid flow. *Nat Cell Biol* 18(6): 657–67. doi: 10.1038/ncb3360
3. Malicki JJ, and Johnson CA (2017). The Cilium: Cellular Antenna and Central Processing Unit. *Trends Cell Biol* 27(2): 126–140. doi: 10.1016/j.tcb.2016.08.002
4. Orhon I, Dupont N, Pampliega O, Cuervo a M, and Codogno P (2014). Autophagy and regulation of cilia function and assembly. *Cell Death Differ* 22(3): 389–397. doi: 10.1038/cdd.2014.171
5. Luijten MNH, Basten SG, Claessens T, Vernooij M, Scott CL, Janssen R, Easton JA, Kamps MAF, Vreeburg M, Broers JLV, van Geel M, Menko FH, Harbottle RP, Nookala RK, Tee AR, Land SC, Giles RH, Coull BJ, and van Steensel MAM (2013). Birt–Hogg–Dubé syndrome is a novel ciliopathy. *Hum Mol Genet* 22(21): 4383–4397. doi: 10.1093/hmg/ddt288
6. Zhong M, Zhao X, Li J, Yuan W, Yan G, Tong M, Guo S, Zhu Y, Jiang YY, Liu Y, and Jiang YY (2016). Tumor Suppressor Folliculin Regulates mTORC1 through Primary Cilia. *J Biol Chem* 291(22): 11689–97. doi: 10.1074/jbc.M116.719997
7. Dunlop EA, Seifan S, Claessens T, Behrends C, Kamps MA, Rozycka E, Kemp AJ, Nookala RK, Blenis J, Coull BJ, Murray JT, van Steensel MA, Wilkinson S, and Tee AR (2014). FLCN, a novel autophagy component, interacts with GABARAP and is regulated by ULK1 phosphorylation. *Autophagy* 10(10): 1749–1760. doi: 10.4161/auto.29640
8. Possik E, Jalali Z, Nouët Y, Yan M, Gingras M-C, Schmeisser K, Panait L, Dupuy F, Kharitidi D, Chotard L, Jones RG, Hall DH, and Pause A (2014). Folliculin Regulates Ampk-Dependent Autophagy and Metabolic Stress Survival. *PLoS Genet* 10(4): e1004273. doi: 10.1371/journal.pgen.1004273
9. Bastola P, Stratton Y, Kellner E, Mikhaylova O, Yi Y, Sartor MA, Medvedovic M, Biesiada J, Meller J, and Czyzyk-Krzeska MF (2013). Folliculin Contributes to VHL Tumor Suppressing Activity in Renal Cancer through Regulation of Autophagy. *PLoS One* 8(7): e70030. doi: 10.1371/journal.pone.0070030
10. Gupta N, Sunwoo BY, and Kotloff RM (2016). Birt-Hogg-Dubé Syndrome. *Clin Chest Med* 37(3): 475–86. doi: 10.1016/j.ccm.2016.04.010
11. Klionsky DJ et al. (2016). Guidelines for the use and interpretation of assays for monitoring autophagy (3rd edition). *Autophagy* 12(1): 1–222. doi: 10.1080/15548627.2015.1100356
12. Baba M, Hong S-B, Sharma N, Warren MB, Nickerson ML, Iwamatsu A, Esposito D, Gillette WK, Hopkins RF, Hartley JL, Furihata M, Oishi S, Zhen W, Burke TR, Linehan WM, Schmidt LS, and Zbar B (2006). Folliculin encoded by the BHD gene interacts with a binding protein, FNIP1, and AMPK, and is involved in AMPK and mTOR signaling. *Proc Natl Acad Sci* 103(42): 15552–15557. doi: 10.1073/pnas.0603781103
13. Yang Y, Padilla-Nash HM, Vira MA, Abu-Asab MS, Val D, Worrell R, Tsokos M, Merino MJ, Pavlovich CP, Ried T, Linehan WM, and Vocke CD (2008). The UOK 257 cell line: a novel model for studies of the human Birt–Hogg–Dubé gene pathway. *Cancer Genet Cytogenet* 180(2): 100–109. doi: 10.1016/j.cancergencyto.2007.10.010
14. Pampliega O, Orhon I, Patel B, Sridhar S, Díaz-Carretero A, Beau I, Codogno P, Satir BH, Satir P, and Cuervo AM (2013). Functional interaction between autophagy and ciliogenesis. *Nature* 502(7470): 194–200. doi: 10.1038/nature12639
15. Boehlke C, Kotsis F, Patel V, Braeg S, Voelker H, Bredt S, Beyer T, Janusch H, Hamann C, Gödel M, Müller K, Herbst M, Hornung M, Dörken M, Köttgen M, Nitschke R, Igarashi P, Walz G, and Kuehn EW (2010). Primary cilia regulate mTORC1 activity and cell size through Lkb1. *Nat Cell Biol* 12(11): 1115–1122. doi: 10.1038/ncb2117
16. Bays JL, Campbell HK, Heidema C, Sebbagh M, and DeMali KA (2017). Linking E-cadherin mechanotransduction to cell metabolism through force-mediated activation of AMPK. *Nat Cell Biol* 19(6): 724–731. doi: 10.1038/ncb3537
17. Tang Z, Lin MG, Stowe TR, Chen S, Zhu M, Stearns T, Franco B, and Zhong Q (2013). Autophagy promotes primary ciliogenesis by removing OFD1 from centriolar satellites. *Nature* 502(7470): 254–257. doi: 10.1038/nature12606
18. Siggs OM, Stockenhuber A, Deobagkar-Lele M, Bull KR, Crockford TL, Kingston BL, Crawford G, Anzilotti C, Steeples V, Ghaffari S, Czibik G, Bellahcene M, Watkins H, Ashrafian H, Davies B, Woods A, Carling D, Yavari A, Beutler B, and Cornall RJ (2016). Mutation of Fnip1 is associated with B-cell deficiency, cardiomyopathy, and elevated AMPK activity. *Proc Natl Acad Sci U S A* 113(26): E3706–15. doi: 10.1073/pnas.1607592113
19. Chebib FT, Sussman CR, Wang X, Harris PC, and Torres VE (2015). Vasopressin and disruption of calcium signalling in polycystic kidney disease. *Nat Rev Nephrol* 11(8): 451–64. doi: 10.1038/nrneph.2015.39
20. Lemos FO, and Ehrlich BE (2018). Polycystin and calcium signaling in cell death and survival. *Cell Calcium* 69: 37–45. doi: 10.1016/j.ceca.2017.05.011
21. Dalagiorgou G, Basdra EK, and Papavassiliou AG (2010). Polycystin-1: Function as a mechanosensor. *Int J Biochem Cell Biol* 42(10): 1610–1613. doi: 10.1016/j.biocel.2010.06.017
22. Hua K, and Ferland RJ (2017). Fixation methods can differentially affect ciliary protein immunolabeling. *Cilia* 6(1): 5. doi: 10.1186/s13630-017-0045-9



Supplementary Figure 1



Supplementary Figure 2

**A****B****C**

Supplementary Figure 3



Contents lists available at ScienceDirect

Biochimie

journal homepage: [www.elsevier.com/locate/biochi](http://www.elsevier.com/locate/biochi)

## Review

## Interplay between primary cilia, ubiquitin-proteasome system and autophagy

Asma Boukhalfa <sup>a, b, 1</sup>, Caterina Miceli <sup>a, b, 1</sup>, Yennifer Ávalos <sup>c, d</sup>, Etienne Morel <sup>a, b, \*</sup>,  
Nicolas Dupont <sup>a, b, \*\*</sup><sup>a</sup> Institut Necker-Enfants Malades (INEM), INSERM U1151-CNRS UMR 8253, F-75993, Paris, France<sup>b</sup> Université Paris Descartes-Sorbonne Paris Cité, F-75993, Paris, France<sup>c</sup> Departamento de Fisiología, Facultad Ciencias Biológicas, Pontificia Universidad Católica de Chile, 7820436, Santiago, Chile<sup>d</sup> Departamento de Biología, Facultad de Química y Biología, Universidad de Santiago de Chile, 8350709, Santiago, Chile

## ARTICLE INFO

## Article history:

Received 15 February 2019

Accepted 13 June 2019

Available online xxx

## Keywords:

Primary cilium

Autophagy

Proteasome

## ABSTRACT

Cilia are microtubule-based organelles located at the cell surface of many eukaryotic cell types. Cilia control different cellular functions ranging from motility (for motile cilia) to signal transduction pathways (for primary cilia). A variety of signaling pathways are coordinated by this organelle during development, cell migration and cell differentiation. Interestingly, aberrant ciliogenesis or altered cilium signaling has been associated with human diseases, notably in cancer. Disruption of cilia through mutation of genes encoding cilia proteins has been also linked to multiple human disorders referred as ciliopathies. Recent studies highlight the interplay between cilia and proteostasis. Here we review findings regarding the crosstalk between cilia and two proteolytic systems, the ubiquitin proteasome system and the autophagy-lysosomal system and discuss the potential implications in human disease including ciliopathies.

© 2019 Elsevier B.V. and Société Française de Biochimie et Biologie Moléculaire (SFBBM). All rights reserved.

## Contents

1. Cilia: from structure to function .....	00
2. Ubiquitin-Proteasome System (UPS) .....	00
3. Crosstalk between cilia and UPS .....	00
4. Autophagy pathway .....	00
5. Crosstalk between cilia and autophagy .....	00
6. Concluding remarks .....	00
Conflicts of interests .....	00
Acknowledgments .....	00
References .....	00

## 1. Cilia: from structure to function

Cilia are tiny cellular membrane protrusions that emanate from the surface of different cell types. The cilia are composed of a microtubule-based core structure (the axoneme) which nucleates from a basal body (BB) that is derived from one centriole of the centrosome (the older one for primary cilia) [1,2]. The axoneme is separated from the rest of the intracellular compartments by the

\* Corresponding author. Institut Necker-Enfants Malades (INEM), INSERM U1151-CNRS UMR 8253, F-75993, Paris, France.

\*\* Corresponding author. Institut Necker-Enfants Malades (INEM), INSERM U1151-CNRS UMR 8253, F-75993, Paris, France.

E-mail addresses: [etienne.morel@inserm.fr](mailto:etienne.morel@inserm.fr) (E. Morel), [nicolas.dupont@inserm.fr](mailto:nicolas.dupont@inserm.fr) (N. Dupont).

<sup>1</sup> These authors contribute equally to this work.

transition zone (TZ) which is a ciliary subdomain highly organized with a molecular structure resembling that of the nuclear pore. It functions as a ciliary gate that strictly controls the molecular composition of the ciliary compartment. Conventionally, cilia are classified as motile and non-motile according to their microtubule pattern and associated motility in the organism. Motile cilium (MC) is formed by an axoneme of 9 outer microtubule doublets and 2 single central microtubules whereas the primary cilium (PC), a solitary non-motile cilium, lacks the 2 single central microtubules and dynein (molecular motors) arms, needed for motility. Cilia are very dynamic organelles since cilia formation and disassembly occur in synchrony with the cell cycle. Ciliogenesis takes place in quiescent cells when cell enter the G0 phase whereas cilia are disassembled as cell progress towards S phase. Due to the fact that no protein synthesis occurs in cilia, cilia growth is maintained by specific bidirectional trafficking system, coordinated by the IFT proteins (Intraflagellar Transport). More specifically, two well conserved IFT protein machineries are known to traffic along the polarized microtubules of the axoneme, through the action of two motor protein families (kinesins and dyneins) termed IFT-A (Retrograde) and IFT-B (Anterograde) with tip-to-base and base-to-tip cargo direction, respectively. Maintenance of the cilia also depends on the Bardet–Biedl syndrome (BBSome) protein complex (consisting of eight BBS proteins) which recognize ciliary targeting sequence on specific proteins (for example RVxP (where x is any amino acid) in the N- terminus of polycystin-2 ciliary protein) that need to be targeted to the cilium. Readers can refer to excellent reviews for more detailed information on the regulation of the dynamic process of the cilia formation and disassembly [3].

MC is a beating organelle which generates fluid flow on the surface of epithelial cells lining the airways and the reproductive tract as well as of the ependyma. Motility of the MC in these epithelial cells is essential for mucociliary clearance and ependymal flow. PC is a sensory non-motile organelle that clusters receptors and signaling molecules and thus PC is recognized as signaling hubs. The ciliary membrane is enriched in signaling receptors such as components of the Hedgehog (Hh) pathway [4], Wnt signaling pathway [5], PDGF alpha receptors and calcium channels among others [6]. The unique localization of the PC allows the activation of these pathways in response to extracellular changes. PC is therefore an organelle critical for vertebrate development, tissue homeostasis, cell migration and differentiation, cell cycle and apoptosis. The importance of cilia in pathophysiology is highlighted by the presence of a group of diseases known as ciliopathies (human disorders associated with abnormalities of cilia structure or/and function). Ciliopathies can affect many organs (including brain, eyes, liver, kidney, skeleton and limbs) with phenotypically variable and overlapping disease manifestations. Despite the fact that more than 50 genes have been linked to ciliopathies, much less is known about the specific molecular mechanisms which could explain the phenotypic characterization of this broad range of disorders. These genes encode for proteins mainly localized at the axoneme or at the transition zone. For example, polycystic kidney disease (PKD), such as autosomal dominant polycystic kidney disease (ADPKD), results from mutations in genes (*PKD1* and *PKD2*) encoding cilia associated mechanosensitive calcium channels (polycystin proteins). We can cite also the Meckel-Gruber syndrome (MKS) or Bardet-Biedl syndrome (BBS) which are characterized by mutations affecting genes (at least 13 genes for MKS: *B9D1*, *B9D2*, *CC2D2A*, *CEP290*, *MKS1*, *RPGRIP1L*, *TCTN2*, *TCTN3*, *TMEM67*, *TMEM107*, *TMEM216*, *TMEM231*, *TMEM237* genes and more than 20 for BBS: *BBS1*, *BBS2*, *ARL6* (*BBS3*), *BBS4*, *BBS5*, *MKKS* (*BBS6*), *BBS7*, *TTC8* (*BBS8*), *BBS9*, *BBS10*, *TRIM32* (*BBS11*), *BBS12*, *MKS1* (*BBS13*), *CEP290* (*BBS14*), *WDRPCP* (*BBS15*), *SDCCAG8* (*BBS16*), *LZTFL1* (*BBS17*), *BBIP1* (*BBS18*), *IFT27* (*BBS19*), *IFT72* (*BBS20*), and *C8ORF37* (*BBS21*)) coding for proteins

associated with the transition zone or with the BBSome. Finally, cilium is not only associated to monogenic inherited disorders but also to many complex human diseases such as chronic obstructive pulmonary disease (COPD) or cancer. Significant cilia shortening is observed in COPD patients which leads to an impairment of mucociliary clearance interfering with the protection of airways from infection. The relation between cilia and cancer seems to be more complex. Indeed, oncogenic signaling pathways (such as Hh pathway) have been shown to be mediated by PC whereas cilia are also known to be lost in some types of cancer.

## 2. Ubiquitin-Proteasome System (UPS)

Two main intracellular protein degradation systems exist in vertebrates, the Ubiquitin-Proteasome System (UPS) and the autophagic-lysosomal pathway. Along with machineries involved in protein biogenesis, folding and trafficking, these two proteolytic systems play an important role in proteostasis [7,8]. Proteostasis is a crucial cellular homeostatic process that allows cells to regulate protein general abundance according to functional need but also to recognize and remove damaged proteins. Thus, proteostasis imbalance leads to the accumulation of misfolded proteins or excessive protein degradation and is associated, directly or indirectly, with many human diseases such as Alzheimer, Parkinson and Prion diseases.

The UPS starts with the ubiquitylation of target proteins. Ubiquitin is a small (8 kDa) and highly conserved protein and expressed in all eukaryotic cells. The C-terminal glycine of this protein can be covalently attached to lysine residues of substrate proteins, which is the process by which target proteins are tagged for degradation. This post-translational modification involves the hierarchical action of three general families of ubiquitin enzymes. An E1 (Ub-activating) enzyme must first activate ubiquitin (Ub). Then, the activated Ub is transferred to E2 (Ub-conjugating) and E3 (Ub Ligase) enzyme which transfer it to the target protein. The E3 Ub ligase dictates substrate specificity. Conversely, ubiquitin tags can be removed from protein substrates by deubiquitinases (DUBs). The human genome encodes two E1s, more than 30 E2 enzymes, nearly 600 E3s and 100 DUBs. There are several types of ubiquitination: fixation of one Ub protein on one lysine residue of the protein substrate (monoubiquitylation, monoUb), fixation of one Ub on several lysines of the same substrate (multi-monoubiquitylation, multimonUb) and fixation of multiple Ub chains (polyubiquitylation, polyUb) on the same lysine residue [9,10]. Since ubiquitin itself contains seven lysines residues (K6, K11, K27, K29, K33, K48 and K63) that can be targeted in recurrent rounds of enzymatic cascade, a great variety of distinct polyubiquitylations can be generated. These different types of ubiquitination are associated with distinct cellular mechanisms including endosomal pathway (for MultimonUb or polyUb K63), post-Golgi trafficking (for polyUb K33), NF- $\kappa$ B signaling (for polyUb K63), proteasomal degradation (for polyUb K48, K11 and K29) and autophagic degradation (see dedicated section for details on autophagic pathway). For example, K48-linked polyubiquitins have been shown to be mainly destined for proteasomal degradation whereas nondegrading K63-linked polyubiquitin or mono and multi-monoubiquitylation are mostly associated with endo-lysosomal trafficking and signal transduction regulation. To achieve its cellular function, the Ub tag added on a substrate needs to be properly decoded by the eukaryotic cells. This step is completed through ubiquitin receptors which possess one or more Ub-binding domains (UBDs) [11]. For example, Rpn10 (Proteasome Regulatory Subunit 10), which belongs to the 19S regulatory subunit of the proteasome, is known to possess ubiquitin-binding domains and function as receptor for ubiquitinated substrates destined for

proteasomal degradation. Once target proteins are recognized, proteins are then degraded thanks to the macromolecular protease activity of the 26S proteasome, a large multi-protein complex of about 1700 kDa which consists of a 20S catalytic subunit (also called core particle, CP), flanked by two 19S regulatory subunits (also called regulatory particle, RP) [12]. It is important to notice that proteasome is not only required for degradation of cytosolic protein but also membrane bound proteins. For example, newly synthesized misfolded membrane proteins are known to be recognized by specific UPS system called ERAD (for ER-associated degradation) [13]. These proteins are ubiquitinated, retro-translocated/dislocated from ER and degraded by the proteasome. Since UPS is a fundamental cellular process involved in proteostasis, the regulation of its dedicated molecular machinery and activity are tightly controlled. First, different factors induce the expression of genes encoding enzymes (involved in different steps of ubiquitylation) or structural proteasomal components. Second, another layer of regulation is added by different kinds of post-translational modifications (such as ubiquitination, phosphorylation) of proteasomal subunits regulating the assembly, the degradative capacity but also the localization of 26S proteasome. Finally, proteasomal activity has been shown to be compromised in age related-human diseases. For example, this defect leads to an accumulation of aberrant proteins such as the tau protein in tauopathy. Here, after reviewing the interplay between cilia and UPS, we will discuss the potential implications of this relationship in ciliopathies.

### 3. Crosstalk between cilia and UPS

The first piece of evidence showing the interplay between cilia and UPS came from proteomic analysis of cilia (Fig. 1) [14,15]. In these studies, authors have identified several UPS proteins associated with cilia proteome such as E1 activating enzymes (including UBA1, UBA6), Ub E3 ligase (including MYCBP2 and NEDD4L) and chaperones involved in Ub signaling quality control (including VCP (also known as p97)). Interestingly, functional analyses through genome-wide RNAi screens have also been performed and lead to propose that UPS-mediated protein degradation is crucial for regulating cilia formation and disassembly [16,17]. Thus, these studies have identified several UPS components as positive or negative regulators of ciliogenesis. Most of them were validated by complementary and dedicated studies [18–20]. For example, UBR5, an E3 ubiquitin ligase frequently misregulated in tumors, is known to ubiquitylate a centrosomal protein called CSPP1 (Centrosome

And Spindle Pole Associated Protein 1) required for cilia formation [21]. Others E3 ligase such as SCF (Skp1-Cul1-F box protein), FBW7, Mib1 (Mindbomb1), KCTD17 and KCTD10 were all also identified to regulate the stability of different centrosomal proteins (CP110, NDE1, Talpid3, Trichoplein, CEP97 respectively) which is crucial for ciliary axoneme extension [22–25]. Others UPS components including DUBs were also identified as a positive regulator of ciliogenesis. The deubiquitylation of Cep70 by the tumor suppressor CYLD (cylindromatosis) favors the cilia assembly [26]. It is important to highlight that UPS consequences on ciliogenesis is not restricted to primary cilia since the DUB activity of CYLD has been shown to contribute to the assembly of both primary and motile cilia in multiple organs [26]. Others ubiquitin-like proteins such as E2 SUMO-conjugating enzyme called UBE21/UBC-9 have also been shown to be a regulator of ciliogenesis in mammalian cells [16]. UBE1/UBC9 sumoylates a small GTPase ARL-13 and this sumoylation is required for the ciliary entry of polycystin-2, the protein mutated in autosomal dominant polycystic kidney disease [27]. Others studies are needed to better investigate the interplay between ubiquitin-like proteins and cilia. One should also better clarify whether cilia homeostasis is also interconnected with other aspects of proteostasis including UPR (Unfolded Protein Response) and proteasome-dependent ERAD (ER-associated degradation system) pathways. During ERAD, as mentioned before, misfolded proteins are recognized and ubiquitinated at ER surface and subsequently retro-translocated/dislocated from ER to the 26S proteasome in the cytosol for proteolytic elimination. Interestingly, polycystin-2 (PC2), a ciliary calcium channel which is mutated in autosomal dominant polycystic kidney disease (ADPKD) has been shown to be degraded by ERAD [28] thus highlighting that UPS not only regulate ciliogenesis but also primary cilia dependent-signal transduction pathways.

The interplay between UPS and cilia homeostasis is not restricted to the effect of UPS on ciliogenesis: this relationship being indeed bilateral (Fig. 1). Different ciliary proteins (including BBS4, OFD1 and RPGRIP1L) have been shown to directly interact with different proteasomal components (such as RPT6 from the 19S subunit) leading to a reduction of proteasomal activity [29,30]. The presence of specific cilia-(or centrosomal)-associated proteasomal activity regulated by ciliary proteins was even suggested [31,32]. However, it is still unclear whether cilia are able to relocate the proteasome complex itself at basal body since a subpopulation of proteasomes, with different subunits composition, possibly exists at the ciliary base. Finally and more interestingly, reduction of UPS activity has been observed in mouse models of ciliopathies. For

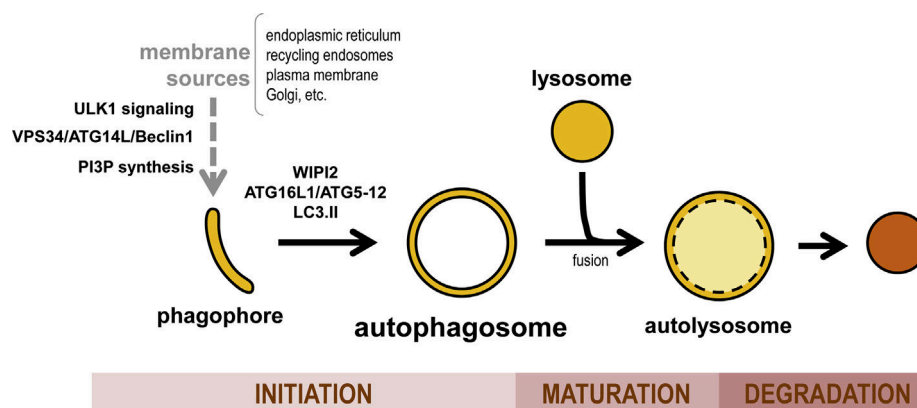


**Fig. 1. The Autophagic pathway.** The autophagic pathway requires three different steps: 1) Initiation in which the cytosolic substrates are sequestered within a double membrane vesicle called phagophore or pre-autophagosome 2) Maturation that is characterized by the elongation and the closure of phagophore forming an « autophagosome » 3) Degradation that includes the fusion of autophagosome-lysosome to form an autolysosome in which the cargo is degraded and recycled.

example, Gerhardt and co-authors have highlighted a specific disruption of proteasomal activity in mouse embryos invalidated for the gene *Rpgrip11* encoding the RPGRIP1L proteins which is mutated in different ciliopathies including the Joubert Syndrome [33]. The most intriguing question that remains to be answered is to what extent this UPS deregulation corresponds to the effect of ciliary protein on UPS. Knowing the fact that this proteasomal activity disruption seems to occur specifically and exclusively at the ciliary base [33], targeting proteasome appears to be an attractive therapeutic strategy to cure human ciliary disorders.

#### 4. Autophagy pathway

Autophagy is a lysosomal degradation and recycling pathway that controls the quality and quantity of cytoplasmic material [34,35]. Autophagy mobilizes nutrient stores such as glycogen, lipid droplets, proteins and organelles and provide nutrients, essential amino acids, fatty acids, glucose allowing cell survival during starvation. It is now widely accepted that autophagy plays crucial roles in cellular and tissue homeostasis as well as metabolism, development, and, through pathogen clearance, immunity. Dysfunctional autophagy, defective or excessive, has been associated to human pathologies ranging from neurodegenerative diseases to cancer and infectious diseases. Growing list of mutations in genes encoding the autophagy-related proteins (ATG) was also identified in various human diseases. In translational terms, autophagy is now recognized as an attractive target for the development of new treatments for human diseases. To this date, three major types of autophagy have been described in mammals: chaperone-mediated autophagy, microautophagy and macroautophagy. During chaperone-mediated autophagy, a subset of cytosolic proteins with KFERQ motifs are recognized by the Hsc70 chaperone and degraded selectively in lysosome. In the case of microautophagy, the cytoplasmic content is directly engulfed by the lysosome by the invagination of the lysosomal membrane itself. The process of macroautophagy (hereafter referred simply to as “autophagy”) requires the formation of a double-membrane vacuole called the autophagosome that sequesters proteins and other cytoplasmic components to be delivered into the lysosome (Fig. 2). Autophagosome biogenesis is mostly orchestrated by autophagy-related proteins (ATGs) and initiated by a complex that is composed of the kinase ULK1/2 and ATG13, FIP200, and ATG101. The activity of this complex is under the control of the mTOR complex 1 (MTORC1), which integrates a variety of signals such as amino acids, glucose, and growth factors. The subsequent step of autophagosome formation relies on VPS34/PIK3C3, a class III phosphatidylinositol kinase responsible for phosphatidylinositol-3-phosphate (PI3P) synthesis, which forms a complex with ATG14L, Beclin1, VPS15, and then with the subsequent, and PI3P-dependent, ATG12—ATG5—ATG16L1 complex. This complex allows the lipidation of LC3-I (ATG8) to form LC3-II which favors maturation of the autophagosome. Finally, fully formed autophagosome will fuse with a lysosome (autolysosome step) to allow the proper breakdown and recycling of the engulfed cargoes by specific lysosomal enzymes. Several trafficking regulators, including Rab small GTPases, SNAREs, and VPS proteins have been shown to be crucial for the last stage of autophagosome maturation for fusion with lysosome. (Fig. 2).

Autophagy takes place at basal levels in all eukaryotic cells. However, autophagy is mostly a stress-response catabolic process that is induced by many different physiological stimuli (among which nutrient starvation, growth factor withdrawal, drug treatment, radiotherapy, oxidative and mechanical stress) and pathophysiological situations. Although in general autophagy is a bulk process, it can also be highly selective. Selective autophagic

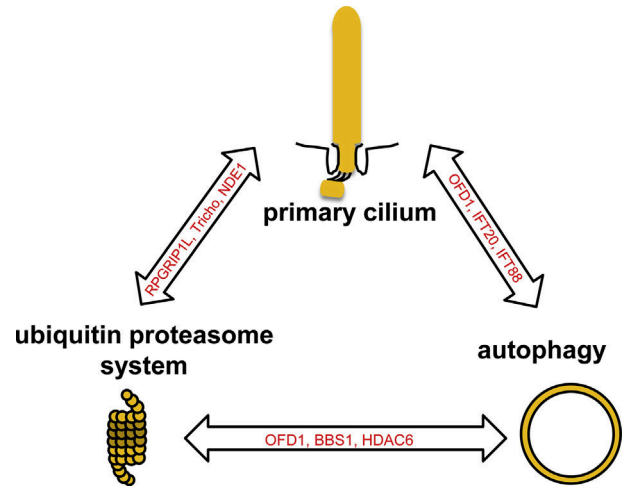


**Fig. 2. Interplay between primary cilium (PC), ubiquitin proteasome system (UPS) and autophagy.** UPS-PC relationship is bilateral: PC can modulate UPS activity whereas UPS components are able to control cilia formation and disassembly via different proteins (such as RPGRIP1L, Tricho and NDE1). Autophagy and PC are also interconnected: PC is a positive modulator of autophagic pathway since compromised ciliogenesis impairs basal autophagy whereas induced autophagy is required for ciliogenesis and cilia length maintenance. Interplay between autophagy and UPS pathways: autophagy directly regulates UPS by degrading the proteasomal machinery through a selective process called proteaphagy. Several key proteins like OFD1, BBS1, HDAC6 and others modulate specifically this UPS and autophagy crosstalk. In addition, when the UPS is not efficient, autophagy can compensate the reduced proteasomal degradative capacity. The two systems can also influence each other through the degradation of mutual key components.

responses are named according to the type of cellular material targeted: aggregated proteins (aggrephagy), mitochondria (mitophagy), peroxisomes (pexophagy), lipid droplets (lipophagy), ribosomes (ribophagy), endoplasmic reticulum (reticulophagy), lysosomes (lysophagy), glycogen (glycophagy), intracellular pathogens (xenophagy) or proteasome components (proteaphagy). Many efforts have been made in understanding certain aspects of selective autophagy especially how cargo(es) is (are) sequestered into autophagosome. Two different cellular pathways (ubiquitin-independent and ubiquitin-dependent) have been shown to recognize signals on cargoes to deliver them into the autophagosome [36]. The ubiquitin independent pathway requires receptors (including NIX for mitophagy or FAM134B for reticulophagy) that bind directly certain substrates and target them for autophagic degradation by interacting with LC3. The ubiquitin dependent pathway involves adaptor proteins (such as p62/SQSTM1, NBR1 or NPD52) which also recognize LC3 and cargoes, however, its ubiquitination is required for its own recognition. As mentioned before, ubiquitination is therefore not only important for substrate degradation by proteasome but also for selective autophagy. The precise mechanism that governs the choice between these two proteolytic systems is still unclear. The lysine residue position, as well as the length and nature of ubiquitin chains have been suggested to be required to pathway selection. Indeed, K48-linked chains lead to proteasomal degradation of the substrates while K63-linked chains or phosphorylated ubiquitin are likely more involved in xenophagy and mitophagy respectively.

Before reviewing data on the interplay between cilia and autophagy, it is important to underline that autophagy and UPS pathways are tightly interconnected [37]. As mentioned before, autophagy directly regulates UPS by degrading the proteasome through a selective autophagy called proteaphagy. However, the relation between UPS, which is the primary proteolytic pathway for short-lived proteins, and autophagy, more dedicated to the long-lived

ones, is not restricted to the effect of autophagy on the regulation of proteasomal degradation. Upon proteasome impairment, autophagy is well known to be able to compensate the reduced cellular proteasomal degradative capacity [38]. Apart from this compensatory function of autophagy, both systems are interconnected by influencing each other through the degradation of key components. This is for example the case of several E3 ligases which control the proteasomal degradation of various autophagy effectors such as ULK1.

## 5. Crosstalk between cilia and autophagy

The crosstalk between cilia and proteolytic systems is not restricted to UPS (Fig. 1). In fact, since 2013 several studies including ours have highlighted the existence of a specific interplay between primary cilia and autophagy (see previously published contributions [39–42]). Here we will summarize and update this research area. Work by Tang and colleagues show that the autophagic degradation of the centriolar satellite protein oral-facial-digital syndrome 1 (OFD1) is necessary for the serum starvation-induced ciliogenesis in mouse embryonic fibroblasts (MEFs) [43]. Accordingly, both ciliogenesis and degradation of OFD1 induced by serum deprivation are partially inhibited in *Atg5*<sup>-/-</sup> MEFs. Indeed, these cells show a lower percentage of ciliated cells and a diminished cilia length. Importantly, the knockdown of OFD1 in autophagy-deficient cells restores the serum deprivation-induced ciliogenesis and cilia length, suggesting that the autophagic degradation of OFD1 is necessary for starvation-induced ciliogenesis [43]. At the same time, Pampliega and colleagues demonstrated a close interaction between PC-dependent signaling pathways, ciliogenesis and autophagy [44]. The authors used two cellular models of impaired ciliogenesis: the knockdown of the ciliary IFT20 protein in MEFs and mouse kidney epithelial cells (KECs) with a hypomorphic mutation of IFT88. In these models, both autophagic maturation and PC formation are significantly reduced in conditions of serum starvation suggesting that compromised ciliogenesis impairs autophagy induction following serum withdrawal. Interestingly, they show that the Hh signaling pathway is necessary for the up-regulation of PC-dependent autophagy following serum withdrawal since the pharmacological or genetic activation of the Hh pathway induces autophagy in wild type MEFs but not in IFT20(-) MEFs or IFT88-/- KECs [44]. This work also shows that autophagy-associated ATG16L1 protein re-localizes at the basal body of the primary cilium after serum starvation or when ciliary Hh signaling is increased. Interestingly, this protein seems to be associated with IFT20, participating in the proper trafficking of the latter from the Golgi to the base of the PC in conditions of ciliogenesis. This study also demonstrates that IFT20 is degraded by basal autophagy, thus maintaining ciliogenesis to a minimum in nutrient rich conditions. Accordingly, in autophagy-deficient *Atg5*<sup>-/-</sup> MEFs the protein IFT20 is accumulated, thus promoting ciliogenesis and cilia growth [44].

Recently, it has been shown that the crosstalk between PC and autophagy involves the mTOR pathway and the ubiquitin-proteasome system [45]. In this work, Wang and colleagues, using epithelial kidney HK2 cells in which IFT88 was knocked down, and C13 cells (epithelial kidney cells with short cilia), demonstrated that both basal and starvation-induced autophagy are reduced in both paradigms of cilia-deficient cells. Interestingly, these cells show higher activation of the mTOR pathway and treatment with rapamycin restores autophagy in both cell types suggesting that the PC depletion inhibits autophagy through the activation of the mTOR signaling pathway [45]. In addition, autophagy induction significantly increases cilium length, while its inhibition reduces cilia length and frequency in IFT88-KD and *Atg7*<sup>-/-</sup> kidney

proximal tubular cells, respectively. Interestingly, the pharmacological inhibition of proteasomal activity reverses the shortening of cilia in autophagy deficient cells, suggesting that the autophagy's inhibition promotes proteasomal degradation of an unknown protein that is necessary for ciliogenesis [45]. Altogether, these results suggest that a PC of "normal length" is necessary for basal and starvation-induced autophagy and, conversely, autophagy is required for ciliogenesis and cilia length maintenance. On the other hand, it is known that the PC acts as a flow sensor that regulates kidney epithelial cell size through the liver kinase B1 (LKB1)-AMPK-mTOR pathway [46]. Interestingly, we have shown that physiological fluid flow induces autophagy and decreases cell volume in a cilium-dependent manner, suggesting that the PC is required for fluid flow-induced autophagy [47]. Unlike PC-induced autophagy following serum withdrawal, Hedgehog signaling pathway is not involved in this setting. So far, this flow-induced autophagy is characterized by the recruitment of ATG16L1 to the basal body of the PC as previously demonstrated by Pampliega and colleagues. These results suggest that ATG16L1 translocation might be one of the hallmarks of PC-dependent autophagy. Additionally, we evaluated the role of the PC *in vivo* in the regulation of autophagy and cell size in kidney epithelial cells. The specific depletion of Kif3a in tubular cells in mice impairs ciliogenesis, reduces autophagy, and enlarges tubular epithelial cells compared with control mice. Altogether, these results indicate that the PC-dependent flow-induced autophagy is required for the control of cell size *in vitro* and *in vivo* [47]. Recently, Park and colleagues studied the role of autophagy and cilia in the development of focal malformations of cortical development (FMCDs) which are a group of cortical abnormalities associated with epilepsy, intellectual disability and developmental delay. These authors demonstrated that brain somatic activating mutations of mTOR decrease neuronal ciliogenesis due to impaired autophagy and the consequent accumulation of the protein OFD1 [48]. Interestingly, the mouse model of the brain somatic mutation of mTOR (p.Cys1483Tyr) exhibits the same phenotype found in FMCDs patients such as cortical dyslamination, seizures, cytomegalic neurons and decreased ciliogenesis which can be rescued by rapamycin treatment or OFD1 knockdown. Altogether these results suggest that the accumulation of OFD1 induced by defective autophagy is responsible for reduced neuronal ciliogenesis. These results were confirmed through the analysis of brain tissues from FMCDs patients which exhibit lower percentage of ciliated neurons, decreased autophagy, and accumulation of OFD1 protein [48]. To date, most of recent data focus on the post-translational mechanisms that control the crosstalk between the PC and autophagy. However, the work of Liu and collaborators delve in the transcriptional control of the PC-autophagy interplay [49]. They indeed show that ciliogenesis is reciprocally controlled by PPARA (peroxisome proliferator activated receptor alpha) and NR1H4/FXR (nuclear receptor subfamily 1, group H, member 4). Specifically, pharmacological activation of PPARA promotes ciliogenesis, induces expression of autophagic genes, and activates autophagy in mammalian cells. Interestingly, ciliogenesis requires PPARA-mediated activation of autophagy since the rapamycin treatment prevents the impaired ciliogenesis in *Pppara*<sup>-/-</sup> MEFs, however knockdown of *Atg7* in *Pppara*<sup>-/-</sup> MEFs abrogates the effect of rapamycin. On the contrary, pharmacological activation of NR1H4 negatively regulates autophagy and ciliogenesis and, conversely, siRNA-mediated knockdown of NR1H4 induces cilia formation and autophagy. Indeed, activation of NR1H4 inhibits the PPARA-dependent ciliogenesis suggesting that ciliogenesis is reciprocally controlled by these two transcription factors [49].

Finally, defective autophagic activity has been linked to different mouse model of ciliopathies such as chronic obstructive pulmonary disease (COPD) or polycystic kidney disease (PKD) models. Thus, as

mentioned before for UPS, we could wonder whether targeting autophagy is an attractive target for the development of new treatments for human ciliary disorders. Along this line, Lin and colleagues have recently demonstrated the beneficial effect of autophagy activation on preventing cystogenesis. In this study, authors have developed zebrafish model of PKD and shown that activating autophagy using mTOR-dependent (rapamycin) or mTOR-independent compounds (carbamazepine, minoxidil) reduces cystogenesis and restores renal function [50]. However, other *in vivo* experiments are needed to study the therapeutic (versus the renal and non-renal toxicity [51,52]) effect of several autophagic activators in PKD models.

## 6. Concluding remarks

Here we focused on the interplay between cilia and two proteolytic systems: autophagy and UPS. Despite several reports that have identified bidirectional crosstalk between autophagy and the PC or UPS and the PC, only a limited number of data have directly focused on the interplay between autophagy, UPS and the PC in the control of cellular functions. It is known that cilium-dependent signaling pathways are necessary for autophagy induction in some cellular models (such as fibroblast and kidney epithelial cells), while both basal or starvation-induced autophagy regulate ciliogenesis and the PC length through the degradation of specific proteins that acts as positive or negative regulators of ciliogenesis. Despite exciting progresses in the understanding of the interplay between autophagy and cilia, many questions remain to be answered: is this interplay between autophagy and the PC also occurring in other cell types? Likewise, as the majority of the published articles show the effect of autophagy on ciliogenesis, or *vice versa*, under serum deprivation conditions, could other stimuli that modulate the autophagic pathway also control ciliogenesis or cilia length? On the other hand, are cilia associated structures and/or complexes also interconnected with other aspects of proteostasis including protein folding and protein synthesis? Is there a relationship between cilia and other forms of autophagy such as chaperone-mediated autophagy or microautophagy? Thus, future research needs to focus on better understanding the translational interplay that exists between autophagy, UPS and ciliogenesis in order to identify therapeutic targets that, through the modulation of these processes, might represent effective treatments for different ciliopathies or non-communicable diseases associated with cilia or proteostasis defects such as insulin resistance, type-2 diabetes, cancer, and neurodegenerative disorders.

## Conflicts of interests

The authors declare that they have no conflict of interest.

## Acknowledgments

We warmly thank Dr Patrice Codogno for constant support, mentoring and fruitful discussions. This study was supported by ANR (agence nationale de la recherche), INSERM (institut national de la santé et de la recherche médicale) and CNRS (centre national de la recherche scientifique). This work was also supported by Fondo Nacional de Desarrollo Científico y Tecnológico Grant 3180209 and the CONICYT Grant RED170147 (to Y. Ávalos).

## References

- [1] J.M. Scholey, Intraflagellar transport motors in cilia: moving along the cell's antenna, *J. Cell Biol.* (2008), <https://doi.org/10.1083/jcb.200709133>.
- [2] H. Ishikawa, W.F. Marshall, Ciliogenesis: building the cell's antenna, *Nat. Rev. Mol. Cell Biol.* (2011), <https://doi.org/10.1038/nrm3085>.
- [3] A. Mourão, S.T. Christensen, E. Lorentzen, The intraflagellar transport machinery in ciliary signaling, *Curr. Opin. Struct. Biol.* (2016), <https://doi.org/10.1016/j.sbi.2016.06.009>.
- [4] F. Bangs, K.V. Anderson, Primary cilia and mammalian Hedgehog signaling, *Cold Spring Harb. Perspect. Biol.* (2017), <https://doi.org/10.1101/cshperspect.a028175>.
- [5] J.M. Gerdes, N. Katsanis, Chapter 7 ciliary function and Wnt signal modulation, *Curr. Top. Dev. Biol.* (2008), [https://doi.org/10.1016/S0070-2153\(08\)00807-7](https://doi.org/10.1016/S0070-2153(08)00807-7).
- [6] R. Pala, N. Alomari, S.M. Nauli, Primary cilium-dependent signaling mechanisms, *Int. J. Mol. Sci.* (2017), <https://doi.org/10.3390/ijms18112272>.
- [7] C.L. Klaips, G.G. Jayaraj, F.U. Hartl, Pathways of cellular proteostasis in aging and disease, *J. Cell Biol.* (2018), <https://doi.org/10.1083/jcb.201709072>.
- [8] J. Labbadia, R.I. Morimoto, The biology of proteostasis in aging and disease, *Annu. Rev. Biochem.* (2015), <https://doi.org/10.1146/annurev-biochem-060614-033955>.
- [9] P.A. Robinson, Ubiquitin-protein ligases, *J. Cell Sci.* (2004), <https://doi.org/10.1242/jcs.01539>.
- [10] I. Dikic, Proteasomal and autophagic degradation systems, *Annu. Rev. Biochem.* (2017), <https://doi.org/10.1146/annurev-biochem-061516-044908>.
- [11] I. Dikic, S. Wakatsuki, K.J. Walters, Ubiquitin-binding domains from structures to functions, *Nat. Rev. Mol. Cell Biol.* (2009), <https://doi.org/10.1038/nrm2767>.
- [12] G.A. Collins, A.L. Goldberg, The logic of the 26S proteasome, *Cell* (2017), <https://doi.org/10.1016/j.cell.2017.04.023>.
- [13] X. Wu, T.A. Rapoport, Mechanistic insights into ER-associated protein degradation, *Curr. Opin. Cell Biol.* (2018), <https://doi.org/10.1016/jceb.2018.04.004>.
- [14] G.J. Pazour, N. Agrin, J. Leszyk, G.B. Witman, Proteomic analysis of a eukaryotic cilium, *J. Cell Biol.* (2005), <https://doi.org/10.1083/jcb.200504008>.
- [15] D.U. Mick, R.B. Rodrigues, R.D. Leib, C.M. Adams, A.S. Chien, S.P. Gygi, M.V. Nachury, Proteomics of primary cilia by proximity labeling, *Dev. Cell* (2015), <https://doi.org/10.1016/j.devcel.2015.10.015>.
- [16] G. Whewey, M. Schmidts, D.A. Mans, K. Szymanska, T.M.T. Nguyen, H. Racher, I.G. Phelps, G. Toedt, J. Kennedy, K.A. Wunderlich, N. Sorousch, Z.A. Abdelhamed, S. Natarajan, W. Herridge, J. Van Reeuwijk, N. Horn, K. Boldt, D.A. Parry, S.J.F. Letteboer, S. Roosing, M. Adams, S.M. Bell, J. Bond, J. Higgins, E.E. Morrison, D.C. Tomlinson, G.G. Slaats, T.J.P. Van Dam, L. Huang, K. Kessler, A. Giessel, C.V. Logan, E.A. Boyle, J. Shendure, S. Anazi, M. Aldahmesh, S. Al Hazzaa, R.A. Hegele, C. Ober, P. Frosch, A.A. Mhanni, B.N. Chodirker, A.E. Chudley, R. Lamont, F.P. Bernier, C.L. Beaulieu, P. Gordon, R.T. Pon, C. Donahue, A.J. Barkovich, L. Wolf, C. Toomes, C.T. Thiel, K.M. Boycott, M. McKibbin, C.F. Inglehearn, F. Stewart, H. Omran, M.A. Huynen, P.I. Sergouniotis, F.S. Alkuraya, J.S. Parboosingh, A.M. Innes, C.E. Willoughby, R.H. Giles, A.R. Webster, M. Ueffing, O. Blacque, J.G. Gleeson, U. Wolfrum, P.L. Beales, T. Gibson, D. Doherty, H.M. Mitchison, R. Roepman, C.A. Johnson, An siRNA-based functional genomics screen for the identification of regulators of ciliogenesis and ciliopathy genes, *Nat. Cell Biol.* (2015), <https://doi.org/10.1038/ncb3201>.
- [17] J. Kim, J.E. Lee, S. Heynen-Genel, E. Suyama, K. Ono, K. Lee, T. Ideker, P. Aza-Blanc, J.G. Gleeson, Functional genomic screen for modulators of ciliogenesis and cilium length, *Nature* (2010), <https://doi.org/10.1038/nature08895>.
- [18] J.J. Malicki, C.A. Johnson, The cilium: cellular antenna and central processing unit, *Trends Cell Biol.* (2017), <https://doi.org/10.1016/j.tcb.2016.08.002>.
- [19] K. Huang, D.R. Diener, J.L. Rosenbaum, The ubiquitin conjugation system is involved in the disassembly of cilia and flagella, *J. Cell Biol.* (2009), <https://doi.org/10.1083/jcb.200903066>.
- [20] R.F. Shearer, D.N. Saunders, Regulation of primary cilia formation by the ubiquitin-proteasome system, *Biochem. Soc. Trans.* (2016), <https://doi.org/10.1042/BST20160174>.
- [21] R.F. Shearer, K.-A.M. Frikstad, J. McKenna, R.A. McCloy, N. Deng, A. Burgess, T. Stokke, S. Patzke, D.N. Saunders, The E3 ubiquitin ligase UBR5 regulates centriolar satellite stability and primary cilia, *Mol. Biol. Cell* (2018), <https://doi.org/10.1091/mbc.E17-04-0248>.
- [22] L. Wang, K. Lee, R. Malonis, I. Sanchez, B.D. Dynlacht, Tethering of an E3 ligase by PCM1 regulates the abundance of centrosomal KIAA0586/Talpid3 and promotes ciliogenesis, *Elife* (2016), <https://doi.org/10.7554/eLife.12950>.
- [23] K. Kasahara, Y. Kawakami, T. Kiyono, S. Yonemura, Y. Kawamura, S. Era, F. Matsuzaki, N. Goshima, M. Inagaki, Ubiquitin-proteasome system controls ciliogenesis at the initial step of axoneme extension, *Nat. Commun.* (2014), <https://doi.org/10.1038/ncomms6081>.
- [24] D. Maskey, M.C. Marlin, S. Kim, S. Kim, E.-C. Ong, G. Li, L. Tsiokas, Cell cycle-dependent ubiquitylation and destruction of NDE1 by CDK5-FBW7 regulates ciliary length, *EMBO J.* (2015), <https://doi.org/10.15252/emboj>.
- [25] V. Dangioliella, V. Donato, S. Vijayakumar, A. Saraf, L. Florens, M.P. Washburn, B. Dynlacht, M. Pagano, SCFCyclinF controls centrosome homeostasis and mitotic fidelity through CP110 degradation, *Nature* (2010), <https://doi.org/10.1038/nature09140>.
- [26] Y. Yang, J. Ran, M. Liu, D. Li, Y. Li, X. Shi, D. Meng, J. Pan, G. Ou, R. Aneja, S.C. Sun, J. Zhou, CYLD mediates ciliogenesis in multiple organs by deubiquitinating Cep70 and inactivating HDAC6, *Cell Res.* (2014), <https://doi.org/10.1038/cr.2014.136>.
- [27] Y. Li, Q. Zhang, Q. Wei, Y. Zhang, K. Ling, J. Hu, SUMOylation of the small GTPase ARL-13 promotes ciliary targeting of sensory receptors, *J. Cell Biol.* (2012), <https://doi.org/10.1083/jcb.201203150>.
- [28] G. Liang, Q. Li, Y. Tang, K. Kokame, T. Kikuchi, G. Wu, X.Z. Chen, Polyubiquitin-2 is regulated by endoplasmic reticulum-associated degradation, *Hum. Mol. Genet.* (2009), <https://doi.org/10.1093/hmg/ddn320>.

- Genet. (2008), <https://doi.org/10.1093/hmg/ddm383>.
- [29] C. Gerhardt, T. Leu, J.M. Lier, U. Rütther, The cilia-regulated proteasome and its role in the development of ciliopathies and cancer, *Cilia* (2016), <https://doi.org/10.1186/s13630-016-0035-3>.
- [30] Y.P. Liu, I.C. Tsai, M. Morleo, E.C. Oh, C.C. Leitch, F. Massa, B.H. Lee, D.S. Parker, D. Finley, N.A. Zaghoul, B. Franco, N. Katsanis, Ciliopathy proteins regulate paracrine signaling by modulating proteasomal degradation of mediators, *J. Clin. Investig.* (2014), <https://doi.org/10.1172/JCI71898>.
- [31] R.P. Fabunmi, W.C. Wigley, P.J. Thomas, G.N. DeMartino, Activity and regulation of the centrosome-associated proteasome, *J. Biol. Chem.* (2000), <https://doi.org/10.1074/jbc.275.1.409>.
- [32] C.W. Wigley, R.P. Fabunmi, M.G. Lee, C.R. Marino, S. Muallem, G.N. DeMartino, P.J. Thomas, Dynamic association of proteasomal machinery with the centrosome, *J. Cell Biol.* (1999), <https://doi.org/10.1083/jcb.145.3.481>.
- [33] C. Gerhardt, J.M. Lier, S. Burmüh, A. Struchtrup, K. Deutschmann, M. Vetter, T. Leu, S. Reeg, T. Grune, U. Rütther, The transition zone protein Rpgrip11 regulates proteasomal activity at the primary cilium, *J. Cell Biol.* (2015), <https://doi.org/10.1083/jcb.201408060>.
- [34] E. Morel, M. Mehrpour, J. Botti, N. Dupont, A. Hamai, A.C. Nascimbeni, P. Codogno, Autophagy: a druggable process, *Annu. Rev. Pharmacol. Toxicol.* 57 (2017) 375–398, <https://doi.org/10.1146/annurev-pharmtox-010716-104936>.
- [35] P. Boya, F. Reggiori, P. Codogno, Emerging regulation and functions of autophagy, *Nat. Cell Biol.* (2013), <https://doi.org/10.1038/ncb2788>.
- [36] V. Rogov, V. Dötsch, T. Johansen, V. Kirkin, Interactions between autophagy receptors and ubiquitin-like proteins form the molecular basis for selective autophagy, *Mol. Cell* (2014), <https://doi.org/10.1016/j.molcel.2013.12.014>.
- [37] Y.T. Kwon, A. Ciechanover, The ubiquitin code in the ubiquitin-proteasome system and autophagy, *Trends Biochem. Sci.* (2017), <https://doi.org/10.1016/j.tibs.2017.09.002>.
- [38] V.I. Korolchuk, F.M. Menzies, D.C. Rubinsztein, Mechanisms of cross-talk between the ubiquitin-proteasome and autophagy-lysosome systems, *FEBS Lett.* (2010), <https://doi.org/10.1016/j.febslet.2009.12.047>.
- [39] M. Cao, Q. Zhong, Cilia in autophagy and cancer, *Cilia* (2016), <https://doi.org/10.1186/s13630-016-0027-3>.
- [40] O. Pampliega, A.M. Cuervo, Autophagy and primary cilia: dual interplay, *Curr. Opin. Cell Biol.* (2016), <https://doi.org/10.1016/j.ceb.2016.01.008>.
- [41] I. Orhon, N. Dupont, O. Pampliega, A.M. Cuervo, P. Codogno, Autophagy and regulation of cilia function and assembly, *Cell Death Differ.* (2015), <https://doi.org/10.1038/cdd.2014.171>.
- [42] Y. Ávalos, D. Peña-Oyázarun, M. Budini, E. Morselli, A. Criollo, New roles of the primary cilium in autophagy, *BioMed Res. Int.* (2017), <https://doi.org/10.1155/2017/4367019>.
- [43] Z. Tang, M.G. Lin, T.R. Stowe, S. Chen, M. Zhu, T. Stearns, B. Franco, Q. Zhong, Autophagy promotes primary ciliogenesis by removing OFD1 from centriolar satellites, *Nature* (2013), <https://doi.org/10.1038/nature12606>.
- [44] O. Pampliega, I. Orhon, B. Patel, S. Sridhar, A. Diaz-Carretero, I. Beau, P. Codogno, B.H. Satir, P. Satir, A.M. Cuervo, Functional interaction between autophagy and ciliogenesis, *Nature* 502 (2013) 194–200, <https://doi.org/10.1038/nature12639>.
- [45] S. Wang, M.J. Livingston, Y. Su, Z. Dong, Reciprocal regulation of cilia and autophagy via the MTOR and proteasome pathways, *Autophagy* (2015), <https://doi.org/10.1080/15548627.2015.1023983>.
- [46] C. Boehlke, F. Kotsis, V. Patel, S. Braeg, H. Voelker, S. Bredt, T. Beyer, H. Janusch, C. Hamann, M. Gödel, K. Müller, M. Herbst, M. Hornung, M. Doerken, M. Köttgen, R. Nitschke, P. Igarashi, G. Walz, E.W. Kuehn, Primary cilia regulate mTORC1 activity and cell size through Lkb1, *Nat. Cell Biol.* (2010), <https://doi.org/10.1038/ncb2117>.
- [47] I. Orhon, N. Dupont, M. Zaidan, V. Boitez, M. Burtin, A. Schmitt, T. Capiod, A. Viau, I. Beau, E. Wolfgang Kuehn, G. Friedlander, F. Terzi, P. Codogno, Primary-cilium-dependent autophagy controls epithelial cell volume in response to fluid flow, *Nat. Cell Biol.* (2016), <https://doi.org/10.1038/ncb3360>.
- [48] S.M. Park, J.S. Lim, S. Ramakrishna, S.H. Kim, W.K. Kim, J. Lee, H.C. Kang, J.F. Reiter, D.S. Kim, H. (Henry) Kim, J.H. Lee, Brain somatic mutations in MTOR disrupt neuronal ciliogenesis, leading to focal cortical dyslamination, *Neuron* (2018), <https://doi.org/10.1016/j.neuron.2018.05.039>.
- [49] Z. qiang Liu, J.N. Lee, M. Son, J.Y. Lim, R.K. Dutta, Y. Maharjan, S.A. Kwak, G.T. Oh, K. Byun, S.K. Choe, R. Park, Ciliogenesis is reciprocally regulated by PPARA and NR1H4/FXR through controlling autophagy in vitro and in vivo, *Autophagy* (2018), <https://doi.org/10.1080/15548627.2018.1448326>.
- [50] P. Zhu, C.J. Sieben, X. Xu, P.C. Harris, X. Lin, Autophagy activators suppress cystogenesis in an autosomal dominant polycystic kidney disease model, *Hum. Mol. Genet.* (2017), <https://doi.org/10.1093/hmg/ddw376>.
- [51] G. Walz, K. Budde, M. Mannaa, J. Nurnberger, C. Wanner, C. Sommerer, U. Kunzendorf, B. Banas, W.H. Horl, N. Obermuller, W. Arns, H. Pavenstadt, J. Gaedeke, M. Buchert, C. May, H. Gschaidmeier, S. Kramer, K.U. Eckardt, Everolimus in patients with autosomal dominant polycystic kidney disease, *[Erratum appears in N Engl J Med 363 (12) (2010 Sep 16) 1190 [Erratum appears in N Engl J Med. 2010 Nov 11;363(20):1977], N. Engl. J. Med.* (2010).
- [52] A.L. Serra, D. Poster, A.D. Kistler, F. Krauer, S. Raina, J. Young, K.M. Rentsch, K.S. Spanaus, O. Senn, P. Kristanto, H. Scheffel, D. Weishaupt, R.P. Wüthrich, Sirolimus and kidney growth in autosomal dominant polycystic kidney disease, *N. Engl. J. Med.* (2010), <https://doi.org/10.1056/NEJMoa0907419>.



## VI. BIBLIOGRAPHY

Abdul-Majeed, S., Moloney, B. C. and Nauli, S. M. (2012) 'Mechanisms regulating cilia growth and cilia function in endothelial cells', *Cellular and Molecular Life Sciences*, 69(1), pp. 165–173. doi: 10.1007/s00018-011-0744-0.

Abou Alaiwi, W. A. *et al.* (2014) 'Survivin-induced abnormal ploidy contributes to cystic kidney and aneurysm formation', *Circulation*, 129(6), pp. 660–672. doi: 10.1161/CIRCULATIONAHA.113.005746.

Avidor-reiss, T. *et al.* (2004) 'Decoding Cilia Function : Defining Specialized Genes Required for Compartmentalized Cilia Biogenesis University of California at San Diego', 117, pp. 527–539.

Baker, K. and Beales, P. L. (2009) 'Making sense of cilia in disease: The human ciliopathies', *American Journal of Medical Genetics, Part C: Seminars in Medical Genetics*, 151(4), pp. 281–295. doi: 10.1002/ajmg.c.30231.

Bangs, F. and Anderson, K. V. (2017) 'Primary cilia and Mammalian Hedgehog signaling', *Cold Spring Harbor Perspectives in Biology*, 9(5), pp. 1–21. doi: 10.1101/cshperspect.a028175.

Di Bartolomeo, S. *et al.* (2010) 'The dynamic interaction of AMBRA1 with the dynein motor complex regulates mammalian autophagy', *Journal of Cell Biology*, 191(1), pp. 155–168. doi: 10.1083/jcb.201002100.

Benmerah, A. (2013) 'The ciliary pocket', *Current Opinion in Cell Biology*, 25(1), pp. 78–84. doi: 10.1016/j.ceb.2012.10.011.

Bershteyn, M. *et al.* (2010) 'MIM and cortactin antagonism regulates ciliogenesis and hedgehog signaling', *Developmental Cell*. Elsevier Ltd, 19(2), pp. 270–283. doi: 10.1016/j.devcel.2010.07.009.

Blacque, O. E. *et al.* (2004) 'Loss of *C. elegans* BBS-7 and BBS-8 protein function results in cilia defects and compromised intraflagellar transport', 1, pp. 1630–1642. doi: 10.1101/gad.1194004.copeptide.

- Blacque, O. E. and Leroux, M. R. (2006) ‘Human Genome & Diseases : Review Bardet-Biedl syndrome : an emerging pathomechanism of intracellular transport’, 63, pp. 2145–2161. doi: 10.1007/s00018-006-6180-x.
- Boada-Romero, E. *et al.* (2013) ‘TMEM59 defines a novel ATG16L1-binding motif that promotes local activation of LC3.’, *The EMBO journal*, 32(4), pp. 566–82. doi: 10.1038/emboj.2013.8.
- Boehlke, C. *et al.* (2010) ‘Primary cilia regulate mTORC1 activity and cell size through Lkb1’, *Nature Cell Biology*, 12(11), pp. 1115–1122. doi: 10.1038/ncb2117.
- Boukhalfa, A. *et al.* (2019) ‘Interplay between Primary cilia, Ubiquitin-Proteasome system and Autophagy’, *Biochimie*. doi: 10.1016/j.biochi.2019.06.009.
- Boya, P., Reggiori, F. and Codogno, P. (2013) ‘Emerging regulation and functions of autophagy’, *Nat Cell Biol*, 15(7), pp. 713–720. Available at: [http://www.ncbi.nlm.nih.gov/entrez/query.fcgi?cmd=Retrieve&db=PubMed&dopt=Citation&list\\_uids=23817233](http://www.ncbi.nlm.nih.gov/entrez/query.fcgi?cmd=Retrieve&db=PubMed&dopt=Citation&list_uids=23817233).
- Braun, D. A. and Hildebrandt, F. (2017) ‘Ciliopathies.’, *Cold Spring Harbor perspectives in biology*, 9(3), p. a028191. doi: 10.1101/cshperspect.a028191.
- Briscoe, J. and Théron, P. P. (2013) ‘The mechanisms of Hedgehog signalling and its roles in development and disease’, *Nature Reviews Molecular Cell Biology*, 14(7), pp. 418–431. doi: 10.1038/nrm3598.
- Bull, M. (2008) ‘基因的改变NIH Public Access’, *Bone*, 23(1), pp. 1–7. doi: 10.1038/jid.2014.371.
- Burtey, S. *et al.* (2008) ‘Centrosome overduplication and mitotic instability in PKD2 transgenic lines’, *Cell Biology International*, 32(10), pp. 1193–1198. doi: 10.1016/j.cellbi.2008.07.021.
- Chang, J. *et al.* (2013) ‘Essential role of Cenexin1 , but not Odf2 , in ciliogenesis’, pp. 655–662.
- Chávez, M. *et al.* (2015) ‘Modulation of Ciliary Phosphoinositide Content Regulates Trafficking and Sonic Hedgehog Signaling Output.’, *Developmental cell*, 34(3), pp. 338–50. doi:

10.1016/j.devcel.2015.06.016.

Cheng, J. *et al.* (2014) ‘Yeast and mammalian autophagosomes exhibit distinct phosphatidylinositol 3-phosphate asymmetries.’, *Nature communications*, 5, p. 3207. doi: 10.1038/ncomms4207.

Cheong, H. *et al.* (2014) ‘Analysis of a lung defect in autophagy-deficient mouse strains’, *Autophagy*, 10(1), pp. 45–56. doi: 10.4161/auto.26505.

Codogno, P., Mehrpour, M. and Proikas-Cezanne, T. (2011) ‘Canonical and non-canonical autophagy: variations on a common theme of self-eating?’, *Nat Rev Mol Cell Biol*, 13(1), pp. 7–12. Available at:  
[http://www.ncbi.nlm.nih.gov/entrez/query.fcgi?cmd=Retrieve&db=PubMed&dopt=Citation&list\\_uids=22166994](http://www.ncbi.nlm.nih.gov/entrez/query.fcgi?cmd=Retrieve&db=PubMed&dopt=Citation&list_uids=22166994).

Cohen, S., Valm, A. M. and Lippincott-Schwartz, J. (2018) ‘Interacting organelles’, *Current Opinion in Cell Biology*, 53, pp. 84–91. doi: 10.1016/j.ceb.2018.06.003.

Cole, D. G. *et al.* (1992) ‘Isolation of a sea urchin egg kinesin-related protein using peptide antibodies’, *Journal of Cell Science*, 101(2), pp. 291–301.

Comartin, D. *et al.* (2013) ‘CEP120 and SPICE1 cooperate with CPAP in centriole elongation’, *Current Biology*, 23(14), pp. 1360–1366. doi: 10.1016/j.cub.2013.06.002.

Corbit, K. C. *et al.* (2005) ‘Vertebrate Smoothed functions at the primary cilium’, *Nature*, 437(7061), pp. 1018–1021. doi: 10.1038/nature04117.

De Craene, J.-O. *et al.* (2017) ‘Phosphoinositides, Major Actors in Membrane Trafficking and Lipid Signaling Pathways’, *International Journal of Molecular Sciences*, 18(3), p. 634. doi: 10.3390/ijms18030634.

Cuervo, A. M. and Dice, J. F. (2000) ‘Unique properties of lamp2a compared to other lamp2 isoforms’, *Journal of Cell Science*, 113(24), pp. 4441–4450.

Cuervo, A. M. and Wong, E. (2014) ‘Chaperone-mediated autophagy: Roles in disease and aging’, *Cell Research*. Nature Publishing Group, 24(1), pp. 92–104. doi: 10.1038/cr.2013.153.

- Delling, M. *et al.* (2016) ‘Primary cilia are not calcium-responsive mechanosensors.’, *Nature*, 531(7596), pp. 656–60. doi: 10.1038/nature17426.
- Delous, M. *et al.* (2007) ‘The ciliary gene RPGRIP1L is mutated in cerebello-oculo-renal syndrome (Joubert syndrome type B) and Meckel syndrome’, *Nature Genetics*, 39(7), pp. 875–881. doi: 10.1038/ng2039.
- Division, C. (2017) ‘How centrioles acquire the ability to reproduce’, pp. 4–7. doi: 10.7554/eLife.20353.
- Dooley, H. C. *et al.* (2014) ‘WIPI2 links LC3 conjugation with PI3P, autophagosome formation, and pathogen clearance by recruiting Atg12-5-16L1’, *Mol Cell*. The Authors, 55(2), pp. 238–252. doi: 10.1016/j.molcel.2014.05.021.
- Downing, K. H. and Sui, H. (2007) ‘Structural insights into microtubule doublet interactions in axonemes’, *Current Opinion in Structural Biology*, 17(2), pp. 253–259. doi: 10.1016/j.sbi.2007.03.013.
- Dudley, L. J. *et al.* (2019) ‘Intrinsic lipid binding activity of ATG16L1 supports efficient membrane anchoring and autophagy.’, *The EMBO journal*, 38(9). doi: 10.15252/emboj.2018100554.
- Dupont, N. and Codogno, P. (2013) ‘Autophagy plays a WASHing game.’, *The EMBO journal*. Nature Publishing Group, 32(20), pp. 2659–60. doi: 10.1038/emboj.2013.202.
- Endoh-Yamagami, S. *et al.* (2009) ‘The Mammalian Cos2 Homolog Kif7 Plays an Essential Role in Modulating Hh Signal Transduction during Development’, *Current Biology*. Elsevier Ltd, 19(15), pp. 1320–1326. doi: 10.1016/j.cub.2009.06.046.
- Fenouille, N. *et al.* (2017) ‘To be or not to be cell autonomous? Autophagy says both’, *Essays In Biochemistry*, 61(6), pp. 649–661. doi: 10.1042/EBC20170025.
- Follit, J. A. *et al.* (2006) ‘The Intraflagellar Transport Protein IFT20 Is Associated with the Golgi Complex and Is Required for Cilia Assembly □ V’, *Molecular Biology of the Cell*, 17, pp. 3781–3792. doi: 10.1091/mbc.E06.

- Follit, J. A. *et al.* (2009) ‘Characterization of mouse IFT complex B’, *Cell Motility and the Cytoskeleton*. doi: 10.1002/cm.20346.
- Franco, I. *et al.* (2014) ‘PI3K class II  $\alpha$  controls spatially restricted endosomal PtdIns3P and Rab11 activation to promote primary cilium function’, *Developmental Cell*. Elsevier Inc., 28(6), pp. 647–658. doi: 10.1016/j.devcel.2014.01.022.
- Fu, J., Hagan, I. M. and Glover, D. M. (2015) ‘The centrosome and its duplication cycle’, *Cold Spring Harbor Perspectives in Medicine*, 5(1), pp. 1–36. doi: 10.1101/cshperspect.a015800.
- Garcia-Gonzalo, F. R. *et al.* (2015) ‘Phosphoinositides Regulate Ciliary Protein Trafficking to Modulate Hedgehog Signaling’, *Developmental Cell*. Cell Press, 34(4), pp. 400–409. doi: 10.1016/J.DEVCEL.2015.08.001.
- Garcia, G., Raleigh, D. R. and Reiter, J. F. (2018) ‘How the Ciliary Membrane Is Organized Inside-Out to Communicate Outside-In’, *Current Biology*. Elsevier Ltd, 28(8), pp. R421--R434. doi: 10.1016/j.cub.2018.03.010.
- Geisler, S. *et al.* (2010) ‘PINK1/Parkin-mediated mitophagy is dependent on VDAC1 and p62/SQSTM1.’, *Nature cell biology*, 12(2), pp. 119–31. doi: 10.1038/ncb2012.
- Geng, J. *et al.* (2010) ‘Post-Golgi Sec proteins are required for autophagy in *Saccharomyces cerevisiae*’, *Mol Biol Cell*, 21(13), pp. 2257–2269. doi: 10.1091/mbc.E09-11-0969.
- Gluezn, E. *et al.* (2010) ‘Beyond 9+0: Noncanonical axoneme structures characterize sensory cilia from protists to humans’, *FASEB Journal*, 24(9), pp. 3117–3121. doi: 10.1096/fj.09-151381.
- Goetz, S. C. and Anderson, K. V (2010) ‘The primary cilium: a signalling centre during vertebrate development.’, *Nature reviews. Genetics*, 11(5), pp. 331–44. doi: 10.1038/nrg2774.
- Goetz, S. C., Liem, K. F. and Anderson, K. V (2012) ‘The spinocerebellar ataxia-associated gene tau tubulin kinase 2 controls the initiation of ciliogenesis’, *Cell*. Elsevier Inc., 151(4), pp. 847–858. doi: 10.1016/j.cell.2012.10.010.
- Gradilone, S. A. *et al.* (2007) ‘Cholangiocyte cilia express TRPV4 and detect changes in luminal

tonicity inducing bicarbonate secretion’, *Proceedings of the National Academy of Sciences of the United States of America*, 104(48), pp. 19138–19143. doi: 10.1073/pnas.0705964104.

Hagenlocher, C. *et al.* (2013) ‘Ciliogenesis and cerebrospinal fluid flow in the developing *Xenopus* brain are regulated by foxj1’, *Cilia*, 2(1), pp. 1–14. doi: 10.1186/2046-2530-2-12.

Haimo, L. T. and Rosenbaum, J. L. (1981) ‘Cilia, Flagella, and Microtubules’, 91(December).

Hamasaki, M. *et al.* (2013) ‘Autophagosomes form at ER-mitochondria contact sites’, *Nature*, 495(7441), pp. 389–393. Available at:

[http://www.ncbi.nlm.nih.gov/entrez/query.fcgi?cmd=Retrieve&db=PubMed&dopt=Citation&list\\_uids=23455425](http://www.ncbi.nlm.nih.gov/entrez/query.fcgi?cmd=Retrieve&db=PubMed&dopt=Citation&list_uids=23455425).

Hanada, T. *et al.* (2009) ‘The amino-terminal region of Atg3 is essential for association with phosphatidylethanolamine in Atg8 lipidation.’, *FEBS letters*, 583(7), pp. 1078–83. doi: 10.1016/j.febslet.2009.03.009.

Hasegawa, J. *et al.* (2016) ‘Autophagosome-lysosome fusion in neurons requires INPP5E, a protein associated with Joubert syndrome.’, *The EMBO journal*, 35(17), pp. 1853–67. doi: 10.15252/emboj.201593148.

Haycraft, C. J. *et al.* (2005) ‘Gli2 and Gli3 localize to cilia and require the intraflagellar transport protein polaris for processing and function’, *PLoS Genetics*, 1(4), pp. 0480–0488. doi: 10.1371/journal.pgen.0010053.

Huang, P. and Schier, A. F. (2009) ‘Dampened Hedgehog signaling but normal Wnt signaling in zebrafish without cilia’, *Development*, 136(18), pp. 3089–3098. doi: 10.1242/dev.041343.

Huangfu, D. *et al.* (2003) ‘Hedgehog signalling in the mouse requires intraflagellar transport proteins’, *Nature*, 426(6962), pp. 83–87. doi: 10.1038/nature02061.

Huangfu, D. and Anderson, K. V. (2005) ‘Cilia and Hedgehog responsiveness in the mouse’, *Proceedings of the National Academy of Sciences of the United States of America*, 102(32), pp. 11325–11330. doi: 10.1073/pnas.0505328102.

Inoko, A. *et al.* (2012) ‘Trichoplein and Aurora A block aberrant primary cilia assembly in

- proliferating cells', *Journal of Cell Biology*, 197(3), pp. 391–405. doi: 10.1083/jcb.201106101.
- Iomini, C. *et al.* (2002) 'Primary cilia of human endothelial cells disassemble under laminar shear stress', pp. 811–817. doi: 10.1083/jcb.200312133.
- Ishikawa, H. *et al.* (2005) 'Odf2-deficient mother centrioles lack distal/subdistal appendages and the ability to generate primary cilia', *Nature Cell Biology*, 7(5), pp. 517–524. doi: 10.1038/ncb1251.
- Ishikawa, H. and Marshall, W. F. (2011) 'Ciliogenesis: Building the cell's antenna', *Nature Reviews Molecular Cell Biology*. Nature Publishing Group, 12(4), pp. 222–234. doi: 10.1038/nrm3085.
- Ishikawa, H. and Marshall, W. F. (2014) 'Mechanobiology of ciliogenesis', *BioScience*, 64(12), pp. 1084–1091. doi: 10.1093/biosci/biu173.
- Jacoby, M. *et al.* (2009) 'INPP5E mutations cause primary cilium signaling defects, ciliary instability and ciliopathies in human and mouse', *Nature Genetics*, 41(9), pp. 1027–1031. doi: 10.1038/ng.427.
- Janke, C. and Kneussel, M. (2010) 'Tubulin post-translational modifications: Encoding functions on the neuronal microtubule cytoskeleton', *Trends in Neurosciences*. Elsevier Ltd, 33(8), pp. 362–372. doi: 10.1016/j.tins.2010.05.001.
- Jenkins, B. V. *et al.* (2017) 'Effects of mutating  $\alpha$ -tubulin lysine 40 on sensory dendrite development', *Journal of Cell Science*, 130(24), pp. 4120–4131. doi: 10.1242/jcs.210203.
- Jerber, J. *et al.* (2014) 'The coiled-coil domain containing protein CCDC151 is required for the function of IFT-dependent motile cilia in animals', *Human Molecular Genetics*, 23(3), pp. 563–577. doi: 10.1093/hmg/ddt445.
- Joachim, J. *et al.* (2015) 'Activation of ULK Kinase and Autophagy by GABARAP Trafficking from the Centrosome Is Regulated by WAC and GM130', *Molecular Cell*. The Authors, 60(6), pp. 899–913. doi: 10.1016/j.molcel.2015.11.018.
- Al Jord, A., Spassky, N. and Meunier, A. (2019) 'Motile ciliogenesis and the mitotic prism',

*Biology of the Cell*, pp. 199–212. doi: 10.1111/boc.201800072.

Joukov and De Nicolo (2019) ‘The Centrosome and the Primary Cilium: The Yin and Yang of a Hybrid Organelle’, *Cells*, 8(7), p. 701. doi: 10.3390/cells8070701.

Jurczyk, A. *et al.* (2004) ‘Pericentrin forms a complex with intraflagellar transport proteins and polycystin-2 and is required for primary cilia assembly’, *Journal of Cell Biology*, 166(5), pp. 637–643. doi: 10.1083/jcb.200405023.

Kabeya, Y. *et al.* (2000) ‘LC3, a mammalian homologue of yeast Apg8p, is localized in autophagosome membranes after processing’, *Embo J*, 19(21), pp. 5720–5728. Available at: [http://www.ncbi.nlm.nih.gov/entrez/query.fcgi?cmd=Retrieve&db=PubMed&dopt=Citation&list\\_uids=11060023](http://www.ncbi.nlm.nih.gov/entrez/query.fcgi?cmd=Retrieve&db=PubMed&dopt=Citation&list_uids=11060023).

Kang, R. S. and Fölsch, H. (2009) ‘An old dog learns new tricks: novel functions of the exocyst complex in polarized epithelia in animals’, *FL000 Biology Reports*, 4(November), pp. 1–4. doi: 10.3410/b1-83.

Karanasios, E. *et al.* (2016) ‘Autophagy initiation by ULK complex assembly on ER tubulovesicular regions marked by ATG9 vesicles.’, *Nature communications*, 7, p. 12420. doi: 10.1038/ncomms12420.

Keady, B. T. *et al.* (2013) ‘NIH Public Access’, 22(5), pp. 940–951. doi: 10.1016/j.devcel.2012.04.009.IFT25.

Kim, J. *et al.* (2010) ‘Functional genomic screen for modulators of ciliogenesis and cilium length’, *Nature*. Nature Publishing Group, 464(7291), pp. 1048–1051. doi: 10.1038/nature08895.

Kim, J. C. *et al.* (2004) ‘The Bardet-Biedl protein BBS4 targets cargo to the pericentriolar region and is required for microtubule anchoring and cell cycle progression’, *Nature Genetics*, 36(5), pp. 462–470. doi: 10.1038/ng1352.

Kim, J., Kato, M. and Beachy, P. A. (2009) ‘Gli2 trafficking links Hedgehog-dependent activation of Smoothened in the primary cilium to transcriptional activation in the nucleus’, *Proceedings of the National Academy of Sciences of the United States of America*, 106(51), pp. 21666–21671. doi: 10.1073/pnas.0912180106.

- Kim, M. *et al.* (2012) ‘Staurosporine and cytochalasin d induce chondrogenesis by regulation of actin dynamics in different way’, *Experimental and Molecular Medicine*, 44(9), pp. 521–528. doi: 10.3858/emm.2012.44.9.059.
- Kitagawa, D. *et al.* (2011) ‘Structural basis of the 9-fold symmetry of centrioles’, *Cell*, 144(3), pp. 364–375. doi: 10.1016/j.cell.2011.01.008.
- Klionsky, D. J. (2007) ‘Autophagy: from phenomenology to molecular understanding in less than a decade’, *Nat Rev Mol Cell Biol*, 8(11), pp. 931–937. Available at: [http://www.ncbi.nlm.nih.gov/entrez/query.fcgi?cmd=Retrieve&db=PubMed&dopt=Citation&list\\_uids=17712358](http://www.ncbi.nlm.nih.gov/entrez/query.fcgi?cmd=Retrieve&db=PubMed&dopt=Citation&list_uids=17712358).
- Klionsky, D. J. *et al.* (2016) ‘Guidelines for the use and interpretation of assays for monitoring autophagy (3rd edition).’, *Autophagy*, 12(1), pp. 1–222. doi: 10.1080/15548627.2015.1100356.
- Kobayashi, T. *et al.* (2011) ‘Centriolar kinesin Kif24 interacts with CP110 to remodel microtubules and regulate ciliogenesis’, *Cell*, 145(6), pp. 914–925. doi: 10.1016/j.cell.2011.04.028.
- Kobayashi, T. *et al.* (2014) ‘play overlapping and distinct roles in cilia assembly’, 204(2), pp. 215–229. doi: 10.1083/jcb.201304153.
- Konno, A., Setou, M. and Ikegami, K. (2012) *Ciliary and Flagellar Structure and Function-Their Regulations by Posttranslational Modifications of Axonemal Tubulin*. 1st edn, *International Review of Cell and Molecular Biology*. 1st edn. Elsevier Inc. doi: 10.1016/B978-0-12-394305-7.00003-3.
- Koyama-Honda, I. *et al.* (2013) ‘Temporal analysis of recruitment of mammalian ATG proteins to the autophagosome formation site’, *Autophagy*, 9(10), pp. 1491–1499. Available at: [http://www.ncbi.nlm.nih.gov/entrez/query.fcgi?cmd=Retrieve&db=PubMed&dopt=Citation&list\\_uids=23884233](http://www.ncbi.nlm.nih.gov/entrez/query.fcgi?cmd=Retrieve&db=PubMed&dopt=Citation&list_uids=23884233).
- Kozminski, K. G., Beech, P. L. and Rosenbaum, J. L. (1995) ‘The Chlamydomonas kinesin-like protein FLA10 is involved in motility associated with the flagellar membrane’, *Journal of Cell Biology*, 131(6 I), pp. 1517–1527. doi: 10.1083/jcb.131.6.1517.

- Kuhns, S. *et al.* (2013) 'The microtubule affinity regulating kinase MARK4 promotes axoneme extension during early ciliogenesis', *Journal of Cell Biology*, 200(4), pp. 505–522. doi: 10.1083/jcb.201206013.
- Kundu, M. *et al.* (2008) 'Ulk1 plays a critical role in the autophagic clearance of mitochondria and ribosomes during reticulocyte maturation', *Blood*, 112(4), pp. 1493–1502. doi: 10.1182/blood-2008-02-137398.
- Kwon, R. Y. *et al.* (2010) 'Primary cilium-dependent mechanosensing is mediated by adenylyl cyclase 6 and cyclic AMP in bone cells', *FASEB Journal*, 24(8), pp. 2859–2868. doi: 10.1096/fj.09-148007.
- Larkins, C. E. *et al.* (2011) 'Arl13b regulates ciliogenesis and the dynamic localization of Shh signaling proteins', *Molecular Biology of the Cell*. doi: 10.1091/mbc.E10-12-0994.
- Lechtreck, K. *et al.* (2009) 'proteins from flagella', 187(7), pp. 1117–1132. doi: 10.1083/jcb.200909183.
- Lee, K. L. *et al.* (2015) 'The primary cilium functions as a mechanical and calcium signaling nexus', *Cilia*. ???, 4(1), pp. 1–13. doi: 10.1186/s13630-015-0016-y.
- Leroux, M. R. (2007) 'Taking Vesicular Transport to the Cilium', *Cell*, 129(6), pp. 1041–1043. doi: 10.1016/j.cell.2007.05.049.
- Lin, Yi-nan *et al.* (2013) 'CEP120 interacts with CPAP and positively regulates centriole elongation', 202(2), pp. 211–219. doi: 10.1083/jcb.201212060.
- Liu, A., Wang, B. and Niswander, L. A. (2005) 'Mouse intraflagellar transport proteins regulate both the activator and repressor functions of Gli transcription factors', *Development*, 132(13), pp. 3103–3111. doi: 10.1242/dev.01894.
- Love, D. *et al.* (2010) 'Altered lung morphogenesis, epithelial cell differentiation and mechanics in mice deficient in the Wnt/ $\beta$ -catenin antagonist chibby', *PLoS ONE*, 5(10). doi: 10.1371/journal.pone.0013600.
- Luo, N., Lu, J. and Sun, Y. (2012) 'Evidence of a role of inositol polyphosphate 5-phosphatase

INPP5E in cilia formation in zebrafish', *Vision Research*, 75, pp. 98–107. doi: 10.1016/j.visres.2012.09.011.

Luyten, A. *et al.* (2010) 'Aberrant regulation of planar cell polarity in polycystic kidney disease', *Journal of the American Society of Nephrology*, 21(9), pp. 1521–1532. doi: 10.1681/ASN.2010010127.

Lystad, A. H. *et al.* (2019) 'Distinct functions of ATG16L1 isoforms in membrane binding and LC3B lipidation in autophagy-related processes', *Nature Cell Biology*. Nature Publishing Group, 21(3), pp. 372–383. doi: 10.1038/s41556-019-0274-9.

Mackeh, R. *et al.* (2013) 'Autophagy and microtubules - new story, old players', *Journal of Cell Science*. doi: 10.1242/jcs.115626.

Malicki, J. and Avidor-Reiss, T. (2014) 'From the cytoplasm into the cilium: Bon voyage', *Organogenesis*, 10(1), pp. 138–157. doi: 10.4161/org.29055.

Marko, K. (2015) 'Precision Agriculture Eats Data, CPU Cycles: It's A Perfect Fit For Cloud Services', *Forbes Tech*, 364(16), p. 2. doi: 10.1056/NEJMra1010172.Ciliopathies.

Marszalek, J. R. *et al.* (1999) 'Situs inversus and embryonic ciliary morphogenesis defects in mouse mutants lacking the KIF3A subunit of kinesin-II', *Proceedings of the National Academy of Sciences of the United States of America*, 96(9), pp. 5043–5048. doi: 10.1073/pnas.96.9.5043.

Matsunaga, K. *et al.* (2009) 'Two Beclin 1-binding proteins, Atg14L and Rubicon, reciprocally regulate autophagy at different stages', *Nat Cell Biol*, 11(4), pp. 385–396. Available at: [http://www.ncbi.nlm.nih.gov/entrez/query.fcgi?cmd=Retrieve&db=PubMed&dopt=Citation&list\\_uids=19270696](http://www.ncbi.nlm.nih.gov/entrez/query.fcgi?cmd=Retrieve&db=PubMed&dopt=Citation&list_uids=19270696).

Meijer, A. J. and Codogno, P. (2004) 'Regulation and role of autophagy in mammalian cells', *Int J Biochem Cell Biol*, 36(12), pp. 2445–2462. Available at: [http://www.ncbi.nlm.nih.gov/entrez/query.fcgi?cmd=Retrieve&db=PubMed&dopt=Citation&list\\_uids=15325584](http://www.ncbi.nlm.nih.gov/entrez/query.fcgi?cmd=Retrieve&db=PubMed&dopt=Citation&list_uids=15325584).

Mercer, C. A., Kaliappan, A. and Dennis, P. B. (2009) 'A novel, human Atg13 binding protein, Atg101, interacts with ULK1 and is essential for macroautophagy', *Autophagy*, 5(5), pp. 649–

662. doi: 10.4161/auto.5.5.8249.

Miki, H., Okada, Y. and Hirokawa, N. (2005) 'Analysis of the kinesin superfamily: Insights into structure and function', *Trends in Cell Biology*, 15(9), pp. 467–476. doi: 10.1016/j.tcb.2005.07.006.

Milenkovic, L., Scott, M. P. and Rohatgi, R. (2009) 'Lateral transport of Smoothed from the plasma membrane to the membrane of the cilium', *Journal of Cell Biology*, 187(3), pp. 365–374. doi: 10.1083/jcb.200907126.

Mizushima, N. and Komatsu, M. (2011) 'Autophagy: renovation of cells and tissues', *Cell*. 2011/11/15, 147(4), pp. 728–741. doi: S0092-8674(11)01276-1 [pii]10.1016/j.cell.2011.10.026.

Molino, D., Nascimbeni, A. C., *et al.* (2017) 'ER-driven membrane contact sites: Evolutionary conserved machineries for stress response and autophagy regulation?', *Communicative & Integrative Biology*, 10(5–6), p. e1401699. doi: 10.1080/19420889.2017.1401699.

Molino, D., Zemirli, N. N., *et al.* (2017) 'The Journey of the Autophagosome through Mammalian Cell Organelles and Membranes', *Journal of Molecular Biology*, 429(4), pp. 497–514. doi: 10.1016/j.jmb.2016.12.013.

Monis, W. J., Faundez, V. and Pazour, G. J. (2017) 'BLOC-1 is required for selective membrane protein trafficking from endosomes to primary cilia', *The Journal of Cell Biology*, 216(7), pp. 2131–2150. doi: 10.1083/jcb.201611138.

Morel, E. *et al.* (2017) 'Autophagy: A Druggable Process', *Annual Review of Pharmacology and Toxicology*, 57(1), pp. 375–398. doi: 10.1146/annurev-pharmtox-010716-104936.

Morel, Etienne (2017) 'La formation de l'autophagosome', *medecine/sciences*, 33(3), pp. 217–220. doi: 10.1051/medsci/20173303004.

Morel, E. (2017) 'The biogenesis of autophagosome: A new challenge for the cell biologist', *Medecine/Sciences*, 33(3). doi: 10.1051/medsci/20173303004.

Nachury, M. V *et al.* (2007) 'A Core Complex of BBS Proteins Cooperates with the GTPase Rab8 to Promote Ciliary Membrane Biogenesis', *Cell*, 129(6), pp. 1201–1213. doi:

10.1016/j.cell.2007.03.053.

Nachury, M. V, Seeley, E. S. and Jin, H. (2010) 'Trafficking to the Ciliary Membrane: How to Get Across the Periciliary Diffusion Barrier?', *Annual Review of Cell and Developmental Biology*. doi: 10.1146/annurev.cellbio.042308.113337.

Nakatsu, F. (2015) 'A Phosphoinositide Code for Primary Cilia.', *Developmental cell*, 34(4), pp. 379–80. doi: 10.1016/j.devcel.2015.08.008.

Narita, K. *et al.* (2012) 'Proteomic analysis of multiple primary cilia reveals a novel mode of ciliary development in mammals', *Biology Open*, 1(8), pp. 815–825. doi: 10.1242/bio.20121081.

Nascimbeni, A. C., Codogno, P. and Morel, E. (2017) 'Phosphatidylinositol-3-phosphate in the regulation of autophagy membrane dynamics', *The FEBS Journal*, 284(9), pp. 1267–1278. doi: 10.1111/febs.13987.

Nauli, S. M. *et al.* (2003) 'Polycystins 1 and 2 mediate mechanosensation in the primary cilium of kidney cells', *Nature Genetics*, 33(2), pp. 129–137. doi: 10.1038/ng1076.

Nechipurenko, I. V, Doroquez, D. B. and Sengupta, P. (2013) 'Primary cilia and dendritic spines: Different but similar signaling compartments', *Molecules and Cells*, 36(4), pp. 288–303. doi: 10.1007/s10059-013-0246-z.

Nishida, Y. *et al.* (2009) 'Discovery of Atg5/Atg7-independent alternative macroautophagy.', *Nature*. Nature Publishing Group, 461(7264), pp. 654–658. doi: 10.1038/nature08455.

Nonaka, S. *et al.* (1998) 'Randomization of left-right asymmetry due to loss of nodal cilia generating leftward flow of extraembryonic fluid in mice lacking KIF3B motor protein', *Cell*, 95(6), pp. 829–837. doi: 10.1016/S0092-8674(00)81705-5.

Ocbina, P. J. R., Tuson, M. and Anderson, K. V. (2009) 'Primary cilia are not required for normal canonical Wnt signaling in the mouse embryo', *PLoS ONE*, 4(8), pp. 1–8. doi: 10.1371/journal.pone.0006839.

Okada, Y. *et al.* (2005) 'Mechanism of nodal flow: A conserved symmetry breaking event in left-right axis determination', *Cell*, 121(4), pp. 633–644. doi: 10.1016/j.cell.2005.04.008.

- Omori, Y. *et al.* (2008) ‘elipsa is an early determinant of ciliogenesis that links the IFT particle to membrane-associated small GTPase’, *10(4)*. doi: 10.1038/ncb1706.
- Orhon, I. *et al.* (2014) ‘Autophagy and regulation of cilia function and assembly’, *Cell Death and Differentiation*. Nature Publishing Group, 22(3), pp. 389–397. doi: 10.1038/cdd.2014.171.
- Orhon, I. *et al.* (2016) ‘Primary-cilium-dependent autophagy controls epithelial cell volume in response to fluid flow.’, *Nature cell biology*, 18(6), pp. 657–67. doi: 10.1038/ncb3360.
- Pampliega, O. *et al.* (2013) ‘Functional interaction between autophagy and ciliogenesis.’, *Nature*, 502(7470), pp. 194–200. doi: 10.1038/nature12639.
- Di Paolo, G. and De Camilli, P. (2006) ‘Phosphoinositides in cell regulation and membrane dynamics’, *Nature*, 443(7112), pp. 651–657. doi: 10.1038/nature05185.
- Patel, V. *et al.* (2008) ‘Acute kidney injury and aberrant planar cell polarity induce cyst formation in mice lacking renal cilia’, *Human Molecular Genetics*, 17(11), pp. 1578–1590. doi: 10.1093/hmg/ddn045.
- Pedersen, L. B., Mogensen, J. B. and Christensen, S. T. (2016) ‘Endocytic Control of Cellular Signaling at the Primary Cilium’, *Trends in Biochemical Sciences*. Elsevier Ltd, 41(9), pp. 784–797. doi: 10.1016/j.tibs.2016.06.002.
- Pedersen, L. B. and Rosenbaum, J. L. (2008) *Intraflagellar Transport (IFT): Role in Ciliary Assembly, Resorption and Signalling*. 1st edn, *Ciliary Function in Mammalian Development*. 1st edn. Elsevier Inc. doi: 10.1016/S0070-2153(08)00802-8.
- Phua, S. C., Nihongaki, Y. and Inoue, T. (2018) ‘Autonomy declared by primary cilia through compartmentalization of membrane phosphoinositides.’, *Current opinion in cell biology*, 50, pp. 72–78. doi: 10.1016/j.ceb.2018.01.008.
- Qian, F. *et al.* (2002) ‘Cleavage of polycystin-1 requires the receptor for egg jelly domain and is disrupted by human autosomal-dominant polycystic kidney disease 1-associated mutations’, *Proceedings of the National Academy of Sciences of the United States of America*, 99(26), pp. 16981–16986. doi: 10.1073/pnas.252484899.

Razi, M., Chan, E. Y. W. and Tooze, S. a. (2009) 'Early endosomes and endosomal coatomer are required for Autophagy', *Journal of Cell Biology*, 185(2), pp. 305–321. doi: 10.1083/jcb.200810098.

Reggiori, F. *et al.* (2003) 'Vps51 is part of the yeast Vps fifty-three tethering complex essential for retrograde traffic from the early endosome and Cvt vesicle completion', *Journal of Biological Chemistry*, 278(7), pp. 5009–5020. doi: 10.1074/jbc.M210436200.

Reiter, J. F. and Leroux, M. R. (2017) 'Genes and molecular pathways underpinning ciliopathies.', *Nature reviews. Molecular cell biology*, 18(9), pp. 533–547. doi: 10.1038/nrm.2017.60.

Retailleau, K. and Duprat, F. (2014) 'Polycystins and partners: Proposed role in mechanosensitivity', *Journal of Physiology*, 592(12), pp. 2453–2471. doi: 10.1113/jphysiol.2014.271346.

Rohatgi, R. *et al.* (2009) 'Hedgehog signal transduction by Smoothed: Pharmacologic evidence for a 2-step activation process', *Proceedings of the National Academy of Sciences of the United States of America*, 106(9), pp. 3196–3201. doi: 10.1073/pnas.0813373106.

Rohatgi, R., Milenkovic, L. and Scott, M. P. (2007) 'Patched1 Regulates Hedgehog Signaling at the Primary Cilium', *Science*, 317(5836), pp. 372–376. doi: 10.1126/science.1139740.

Ropolo, A. *et al.* (2007) 'The pancreatitis-induced vacuole membrane protein 1 triggers autophagy in mammalian cells', *J Biol Chem*. 2007/10/18, 282(51), pp. 37124–37133. doi: M706956200 [pii]10.1074/jbc.M706956200.

Ruiz-Perez, V. L. *et al.* (2003) 'Mutations in two nonhomologous genes in a head-to-head configuration cause Ellis-van Creveld syndrome', *American Journal of Human Genetics*, 72(3), pp. 728–732. doi: 10.1086/368063.

Russell, R. C. *et al.* (2013) 'ULK1 induces autophagy by phosphorylating Beclin-1 and activating VPS34 lipid kinase', *Nat Cell Biol*, 15(7), pp. 741–750. doi: 10.1038/ncb2757.

Satir, P. (2017) 'CILIA: Before and after', *Cilia*. BioMed Central, 6(1), pp. 1–11. doi: 10.1186/s13630-017-0046-8.

- Schink, K. O., Tan, K.-W. and Stenmark, H. (2016) 'Phosphoinositides in Control of Membrane Dynamics.', *Annual review of cell and developmental biology*. doi: 10.1146/annurev-cellbio-111315-125349.
- Schmidt, T. I. *et al.* (2009) 'Report Control of Centriole Length by CPAP and CP110', pp. 1005–1011. doi: 10.1016/j.cub.2009.05.016.
- Scholey, J. M. (2008) 'Intraflagellar transport motors in cilia: moving along the cell's antenna', *The Journal of Cell Biology*, 180(1), pp. 23–29. doi: 10.1083/jcb.200709133.
- Schröder, J. M. *et al.* (2011) 'EB1 and EB3 promote cilia biogenesis by several centrosome-related mechanisms', *Journal of Cell Science*, 124(15), pp. 2539–2551. doi: 10.1242/jcs.085852.
- Schurmans, S., Inoue, T. and Reiter, J. F. (2016) 'HHS Public Access', 34(4), pp. 400–409. doi: 10.1016/j.devcel.2015.08.001.Phosphoinositides.
- Scrivo, A., Codogno, P. and Bomont, P. (2019) 'Gigaxonin E3 ligase governs ATG16L1 turnover to control autophagosome production', *Nature Communications*. Springer US, 10(1), pp. 1–14. doi: 10.1038/s41467-019-08331-w.
- Sedmak, T. and Wolfrum, U. (2010) 'Intraflagellar transport molecules in ciliary and nonciliary cells of the retina', *Journal of Cell Biology*, 189(1), pp. 171–186. doi: 10.1083/jcb.200911095.
- Sharma, N. *et al.* (2011) 'Soluble levels of cytosolic tubulin regulate ciliary length control', *Molecular Biology of the Cell*, 22(6), pp. 806–816. doi: 10.1091/mbc.E10-03-0269.
- Singla, V. *et al.* (2010) 'Ofd1, a Human Disease Gene, Regulates the Length and Distal Structure of Centrioles', *Developmental Cell*. Elsevier Ltd, 18(3), pp. 410–424. doi: 10.1016/j.devcel.2009.12.022.
- Spektor, A. *et al.* (2007) 'Cep97 and CP110 Suppress a Cilia Assembly Program', *Cell*, 130(4), pp. 678–690. doi: 10.1016/j.cell.2007.06.027.
- Stenmark, H. (2009) 'Rab GTPases as coordinators of vesicle traffic', *Nature Reviews Molecular Cell Biology*, 10(8), pp. 513–525. doi: 10.1038/nrm2728.
- Sui, H. and Downing, K. H. (2006) 'Molecular architecture of axonemal microtubule doublets

revealed by cryo-electron tomography’, *Nature*, 442(7101), pp. 475–478. doi: 10.1038/nature04816.

Suzuki, K. and Ohsumi, Y. (2007) ‘Molecular machinery of autophagosome formation in yeast, *Saccharomyces cerevisiae*’, *FEBS Letters*, 581(11), pp. 2156–2161. doi: 10.1016/j.febslet.2007.01.096.

Takeda, S. and Narita, K. (2012) ‘Structure and function of vertebrate cilia, towards a new taxonomy’, *Differentiation*. Elsevier, 83(2), pp. S4--S11. doi: 10.1016/j.diff.2011.11.002.

Talbot, P., Geiske, C. and Knoll, M. (1999) ‘Oocyte pickup by the mammalian oviduct’, *Molecular Biology of the Cell*, 10(1), pp. 5–8. doi: 10.1091/mbc.10.1.5.

Tan, J. M. J. *et al.* (2018) ‘An ATG16L1-dependent pathway promotes plasma membrane repair and limits *Listeria monocytogenes* cell-to-cell spread’, *Nature Microbiology*, 3(12), pp. 1472–1485. doi: 10.1038/s41564-018-0293-5.

Tang, Z. *et al.* (2013) ‘Autophagy promotes primary ciliogenesis by removing OFD1 from centriolar satellites’, *Nature*. 2013/10/04, 502(7470), pp. 254–257. doi: 10.1038/nature12606.

Tanida, I. *et al.* (2005) ‘Lysosomal turnover, but not a cellular level, of endogenous LC3 is a marker for autophagy’, *Autophagy*, 1(2), pp. 84–91. Available at: [http://www.ncbi.nlm.nih.gov/entrez/query.fcgi?cmd=Retrieve&db=PubMed&dopt=Citation&list\\_uids=16874052](http://www.ncbi.nlm.nih.gov/entrez/query.fcgi?cmd=Retrieve&db=PubMed&dopt=Citation&list_uids=16874052).

Tateishi, K. *et al.* (2013) ‘Two appendages homologous between basal bodies and centrioles are formed using distinct Odf2 domains’, *Journal of Cell Biology*. doi: 10.1083/jcb.201303071.

Taylor, S. P. *et al.* (2015) ‘Mutations in DYNC2LI1 disrupt cilia function and cause short rib polydactyly syndrome’, *Nature Communications*. Nature Publishing Group, 6(1). doi: 10.1038/ncomms8092.

Thauvin-robinet, C. *et al.* (2015) ‘HHS Public Access’, 46(8), pp. 905–911. doi: 10.1038/ng.3031.The.

Thauvin-Robinet, C. *et al.* (2014) ‘The oral-facial-digital syndrome gene C2CD3 encodes a

positive regulator of centriole elongation', *Nature Genetics*. Nature Publishing Group, 46(8), pp. 905–911. doi: 10.1038/ng.3031.

Tobin, J. L. and Beales, P. L. (2009) 'The nonmotile ciliopathies THE IMPORTANCE OF UNDERSTANDING', 11(6). doi: 10.1097/GIM.0b013e3181a02882.

Travassos, L. H. *et al.* (2010) 'Nod1 and Nod2 direct autophagy by recruiting ATG16L1 to the plasma membrane at the site of bacterial entry', *Nature Immunology*. Nature Publishing Group, 11(1), pp. 55–62. doi: 10.1038/ni.1823.

Tsao, C. and Gorovsky, M. A. (2008) 'Different Effects of Tetrahymena IFT172 Domains on Anterograde and Retrograde Intraflagellar Transport', 19(April), pp. 1450–1461. doi: 10.1091/mbc.E07.

Uzbekov, R. E. *et al.* (2012) 'Centrosome fine ultrastructure of the osteocyte mechanosensitive primary cilium', *Microscopy and Microanalysis*, 18(6), pp. 1430–1441. doi: 10.1017/S1431927612013281.

Veleri, S. *et al.* (2014) 'Ciliopathy-associated gene Cc2d2a promotes assembly of subdistal appendages on the mother centriole during cilia biogenesis', *Nature Communications*. Nature Publishing Group, 5(May), pp. 1–12. doi: 10.1038/ncomms5207.

Vivar, O. I. *et al.* (2016) 'IFT20 controls LAT recruitment to the immune synapse and T-cell activation in vivo', *Proceedings of the National Academy of Sciences of the United States of America*. doi: 10.1073/pnas.1513601113.

Walentek, P. *et al.* (2016) 'Ciliary transcription factors and miRNAs precisely regulate Cp110 levels required for ciliary adhesions and ciliogenesis', pp. 1–24. doi: 10.7554/eLife.17557.

Wang, C. *et al.* (2018) 'Centrosomal protein Dzip11 binds Cby, promotes ciliary bud formation, and acts redundantly with Bromi to regulate ciliogenesis in the mouse.', *Development (Cambridge)*. Company of Biologists, 145(6). doi: 10.1242/dev.164236.

Weatherbee, S. D., Niswander, L. A. and Anderson, K. V. (2009) 'A mouse model for Meckel syndrome reveals Mks1 is required for ciliogenesis and Hedgehog signaling', *Human Molecular Genetics*, 18(23), pp. 4565–4575. doi: 10.1093/hmg/ddp422.

- Webber, W. A. and Lee, J. (1975) 'Fine structure of mammalian renal cilia', *The Anatomical Record*, 182(3), pp. 339–343. doi: 10.1002/ar.1091820307.
- Werner, S., Pimenta-marques, A. and Bettencourt-dias, M. (2017) 'Maintaining centrosomes and cilia', 1, pp. 3789–3800. doi: 10.1242/jcs.203505.
- Wiens, C. J. *et al.* (2010) 'Bardet-biedl syndrome-associated small GTPase ARL6 (BBS3) functions at or near the ciliary gate and modulates Wnt signaling', *Journal of Biological Chemistry*, 285(21), pp. 16218–16230. doi: 10.1074/jbc.M109.070953.
- Wong, S. Y. and Reiter, J. F. (2009) 'THE PRIMARY CILIUM : AT THE CROSSROADS OF MAMMALIAN', 2153(08). doi: 10.1016/S0070-2153(08)00809-0.THE.
- Wood, C. R. *et al.* (2012) 'IFT proteins accumulate during cell division and localize to the cleavage furrow in chlamydomonas', *PLoS ONE*, 7(2). doi: 10.1371/journal.pone.0030729.
- Xiong, Q. *et al.* (2018) 'The Role of ATG16 in Autophagy and The Ubiquitin Proteasome System', *Cells*, 8(1), p. 2. doi: 10.3390/cells8010002.
- Xu, C. and Min, J. (2011) 'Structure and function of WD40 domain proteins.', *Protein & cell*, 2(3), pp. 202–14. doi: 10.1007/s13238-011-1018-1.
- Xu, Q. *et al.* (2016) 'Phosphatidylinositol phosphate kinase PIPKI $\gamma$  and phosphatase INPP5E coordinate initiation of ciliogenesis.', *Nature communications*, 7(1), p. 10777. doi: 10.1038/ncomms10777.
- Xu, W. *et al.* (2017) 'The Joubert Syndrome Protein Inpp5e Controls Ciliogenesis by Regulating Phosphoinositides at the Apical Membrane', *Journal of the American Society of Nephrology*, 28(1), pp. 118–129. doi: 10.1681/ASN.2015080906.
- Xu, W. *et al.* (2019) 'Apical PtdIns(4,5)P<sub>2</sub> is required for ciliogenesis and suppression of polycystic kidney disease', *The FASEB Journal*, 33(2), pp. 2848–2857. doi: 10.1096/fj.201800385RRR.
- Yin, Y. *et al.* (2009) 'The Talpid3 gene (KIAA0586) encodes a centrosomal protein that is essential for primary cilia formation', *Development*, 136(4), pp. 655–664. doi:

10.1242/dev.028464.

Zemirli, N. *et al.* (2019) ‘The primary cilium protein folliculin is part of the autophagy signaling pathway to regulate epithelial cell size in response to fluid flow’, *Cell Stress*. Shared Science Publishers, 3(3), pp. 100–109. doi: 10.15698/cst2019.03.180.

Zuo, X., Fogelgren, B. and Lipschutz, J. H. (2011) ‘The small GTPase Cdc42 is necessary for primary ciliogenesis in renal tubular epithelial cells’, *Journal of Biological Chemistry*, 286(25), pp. 22469–22477. doi: 10.1074/jbc.M111.238469.